Boston University

OpenBU **http://open.bu.edu**

Boston University Theses & Dissertations Boston University Theses & Dissertations

2023

Topology in quasiperiodically driven systems

https://hdl.handle.net/2144/49211

Downloaded from DSpace Repository, DSpace Institution's institutional repository

BOSTON UNIVERSITY

GRADUATE SCHOOL OF ARTS AND SCIENCES

Dissertation

TOPOLOGY IN QUASIPERIODICALLY DRIVEN SYSTEMS

by

DAVID MERRICK LONG

B. Sci. (Adv.) (Hons.), The University of Sydney, 2018

Submitted in partial fulfillment of the
requirements for the degree of
Doctor of Philosophy
2023

© 2023 by
DAVID MERRICK LONG
All rights reserved, except for chapters 2-5 which are ©2021-2022 American Physical Society

Approved by

First Reader

Anushya Chandran, PhD
Assistant Professor of Physics

Second Reader

Claudio Chamon, PhD
Professor of Physics

Art is never finished, only abandoned. Leonardo da Vinci

Universities are truly storehouses for knowledge: students arrive from school confident they know nearly everything, and they leave five years later certain that they know practically nothing. Where did the knowledge go in the meantime? In the university, of course, where it is dried and stored. Terry Pratchett

Acknowledgments

The success of my PhD is owed to the support and encouragement of many people. The first and foremost is, of course, my advisor, Anushya Chandran. Anushya's help in a scientific, professional, and personal capacity has been crucial throughout the five years of my PhD studies. I am particularly grateful for her emphasis on making contact with experiment, a habit I think I lacked before studying with her.

Many other scientific collaborators have lent me their expertise. Special mention should go to Philip Crowley, who has been a perennial presence in my list of coauthors, and from whom I have learned a great deal. Other close collaborators of mine include Marin Bukov, Pieter Claeys, Andrew Doherty, Dominik Hahn, Vedika Khemani, Alicia Kollár, Ali Lavasani, Nehal Mittal, Anatoli Polkovnikov, Martin Ritter, Antonello Scardicchio, Long Hin Tang, Carlo Vanoni, and Dominik Vuina. I have also benefited from discussions with and comments by Oleksandr Balabanov, Eric Boyers, Fiona Burnell, Claudio Chamon, Dominic Else, Michael Flynn, Maria Hermanns, David Huse, Michael Kolodrubetz, Christopher Laumann, Ben Lev, Ivar Martin, Alan Morningstar, Titus Neupert, Carlos Ortega-Taberner, Robin Schäfer and Alex Sushkov. While teaching at BU, I learned from Anushya Chandran, Andrew Duffy, Ken Lane, Robert Marsland III, and Anatoli Polkovnikov.

My final scientific thanks go to my dissertation committee: Caludio Chamon, Anushya Chandran, Shyamsunder Erramilli, Ami Katz, and Alex Sushkov.

Among my nonscientific support, my family deserves pride of place. My mum Marija, my dad Tim, and my sisters Jenny and Felicity have been an inexhaustible source of care and love throughout my move to, and stay in, the USA. Our calls are the bright spot of my week.

I would also like to thank all my friends in the BU Physics Department. Listing every student in the program would not be a good use of space, but particular mention

should go to Matteo Bellitti, Eric Boyers, Chris Cosby, Brian Dawes, Sumner Hearth, Julian Ingham, Gautam Naik, Nick Russo, Gabe Schumm, Long Hin Tang, Tamiro Villazon, Dominik Vuina, Thomas Wester, Maria Yampolskaya, Shiyu Zhou, and all the members of the Graduate Student Council not included in this list. Many staff and faculty have also helped me along the way, including Despina Bokios, Mirtha Cabello, David Campbell, Kelly Capri, Vikram Chowdary, Christina Crabtree, Grace Lillibridge, and Andrei Ruckenstein.

Several parts of this dissertation are reproduced from my published work, Refs. [1–4]. During my PhD, I was supported by Teaching Fellowships from Boston University, and Research Fellowships funded by NSF Grant No. DMR-1752759, and AFOSR Grant No. FA9550-20-1-0235. Some of my PhD research was performed while visiting the Kavli Institute for Theoretical Physics at the University of California, Santa Barbara (supported by NSF Grant No. PHY-1748958), and the Max Planck Institute for the Physics of Complex Systems in Dresden as part of that institute's visitors program. Much of my numerical work during my PhD was performed on the BU Shared Computing Cluster, administered by Boston University's Research Computing Services. I also made extensive use of the Python package Quspin [5, 6].

Finally, I would to thank my cats: Sheba, Hobbes, and Polska. Sheba and Hobbes are sorely missed.

David M. Long
PhD Candidate
Boston University Department of Physics

TOPOLOGY IN QUASIPERIODICALLY DRIVEN SYSTEMS

DAVID MERRICK LONG

Boston University, Graduate School of Arts and Sciences, 2023

Major Professor: Anushya Chandran, PhD
Assistant Professor of Physics

ABSTRACT

Periodic driving is a ubiquitous tool for controlling experimental quantum systems. When the drive fields are of comparable, incommensurate frequencies, new theoretical tools are required to treat the resulting quasiperiodic time dependence. Similarly, new and surprising phenomena of topological origin may emerge in this regime, including the quantized pumping of energy from one drive field to another. This dissertation will describe how to exploit this energy pumping to coherently translate—or *boost*—quantum states of a cavity in the Fock basis. This protocol enables the preparation of highly excited Fock states for use in quantum metrology—one need only boost low occupation Fock states. Energy pumping, and hence boosting, may be achieved nonadiabatically as a robust edge effect associated to an *anomalous localized topological phase* (ALTP) of fermions on a wire, called the *quasiperiodic Floquet-Thouless energy pump* (QP pump). We present a simple coupled-layer model for the QP pump, and describe the broader topological classification which characterizes its robust properties. Finally, we argue that energy pumping by the edge modes is robust to the introduction of weak interactions between fermions, making the QP pump a stable, interacting, non-equilibrium phase of matter.

Contents

1 Introduction 1

2 Background 6

2.1 Quasiperiodic Driving 6

2.2 The Frequency Lattice 10

2.2.1 One Drive—Floquet Theory 10

2.2.2 The Frequency Lattice For Multiple Tones 14

3 Boosting 19

3.1 Phenomenology 19

3.2 Frequency Lattice Explanation 23

3.3 Boosting in the time domain 25

3.4 Experimental considerations 32

3.5 Predicting Rephasings 34

3.5.1 Renormalization of Cavity Frequency 35

3.5.2 Almost Periods 37

3.6 Quality of Rephasings 39

3.6.1 Semiclassical Picture 39

3.6.2 Including the Effect of the Spin 40

3.7 Comparing Semiclassical and Quantum Evolution 43

3.7.1 Semiclassical Evolution 43

3.7.2 Quantum Evolution 45

3.8 Summary and Discussion 49

4 Anomalous Localized Topological Phases 52

4.1 Quasiperiodic Floquet-Thouless Energy Pump 56

4.2 Coupled layer model for the QP pump 58

4.2.1 Sites 61

4.2.2 Coupled layer model 62

4.3 Numerical Characterization 65

4.3.1 Phases 65

4.3.2 Frequency Lattice Localization 70

4.3.3 Critical point 74

4.4 Effect of Interactions 78

4.5 General Construction 81

4.5.1 Four-dimensional quantum Hall edge states 83

4.6 Topological Classification 87

4.6.1 Gauge invariance of $W[V]$ 89

4.6.2 Proof of classification 91

4.7 Observable Consequences 93

4.7.1 Quantized Energy Circulation 95

4.7.2 Quantized Edge Pumping 105

4.8 Summary and Discussion 112

5 Many-Body Localization With Quasiperiodic Driving 115

5.1 Frequency lattice for interacting systems 118

5.2 Quasiperiodically-driven Many-Body Localization 123

5.2.1 Equivalence of Definitions of Quasiperiodically-Driven MBL . 126

5.3 Thermal Region Ansatz 127

5.3.1 Model 131

5.3.2 Statistics of Matrix Elements in Commensurate Approximations 132

5.4 Spatial Localization Assuming Synthetic Localization 137

5.4.1 Model 139

5.4.2 Thermal Avalanches 140

5.5 Synthetic Localization for Two-Tone Driving 147

5.5.1 Localization in the Anderson Model 150

5.5.2 Localization in the Quasiperiodic Model 151

5.5.3 Numerical Evidence of Synthetic Localization for Two-Tone Driving 155

5.6 Absence of Synthetic Localization with Three or More Tones 160

5.7 Many-Body Resonances 161

5.8 Summary and Discussion 165

6 Conclusion **169**

Curriculum Vitae **199**

List of Figures

2·1 Frequency lattice for periodic driving 12

2·2 Frequency lattice for D tones 16

3·1 Cavity state boosting 21

3·2 Boosting snapshots 22

3·3 Semiclassical rephasings 28

3·4 Alignment of the spin and field 30

3·5 Cavity state boosting in the lab frame 34

3·6 Correction to cavity frequency 36

3·7 Comparison of semiclassical evolution to quantum evolution 44

3·8 Q-functions of an initial coherent state 46

3·9 Entanglement between the spin and cavity 47

3·10 Comparison of coherent state ensemble to non-classical state evolution 48

3·11 Holonomy of boosting 50

4·1 Correspondence between ALTPs with the same frequency lattice dimension 53

4·2 The QP pump 54

4·3 Coupled layer model for the QP pump 59

4·4 Coupled layer Chern numbers 60

4·5 Localization length in the coupled layer model 67

4·6 Data collapse in site occupations 68

4·7 Edge modes in the coupled layer model 69

4·8 Spectral entropy in the coupled layer model. 71

4·9 Working parameters for the coupled layer model 72

4·10 Finite size scaling in the coupled layer model 76
4·11 Interactions in the coupled layer model 80
4·12 Synthetic four-dimensional quantum Hall effect 85
4·13 Quantized energy circulation in a qubit 94
4·14 Geometry of Sec. 4.7.1.3 102
4·15 Edge states in a commensurate approximation 106

5·1 Thermal inclusions in disordered chains 116
5·2 The frequency lattice 120
5·3 Frequency lattice quasienergy state 133
5·4 Matrix elements perpendicular to $\vec{\Omega}$ 135
5·5 Matrix elements parallel to $\vec{\Omega}$ 136
5·6 Quasi-one-dimensional model 149
5·7 IPR in commensurate approximations 153
5·8 Scaling of ζ_f in a one-dimensional approximation 158

List of Abbreviations

AFAI	....	Anomalous Floquet-Anderson insulator
ALTP	....	Anomalous localized topological phase
ETH	....	Eigenstate thermalization hypothesis
Fig.	....	Figure
GUE	....	Gaussian unitary ensemble
l-bit	....	Quasilocal integral of motion
MBL	....	Many-body localization
QED	....	Quantum electodynamics
QP	....	Quasiperiodic
QPMBL	....	Many-body localization with quasiperiodic disorder
QP pump	....	Quasiperiodic Floquet-Thouless energy pump
Ref.	....	Reference
rms	....	Root mean square
RMT	....	Random matrix theory
Sec.	....	Section
TLI	....	Topological localized insulator

Chapter 1

Introduction

Periodic driving is a ubiquitous tool in the experimental control of quantum systems. It underlies almost all techniques used to manipulate quantum states, from Rabi oscillations [7] to Floquet engineering of exotic states [8–12].

In many experimental settings, more than one driving frequency must be used in controlling the system. When those frequencies are all well-separated, they may each be treated separately. Such a regime of operation imposes a strict hierarchy of scales—each control frequency must be separated by roughly an order of magnitude, depending on the specific experiment. There is only so much frequency bandwidth which is available to an experiment, which harshly limits the number of control drives which can be employed.

A new paradigm is opened when the control frequencies are taken to be comparable. However, conventional tools used to treat periodically driven systems fail to capture this regime. Indeed, when the frequencies are incommensurate (none sharing a common period) the driving field is not periodic at all, but rather *quasiperiodic* [13–27].

Employing quasiperiodic driving provides new options for experimental control, but there are two challenges obstructing its widespread adoption. One challenge is experimental, while the other is theoretical.

Unique features of quasiperiodic driving—as opposed to those shared by periodically driven systems or those with less structured drives—only become apparent after a long enough time for the driving waveform to be resolved as quasiperiodic. As an extreme illustration, observing a quasiperiodically driven system for less than one period of each constituent driving tone reveals no special structure of the drive.

Thus, quantum experiments must have lifetimes which are long enough to resolve quasiperiodicity. Fortunately, rapid recent progress has resulted in many experimental platforms where coherence times are tens or even thousands of times longer than the timescale of microscopic dynamics, lending experimental legitimacy to the theoretical study of quasiperiodically driven quantum systems [23, 28, 29].

The theoretical challenge—to be addressed by this dissertation—is then to predict the behavior of a quantum system under quasiperiodic driving, and design driving protocols which accomplish useful tasks. While quasiperiodic driving has a long history in both the mathematics and physics literature [13–27, 30–35], the lack of any separation of scales between the driving frequencies can make its treatment difficult. Quasiperiodic driving is unlikely to become a widespread tool if it is onerous to predict what the effect of the drive will be. Thus, there is a need for a transparent and tractable theoretical framework to treat quasiperiodic drives.

My PhD research has employed the *frequency lattice* [13, 30, 36–38] formalism to reveal effects of quasiperiodic driving which are both interesting from a theoretical perspective and technologically useful. The frequency lattice method relates the problem of identifying the long-time dynamics of a quasiperiodically driven system to a lattice tight-binding model in frequency space. The latter is a familiar object in condensed matter physics, where tight-binding models serve as simple models of, for instance, electronic properties of solids. The frequency lattice thus allows us to bring the well-developed machinery and intuition of condensed matter to bear on quasiperiodic driving.

This condensed matter perspective also reveals useful tasks which can be accomplished with quasiperiodic driving. *Topological* properties of condensed matter systems have been shown to underlie phenomena from the archetypal quantum Hall effect [39–41] to exotic quasiparticle exchange statistics [42, 43]. Crucially, any phenomenology associated to topology is inherently robust to small imperfections. Driving protocols which engineer topological features in the frequency lattice thus have effects which are similarly robust to mistakes in the execution of the protocol, or certain forms of external noise [44–48].

One such protocol is *cavity state boosting* [3]. When the frequency lattice model has a nonzero Chern number, it exhibits an anomalous quantum Hall effect. In the language of the original two-tone-driven problem, this manifests as the pumping of energy from one drive to the other by a few-level quantum system, such as a spin-1/2 [37, 38, 49, 50]. The spin preferentially absorbs energy at one frequency, and emits at the other. Thus, one drive is attenuated, while the other is enhanced. When one of the drives is trapped in a cavity, energy pumping can be used to manipulate the cavity state [51]. While an immediate application of this pumping is to increase the energy inside the cavity, the coherent nature of the process allows for more useful forms of control. An initial product state of the spin and cavity

$$|\psi(0)\rangle = |s\rangle \otimes \sum_n c_n |n\rangle \tag{1.1}$$

may be *boosted* to

$$|\psi(T_N)\rangle \approx |s\rangle \otimes \sum_n c_n |n + P_{\text{top}} T_N/\hbar\omega\rangle , \tag{1.2}$$

where T_N is one of a sequence of predictable times—the *almost periods*—P_{top} is the average topological pumping rate, $\hbar\omega$ is the cavity energy quantum, and $P_{\text{top}} T_N/\hbar\omega$ is an integer. The boosted state $|\psi(T_N)\rangle$ is a translation of the initial state in Fock space.

Boosting provides a technique to prepare highly excited nonclassical cavity states, such as Fock states. One need only boost a Fock state prepared at lower occupations. Highly excited nonclassical states serve as a resource for difficult, or even classically forbidden, tasks [52–63]. For instance, Fock states allow for extremely sensitive interferometry. Boosting thus serves as proof, by explicit example, that quasiperiodic driving allows for novel and useful forms of quantum control.

However, boosting is a slow process. It is robust only in the adiabatic limit of very slow driving [38, 64]. In the frequency lattice picture, this can be viewed as scattering of the pumping modes, resulting in non-pumping steady states. This can be overcome by employing more condensed matter machinery and intuition. Designing a one-dimensional model of quasiperiodically driven sites allows the construction of edge modes which pump energy nonadiabatically [4, 65].

This two-tone-driven chain belongs to a broader class of *anomalous localized topological phases* (ALTPs) [1]. Tight-binding models of localized fermions in d dimensions driven by D incommensurate frequencies may support nontrivial topological phases whenever $d + D$ is odd [4, 65, 66]. That the classification only depends on the sum $d+D$ can also be understood through the lens of the frequency lattice. The frequency lattice model in this case just a $(d + D)$-dimensional tight-binding model—the d spatial dimensions may be freely exchanged for *synthetic* dimensions associated to the drives without changing the mathematical description of the model.

The frequency lattice formalism lets us answer more conventional condensed matter questions too. Localization of fermions in one spatial dimension is believed to be stable to the intoduction of short-range interactions between the fermions [67–71] (though there has been recent debate around this claim [72–77]). The same arguments which indicate the stability of this *many-body localization* (MBL) may be adapted to the quasiperiodically driven setting through careful use of the frequency lattice [2, 78]. The conclusion in this case is that MBL continues to be stable with two-tone-driving, but not when driven by three tones or more.

Quasiperiodic driving offers an under-explored space for the construction of useful experimental protocols. The theoretical study of these systems is littered with questions. This dissertation will demonstrate some of the power of quasiperiodic driving for technological applications, and the power of the frequency lattice to tackle the associated theoretical puzzles.

Chapter 2

Background

2.1 Quasiperiodic Driving

The phenomena we describe in this dissertation may all be identified as novel effects in quantum dynamics. We seek to uncover the interesting and useful properties that quantum mechanical systems may exhibit when out of equilibrium—when evolving in time, as opposed to when they are in a static steady state.

There are many physical scenarios in which a system may exist out of equilibrium. After a sudden quench in the system parameters, such as temperature or pressure, systems take a finite time to relax from their initial state to the new equilibrium [79]. Some strongly disordered systems, those which exhibit Anderson localization or many-body localization, are believed to never relax to equilibrium at all [67–71].

Continuous or transient driving may also be used to push a system out of equilibrium [80–86]. As a basic example, by shining a laser on an atom it may be excited out of its ground state. The physics of a driven system can often be captured by introducing time dependence to the Hamiltonian which describes a system, $H(t)$. The evolution of the quantum state $|\psi(t)\rangle$ is then governed by the time-dependent Schrödinger equation (we set $\hbar = 1$),

$$i\partial_t \left|\psi(t)\right\rangle = H(t) \left|\psi(t)\right\rangle . \tag{2.1}$$

In adopting this formalism, we are assuming that the system of interest remains isolated, so that $|\psi(t)\rangle$ is always a pure state. If there can be back-action by the system on the drive, then the drive must also be treated as a dynamical degree of freedom.

It is frequently useful to describe evolution under Eq. (2.1) in terms of a unitary evolution operator $U(t, t')$ such that $U(t_1, t_0) \left|\psi(t_0)\right\rangle = \left|\psi(t_1)\right\rangle$. This operator also obeys the Schrödinger equation $i\partial_{t_1} U(t_1, t_1) = H(t_1)U(t_1, t_0)$, and is often expressed as the time ordered exponential

$$U(t_1, t_0) = \mathcal{T} \exp \left[-i \int_{t_0}^{t_1} H(s) \, \mathrm{d}s \right]. \tag{2.2}$$

This formal solution is typically not very useful. More useful expressions can be found when specific properties of $H(t)$ are assumed.

The most restrictive form of time dependence one can assume is that $H(t) = H$ is constant. Then $U(t_1, t_0) = \exp[-i(t_1 - t_0)H]$ is given by the usual matrix exponential. The time evolution of an arbitrary state $\left|\psi(t)\right\rangle$ can be found efficiently by decomposing $\left|\psi(0)\right\rangle$ in the eigenstates $\left|\phi_\alpha\right\rangle$ of H, each of which only accrue a phase $(t_1 - t_0)E_\alpha$. We can express this procedure mathematically by defining the rotation matrix $V = \sum_\alpha \left|\phi_\alpha\right\rangle\!\left\langle\alpha\right|$ which transforms some computational basis $\{\left|\alpha\right\rangle\}$ to the eigenbasis of H. Then we have the expression

$$U(t_1, t_0) = V e^{-i(t_1 - t_0)H_F} V^\dagger, \quad \text{where} \quad H_F = \sum_\alpha E_\alpha \left|\alpha\right\rangle\!\left\langle\alpha\right|. \tag{2.3}$$

This just expresses that U is diagonal in the same basis as H, with eigenvalues $e^{-i(t_1 - t_0)E_\alpha}$. In principle, Eq. (2.3) allows for the study of dynamics through a detailed understanding of the eigenstates and eigenvalues of H.

What of more general forms of time dependence? The dynamical effects which can occur with an arbitrary $H(t)$ must be richer than with a static Hamiltonian, but the prospect of making significant progress in understanding such dynamics seems poor. In this dissertation, we will restrict to Hamiltonians with *multi-tone* time dependence.

That is, where we can parameterize $H(t)$ in terms of D phase variables,

$$H(t) = H(\theta_1(t), \theta_2(t), \ldots, \theta_D(t)) = H(\vec{\theta}_t), \quad \vec{\theta}_t = \sum_j \theta_j(t)\hat{e}_j = \sum_j (\Omega_j t + \theta_{0j})\hat{e}_j, \tag{2.4}$$

such that $H(\vec{\theta})$ is periodic with respect to each phase

$$H(\vec{\theta}) = H(\vec{\theta} + 2\pi\hat{e}_j) \quad \text{for all } j \in \{1, \ldots, D\}. \tag{2.5}$$

For brevity of notation, we have assembled the phase variables into a vector $\vec{\theta}_t$. Similarly, the angular frequencies Ω_j may be assembled into $\vec{\Omega} = \sum_j \Omega_j \hat{e}_j$, so that

$$\vec{\theta}_t = \vec{\Omega} t + \vec{\theta}_0. \tag{2.6}$$

As the Hamiltonian is periodic in $\vec{\theta}$, the phase angles should be regarded as being defined on a torus; $\vec{\theta} \in \mathbb{T}^D = \mathbb{R}^D / 2\pi\mathbb{Z}^D$.

The multi-tone time dependence is called *quasiperiodic* or *incommensurate* if the frequencies $\vec{\Omega}$ share no rational dependencies—so that they share no common period. Mathematically, this condition is expressed as

$$\vec{n} \in \mathbb{Z}^D \text{ and } \vec{\Omega} \cdot \vec{n} = 0 \iff \vec{n} = 0. \tag{2.7}$$

A *Floquet-Bloch decomposition* for a quasiperiodic Hamiltonian generalizes the eigenstate decomposition of Eq. (2.3),

$$\begin{aligned} &U(t_1, t_0) = V(\vec{\theta}_{t_1}) e^{-i(t_1 - t_0)H_F} V(\vec{\theta}_{t_0})^\dagger, \\ &\qquad\qquad \text{where} \quad H_F = \sum_\alpha \epsilon_\alpha \, |\alpha\rangle\langle\alpha| \text{ and } V(\vec{\theta}) = \sum_\alpha |\phi_\alpha(\vec{\theta})\rangle\langle\alpha|. \end{aligned} \tag{2.8}$$

The special states $|\phi_\alpha(\vec{\theta})\rangle$ are known as *quasienergy states*, while ϵ_α is called its associated *quasienergy*. These are the analogues of the eigenstates and eigenvalues of

H in the static case. Indeed, the state $|\psi_\alpha(t)\rangle = e^{-i\epsilon_\alpha t}\,|\phi_\alpha(\vec{\theta}_t)\rangle$ solves the Schrödinger equation. The static operator H_F is called the *Floquet Hamiltonian*, while the unitary $V(\vec{\theta})$ is called the *micromotion operator*.

For the special case of $D = 1$, it has been known for centuries that such a decomposition always exists, a result known as *Floquet's theorem* [87]. Ref. [2] argued that the existence of such a decomposition is generic for $D = 2$, though finely-tuned counterexamples are known [38]. For high frequency driving perturbative expansions produce good approximations to Eq. (2.8) [10, 33, 88], but in general, we cannot always find such Floquet-Bloch decompositions in quasiperiodically driven systems.

The existence of a Floquet-Bloch decomposition implies powerful consequences. One immediate consequence is the quasiperiodic time dependence of local observables. This follows from the decomposition of an observable $O(t)$ in the Heisenberg picture in the basis of quasienergy states,

$$O(t) = \sum_{\alpha,\beta} O_{\alpha\beta}(\vec{\theta}_t) e^{-i(\epsilon_\beta - \epsilon_\alpha)t} |\phi_\alpha(\vec{\theta}_0)\rangle\langle\phi_\beta(\vec{\theta}_0)|, \tag{2.9}$$

where $O_{\alpha\beta}(\vec{\theta}_t) = \langle\phi_\alpha(\vec{\theta}_t)|\,O(0)\,|\phi_\beta(\vec{\theta}_t)\rangle$ is quasiperiodic. (We have assumed O does not have explicit time dependence.) Roughly, normalizability of $|\phi_\alpha(\vec{\theta}_t)\rangle$ implies that only finitely many of the terms $O_{\alpha\beta}(\vec{\theta}_t)$ contribute significantly to expectation values, so that $\langle O(t)\rangle$ is explicitly quasiperiodic. More precisely, the power spectrum of all local observables in a system with a Floquet-Bloch decomposition are pure point [16, 17].

The existence of a Floquet-Bloch decomposition will also frequently let us apply notions of *topology*, and discover robust effects in quasiperiodically driven quantum systems.

2.2 The Frequency Lattice

To study the long-time dynamics of a quasiperiodically driven system, we wish to find the quasienergies and quasienergy states. For periodically driven systems, this can be done by diagonalizing the *Floquet operator* $U(T, 0)$, which describes evolution over one period. However, no analogous procedure exists for multi-tone driving. Instead, we use a powerful construction known as the *frequency lattice* [13, 30, 36–38].

The frequency lattice provides a formal mapping between a tight-binding model in d dimensions driven by D incommensurate tones and a static system with an additional D *synthetic dimensions*. We first review the construction for the case of a single periodic drive ($D = 1$) and recover the results of Floquet theory. We then make a straightforward generalization to the multiple-tone case.

2.2.1 One Drive—Floquet Theory

When the driving is periodic, $H(t + T) = H(t) = H(\theta_t)$, Floquet's theorem states that a Floquet-Bloch decomposition always exists. In more detail, it is possible to identify a complete set of solutions to the Schrödinger equation of the form

$$|\psi_\alpha(t)\rangle = e^{-i\epsilon_\alpha t} |\phi_\alpha(t)\rangle \tag{2.10}$$

where $|\phi_\alpha(t + T)\rangle = |\phi_\alpha(t)\rangle$ is periodic and α indexes a basis of the Hilbert space. Due to the formal similarity to the evolution static eigenstates, ϵ_α is called the quasienergy and $|\phi_\alpha(t)\rangle$ is called the quasienergy state.

The decomposition of the solutions (2.10) implies the corresponding decomposition of the evolution operator

$$U(t_1, t_0) = V(t_1) e^{-i(t_1 - t_0) H_F} V^\dagger(t_0), \tag{2.11}$$

where $H_F = \sum_\alpha \epsilon_\alpha |\alpha\rangle\langle\alpha|$ is called the Floquet Hamiltonian, the micromotion $V(t) =$

$\sum_\alpha |\phi_\alpha(t)\rangle\langle\alpha|$ is also periodic and $|\alpha\rangle$ is an arbitrary fixed basis for the system's Hilbert space. We will prove the same result using the frequency lattice.

Before we do so, it is important to note that there is a gauge freedom in this decomposition; as $e^{in\Omega t}$ for $n \in \mathbb{Z}$ and $\Omega = 2\pi/T$ is itself periodic with period T, the form of the Floquet decomposition is preserved by the map

$$\epsilon_\alpha \mapsto \epsilon_\alpha + n_\alpha\Omega, \quad |\phi_\alpha(t)\rangle \mapsto e^{in_\alpha\Omega t}\,|\phi_\alpha(t)\rangle\,. \tag{2.12}$$

The quasienergy can be shifted by an integer multiple of Ω without affecting the actual solution (2.10), provided a gauge transformation is made to the quasienergy state $|\phi_\alpha(t)\rangle$. As such, the quasienergy should be regarded as being defined modulo Ω. This is the origin of the distinct topology possible in the structure of Floquet systems when compared to static systems [9, 89, 90].

Floquet's theorem can be proved using elementary techniques in linear ordinary differential equations, but these techniques are not easily transferable to the quasiperiodic case. We will now describe how the time dependent Floquet problem can be understood as a static lattice problem with one synthetic dimension—the frequency lattice—and how this interpretation naturally leads to Floquet's theorem.

By Fourier transforming the Schrödinger equation we can map (2.1) into a lattice problem in frequency space. That is, if we write $H(t) = H(\theta_t)$ with $\theta_t = \Omega t + \theta_0$ defined modulo 2π, then we can express H in terms of its Fourier series as

$$H(\theta) = \sum_{m\in\mathbb{Z}} H_m e^{-im\theta}. \tag{2.13}$$

Similarly writing $|\phi_\alpha(\theta_t)\rangle = \sum_{m\in\mathbb{Z}} |\phi_{\alpha m}(\theta_0)\rangle\, e^{-im\theta_t}$, the Schrödinger equation becomes

$$\epsilon_\alpha\,|\phi_{\alpha n}(\theta_0)\rangle = \sum_{m\in\mathbb{Z}} \left(H_{n-m}e^{-i(n-m)\theta_0} - n\Omega\delta_{nm}\right)|\phi_{\alpha m}(\theta_0)\rangle\,. \tag{2.14}$$

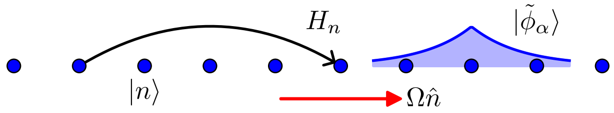

Figure 2·1: *Frequency lattice for periodic driving.*—The problem of finding quasienergy states in a periodically driven (Floquet) system can be mapped onto a static frequency lattice problem with one synthetic dimension, with sites labeled by $|n\rangle$. The lattice Hamiltonian—the quasienergy operator $K(\theta_0)$—has a linear potential $-n\Omega$, as might arise from an electric field $\Omega\hat{n}$, and hopping matrices given by the Fourier components H_m of $H(\theta)$. Floquet's theorem follows from the localization of the frequency lattice eigenstates $|\tilde{\phi}_\alpha\rangle$, which can be seen as a consequence of Stark localization by $\Omega\hat{n}$.

This is the form of a tight-binding model on a one-dimensional lattice with sites labeled by n, and a local Hilbert space given by that of the original system. Indeed, defining an auxiliary Hilbert space spanned by $|n\rangle$, and defining

$$|\tilde{\phi}_\alpha(\theta_0)\rangle = \sum_{n\in\mathbb{Z}} |\phi_{\alpha m}(\theta_0)\rangle \otimes |n\rangle \,, \tag{2.15}$$

$$K(\theta_0) = \sum_{n,m\in\mathbb{Z}} \left(H_{n-m}e^{-i(n-m)\theta_0} - n\Omega\delta_{nm}\right) \otimes |n\rangle\langle m|, \tag{2.16}$$

then (2.14) becomes an eigenvalue equation for the *quasienergy operator* $K(\theta_0)$, which has the form of a lattice Hamiltonian (Fig. 2·1).

We have kept the dependence of $|\phi_{\alpha n}(\theta_0)\rangle$ and $K(\theta_0)$ on the initial phase (equivalently initial time) explicit, though we have not written it for ϵ_α. Indeed, inspecting (2.16) shows that the initial phase θ_0 enters the quasienergy operator like a constant vector potential. This is a pure gauge term, unless our synthetic lattice has non-contractible loops, which it does not. Thus the quasienergies ϵ_α can't depend on initial phase. The dependence of the quasienergy states $|\tilde{\phi}_\alpha(\theta_0)\rangle$ on θ_0 only encodes the choice of the origin of time in the temporal domain.

The other terms in $K(\theta_0)$ also admit translation into the language of a tight-binding model. The Fourier amplitudes H_m are mth nearest-neighbor hopping terms, and when $H(t)$ is smooth in the sense that its Fourier components H_m decay exponentially $\|H_m\| \lesssim e^{-\kappa m}$ (κ being a positive dimensionless constant), then the lattice model defined by K is also quasilocal. The term $\sum_n -n\Omega|n\rangle\langle n|$ is an on-site potential of constant gradient $-\Omega\hat{n}$. This gives $\Omega\hat{n}$ a natural interpretation as an electric field (in units where $\hbar = e = 1$). This geometry is shown in Fig. 2·1.

The presence of the electric field $\Omega\hat{n}$ implies that the eigenstates of K must be exponentially localized by Stark localization [91]. The eigenstates have a particular energy, and so can only have very small tails on sites with very far detuned energies. Thus, their Fourier transforms $|\phi_\alpha(\theta)\rangle$ are well defined and smooth as functions of θ. This is the proof of the existence of the quasienergy states via the frequency lattice—that is, Floquet's theorem.

While this is a less elementary than possible proof of Floquet's theorem, the frequency lattice construction has been used in Floquet theory many times before. For instance, various high-frequency expansions for the Floquet Hamiltonian and quasienergy states can be obtained through conventional perturbation theory in the frequency lattice [88].

One may be concerned that we have introduced many more degrees of freedom in our problem than are physical. For example, for a driven qudit with only N states, K certainly has many more eigenstates than N. These extra quasienergy states are a result of the gauge invariance (2.12); the eigenstates of K fall into N classes related by translation in the frequency lattice (multiplication by $e^{in\Omega t}$ in the time domain) and a shift in quasienergy due to the change in potential from the electric field $\Omega\hat{n}$. This is exactly the transformation (2.12). In the frequency lattice language, the eigenstates of K form a Stark ladder, and the gauge freedom relates states on different rungs of the ladder.

We will see in the next section that the frequency lattice picture can be adapted to the case of driving by multiple tones. This picture will allow us to import our intuition and known results about static lattice problems to quasiperiodically driven tight-binding models.

2.2.2 The Frequency Lattice For Multiple Tones

In the multi-tone case, the Hamiltonian is not necessarily periodic, but has the structure

$$H(t) = H(\vec{\theta}_t) = H(\vec{\Omega}t + \vec{\theta}_0) \tag{2.17}$$

where the phase angles $\vec{\theta}_t$ should be considered to be defined on a torus; $\vec{\theta} \in \mathbb{T}^D = \mathbb{R}^D/2\pi\mathbb{Z}^D$.

When the frequencies $\vec{\Omega}$ are incommensurate in the sense that $\vec{n}\cdot\vec{\Omega} = 0$ only when $\vec{n} = 0$ for $\vec{n} \in \mathbb{Z}^D$, then Floquet's theorem does not apply. However, we can still make use of the frequency lattice to understand the structure of the solutions to the Schrödinger equation.

To find a Floquet decomposition in analogy to (2.10), we are seeking solutions to the Schrödinger equation of the form

$$|\psi_\alpha(t;\vec{\theta}_0)\rangle = e^{-i\epsilon_\alpha(\vec{\theta}_0)}\,|\phi_\alpha(\vec{\theta}_t)\rangle\,, \tag{2.18}$$

where we have kept the dependence $\epsilon_\alpha(\vec{\theta}_0)$ for now in order to treat commensurate and incommensurate drives within the same formalism. Fourier transforming the Schrödinger equation with respect to time gives a D-dimensional lattice model

$$\epsilon_\alpha(\vec{\theta}_0)\,|\tilde{\phi}_\alpha(\vec{\theta}_0)\rangle = K(\vec{\theta}_0)\,|\tilde{\phi}_\alpha(\vec{\theta}_0)\rangle \tag{2.19}$$

where

$$|\tilde{\phi}_\alpha(\vec{\theta}_0)\rangle = \sum_{\vec{n}} |\phi_{\alpha\vec{n}}(\vec{\theta}_0)\rangle \otimes |\vec{n}\rangle \, , \tag{2.20}$$

$$K(\vec{\theta}_0) = \sum_{\vec{n},\vec{m}} \left(H_{\vec{n}-\vec{m}} e^{-i(\vec{n}-\vec{m})\cdot\vec{\theta}_0} - \vec{n}\cdot\vec{\Omega}\delta_{\vec{n}\vec{m}} \right) \otimes |\vec{n}\rangle\langle\vec{m}|, \tag{2.21}$$

and $H_{\vec{n}}$ ($|\phi_{\alpha\vec{n}}(\vec{\theta}_0)\rangle$) labels the Fourier components of $H(\vec{\theta})$ ($|\phi_\alpha(\vec{\theta})\rangle$) as before.

If the frequencies are incommensurate, then the frequency lattice again has no non-trivial loops, and the vector potential $\vec{\theta}_0$ is again purely a gauge choice which does not affect the spectrum of $K(\vec{\theta}_0)$. Once more, the only effect of initial phase $\vec{\theta}_0$ on $|\tilde{\phi}_\alpha(\vec{\theta}_0)\rangle$ in the incommensurate case is to encode the origin of time.

The rest of the structure of K is essentially the same as the Floquet case. The Fourier amplitudes $H_{\vec{m}}$ appear as hopping amplitudes along the vector $\vec{m}$, and the smoothness of $H(\vec{\theta})$ translates into the hopping being quasilocal. The driving frequencies $\vec{\Omega}$ appear as an electric field, and thus imply that the quasienergy states $|\tilde{\phi}_\alpha(\vec{\theta}_0)\rangle$ are Stark localized along the $\vec{\Omega}$ direction whenever $|\vec{\Omega}| > 0$ (Fig. 2·2(a)). Unlike the periodic case, this Stark localization is not sufficient to conclude that the time domain states $|\phi_\alpha(\vec{\theta}_t)\rangle$ are well defined. The frequency lattice states may be delocalized along other directions in the frequency lattice, preventing their Fourier series from converging to a continuous function. At a technical level, it is the convergence or non-convergence of this Fourier series which determines whether we can find a Floquet decomposition (2.18) for the quasiperiodically driven system.

A similar gauge freedom to the periodic case appears here, as it must for this prescription to make any sense; otherwise we would have many more solutions to the Schrödinger equation than there are states in the system's Hilbert space. Just as in the periodic case, any eigenstates of K may be translated by $-\vec{n}$ to obtain a new eigenstate of K with an energy shifted by $\vec{n}\cdot\vec{\Omega}$ due to the change of its position in

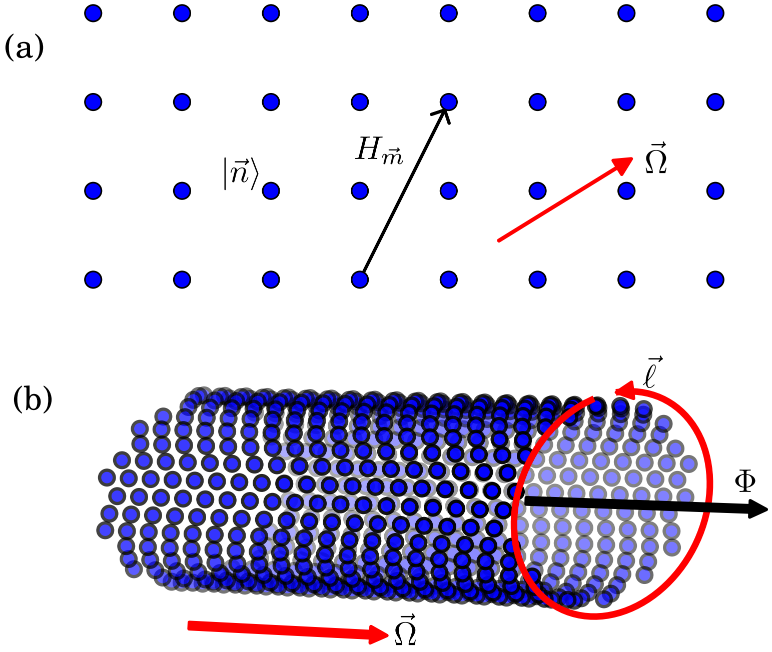

Figure 2·2: *Frequency lattice for D tones.*—**(a)** The quasienergy states of (2.18) can be identified from the eigenstates of a quasienergy operator K (2.21) in a frequency lattice with D synthetic dimensions (illustrated for $D = 2$), with sites labeled by $|\vec{n}\rangle$. K consists of hopping matrices $H_{\vec{m}}$ between sites separated by $\vec{m}$ and an electric field $\vec{\Omega}$. **(b)** When $\vec{\Omega}$ is commensurate, so that $\vec{\ell}_j \cdot \vec{\Omega} = 0$ for some integer $\vec{\ell}_j \neq 0$, the frequency lattice compactifies into a cylinder with circumference $\vec{\ell}_j$. In addition to the hopping matrices and electric field of the incommensurate case, there is now a flux $\Phi_j = \vec{\ell}_j \cdot \vec{\theta}_0$ proportional to the initial phase of the drives which threads the cylinder.

the electric potential. In the time domain, this corresponds to the transformation

$$\epsilon_\alpha \mapsto \epsilon_\alpha + \vec{n}\cdot\vec{\Omega}, \quad |\phi_\alpha(\vec{\theta})\rangle \mapsto e^{i\vec{n}\cdot\vec{\theta}}\,|\phi_\alpha(\vec{\theta})\rangle\,, \tag{2.22}$$

which only introduces a static phase to the actual solution $|\psi_\alpha(t)\rangle$. Thus, the quasienergy should be regarded as being defined only modulo $\mathbb{Z}^D \cdot \vec{\Omega}$. In the quasiperiodic case the set $\mathbb{Z}^D \cdot \vec{\Omega}$ is dense in the real line, making the actual value of the quasienergy rarely useful.

The frequency lattice helps us to unpack and separate this gauge freedom. In later chapters we will use α to index the driven system's Hilbert space and γ to index the expanded frequency lattice Hilbert space. Equivalently, α may index equivalence classes of $|\tilde{\phi}_\gamma\rangle$ under the gauge transformation (2.22). We must keep in mind that most of the degrees of freedom γ in the lattice problem are only calculational tools, and shouldn't affect any prediction we make about the time domain.

There is a subtlety in the case of *commensurate* drives that is absent in (2.16). If the frequencies $\vec{\Omega}$ are rationally dependent (commensurate), so that there is some $\vec{\ell} \in \mathbb{Z}^D$ such that $\vec{\ell}\cdot\vec{\Omega} = 0$, then the time-domain frequencies $\vec{n}\cdot\vec{\Omega}$ and $(\vec{n}+\vec{\ell})\cdot\vec{\Omega}$ are the same, and should not be regarded as distinct in the frequency lattice. Thus, rational dependencies $\vec{\ell}_j \neq 0$ between the frequencies $\vec{\Omega}$ compactify the full frequency lattice from $\mathbb{Z}^D$ to a cylinder with closed non-contractible loops given by $\vec{\ell}_j$ (Fig. 2·2(b)).

In this case one must keep the explicit dependence of $\epsilon_\alpha(\vec{\theta}_0)$ on initial phase. As in the periodic case, the initial phase appears in $K(\vec{\theta}_0)$ as a constant vector potential. However, due to the presence of these non-contractible loops in the frequency lattice, this *can* affect the spectrum through the presence of the physically measurable fluxes

$$\Phi_j = \vec{\ell}_j \cdot \vec{\theta}_0. \tag{2.23}$$

It would then be more correct to write $\epsilon_\alpha(\vec{\theta}_0) = \epsilon(\vec{\Phi})$. In particular, $\epsilon_\alpha(\vec{\theta}_0) = \epsilon_\alpha(\vec{\Omega}t +$

$\vec{\theta}_0$) is still constant along trajectories in the phase torus.

The quasienergy then forms *bands*, again in complete analogy to non-interacting solid-state systems. The fluxes Φ_j parameterize some dependence of the quasienergies $\epsilon_\alpha(\vec{\Phi})$ on the initial relative phase. Many of the usual ideas of band theory will find application in this setting, but will not be relevant to the incommensurate driving we focus on in this dissertation.

Chapter 3

Boosting

Non-classical states of cavity and circuit QED systems [92–95] serve as a resource for difficult, or even classically forbidden, tasks [52–63]. However, preparing these states is itself difficult, as it requires strong nonlinearity [93, 95]. In this chapter, we present an experimentally feasible scheme for the on-demand preparation of highly excited non-classical states, such as Fock and Schrödinger cat states. The scheme exploits topological energy pumping—the quantized pumping of energy into a cavity by a strongly-coupled periodically-driven spin [1, 37, 38, 51]—which acts to coherently translate, or *boost*, a quantum state of the cavity in the Fock basis.

In Sec. 3.1 we describe the boosting at a phenomenological level. We proceed to give a transparent explanation of why and how boosting works by appealing to a frequency lattice picture in Sec. 3.2. In this case, the frequency lattice does not provide significant quantitative insight, and it is more convenient to make detailed analysis in the time domain (Sec. 3.3). Sec. 3.4 describes, in broad terms, how boosting may be achieved in current experiments. Remaining sections contain additional details of our calculations, and we conclude in Sec. 3.8.

3.1 Phenomenology

Boosting occurs in the strong-coupling regime of cavity and circuit QED. The model systems of interest in this case are of qubits (two-level quantum systems) coupled to single-mode bosonic cavities. By engineering an appropriate slow periodic drive on the qubit, the cavity state may be indirectly manipulated.

In particular, we consider a Floquet Jaynes-Cummings model with a periodically driven spin,

$$H(t) = \hbar\omega\hat{n} - \mu\vec{B}_c(\theta_1(t)) \cdot \vec{S} + \frac{\mu B_0}{2}(\hat{a}S^+ + \hat{a}^\dagger S^-). \tag{3.1}$$

Here, μ is the spin magnetic moment, B_0 is a coupling strength between the cavity and spin, $\hat{a}^{(\dagger)}$ are cavity annihilation (creation) operators, and $S^\pm$ are spin raising (lowering) operators. The spin is driven by a circularly polarized classical field with frequency Ω:

$$\vec{B}_c(\theta_1) = (B_m - B_d \sin\theta_1)\hat{\mathbf{x}} + B_d \cos\theta_1 \hat{\mathbf{z}}. \tag{3.2}$$

Later, we will show how this model may be achieved within a rotating frame of a typical cavity or circuit QED Hamiltonian.

Energy pumping (also called frequency conversion) is well understood in the semi-classical regime, when the cavity is in a coherent state [28, 37, 38, 48, 51, 64]. The spin experiences two strong periodically oscillating fields (Fig. 3·1(a))—one from the external drive with phase variable $\theta_1(t) = \Omega t + \theta_{01}$, and an effective field from the cavity with phase $\theta_2(t) = \omega t + \theta_{02}$. The spin follows this magnetic field adiabatically, and in so doing winds around the Bloch sphere. If the frequency ratio $\Omega/\omega \notin \mathbb{Q}$ is irrational, and the motion of the spin covers the Bloch sphere with Chern number $C \in \mathbb{Z}$, then the spin mediates a quantized *average* number current into (or out of) the cavity,

$$[\dot{n}]_t = \frac{\Omega}{2\pi}C. \tag{3.3}$$

We use square brackets $[\cdot]_x$ to denote averages over the variable x, which in Eq. (3.3) is time.

The instantaneous number current, $\dot{n}(t)$, is *not* quantized. It may vary substantially within the periods $2\pi/\Omega$ and $2\pi/\omega$. Thus, it is remarkable that there are special times—the *almost periods* $T_N = (2\pi/\Omega)h_N$ (where h_N is an integer)—at which the number of photons pumped into the cavity is almost exactly given by $[\dot{n}]_t T_N = Ch_N$,

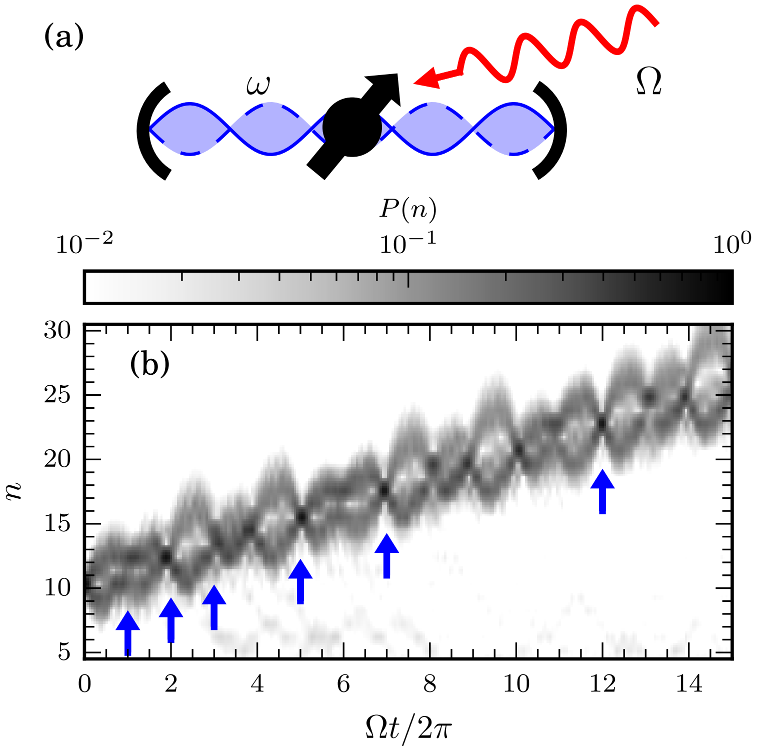

Figure 3·1: (**a**) *Model.*—A spin coupled to a quantum cavity with frequency ω and subject to an external periodic drive of frequency Ω, such that $\Omega/\omega \notin \mathbb{Q}$. The frequencies $\hbar\omega$ and $\hbar\Omega$ are smaller than all other energy scales in the problem. (**b**) *Cavity state boosting in a Fock state.*—A plot of the Fock state occupation $P(n) = \langle n| \rho_{\text{cav}}(t) |n\rangle$, where $\rho_{\text{cav}}(t)$ is the reduced density matrix of the cavity, shows *rephasings*, marked by blue arrows. These represent the cavity state becoming near-Fock with a larger occupation number than the initial state. *Parameters in model* (3.1)*:* $\Omega/\omega = (1+\sqrt{5})/2$, $\mu B_m/\hbar\omega = \mu B_d/\hbar\omega = 6$, $\mu B_0/\hbar\omega = 1.5$, $\theta_{01} = 3\pi/2$, initial state $|\psi_0\rangle = |+\rangle_{\hat{\mathbf{x}}} |n_0\rangle$ being a product of $|+\rangle_{\hat{\mathbf{x}}}$ (the $+S$ eigenstate of S_x), and $|n_0\rangle$ (a Fock state) with $n_0 = 10$, and spin $S = 1/2$ (that is, a two-level system).

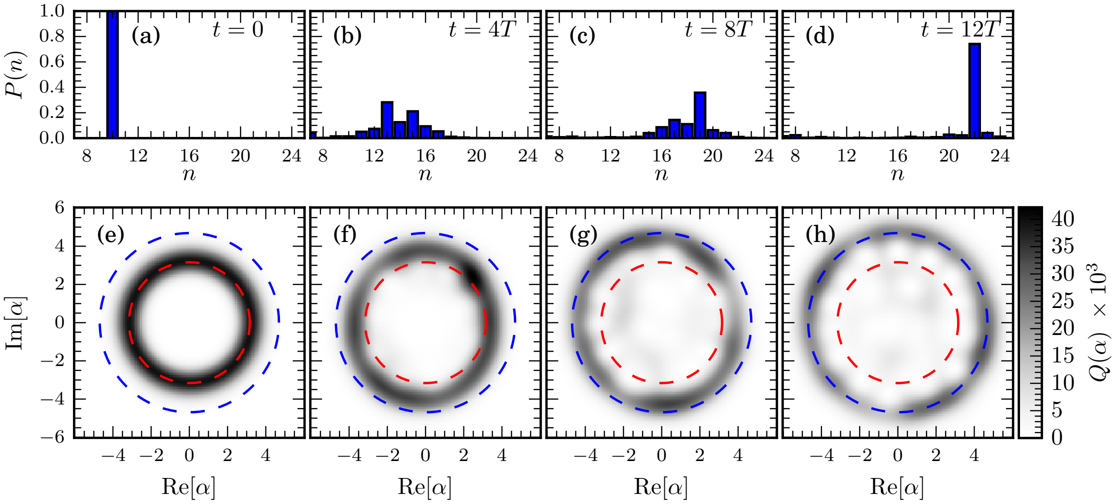

Figure 3·2: *Boosting snapshots.*—(**a-d**) The photon number distribution $P(n) = \langle n| \rho_{\text{cav}}(t) |n\rangle$ in Fig. 3·1 at multiples of the period of the classical drive $T = 2\pi/\Omega$. The distribution broadens from the initial Fock state (**a**), but narrows again at special times to produce a near-Fock state again (**d**). (**e-h**) The Husimi Q-function $Q(\alpha) = \frac{1}{\pi} \langle \alpha| \rho_{\text{cav}}(t) |\alpha\rangle$. Initially (**e**) the cavity is in a Fock state, with a circularly symmetric Q-function. At most times (**f**, **g**), the Q-function is displaced from the center of the quadrature plane, and is not circular. At special times (**h**) the Q-function is again centered and approximately circularly symmetric about the origin, but now with a larger radius. The initial radius ($n = 10$, red) and predicted final radius ($n = 22$, blue) are marked by dashed circles for reference. *Parameters:* as in Fig. 3·1.

regardless of the initial phase of the drive and cavity field. At these times $\theta_1(t)$, $\theta_2(t)$, and the spin state all return close to their initial values, with a deviation decreasing like $1/h_N$. Thus, an ensemble of spin-cavity states will *rephase* to form a boosted ensemble with a larger n at the times T_N. This is the semiclassical mechanism underlying cavity state boosting.

Strikingly, the boosting effect persists into the quantum regime of the cavity, and also applies to non-classical initial states. By decomposing the initial non-classical state into a superposition of coherent states, we relate boosting in the quantum system to the corresponding semiclassical effect. An initial product state of the spin and cavity

$$|\psi(0)\rangle = |s\rangle \otimes \sum_n c_n |n\rangle \tag{3.4}$$

is, if the spin state is initialized correctly and the distribution of $|c_n|^2$ is sufficiently narrow, boosted to

$$|\psi(T_N)\rangle \approx |s\rangle \otimes \sum_n c_n |n + Ch_N\rangle . \tag{3.5}$$

Fig. 3·1(b) shows that an initial Fock state presents the boosting phenomenon. At the almost periods, the cavity's n distribution $P(n) = \langle n| \rho_{\text{cav}}(t) |n\rangle$ narrows substantially (where $\rho_{\text{cav}}(t)$ is the reduced density matrix of the cavity). The cavity state has been boosted to an approximate Fock state with a larger occupation number (Fig. 3·2). By decoupling the spin at one of these almost periods, the boosted state can be preserved in the cavity.

More generally, highly-excited non-classical cavity states (Fock states, Schrödinger cat states, etc.) may be prepared by boosting states from lower occupations.

3.2 Frequency Lattice Explanation

The average energy pumping rate (3.3) depends on a Chern number describing the qubit motion—a topological invariant characterising how many times the qubit state wraps around the Bloch sphere throughout its evolution. A more familiar example from condensed matter physics where the Chern number of a state determines observable properties is the quantum Hall effect, where the Chern number fixes the transverse conductivity. That is, it fixes the rate of charge transfer.

Topological energy pumping is closely related to the quantum Hall effect. Indeed, energy pumping is essentially the quantum Hall effect in the frequency lattice. The fixed rate of charge transfer in the quantum Hall effect becomes a fixed rate of energy transfer in the frequency lattice.

We can write the model (3.1) as a tight-binding model in Fock space by treating Fock states as "lattice sites" between which a single particle is hopping. The synthetic dimension of the frequency lattice gives a second dimension. Denoting the cavity Fock states by $|n\rangle$, the synthetic frequency lattice sates as $|m\rangle$ and using $\vec{n} = n\hat{e}_1 + m\hat{e}_2$, the quasienergy operator is written[1]

$$K = \sum_{\vec{n},\vec{m}} (H_{\vec{n},\vec{m}} + \vec{n} \cdot \hbar\vec{\Omega}\delta_{\vec{n}\vec{m}})|\vec{n}\rangle\langle\vec{m}|, \tag{3.6}$$

where $\vec{\Omega} = \omega\hat{e}_1 + \Omega\hat{e}_2$ and

$$H_{\vec{n},\vec{m}} = \begin{cases} -\mu B_m S_x & \text{for } \vec{n} = \vec{m}, \\ -\mu\frac{B_d}{2}(S_z + iS_x) & \text{for } \vec{n} = \vec{m} + \hat{e}_2, \\ \mu\frac{B_0}{2}\sqrt{n}S^+ & \text{for } \vec{n} = \vec{m} - \hat{e}_1 \text{ and } \vec{n}\cdot\hat{e}_1 = n. \end{cases} \tag{3.7}$$

In the large n limit, with $B_0\sqrt{n} = O(1)$, this model becomes n independent, except for the linear potential. In fact, the limit model is the famous BHZ model, which for certain choices of parameters is a Chern insulator [37, 38, 51, 96, 97].

We have a Hamiltonian with a Chern number in the presence of a weak electric field. This is precisely the regime where we should have an anomalous quantum Hall effect. If we prepare a wavepacket in the lower band—that is, a state which has support on only a few Fock states and for which the spin state is aligned to the field it experiences—then the wavepacket will be transported perpendicular to the electric field. Further, the average velocity of the wavepacket is proportional to the Chern number of the lower band. As the wavepacket moves in the $\vec{\Omega}_\perp = \Omega\hat{e}_1 - \omega\hat{e}_2$ direction (say), it is increasing in cavity occupation, while the classical drive is decreasing in occupation. Photons are being moved from the classical drive to the cavity. This is the topological energy pumping effect.

---

[1] The sign of the potential here is opposite to chapter 2, which corresponds to a $+i$ in the definition of the Fourier transform, rather than a $-i$. This choice has been made so that the synthetic electric potential has the same sign as the cavity energy.

The other crucial element of boosting is the rephasings exhibited by initial non-classical states. This feature can also be understood through an analogy to solid state physics. Indeed, it is a manifestation of *Bloch oscillations*. Electronic wavepackets in an electric field show center-of-mass oscillations. If the initial wavepacket is very well-localized (as a Fock state is) it should be viewed as a superposition of many wavepackets, each of which has center of mass oscillations. This results in an initial broadening of the wavepacket. However, the dynamics are coherent, so the component packets subsequently rephase and the whole wavepacket contract back into its initial shape [98]. If the packet also has a non-zero Hall velocity, then at Bloch periods it has the same shape, but is translated perpendicular to the electric field—that is, it has been boosted.

3.3 Boosting in the time domain

While the frequency lattice gives a straightforward relation between boosting and well known solid state phenomena, it is not convenient for the quantitative study of the boosting effect. This is because the quasienergy states for a system which exhibits topological energy pumping are delocalized in the frequency lattice—as they must be to carry a current. The frequency lattice is most powerful when the quasienergy states are localized (equivalently, when a Floquet-Bloch decomposition exists).

To make quantitative predictions regarding boosting, we instead choose to work in the time domain.

A semiclassical description suffices to study boosting. The semiclassical model related to Eq. (3.1) is obtained by taking the expectation value of H in a cavity coherent state $|\alpha\rangle = |\sqrt{n}e^{-i\theta_2}\rangle$, giving an effective model for the spin alone

$$H_{\text{eff}}(\theta_1, \theta_2, n) = \langle\alpha| H |\alpha\rangle - \hbar\omega n = -\mu \vec{B}_{\text{eff}} \cdot \vec{S}, \tag{3.8}$$

where

$$\vec{B}_{\text{eff}}(\theta_1, \theta_2, n) = (B_m - B_d \sin\theta_1 - B_0\sqrt{n}\cos\theta_2)\hat{\mathbf{x}} - B_0\sqrt{n}\sin\theta_2\hat{\mathbf{y}} + B_d\cos\theta_1\hat{\mathbf{z}} \tag{3.9}$$

is related to the BHZ model [96, 97]. For now, we assume that the motion of the cavity is unaffected by the spin, so that the phase variable arising from the cavity field $\theta_2(t) = \omega t + \theta_{02}$ rotates at a constant angular velocity. This occurs in the limit $n \to \infty$ with $B_0\sqrt{n} = O(1)$.

The spin model (3.8) has been shown to exhibit energy pumping in the adiabatic limit, where $\hbar\Omega$ and $\hbar\omega$ are much less than all other energy scales in the problem [37]. Energy pumping proceeds with $C = \pm 1$ if the spin is initially aligned with the field, $\Omega/\omega \notin \mathbb{Q}$ is irrational, and $(|B_m| - |B_d|)^2 < B_0^2 n < (|B_m| + |B_d|)^2$ [51].

In this regime, the spin follows the effective field, $\langle\vec{S}\rangle = S\hat{B}_{\text{eff}} + O(\Omega)$. Importantly, the spin state only depends on the instantaneous values of θ_1, θ_2, and n. Explicitly calculating the instantaneous rate of change of n using $\hbar\dot{n} = -\langle\partial_{\theta_2} H_{\text{eff}}\rangle$ gives [64]

$$\hbar\dot{n}(\theta_1, \theta_2, n) = \mu S \partial_{\theta_2}|\vec{B}_{\text{eff}}| + \hbar\Omega F + O(\Omega^2), \tag{3.10}$$

where

$$F = S\hat{B}_{\text{eff}} \cdot (\partial_{\theta_1}\hat{B}_{\text{eff}} \times \partial_{\theta_2}\hat{B}_{\text{eff}}), \tag{3.11}$$

is the Berry curvature of the spin state aligned to the field $\vec{B}_{\text{eff}}$ [99]. The integral of F over the torus is $2\pi C$, where C is the Chern number.

We neglect the effect of the changing cavity population n on the spin dynamics, and so fix $n = n_0$ in the right hand side of Eq. (3.10). This is justified if the right hand side of Eq. (3.10) changes slowly with n. Then the change in cavity population

$$\Delta n(t, \vec{\theta}_0, n_0) = \int_0^t \dot{n}(\vec{\theta}_s, n_0)\mathrm{d}s \tag{3.12}$$

is computed as the integral of a quasiperiodic function over the trajectory $\vec{\theta}_t = (\theta_1(t), \theta_2(t))$ on the torus. As Ω/ω is irrational, this trajectory densely fills the torus as $t \to \infty$, and the integral (3.12) approximates the uniform integral of $\dot{n}$ over the torus. At the *almost periods*, T_N, the trajectory comes close to its initial position ($\vec{\theta}_{T_N} \approx \vec{\theta}_0$), and Eq. (3.12) approximates the uniform integral, the Chern number, especially well:

$$\begin{aligned}\Delta n(T_N, \vec{\theta}_0, n_0) &= \frac{T_N}{(2\pi)^2}\int \dot{n}(\vec{\theta}, n_0)\mathrm{d}^2\theta + O(T_N^{-1}) \\ &= \frac{\Omega T_N}{2\pi}C + O(T_N^{-1}).\end{aligned} \tag{3.13}$$

These almost periods may be computed from the continued fraction expansion of Ω/ω [100] (Sec. 3.5).

Crucially, Eq. (3.13) implies that $\Delta n(T_N)$ is only $O(T_N^{-1})$ different between trajectories with different initial conditions $\vec{\theta}_0$. An ensemble of spins initiated in coherent cavity states with different θ_{02} will each pump the same number of photons into the cavity at the almost periods, with a correction which decays as larger almost periods are considered (Fig. 3·3). We say the ensemble *rephases*.

In contrast, if $\Omega/\omega = p/q \in \mathbb{Q}$ are rationally related [37, 50], then trajectories do not densely fill the torus, and the long-time averages $[\dot{n}]_t$ depend on $\vec{\theta}_0$, so that

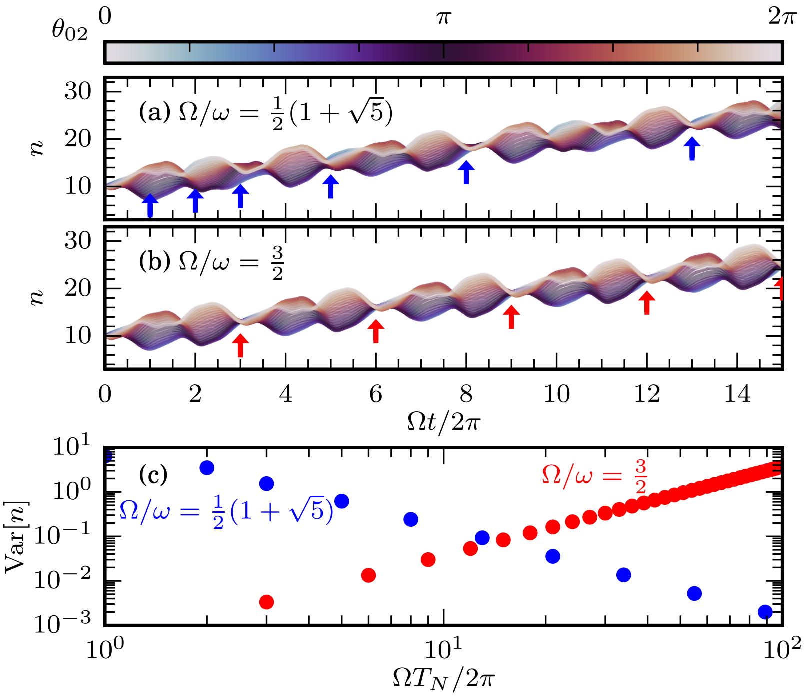

Figure 3·3: *Semiclassical rephasings.*—The prediction for the Fock occupation number $n(t)$ (3.12) for an ensemble of initial phases $\vec{\theta}_0$ and a (**a**) quasiperiodic and (**b**) periodic drive. Both show rephasings at their almost periods and periods respectively. (**c**) Inspecting the variance of $n(t)$ between $N_\theta = 32$ different values of θ_{02} shows that the rephasings improve in quality with increasing T_N for quasiperiodic drives, but decay linearly for periodic drives.

rephasings at subsequent periods $T_N = N(2\pi/\Omega)p$ decay in quality linearly with T_N.

The rephasing of the classical ensemble of states initiated with different θ_{02} can be used to explain cavity state boosting in the full quantum model (3.1). An arbitrary initial state $|\psi(0)\rangle$ of the spin and cavity can be decomposed into a superposition of coherent states $|\alpha\rangle = |\sqrt{n}e^{-i\theta_2}\rangle$ and spin states $|m\rangle_{\hat{B}_{\text{eff}}}$ ($m \in \{-S, \ldots, S\}$) quantized along the axis $\hat{B}_{\text{eff}}$ defined by n and θ_2. For the simplest case of a spin-$\frac{1}{2}$, we have

$$|\psi(0)\rangle = \int \mathrm{d}^2\alpha \, \left[c_+(\alpha)\,|+\rangle_{\hat{B}_{\text{eff}}} + c_-(\alpha)\,|-\rangle_{\hat{B}_{\text{eff}}}\right]|\alpha\rangle \,, \tag{3.14}$$

where $\mathrm{d}^2\alpha$ is a normalized measure on the coherent states[2]. When $c_- \approx 0$, the initial state is approximately a superposition of states where the spin is aligned with an effective field $\vec{B}_{\text{eff}}$. The dynamics of each component of this superposition can then be described semiclassically. The requirement $c_- \approx 0$ is typically unrestrictive, and for the model (3.1) an initial product state $|\psi(0)\rangle = |+\rangle_{\hat{\mathbf{x}}}|\psi_0\rangle$ is sufficient.

In each component of the superposition (3.14), the dynamics of the spin is described by the semiclassical description leading to Eq. (3.13)—the spin remains aligned with the effective field as it evolves under the cavity dynamics (Fig. 3·4). Thus, at the almost periods the spin will return to its initial state in each component of the superposition, while the cavity coherent state returns to the same angular position $\theta_2(T_N) \approx \theta_{02}$ but with a larger $n(T_N) \approx n_0 + T_N[\dot{n}]_t$.

Furthermore, the quantum mechanical phase accumulated by each component may be expressed within the semiclassical approximation as the integral of the energy. In

---

[2] The relation of the decomposition Eq. (3.14) to the classic quasiprobability distributions for ρ_{cav} (Wigner function, Husimi Q fuction, Glauber–Sudarshan P representation) does not seem to be straightforward. Eq (3.14) is also a decomposition into an overcomplete combination of coherent states. However, being a decomposition of the wavefunction, Eq. (3.14) is non-trivially related to more standard quasiprobability distributions based on the density matrix.

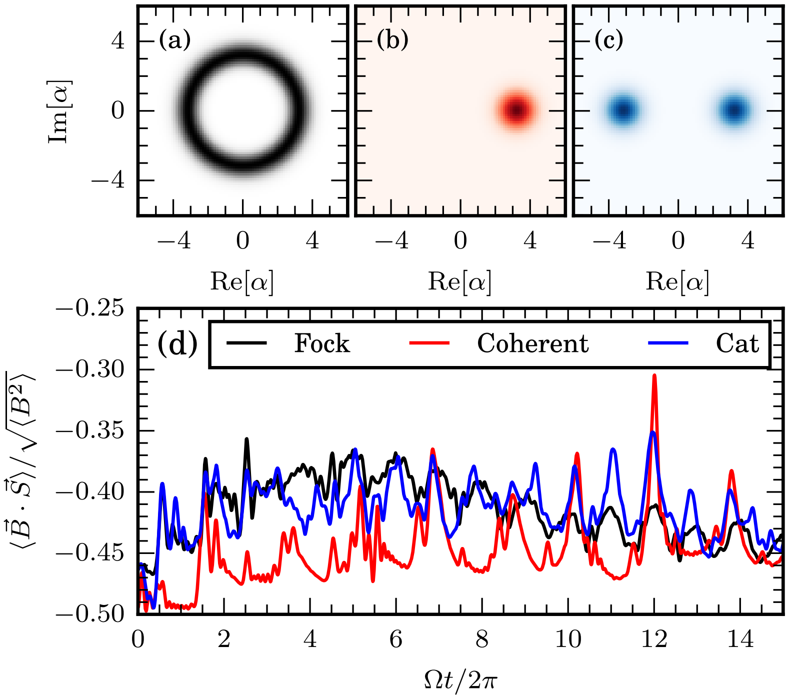

Figure 3·4: *Alignment of spin and field.*—(**a-c**) Cavity Q-functions for different initial states, $|+\rangle_{\hat{\mathbf{x}}}|\psi_0\rangle$, with: (**a**) $|\psi_0\rangle = |n=10\rangle$ a Fock state, (**b**) $|\psi_0\rangle = |\alpha=\sqrt{10}\rangle$ a coherent state, and (**c**) $|\psi_0\rangle \propto |\alpha=\sqrt{10}\rangle + |\alpha=-\sqrt{10}\rangle$ a Schrödinger cat state. (**d**) The expectation value $M = \langle \vec{B}\cdot\vec{S}\rangle/\sqrt{\langle \vec{B}^2\rangle}$ quantifies how closely aligned the spin is to an effective cavity field in a basis of coherent states. We see that M remains close to its extremal value of $-S$. *Parameters:* as in Fig. 3·1.

the c_+ components of Eq. (3.14), this is

$$\phi(t, \vec{\theta}_0, n_0) = \frac{1}{\hbar} \int_0^t \left(\hbar \omega n_0 - \mu S |\vec{B}_{\text{eff}}(\vec{\theta}_s, n_0)| \right) \mathrm{d}s. \tag{3.15}$$

The phase ϕ is also an integral of a quasiperiodic function, just as Δn in Eq. (3.12). Thus, $\phi(T_N, \vec{\theta}_0, n_0)$ rephases at the almost periods T_N, becoming almost $\vec{\theta}_0$ independent. This extends our observations about rephasings in a classical ensemble to rephasings in the full quantum superposition.

The result of this rephasing is the boosting phenomenon: at the almost periods T_N, the quantum state of the cavity rephases to form a state which has been boosted in the Fock basis, as described in Eq. (3.5) (up to a global phase).

We have neglected several effects in the above arguments. We enumerate these approximations below, and determine the regime in which the boosting phenomenon survives.

The most significant feature we have neglected is that the Fock occupation $n(t)$ changes with time, which in turn affects the integrand in Eq. (3.12). In Sec. 3.6, we show that the consequent deviation from perfect rephasings scales as $\sqrt{n(T_N)} - \sqrt{n_0}$. For a constant boost Ch_N, this error is $O(n_0^{-1/2})$, and thus can be reduced by increasing the initial cavity population n_0. The accumulated phase (3.15) depends on n linearly, but for equal initial n_0, the linear term only contributes a global phase, so similar estimates hold for the phase as for n. Our numerical simulations of the model (3.1) show that these estimates are likely pessimistic for short times, where we see the quality of the rephasings improve with time.

The cavity's coupling to the spin also affects the evolution of the phase $\theta_2(t) = -\arg\langle \hat{a}(t) \rangle$ in a coherent state. The most significant effect here is a renormalization of the cavity frequency to $\omega' = \omega + \delta\omega$, as $\delta\omega$ has an Ω independent contribution that can be non-negligible even deep in the adiabatic regime. This correction must be accounted for in order to correctly predict the almost periods (Sec. 3.5), but does not affect the quality of the rephasings.

The rephasings are of highest quality when the distribution $P(n) = \langle n| \rho_{\text{cav}}(0) |n\rangle$ is narrow in n, as components of Eq. (3.14) with different n_0 can dephase rapidly. Indeed, in Sec. 3.6 we show that the rate of dephasing is proportional to the width of the distribution $P(n)$. Fortunately, many non-classical states of interest have essentially a single n_0 value, including Fock states and Schrödinger cat states.

The initial state of the spin and classical drive should furthermore be chosen so as to minimize the magnitude of the c_- component in the decomposition (3.14). In general, this would involve preparing a complicated entangled state of the spin and cavity, so as to align the spin to $\vec{B}_{\text{eff}}$ for all θ_{02}. For the model (3.1), initiating the classical drive with $\theta_{01} = 3\pi/2$ ensures $\hat{B}_{\text{eff}}$ is close to $\hat{\mathbf{x}}$ for all values of θ_{02}. The c_- component is minimized just by preparing a product state with the spin polarized along $\hat{\mathbf{x}}$.

3.4 Experimental considerations

Cavity boosting requires a periodic classical drive, which is routine in essentially all experimental architectures. In Eq. (3.1), it also requires that $\hbar\Omega$ and $\hbar\omega$ be the smallest energy scales in the problem, which, naively, necessitates ultra-strong coupling [101–104]. However, this heirarchy can be achieved in a rotating frame starting from a strong coupling Hamiltonian in the lab frame.

A typical lab frame cavity QED Hamiltonian takes the form [92–95]

$$H_{\text{lab}}/\hbar = \omega_{\text{cav}}\hat{n} + (\omega_q + f(t))S_z + g(\hat{a} + \hat{a}^\dagger)S_x + 2V(t)\cos(\omega_q t)S_x, \tag{3.16}$$

where ω_{cav} is the lab frame cavity frequency, and ω_q is the mean level splitting of the spin. The splitting of the spin is modulated slowly by $f(t)$, while the x field on the spin is amplitude modulated by $2V(t)$ at the resonant carrier frequency ω_q.

Making a rotating frame transformation $|\psi\rangle \to U|\psi\rangle$ with $U(t) = \exp[i\omega_q t(\hat{n}+S_z)]$ and dropping terms which oscillate rapidly with frequency $2\omega_q$ produces a Hamiltonian

$$H_{\text{rot}}/\hbar = (\omega_{\text{cav}} - \omega_q)\hat{n} + f(t)S_z + \frac{g}{2}(\hat{a}S^+ + \hat{a}^\dagger S^-) + V(t)S_x, \tag{3.17}$$

at leading order in ω_q^{-1}. Making the identifications

$$\begin{aligned} \omega_{\text{cav}} - \omega_q &= \omega, \\ \hbar f(t) &= -\mu B_d \cos(\Omega t), \\ \hbar g &= \mu B_0, \\ \hbar V(t) &= -\mu(B_m - B_d \sin(\Omega t)) \end{aligned} \tag{3.18}$$

reproduces Eq. (3.1) in the rotating frame. As the transformation U rigidly rotates the phase space of the cavity, boosting in the rotating frame implies boosting in the lab frame.

Indeed, Fig. 3·5 shows the cavity occupation as a function of time when evolving an initial Fock state under the lab frame Hamiltonian (3.16). Parameters are chosen identically to the analogous rotating frame calculation leading to Fig. 3·1, with the additional parameter ω_q taken to be large, $\omega_q = 100\omega$. The cavity occupations in Fig. 3·5 are indistinguishable from those of Fig. 1(b) by eye, and in particular continue to show rephasings at the almost periods.

This is as expected: the only approximation in the rotating frame transformation relating Eq. (3.16) to Eq. (3.1) is to drop rapidly oscillating terms with frequency $2\omega_q$. Furthermore, the transformation itself does not affect the operator $\hat{n}$, so boosting in the rotating frame implies boosting in the lab frame.

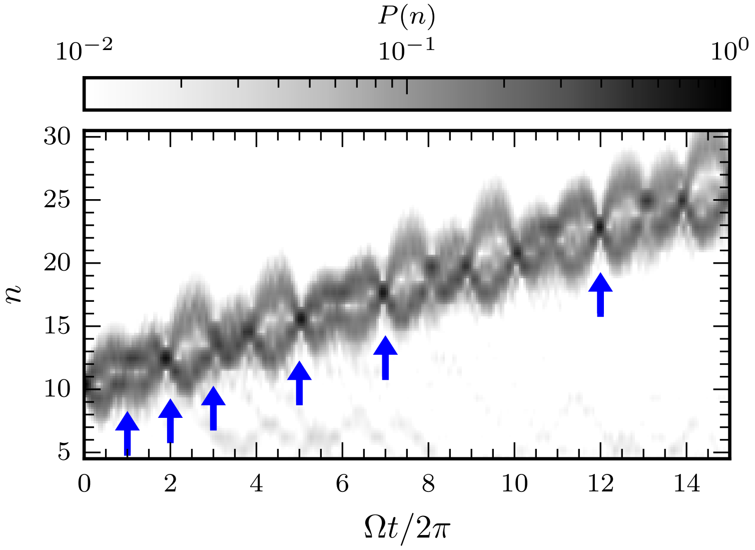

Figure 3·5: *Cavity state boosting in the lab frame.*—A plot of the Fock state occupation $P(n)$ as in Fig. 3·1(b), but now using the lab frame Hamiltonian (3.16). Rephasings at the almost periods are still clearly visible. Indeed, this $P(n)$ cannot be distinguished from Fig. 3·1(b) by eye. *Parameters:* as in Fig. 3·1, and with $\omega_q/\omega = 100$.

This also indicates that boosting requires a hierarchy of scales

$$\omega_{\text{cav}} - \omega_q, \Omega \ll f, g, V \ll \omega_q. \tag{3.19}$$

This hierarchy is achievable in a variety of microwave-frequency superconducting architectures, where naturally high coupling strengths, on the order of 100 MHz, and lifetimes in excess of 100 μs provide an ample window for the required slow drive timescales $\omega_{\text{cav}} - \omega_q$ and Ω [94, 95]. It is also possible to satisfy this hierarchy in optical cavity QED, although the achievable separation of scales between dissipation rates and light-matter couplings is typically smaller [92, 93].

3.5 Predicting Rephasings

In this section, we predict the almost periods T_N at which cavity state boosting occurs.

3.5.1 Renormalization of Cavity Frequency

The almost periods are determined by the ratio of the classical drive frequency Ω and the cavity frequency. The cavity frequency is renormalized from its bare value ω by the coupling to the spin, and the correction in the renormalized value $\omega' = \omega + \delta\omega$ can be significant.

In this section, we calculate the leading correction $\delta\omega_0$. Implicit in this statement is the assumption that the phase of the cavity advances approximately linearly, $\theta_2(t) = -\arg \langle\alpha|\,\hat{a}(t)\,|\alpha\rangle \approx \omega' t + \theta_{02}$ with $|\alpha\rangle$ an initial coherent state. We also assess this assumption below.

In the adiabatic limit, the correction can be calculated by assuming the spin is always aligned to the instantaneous effective field $\vec{B}_{\text{eff}}$, so that $\langle\vec{S}\rangle = S\hat{B}_{\text{eff}}$. Making this replacement in Eq. (3.1) gives an effective Hamiltonian for the cavity [48]

$$H_{\text{cav}} = \hbar\omega\hat{n} - \mu S|\vec{B}_{\text{eff}}|. \tag{3.20}$$

To extract a frequency from this Hamiltonian, we would like to find the ω' so that

$$\langle[\hat{a}, H_{\text{cav}}]\rangle = \hbar\omega'(n, \theta_1, \theta_2)\langle\hat{a}\rangle, \tag{3.21}$$

in a coherent state $|\alpha\rangle = |\sqrt{n}e^{-i\theta_2}\rangle$. A straightforward way to do this is to replace $(\hat{a}, \hat{a}^\dagger)$ by $\sqrt{n}(e^{-i\theta_2}, e^{i\theta_2})$ and compute $\hbar\omega' = \partial_n H_{\text{cav}}$. This provides a renormalized frequency as a function of n, θ_1, θ_2, and the parameters of the model. Observe that this correction need not go to zero as ω decreases.

More explicitly, we have $\delta\omega = \omega' - \omega = \delta\omega_0 + \Omega\delta\omega_1 + \ldots$, where the constant order correction

$$\delta\omega_0(n, \vec{\theta}) = -\frac{\mu S}{\hbar}\frac{\vec{B}_{\text{eff}} \cdot \partial_n \vec{B}_{\text{eff}}}{|\vec{B}_{\text{eff}}|}, \tag{3.22}$$

is sufficient for our purposes.

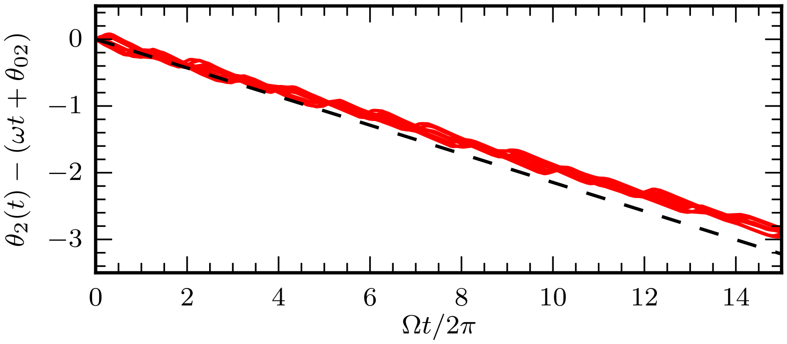

Figure 3·6: *Correction to cavity frequency.*—The bare cavity frequency is corrected from ω by the coupling to the spin. Measuring $\theta_2(t) = -\arg\langle\hat{a}(t)\rangle$ for $N_\theta = 8$ initial coherent states (red) shows that $\theta_2(t)$ differs from the bare prediction of $\omega t + \theta_{02}$. The leading correction gives $\theta_2(t) = (\omega + [\delta\omega_0]_{\vec{\theta}})t + \theta_{02}$ (3.23) (black dashed), and predicts the initial behavior of $\theta_2(t)$ accurately up to $\Omega t/(2\pi) \approx 10$. As the correction is n-dependent, and n varies due to pumping, $\theta_2(t) - (\omega t + \theta_{02})$ deviates from the correction $[\delta\omega_0]_{\vec{\theta}} t$ at longer times. *Parameters*: as in Fig. 3·1.

Furthermore, if $\delta\omega_0$ varies slowly with n in comparison to $\vec{\theta}$, then we can make a quasistatic approximation in replacing $\delta\omega_0$ with its average over $\vec{\theta}$, which we denote with square brackets, $[\delta\omega_0]_{\vec{\theta}}$. The average $[\delta\omega_0]_{\vec{\theta}}$ controls the motion of an ensemble of coherent states with different initial phases θ_{02}. We are neglecting fluctuations around this average drift in θ_2.

Specifically, for the parameters in Fig. 3·1, we find

$$[\delta\omega_0]_{\vec{\theta}}/\omega = -5.52\ldots \times 10^{-2}. \tag{3.23}$$

This prediction for the correction to the frequency can be compared to data. We compute $\theta_2(t) = -\arg\langle\hat{a}(t)\rangle$ for several initial coherent states and compare the curve to the linear prediction (3.23). Fig. 3·6 shows both the deviation of $\theta_2(t)$ from the bare value of $\omega t + \theta_{02}$ and the predicted average correction $[\delta\omega_0]_{\vec{\theta}} t$. The predicted correction accounts for the early-time average motion of $\theta_2(t)$ across different initial phases θ_{02}. At moderate and late times $\theta_2(t)$ deviates from being linear, as pumping causes n to change with time, and this in turn affects the instantaneous frequencies. At the time scales we are considering, this deviation is insignificant.

At longer time scales, this drift in $[\delta\omega_0(n)]_{\vec{\theta}}$ does not destroy the rephasings; their presence relies on ergodicity of $(\theta_1(t), \theta_2(t))$ in the torus, which is generic. However, if $[\delta\omega_0(n)]_{\vec{\theta}}$ drifts too far from $[\delta\omega_0(n_0)]_{\vec{\theta}}$, then the almost periods become less predictable. Essentially, one must simulate the evolution beforehand and identify the almost periods from numerics, or use a more refined approximation which takes this drift into account. This is not necessary when the unaccounted drift in $\theta_2(t)$ remains small compared to 2π.

3.5.2 Almost Periods

There are well-established methods for predicting the almost periods from the corrected frequencies (Ω, ω'). Indeed, the almost periods relate to the *convergents* and *semiconvergents* of the ratio $\Omega/\omega' = \beta$ [100].

If β has continued fraction expansion

$$\beta = a_0 + \frac{1}{a_1 + \frac{1}{a_2 + \cdots}} \tag{3.24}$$

then the convergents, which are the best rational approximation to β, may be calculated as h_N/k_N, where

$$h_N = a_N h_{N-1} + h_{N-2}, \quad \text{and} \quad k_N = a_N k_{N-1} + k_{N-2} \tag{3.25}$$

are defined recursively, with $(h_{-2}, h_{-1}) = (0, 1)$ and $(k_{-2}, k_{-1}) = (1, 0)$. These rational approximations are “the best” in the sense that, for any other rational p/q with $0 < q \leq k_N$, we have

$$|k_N \beta - h_N| < |q\beta - p|. \tag{3.26}$$

The *almost periods* of the drive with frequencies (Ω, ω') are given by

$$T_N = \frac{2\pi}{\Omega} h_N \approx \frac{2\pi}{\omega'} k_N \tag{3.27}$$

Rephasing of a cavity state occurs at any of the almost periods.

The semiconvergents

$$\frac{h_{N,m}}{k_{N,m}} = \frac{m h_N + h_{N-1}}{m k_N + k_{N-1}} \tag{3.28}$$

also serve as rational approximations to β. Here, m is an integer with $0 < m < a_{N+1}$. These rational approximations obey a weaker condition than Eq. (3.26): for any p/q with $0 < q \le k_{N,m}$, we have

$$\left| \beta - \frac{h_{N,m}}{k_{N,m}} \right| < \left| \beta - \frac{p}{q} \right| . \tag{3.29}$$

The semiconvergents also have associated almost periods,

$$T_{N,m} = \frac{2\pi}{\Omega} h_{N,m}. \tag{3.30}$$

For the parameters in Fig. 3·1, we have a correction to the frequency given by Eq. (3.23), and a corresponding corrected ratio

$$\frac{\Omega}{\omega'} \approx \frac{\Omega}{\omega + [\delta\omega_0]_{\vec{\theta}}} = 1.71... \tag{3.31}$$

and hence a continued fraction expansion

$$[a_0; a_1, a_2, a_3, \ldots] = [1; 1, 2, 2, \ldots], \tag{3.32}$$

and almost periods

$$\begin{aligned} &h_0 = 1, \\ &h_1 = 2, \quad h_{1,1} = 3, \\ &h_2 = 5, \quad h_{2,1} = 7, \\ &h_3 = 12 \quad \dots \end{aligned} \tag{3.33}$$

These are the almost periods plotted in Fig. 3·1. They accurately predict the times at which rephasing occurs, though the rephasing for the convergent $h_0 = 1$ is of very poor quality, as is that of its associated semiconvergent $h_{1,1} = 3$.

If we had not first calculated the correction to the cavity frequency, the predicted almost periods would be given by Fibonacci numbers. The last two almost periods would be incorrect in that case, with a bare prediction of $h = 8, 13$, rather than $h = 7, 12$.

3.6 Quality of Rephasings

In this section, we estimate the scaling of the quality of rephasings with T_N, both in the semiclassical picture and including effects of the spin on the cavity dynamics in the large n regime.

3.6.1 Semiclassical Picture

In the coarsest semiclassical approximation to the evolution of the coupled spin-cavity system, the rephasings at the almost periods improve monotonically. As discussed in Sec. 3.3, the rephasings occur because integrals like

$$A(T_N, \vec{\theta}_0) = \int_0^{T_N} a(\vec{\theta}_t)\mathrm{d}t, \tag{3.34}$$

become approximately $\vec{\theta}_0$ independent at the almost periods T_N. Such integrals give, for instance, $\Delta n(T_N)$ and $\phi(T_N)$.

As the trajectory $\vec{\Omega}t + \vec{\theta}_0$ is dense in the $\vec{\theta}$ torus, at the almost periods we have

$$A(T_N, \vec{\theta}_0) = \int a(\vec{\theta})\mathrm{d}^2\theta + O(1/T_N) \tag{3.35}$$

where the error estimate $O(1/T_N)$ comes from estimating the perpendicular distance between the closest windings of the trajectory around the torus. This can be checked numerically by integrating Eq. (3.34) for different initial θ_{02}, as shown in Fig. 3·3 for $A = \Delta n$.

This improvement of the subsequent rephasings is a property characteristic of *quasiperiodic* systems. If $\Omega/\omega \in \mathbb{Q}$, so that the system is periodic, then rephasings at subsequent *periods* get worse. In this case, the trajectory does not densely cover the torus, so at the period T we have

$$A(T, \vec{\theta}_0) = \int a(\vec{\theta})\mathrm{d}^2\theta + O(1/T), \tag{3.36}$$

as before. However, at subsequent periods NT, we have

$$A(NT, \vec{\theta}_0) = NA(T, \vec{\theta}_0) = N\int a(\vec{\theta})\mathrm{d}^2\theta + O(N/T). \tag{3.37}$$

As the trajectories $\vec{\theta}_t$ do not densely cover the torus, $A(T, \vec{\theta}_0)$ depends on $\vec{\theta}_0$. This results in a deviation of $A(NT, \vec{\theta}_0)$ from the average value $(2\pi)^2N[a]_{\vec{\theta}}$ which grows linearly in time. This is also visible in Fig. 3·3.

3.6.2 Including the Effect of the Spin

To include the effect of the coupling to the spin on the cavity dynamics, still at a semiclassical level, we can augment Eq. (3.34) with a dependence of the integrand on

$n(t)$.

$$A(T_N, \vec{\theta}_0, n_0) = \int_0^{T_N} a(\vec{\theta}_t, n(t))\mathrm{d}t. \tag{3.38}$$

Both Eqs. (3.12) and (3.15) are of this form.

The leading n dependence in Eq. (3.38) for large $n \gg 1$ is at the order $\sqrt{n}$ (from Eq. (3.10)):

$$a(\vec{\theta}_t, n) = a_0(\vec{\theta}_t) + a_1(\vec{\theta}_t)\sqrt{n} + \cdots . \tag{3.39}$$

Here, "$\cdots$" denotes higher order (in Ω or n^{-1}) terms we neglect.

Furthermore, the average of a_1 vanishes, $[a_1]_{\vec{\theta}} = 0$. For Eq. (3.12), this follows from the statement that the average pumping rate does not depend on n (except where it changes as a step function when the Chern number changes). Then we may express

$$a_1 = \vec{\Omega} \cdot \nabla A_1(\vec{\theta}). \tag{3.40}$$

Integrating by parts gives

$$\begin{aligned} A &= [a_0]_{\vec{\theta}} T_N + A_1(\vec{\theta}_{T_N})\sqrt{n(T_N)} - A_1(\vec{\theta}_0)\sqrt{n_0} + \cdots \\ &= [a_0]_{\vec{\theta}} T_N + A_1(\vec{\theta}_0)\left(\sqrt{n(T_N)} - \sqrt{n_0}\right) + \cdots , \end{aligned} \tag{3.41}$$

where we again dropped terms higher order in n^{-1} and used $A_1(\vec{\theta}_{T_N}) = A_1(\vec{\theta}_0) + O(1/T_N)$.

Comparing the value of A between trajectories with different initial $\vec{\theta}_0$ and equal n_0 gives

$$A(T_N, \vec{\theta}_0, n_0) - A(T_N, \vec{\theta}'_0, n_0) \approx \left(A_1(\vec{\theta}_0) - A_1(\vec{\theta}'_0)\right)\left(\sqrt{n(T_N)} - \sqrt{n_0}\right). \tag{3.42}$$

In words, the rephasings in A have a width which broadens like $\sqrt{n(T_N)} - \sqrt{n_0} = O(\sqrt{T_N})$, to leading order in n and Ω. Then it is consistent to use $n(T_N) = n_0 +$

$Ch_N + O(\sqrt{T_N})$. Considering a constant target increase $\Delta n = Ch_N$, we have, for increasing n_0,

$$A(T_N, \vec{\theta}_0, n_0) - A(T_N, \vec{\theta}_0', n_0) \approx \left(A_1(\vec{\theta}_0) - A_1(\vec{\theta}_0')\right) \frac{Ch_N}{2\sqrt{n_0}}. \tag{3.43}$$

The width may thus be reduced by taking n_0 larger.

The integrand for the accumulated phase (3.15) involves a term $\omega n(t)$ with $O(n)$ dependence. However, only phase *differences* are physically meaningful. Eq. (3.41), applied to Δn, shows $n(t) = [\dot{n}]_{\vec{\theta}} t + O(\sqrt{n})$, so that the n dependence in the integrand of

$$\phi(t, \vec{\theta}_0, n_0) - \phi(t, \vec{\theta}_0', n_0) = \frac{1}{\hbar} \int_0^t \left(\hbar\omega O(\sqrt{n(s)}) - \mu S(|B_{\text{eff}}(s, \vec{\theta}_0)| - |B_{\text{eff}}(s, \vec{\theta}_0')|)\right) \mathrm{d}s \tag{3.44}$$

cancels at $O(n)$. Then the phase difference obeys the condition (3.39), and so Eq. (3.42) applies.

As we have observed, boosting works best for initial states with a narrow distribution $P(n) = \langle n| \rho_{\text{cav}} |n\rangle$, as we now investigate. Considering states with differing n_0 gives, for quantities obeying the condition (3.39),

$$\begin{aligned} A(T_N, \vec{\theta}_0, n_0) - A(T_N, \vec{\theta}_0', n_0') \approx{} & A_1(\vec{\theta}_0) \left(\sqrt{n(T_N, n_0)} - \sqrt{n_0}\right) \\ & - A_1(\vec{\theta}_0') \left(\sqrt{n(T_N, n_0')} - \sqrt{n_0'}\right). \end{aligned} \tag{3.45}$$

The right hand side still asymptotically broadens as $O(\sqrt{T_N})$ for large T_N, and can be reduced as $O(n_0^{-1/2}, (n_0')^{-1/2})$ with increasing n_0 and n_0'. The accumulated phase, which does not obey (3.39), is more severely affected by differing values of n_0. A phase difference with differing initial values of n diverges linearly in time:

$$\phi(T_N, \vec{\theta}_0, n_0) - \phi(T_N, \vec{\theta}_0', n_0') \approx \omega(n_0 - n_0')T_N. \tag{3.46}$$

For general non-classical initial states, this makes the condition of having a narrow initial distribution $P(n) = \langle n| \rho_{\text{cav}} |n\rangle$ quite strict. An error on the order of 2π can accumulate in the phase within just a few periods.

In short time numerics, we see rephasings in Fock states improve with T_N (Fig. 3·10). This is likely because the short time behavior is still dominated by the $O(1/T_N)$ improvement in quality derived in Sec. 3.6.1. It is also possible that higher-order terms we have neglected in the above estimates conspire to suppress the error below our prediction for moderate Ω and n_0.

3.7 Comparing Semiclassical and Quantum Evolution

The core of our understanding of cavity boosting is semiclassical. In this section we enumerate the various levels of semiclassical approximation we employ, and numerically compare them to quantum evolution.

3.7.1 Semiclassical Evolution

The coarsest description of the spin-cavity dynamics treats the cavity as completely classical when it begins in a coherent state, and neglects the effects of the spin on the cavity. Then the state of the cavity—now a classical drive—is prescribed:

$$n(t) = n_0, \quad \text{and} \quad \theta_2(t) = \omega' t + \theta_{02}. \tag{3.47}$$

The cavity occupation is constant, and the angular motion progresses at a constant angular frequency ω' (which may be corrected from the bare ω, see Sec. 3.5.1). If $\Omega/\omega' \notin \mathbb{Q}$, the resulting spin model

$$H_{\text{eff}} = -\mu \vec{B}_{\text{eff}}(\theta_1, \theta_2, n) \cdot \vec{S} \tag{3.48}$$

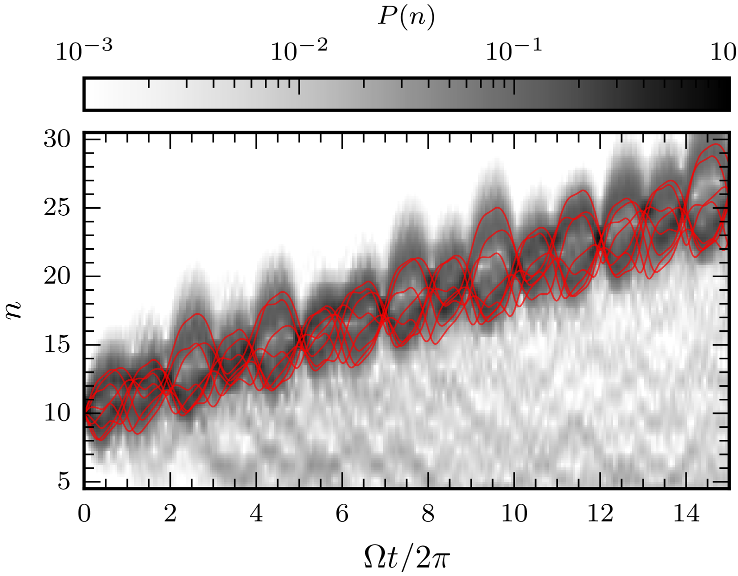

Figure 3·7: *Comparison of semiclassical evolution to quantum evolution.*—The cavity occupation from exact quantum evolution in an initial Fock state (grey image) and the predicted $n(t)$ from integrating Eq. (3.50) (red) for $N_\theta = 8$ different initial phases θ_{02}, assuming a constant frequency $\theta_2(t) = \omega' t + \theta_{02}$. The semiclassical equations reproduce the qualitative features of the quantum evolution, including average pumping and rephasings. *Parameters:* as in Fig. 3·1, with $\omega' = \omega + [\delta\omega_0]_{\vec{\theta}}$ as in Sec. 3.5.

is of a quasiperiodically driven spin, as studied in Refs. [37, 38, 64]. It exhibits energy pumping and implies the presence of rephasings, as described above. The solution for Δn in the adiabatic limit of this model is shown in Fig. 3·3. It reproduces the qualitative features of energy pumping and boosting.

Some component of the effect of the spin on the cavity may be accounted for by explicitly accounting for the change in $n(t)$ implied by the pumping. That is, by solving the differential equation for n,

$$\hbar\dot{n}(t) = -\left\langle\psi(t)\right| \partial_{\theta_2} H_{\text{eff}}(\theta_1, \theta_2, n) \left|\psi(t)\right\rangle, \tag{3.49}$$

with the initial condition $n(0) = n_0$. In the adiabatic limit, this may be approximated as

$$\hbar\dot{n}(\theta_1, \theta_2, n) = \mu S \partial_{\theta_2} |\vec{B}_{\text{eff}}| + \hbar\Omega F, \tag{3.50}$$

where F is a Berry curvature. We still prescribe that $\theta_2(t) = \omega' t + \theta_{02}$.

In Fig. 3·7 we compare the evolution of $n(t)$ given by Eq. (3.50) to the full quantum evolution in a Fock state. It is clearly visible that the semiclassical approximation captures both the qualitative and, to some extent, quantitative aspects of the quantum evolution.

At a further level of complication, we could include the effect of the spin on both $n(t)$ and $\theta_2(t)$, but continue to treat the cavity as classical. This is not an approximation we have considered here.

3.7.2 Quantum Evolution

Lastly, making no approximation, we can consider the full quantum evolution. This regime we investigate numerically.

Our understanding of this regime is still based on semiclassical notions. Namely, we decompose an arbitrary initial cavity state into a superposition of coherent states

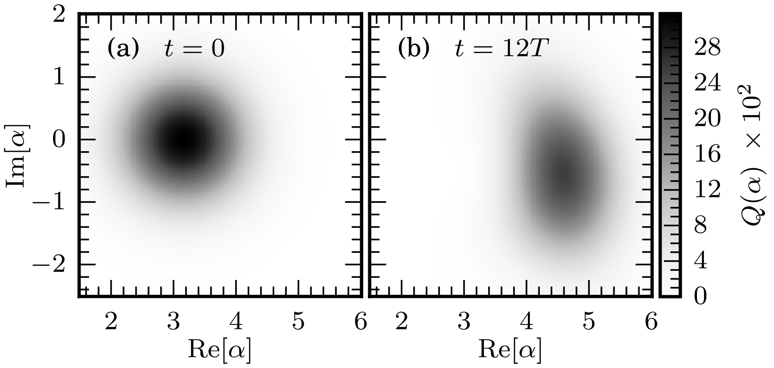

Figure 3·8: *Q-functions of an initial coherent state.*—(**a**) Q-function $Q(\alpha) = \frac{1}{\pi} \langle\alpha| \rho_{\text{cav}}(t) |\alpha\rangle$ at $t = 0$ and (**b**) $t = 12T$. The initially coherent state, $|\psi(0)\rangle = |\alpha = \sqrt{10}\rangle$ evolves to a state which is not exactly coherent, but with a Q-function well-localized in α.

with spin states aligned to $\vec{B}_{\text{eff}}$, and consider the evolution of each component of the superposition individually. In our semiclassical arguments, we assume that these states remain tensor products of cavity coherent states and polarized spin states, and that we can understand the properties of the superposition state by considering an ensemble of coherent states. We investigate each of these assumptions below, and find that they are valid.

3.7.2.1 Coherent State Dynamics

In the semiclassical limit of $n \to \infty$ with $\mu B_0\sqrt{n} = O(1)$, the effect of the qubit on the cavity is negligible, and the cavity is well-approximated as being harmonic at times short compared to $\hbar\sqrt{n}/\mu B_0 S$. (This timescale comes from comparing the cavity energy $\hbar\omega n$ to the spin energy $\mu B_0 S\sqrt{n}$.) In this regime, an initial coherent state $|\alpha\rangle$ evolves to another coherent state $|\alpha(t)\rangle$. This is the assumption we make in treating the cavity semiclassically.

In our numerics, and in any experiment, we are not strictly in this regime. Nonetheless, Fig. 3·8 shows qualitatively that an initial coherent state evolves into a state which is well-localized in the cavity quadratures.

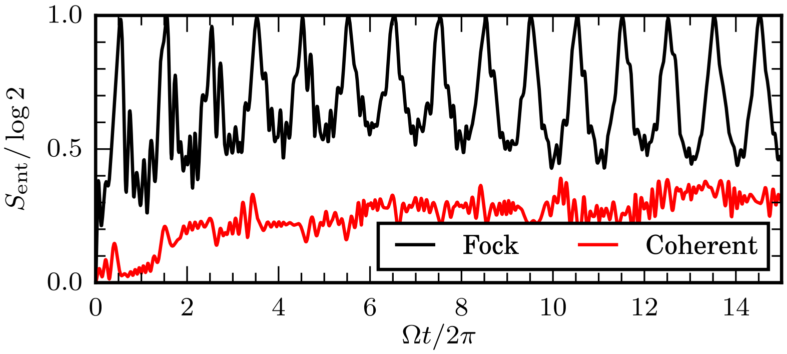

Figure 3·9: *Entanglement between the spin and cavity.*—In an initial coherent state with $\theta_{02} = 0$ (red) the spin and cavity remain largely unentangled. In contrast, an initial Fock state (black) periodically entangles with the spin. *Parameters:* as in Fig. 3·1.

Visualized in terms of the Husimi Q-function, $Q(\alpha) = \frac{1}{\pi} \langle\alpha|\, \rho_{\mathrm{cav}}(t)\, |\alpha\rangle$ remains well-localized in α. In particular, a spin strongly coupled to the cavity still follows a field $\vec{B}_{\mathrm{eff}}$ closely, where $\vec{B}_{\mathrm{eff}}$ is determined by the center-of-mass of Q. Some broadening of Q into a "banana" shape is visible along the circle of constant $|\alpha|^2$, but for our parameters and time scales this broadening remains small.

3.7.2.2 Cavity-Spin Entanglement

With strong coupling, the entanglement entropy between the cavity and spin is generically expected to grow quickly. Fig. 3·9 shows that this is indeed what occurs for an initial Fock state, which reaches the maximal possible entropy of $S_{\mathrm{ent}} = \log 2$ within one period of the classical drive. Even so, an initial coherent state in the cavity develops little entanglement.

Both these observations are consistent with our description of the dynamics—that the quantum state of the full system is a superposition of coherent states tensor multiplied by spin states aligned to an effective field. For an initial coherent state, this superposition consists of just one term, so the spin remains in a product state with the cavity. The slight growth in the entanglement entropy for an initial coherent

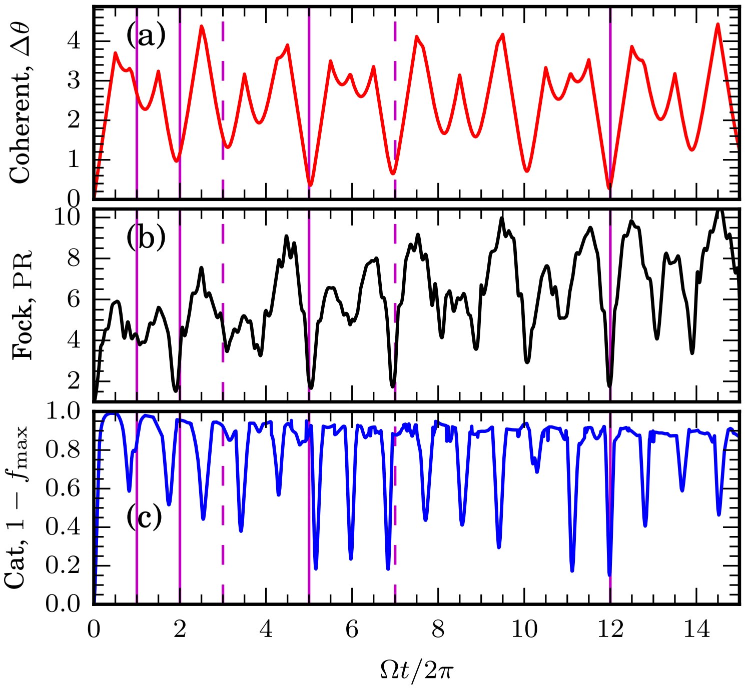

Figure 3·10: *Comparison of coherent state ensemble to non-classical state evolution.*—We compare metrics of rephasing in non-classical states to rephasing in an ensemble of $N_\theta = 8$ initial coherent states with constant n_0 and varying θ_{02}, with spins initially aligned to $\vec{B}_{\text{eff}}$. Predicted almost periods are marked as purple lines. Dashed lines correspond to semiconvergents (Sec. 3.5.2). (**a**) The distance $\Delta\theta(t) = \max_{\theta_{02}} \|\vec{\theta}_t - \vec{\theta}_0\|$ has a local minimum at almost periods of the quasiperiodic drive with frequencies Ω and ω'. (The additional minimum at $t = 10T$ may be an artifact of the almost period at $t = 5T$, or may be due to $\theta_2(t)$ not being a linear function of time in the quantum system.) (**b**) The ensemble rephasings coincide with rephasings of a boosted Fock state, as measured by the participation ratio $\text{PR} = 1/\sum_n P(n)^2$. The participation ratio is 1 in a Fock state, and drops below 2 at all of the marked almost periods except $t = T, 3T$. (**c**) The rephasings of an initial Schrödinger cat state at almost periods are not as clear, possibly because of the metric we use. We use the maximum fidelity: $1 - f_{\max} = 1 - \max_{\alpha \in \mathbb{R}} \langle \text{cat}(\alpha) | \rho_{\text{cav}} | \text{cat}(\alpha) \rangle$, where $|\text{cat}(\alpha)\rangle \propto |\alpha\rangle + |-\alpha\rangle$ is an even superposition of coherent states. There are minima in this quantity close to the almost periods, with the almost period at $t = 12T$ being particularly prominent. *Parameters:* as in Fig. 3·1.

state shows that this picture is not exact, but that it is an effective description of the dynamics at short times (Sec. 3.7.2.1).

In a Fock state, when $\theta_1(t) = 3\pi/2$ in the model (3.1), the effective field $\hat{B}_{\text{eff}}$ does not vary much with θ_2. Then the Fock state may be thought of as a superposition of states $|+\rangle_{\hat{B}_{\text{eff}}} |\alpha\rangle$ where all the spins point approximately in the $\hat{\mathbf{x}}$ direction. This results in a dip in S_{ent} with a frequency Ω. On the other hand, when $\hat{B}_{\text{eff}}$ varies greatly with θ_2 the entanglement between the spin and cavity becomes very large—indeed, Fig. 3·9 shows it reaches $\log 2$.

3.7.2.3 Coherent State Ensembles

In Fig. 3·10 we investigate our final assumption—that the evolution of an ensemble of initial coherent states captures the evolution of a superposition state.

Namely, we compare a metric for rephasing in the ensemble—the maximum distance $\|\vec{\theta}_t - \vec{\theta}_0\|$ within the ensemble—to the participation ratio (PR) of an initial Fock state and the maximum fidelity of an initial Schrödinger cat state. We find that rephasings in the coherent state ensemble coincide with rephasings of the other non-classical states. This shows empirically that our semiclassical picture of the quantum dynamics is effective.

3.8 Summary and Discussion

This chapter showed how boosting may be understood through the lens of the frequency lattice, and provided a more quantitative analysis based in the time domain.

Cavity state boosting allows the preparation of non-classical states of a quantum cavity with larger occupation number n than may otherwise be possible. The potential to realize boosting in optical cavities is particularly intriguing, as deterministic generation of even single photons is challenging in this regime.

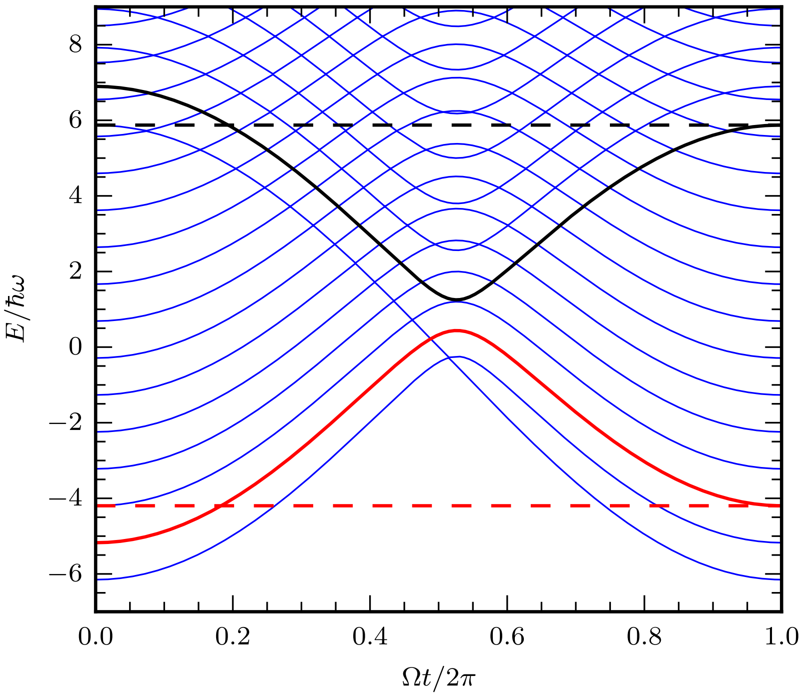

Figure 3·11: *Holonomy.*—Adiabatically following an eigenstate of the Hamiltonian (3.1) throughout a period of the classical drive brings the system to a different eigenstate with one more (red) or one fewer (black) quanta of energy. This feature is known as non-trivial holonomy.

Boosting is topological, in the sense that it occurs even if the instantaneous Hamiltonian is continuously deformed, provided the drive frequency Ω remains incommensurate to the cavity frequency. Changing the parameters of the Hamiltonian may alter the positions of the almost periods, but will not change the fact that they occur.

Boosting is also prethermal. At very long times, nonadiabatic processes cause the spin to no longer be aligned with the effective field, destroying the energy pumping effect [38, 64]. However, at earlier times, n exceeds $(B_m + B_d)^2/B_0^2$, and so exits the topological pumping regime [51].

Recently, Ref. [105] exploited quantum holonomy [106, 107] to achieve the topological pumping of energy in a one-dimensional quantum gas. Boosting may also be understood in terms of holonomy (Fig. 3·11).

If photon losses in the cavity, or dephasing of the qubit, are significant, boosting degrades in quality. As the rate of photon loss from the cavity increases with increasing n, the cavity populations achievable with boosting (and all methods) are limited by the cavity quality factor. Quality factors larger than 10^6 have been reported in many architectures [108–110].

Boosting offers a qualitatively distinct method of preparing highly non-classical cavity states—for instance, Fock states—compared to current methods [111–113]. Presently, preparing Fock states requires detailed and precise control of the coupled spin [111–113]. In contrast, boosting has an immensely simpler drive protocol for the spin—a sine wave in Eq. (3.1). Related protocols may also be used to prepare many-body scar states in other systems [105].

Boosting also provides a way of preparing Schrödinger cat states for use in bosonic encoded qubits [56–63]. Remarkably, the drive protocol to boost a cat state is the same as for a Fock state. Indeed, boosting does not require any knowledge of the current state of the cavity.

Chapter 4

Anomalous Localized Topological Phases

Time dependent driving can create new nonequilibrium phases of matter [10, 12, 114–116]. The most studied example is periodic (Floquet) driving [10, 12, 114, 115, 117, 118]. In the steady state, Floquet phases can exhibit period doubling [119–122] and topological phases [8, 9, 11, 44, 89, 90, 123–131], some of which are impossible in equilibrium.

For instance, two-dimensional fermionic systems support a topological phase with chiral current-carrying edge modes [8, 9, 11, 89, 126, 128, 131]. Such behavior is only possible in a two-dimensional static insulator when populated bands have a nontrivial Chern number, but this requirement is evaded in the driven setting. The drive is engineered to move fermions in short loops—similar to cyclotron orbits—which results in skipping orbits at the edge of the system, while the bulk may be fully localized. These *anomalous Floquet-Anderson insulators* (AFAIs) have prompted keen interest in the nonadiabatic properties of driven phases of matter [45, 90, 116, 127, 128].

In this chapter, we explore a class of nonequilibrium topological phases which emerge under quasiperiodic driving called *anomalous localized topological phases* (ALTPs). In fact, there is an intimate connection between quasiperiodically driven topological phases and Floquet phases in higher dimensions [1, 65]. Specifically, the steady states of a d-dimensional tight-binding model driven by D incommensurate tones follow from the eigenstates of a $(d + D)$-dimensional static model on a *frequency lattice* [13, 30, 36, 37] (chapter 2). This construction relates the AFAI with $(d + D) = (2 + 1)$ to a $(1 + 2)$ *quasiperiodic Floquet-Thouless energy pump* (QP pump)—a one-dimensional phase of two-tone-driven fermions, and a member of the broader class of ALTPs (Fig. 4·1). This connection reveals that the QP pump supports localized edge

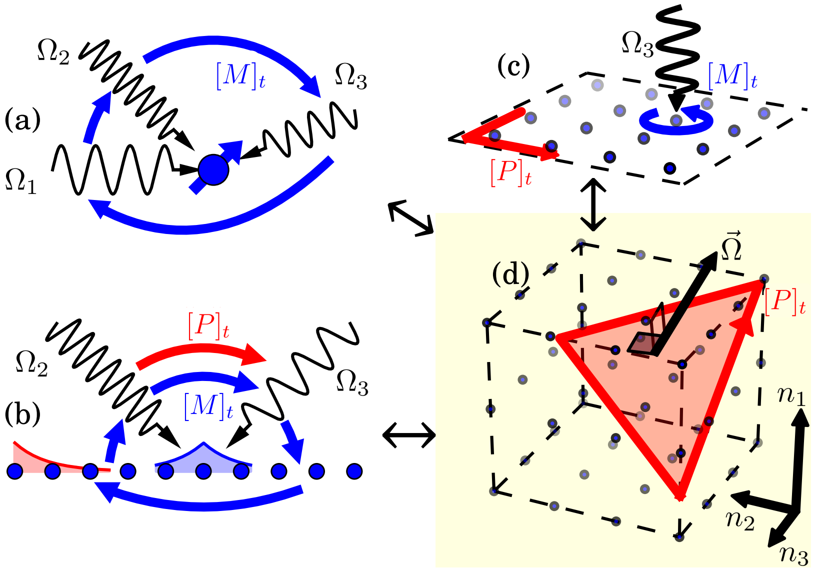

Figure 4·1: *Correspondence between ALTPs with fixed* $d+D=3$.—**(a)** $(0+3)$: A qudit driven by three incommensurate frequencies showing chiral circulation of energy $[M]_t$ between the drives. **(b)** $(1+2)$: A localized fermionic chain driven by two tones (the QP pump) also exhibits an energy-charge circulation in the bulk, and topological edge states that pump energy between the drives $[P]_t$. **(c)** $(2+1)$: A localized two-dimensional system driven by one tone has a quantized bulk magnetization, and quantized edge currents [11, 126]. **(d)** $(3+0)$: All three systems have a unifying description in terms of a static frequency lattice with localized bulk eigenstates and an electric field $\vec{\Omega}$ [66].

modes which mediate an energy current between the drives (Fig. 4·2). This energy current has a quantized average value,

$$[P]_t = P_{\text{top}} W, \quad \text{where} \quad P_{\text{top}} = \frac{\Omega_1 \Omega_2}{2\pi}, \tag{4.1}$$

$W \in \mathbb{Z}$ is a winding number invariant, and $[\cdot]_x$ again represents an average with respect to the variable x (which here is time, t).

Further, the QP pump has the same remarkable coherence properties which allow for the preparation of highly excited nonclassical states in quantum cavities [3]. Unlike the qubit system considered in chapter 3, the existence of the QP pump's pumping

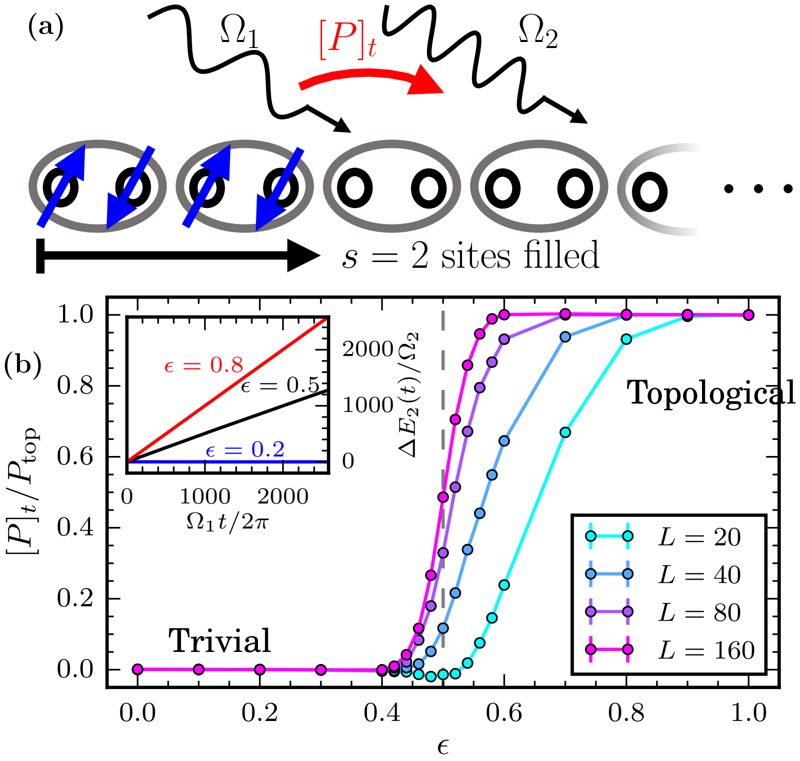

Figure 4·2: *The QP pump.*—(**a**) The quasiperiodic Floquet-Thouless energy pump (QP pump) is a nonequilibrium phase of disordered fermionic chains driven by incommensurate frequencies Ω_1 and Ω_2. When sufficiently many sites (s) from one edge are filled, the chain mediates a topologically quantized average energy current between the drives, $[P]_t = P_{\rm top}W$ ($W \in \mathbb{Z}$). (**b**) The parameter ϵ deforms a coupled layer model of (**a**) from the trivial phase (average energy current $[P]_t = 0$) to the topological phase ($[P]_t = P_{\rm top}$). The transition between the phases sharpens with increasing chain length L. At the critical point ($\epsilon = 1/2$), the pumping rate is half the topological value. (Inset) The total energy pumped into drive 2, ΔE_2, is linear in time in both phases and at the transition. *Parameters in model* (4.15): $s = L/4$, $[P]_t$ is averaged over 200 disorder configurations and initial phases, and as in Fig. 4·5.

states does *not* rely on adiabaticity. Thus, by using these edge states to perform boosting, the lower inequality in the hierarchy of scales Eq. (3.19) may be substantially relaxed. This is a significant advantage in implementing boosting. (Though it must be balanced against the disadvantage of using a more complicated system.)

The QP pump is only one member of the class of ALTPs. In Sec. 4.6, we make a topological classification of localized tight-binding models with any $d + D$. Our key observation is that the frequency lattice treats spatial and synthetic dimensions on an equal footing when its eigenstates are localized (Fig. 4·1). More formally, the topological classification of localized phases of d-dimensional tight-binding models driven by D incommensurate periodic tones depends only on the total frequency lattice dimension $d + D$. The classification is by an integer when $d + D > 1$ is odd and is trivial otherwise. The nontrivial phases are the ALTPs.

However, the abstract classification does not reveal observable properties of these phases. While we identify observable consequences of topology for $(d + D) = 3$ in Sec. 4.7, it is useful to have simple models for each ALTP which make such properties transparent. Such models would also guide experimental realizations of these phases.

In Sec. 4.2 and Sec. 4.5, we devise a coupled layer construction for any $(1 + D)$-dimensional ALTP. We demonstrate the construction in detail for the simplest example of the QP pump (Sec. 4.2). Exploiting the mapping to the frequency lattice, we show the QP pump can be constructed from layers supporting delocalized chiral modes, just as in familiar integer quantum Hall phases [39, 40, 132–134]. The layers for the QP pump are fermionic sites, finely tuned to support pumping modes with equal and opposite average energy currents between the drives. These pumping modes can be coupled in one of two ways: within a site, resulting in a trivial phase; or between sites, resulting in a topological phase with dangling edge modes (Fig. 4·3).

The coupled layer construction can also be adapted to produce a (2+3)-dimensional

ALTP with edge states exhibiting a synthetic four-dimensional quantum Hall effect (Sec. 4.5) [135]. The physical response is an energy current between two of the drives supported at one of the (one-dimensional) edges,

$$[P]_t = \frac{\Omega_3 \Omega_4}{(2\pi)^2} B L_y W + O(B^2). \tag{4.2}$$

Here, B is a synthetic magnetic field, and L_y is the linear dimension of the pumping edge.

We numerically investigate the QP pump coupled layer model, and obtain the phase diagram shown in Fig. 4·2(b) as a function of the interlayer coupling strength ϵ. The model has two localized phases—one topological and one trivial (Sec. 4.3.1)—separated by an isolated critical point (Sec. 4.3.3). The critical point exhibits a half-integer energy current, $[P]_t = P_{\text{top}}/2$, with critical exponents suggestive of the two-dimensional integer quantum Hall universality class. In the topological phase, the energy current is very robust to weak interactions (Sec. 4.4). It persists for an extremely long time, even when interactions cause the system to ultimately thermalize.

4.1 Quasiperiodic Floquet-Thouless Energy Pump

While ALTPs may be classified in all dimensions (Sec. 4.6), the best understood example with $D > 1$ is the QP pump [1, 44, 65]. The QP pump is the ALTP with spatial dimension $d = 1$ and two incommensurate drives, $D = 2$ (the $(1+2)$-dimensional ALTP). This section summarizes some known facts regarding this phase. (See Ref. [66] for the related $(3+0)$-dimensional phase.)

The bulk topological invariant associated to ALTPs is a winding number, W. In the QP pump, the corresponding signature at the edge of the system is a quantized average pumping of energy between the drives. The direction in which this pumping proceeds is fixed by the sign of W and which edge is being considered.

Localization of the quasienergy states in the synthetic dimensions is crucial here. Without this, one cannot define steady states as in Eq. (2.15). In the frequency lattice tight-binding model (2.16), localization may occur due to the inhomogeneous potential $\vec{n} \cdot \vec{\Omega}$. The topological classification of ALTPs further assumes localization in the spatial dimensions [1, 65, 66]. The specific mechanism of localization—random or correlated spatial disorder, Stark localization through a linear potential, or otherwise—is unimportant.

The observable which measures the rate of energy transfer into the second drive is

$$P(t) = -\Omega_2 \partial_{\theta_2} H(\vec{\theta}_t). \tag{4.3}$$

Writing ρ_s for the Slater determinant state with the first s states from the edge filled (and potentially other states in the bulk), we have

$$[P]_t := \lim_{T\to\infty} \frac{1}{T} \int_0^T \mathrm{d}t \ \mathrm{Tr}\, P(t)\rho_s(t) = \frac{\Omega_1\Omega_2}{2\pi} W, \tag{4.4}$$

where $\rho_s(t)$ is the time evolved state from the initial state ρ_s (we will usually leave the dependence of $[P]_t$ on s implicit), and $W \in \mathbb{Z}$ is the winding number [1, 44, 65]. We denote the topological pumping rate as

$$[P]_t = P_{\mathrm{top}} W + O(e^{-s/\zeta}) \tag{4.5}$$

with $P_{\mathrm{top}} = \frac{\Omega_1\Omega_2}{2\pi}$ as in Eq. (4.1), and where ζ is the single-particle localization length. (Equation (4.5) holds for any initial phase and disorder realization which results in localization. However, the data we plot in Fig. 4·2 and later figures include an average over initial phases $\vec{\theta}_0$ and disorder. This reduces the $O(T^{-1})$ noise due to calculating the average $[P]_t$ over a finite time T.)

In terms of the frequency lattice, the pumping states correspond to delocalized edge states. A state initialized with photon numbers n_1 and n_2 can evolve into another with $n_1 + [P]_t t/\Omega_1$ and $n_2 - [P]_t t/\Omega_2$. As such, if $[P]_t \neq 0$, the eigenstates at the edge must be delocalized in the direction

$$\hat{\Omega}_\perp \propto \Omega_2 \hat{e}_1 - \Omega_1 \hat{e}_2. \tag{4.6}$$

That is, perpendicular to $\vec{\Omega}$. We will write $n_\perp = \vec{n}\cdot\hat{\Omega}_\perp$ for the corresponding frequency lattice coordinate (Figs. 4·3 and 4·4).

There is another observable which reveals the topology of the QP pump, in addition to the edge modes. This is a circulation of energy between the drives in the bulk [1, 65]. We will not focus on this observable in the context of the coupled layer model, so a cartoon picture for it suffices for now. Fermions move right (say) then absorb a photon, move left, and emit a photon. This results in a small loop in the frequency lattice (Fig. 4·3), and an observable associated to this motion turns out to have a quantized averaged expectation value proportional to the winding number W (Sec. 4.7.1).

4.2 Coupled layer model for the QP pump

The existence of delocalized edge states in the QP pump (Sec. 4.1) suggests it may be possible to create a kind of coupled layer construction for this phase (Fig. 4·3). By taking sites tuned to criticality—in the sense of having delocalized energy pumping modes (Sec. 4.2.1)—and coupling them so as to either cancel all pumping or leave dangling edge modes (Sec. 4.2.2), we can construct models of the trivial phase and of the QP pump, respectively.

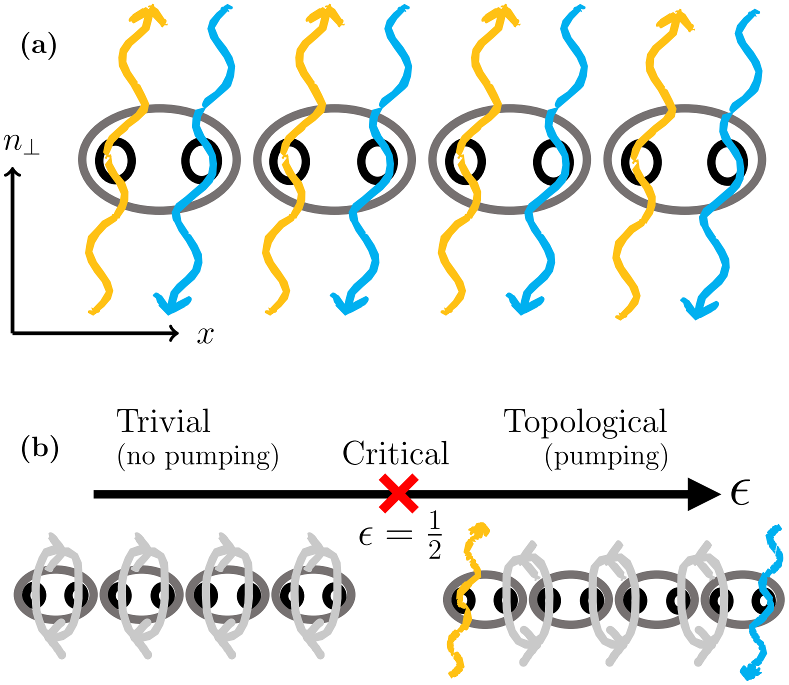

Figure 4·3: *Coupled layer model for the QP pump.*—The QP pump may be constructed from a chain of sites in a coupled layer model. (**a**) The building blocks of the model are counter-diabatically driven spinful fermionic sites. The quasienergy states of a fermion on a site pump energy between the two drives at a quantized rate. In the frequency lattice, this is a current along the $\hat{\Omega}_\perp$ direction, with coordinate $n_\perp$ (Fig. 4·4). (**b**) Coupling the sites causes the pumping modes to hybridize and localize. The tuning parameter ϵ interpolates between a trivial pattern of hybridization, where all states are localized ($\epsilon = 0$), and a topological one, where pumping modes remain at the edge ($\epsilon = 1$). Finite-size scaling (Sec. 4.3.3) suggests the model has a single critical point at $\epsilon = 1/2$.

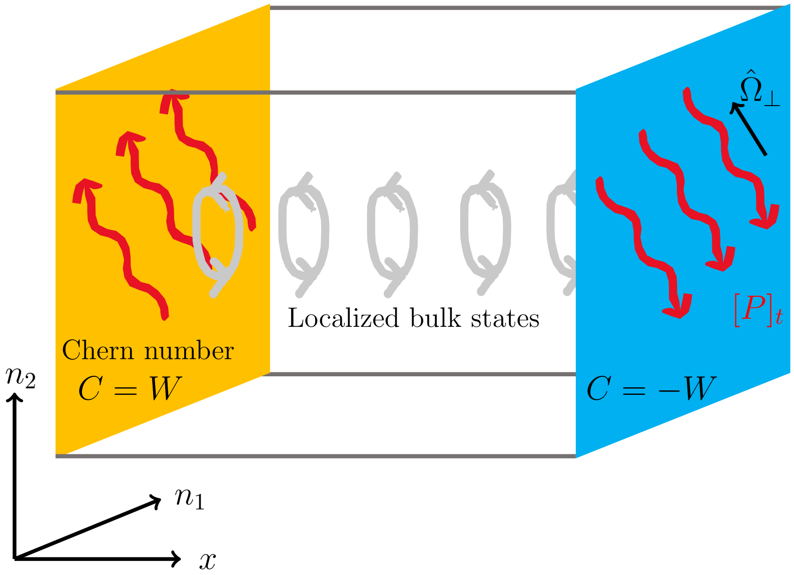
$\hat{\Omega}_\perp$
Localized bulk states
$[P]_t$
Chern number
$C = W$
$C = -W$
n_2
n_1
x

Figure 4·4: *Edge state Chern numbers.*—In the topological phase of the QP pump, the (single-particle) edge states have a Chern number in the frequency lattice. The Chern number C is given by the bulk winding number W, up to a sign depending on which edge is considered. The frequency lattice electric field $\vec{\Omega}$ induces a transverse current (along $\hat{\Omega}_\perp$) through the quantum Hall effect when one Chern state is completely filled. This is the energy pumping response of the edge, $[P]_t$. (See also Ref. [66].)

4.2.1 Sites

Generic two-tone driven few-level systems are localized in the frequency lattice when $|\vec{\Omega}| > 0$ [2, 38]. As such, they do not pump energy in the steady state. However, fine tuning in the form of an additional counterdiabatic drive can produce delocalized modes which support quantized energy pumping [38]. Such finely tuned two-level systems will form the sites of the coupled layer construction.

The model is defined in terms of a one-dimensional chain of spinful fermionic sites, with corresponding annihilation operators $c_{x\mu}$, where x labels position and μ is a spin index.

Explicitly, the Hamiltonian with L sites is

$$H_0(\vec{\theta}) = \sum_{x=0}^{L-1} c^\dagger_{x\mu} \left[-(\vec{B} + \vec{B}_{\mathrm{CD}}) \cdot \vec{\sigma}_{\mu\nu}/2 \right] c_{x\nu}, \tag{4.7}$$

where $\vec{\sigma}$ is a vector of Pauli matrices, summation over the spin indices is implied, and

$$\vec{B}(\vec{\theta}) = B_0 \left[\sin\theta_1 \hat{\mathbf{x}} + \sin\theta_2 \hat{\mathbf{y}} + (1 - \cos\theta_1 - \cos\theta_2)\hat{\mathbf{z}} \right], \tag{4.8}$$

while

$$\vec{B}_{\mathrm{CD}}(\vec{\theta}) = \frac{(\vec{\Omega} \cdot \nabla_\theta \vec{B}) \times \vec{B}}{|\vec{B}|^2} \tag{4.9}$$

is the counterdiabatic drive [136].

The counterdiabatic drive is carefully chosen so that the quasienergy states are created by

$$\begin{aligned} c^\dagger_{x+} &= \frac{1}{\sqrt{2(1+\hat{B}_z)}} \left[(1+\hat{B}_z) c^\dagger_{x\uparrow} + (\hat{B}_x + i\hat{B}_y) c^\dagger_{x\downarrow} \right], \\ c^\dagger_{x-} &= \frac{1}{\sqrt{2(1-\hat{B}_z)}} \left[-(1-\hat{B}_z) c^\dagger_{x\uparrow} + (\hat{B}_x + i\hat{B}_y) c^\dagger_{x\downarrow} \right]. \end{aligned} \tag{4.10}$$

Indeed, the counterdiabatic part $\vec{B}_{\mathrm{CD}}$ is constructed to cancel the inertial term when moving to a frame co-rotating with $\vec{B}$. The $c^\dagger_{x\pm}$ operators have the property that

$$n_{x\pm} = c^\dagger_{x\pm} c_{x\pm} = c^\dagger_{x\mu} \left[\tfrac{1}{2}(\mathbb{1} \pm \hat{B}\cdot\vec{\sigma})\right]_{\mu\nu} c_{x\nu} \tag{4.11}$$

projects onto states with a fermion on site x with its spin aligned along $\hat{B} = \vec{B}/|\vec{B}|$.

The single-particle quasienergy states $c^\dagger_{x\pm}(\vec{\theta})\,|0\rangle$ (where $|0\rangle$ is vacuum state) carry equal and opposite Chern numbers [38]. That is, the Berry curvature

$$F = \nabla_\theta \times A, \quad \text{with} \quad A = i\,\langle 0|\, c_{x\pm} \nabla_\theta c^\dagger_{x\pm}\,|0\rangle\,, \tag{4.12}$$

has a nonzero quantized integral over the torus. (The Chern number is $C = \pm 1$ when $\vec{B}$ is given by Eq. (4.8).) The quantized average energy pumping between the drives is, in frequency lattice language, the quantized Hall current induced by the electric field $\vec{\Omega}$ in the states $c^\dagger_{x\pm}(\vec{\theta})\,|0\rangle$. The $(\pm)$ modes each pump energy in a different direction—if $(+)$ pumps energy from drive 1 to 2, then $(-)$ pumps from drive 2 to 1 (Fig. 4·4; cf. Ref. [66]).

We refer to the modes $c^\dagger_{x\pm}$ as *pumping modes.*

4.2.2 Coupled layer model

To complete the coupled layer construction we must add hopping terms between the sites.

However, there is a complication because the pumping mode creation operators (4.10) cannot be defined with a smooth gauge as a function of $\vec{\theta}$. In Eq. (4.10), we have chosen a particular gauge with a phase singularity at the south pole of the Bloch sphere for $c^\dagger_{x+}$, and at the north pole for $c^\dagger_{x-}$.

The number operators are gauge invariant, and so do not have this discontinuity, but a hopping term like $c^\dagger_{x+}c_{x'-}$ will. Indeed,

$$c^\dagger_{x+}c_{x'-} = -\frac{1}{2}\sqrt{1-\hat{B}_z^2}\left[c^\dagger_{x\uparrow}c_{x'\uparrow} - c^\dagger_{x\downarrow}c_{x'\downarrow}\right. \\ \left. + \frac{-\hat{B}_x + i\hat{B}_y}{1-\hat{B}_z}c^\dagger_{x\uparrow}c_{x'\downarrow} + \frac{\hat{B}_x + i\hat{B}_y}{1+\hat{B}_z}c^\dagger_{x\downarrow}c_{x'\uparrow}\right] \tag{4.13}$$

has a phase singularity in the spin-flipping terms near $\hat{B}_z = \pm 1$. This term cannot be included in the Hamiltonian if it is not a smooth quasiperiodic function. Fortunately, the norm of the hopping term need not be constant, so one can just arrange for the hopping term to vanish when it would otherwise have a singularity. The term

$$h_{x+,x'-} = \sqrt{1-\hat{B}_z^2}\, c^\dagger_{x+}c_{x'-} \tag{4.14}$$

has no singularity, and is proportional to the desired hop.

The full coupled layer Hamiltonian consists of three terms,

$$H(\vec{\theta}) = H_0 + H_{\text{dis}} + H_{\text{hop}}. \tag{4.15}$$

The single-site part H_0 is defined in Eq. (4.7).

The hopping term, written for open boundary conditions as

$$H_{\text{hop}} = J\sum_{x=0}^{L-2}(1-\epsilon)h_{x+,x-} + \epsilon h_{(x+1)+,x-} + J(1-\epsilon)h_{(L-1)+,(L-1)-} + \text{H.c.}, \tag{4.16}$$

couples a $(+)$ mode to a $(-)$ mode, either within a site or between sites (Fig. 4·3). The tuning parameter ϵ, which controls how large intersite hops are compared to intrasite hops, is the main variable of concern. All other parameters of the model will typically be fixed. H_{hop} should be regarded as a Su-Schrieffer-Heeger (SSH) hopping term in a quasiperiodically rotating frame [137].

Finally, the disorder term

$$H_{\text{dis}} = \sum_{x=0}^{L-1} \delta_{x+} n_{x+} + \delta_{x-} n_{x-} \tag{4.17}$$

ensures the localization of fermions in the model [67, 68]. Each $\delta_{x\pm}$ is taken to be uniformly random in $\pm\Delta + [-\delta, \delta]$. We have included an on-site splitting of 2Δ for greater control over the localization properties of the model (Sec. 4.3.2).

Inspection of the limits $\epsilon \in \{0, 1\}$ reveals the properties of this model. When $\epsilon = 0$, the Hamiltonian (4.15) does not couple different sites and so is topologically trivial for any $J \neq 0$ ($W = 0$)—it is an atomic insulator. On the other hand, when $\epsilon = 1$ and with open boundary conditions, the edge modes n_{0+} and n_{L-} are uncoupled, and thus each pumps energy between the drives ($W = 1$ when $\vec{B}$ is given by Eq. (4.8)) (Figs. 4·3 and 4·4). Between these two limits, the edge states are deformed away from being perfectly localized to a single site, but cannot be destroyed unless the bulk delocalizes in either real space or in the synthetic dimensions, or both.

With periodic boundary conditions, the ensemble of Hamiltonians also has a duality

$$\epsilon \mapsto 1 - \epsilon, \quad c_{x+} \mapsto c_{x-}, \quad c_{x-} \mapsto c_{(x+1)+}, \tag{4.18}$$

which maps topological phases to trivial phases, and vice versa. Thus, if there is a unique critical point between these phases, it must be at the self-dual point $\epsilon = \epsilon_c = 1/2$.

We note that the coupled layer construction also makes the bulk circulation of energy in the QP pump intuitive (Sec. 4.1). When pumping modes between different sites are coupled, they (at a cartoon level) hybridize into small circulating loops (Fig. 4·3). This is the bulk energy circulation.

4.3 Numerical Characterization

The edge states of model (4.15) can be found exactly when $\epsilon = 1$. They are created by $c^\dagger_{0+}$ and $c^\dagger_{(L-1)-}$. At $\epsilon = 0$ all couplings are intrasite, and the phase is trivial. At $\epsilon = 1/2$ the model is self-dual, and cannot be localized. Away from these limits, we resort to numerics to find properties of the coupled layer model (4.15).

The steady states of localized quasiperiodically driven models may be extracted through exact diagonalization of the frequency lattice quasienergy operator (2.16). This method is resource-intensive. It requires expanding the Hilbert space with the auxiliary drive states $|\vec{n}\rangle$ and truncating the frequency lattice Hilbert space. We will instead focus on observables that can be measured from real time dynamics using a numerical solution of the Schrödinger equation (for which we use the ordinary differential equation methods of QUSPIN [5, 6]), namely, the lattice site occupation numbers and the energy transferred between the drives (more precisely, the work done on the system by the drives (4.3)).

Our numerics recover expected properties of the topological and trivial phases of the QP pump, including localization and the pumping of energy at the edge (Sec. 4.3.1). Finite-size scaling analysis of the energy transferred between the drives finds a scaling collapse consistent with a single critical point (Sec. 4.3.3). The phenomenology and critical exponents of the transition suggest it lies in the universality class of the two-dimensional quantum Hall transition.

4.3.1 Phases

Localization underlies our understanding of the QP pump. To probe localization numerically, we compute the lattice site occupation numbers of an initially localized fermion:

$$n_x(t) = \langle\psi_0(t)|\,(c^\dagger_{x\uparrow}c_{x\uparrow} + c^\dagger_{x\downarrow}c_{x\downarrow})\,|\psi_0(t)\rangle\,. \tag{4.19}$$

Here, $|\psi_0(0)\rangle = c^\dagger_{0\uparrow}|0\rangle$ is the initial state with one spin up fermion at $x = 0$, $|\psi_0(t)\rangle$ is the corresponding time evolved state under Hamiltonian (4.15), and $c^{(\dagger)}_{x\mu}$ is a fermion annihilation (creation) operator at site x and with spin μ. Calculations of $n_x(t)$ are performed with periodic boundary conditions to avoid the effects of the pumping edge modes.

The typical late time value of $n_x(t)$ is computed as

$$\ln[n_x]_{\mathrm{typ}} = \left[\frac{2}{T}\int\limits_{T/2}^{T} \mathrm{d}t \ln n_x(t)\right]_{\mathrm{dis}} , \tag{4.20}$$

where $[\cdot]_{\mathrm{dis}}$ denotes an average over the disorder realization $\{\delta_{x\pm}\}$ and initial phase $\vec{\theta}_0$, and T is a time much larger than all inverse energy scales in the problem. We use the typical value (geometric mean) for n_x as a forward scattering approximation predicts that n_x is log-normally distributed across disorder realizations for fixed x [68]. This makes the typical value a more meaningful estimate for the center of the distribution.

The occupation $\ln[n_x]_{\mathrm{typ}}$ is plotted for several different values of ϵ in Fig. 4·5(a).

Many features of $[n_x]_{\mathrm{typ}}$ follow from the coupled layer construction, or standard results in the theory of Anderson localization [67, 68]. When $\epsilon \in \{0, 1\}$, the model is perfectly localized—the occupations $n_x(t)$ can only be nonzero for $x = 0$ in the trivial phase, or $x \in \{0, \pm 1\}$ in the topological phase.

As ϵ is moved away from these limits, $[n_x]_{\mathrm{typ}}$ remains exponentially decaying in $|x|$, but the localization length ζ increases. Standard estimates from Anderson localization give that $\zeta^{-1} = O(\ln t/\delta)$, where t is a hopping amplitude, δ is the disorder strength, and $t \ll \delta$. The coupled layer model has modulated strong and weak hops between pumping modes, so it is more meaningful to use an amplitude associated to double hops spanning both a weak and strong bond—from n_{x+} to $n_{(x+1)+}$. Second order perturbation theory predicts that this effective hopping is proportional to $t =$

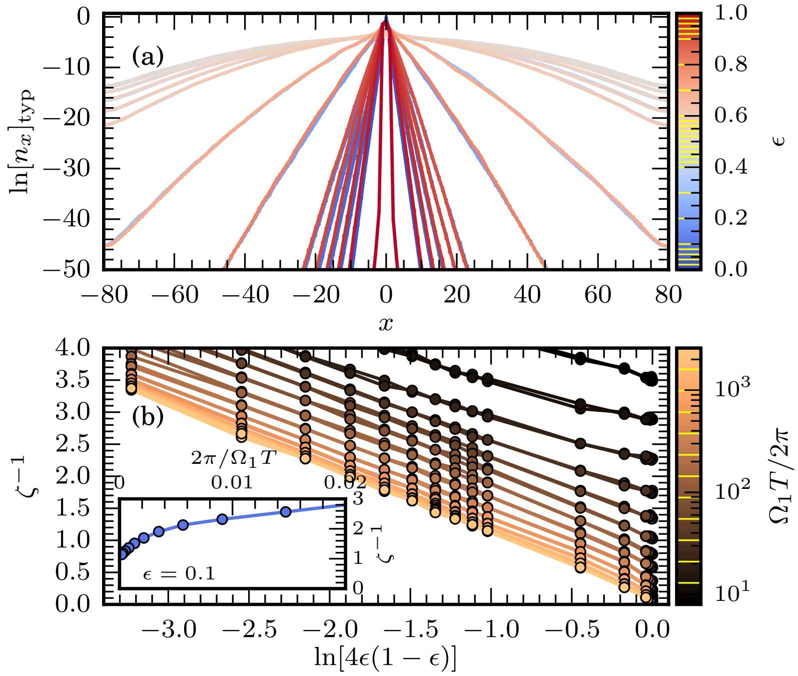

Figure 4·5: *Localization in the coupled layer model.*—(**a**) The typical occupation $\ln[n_x]_{\rm typ}$ decays for different ϵ. There is clear exponential decay for small $\epsilon(1-\epsilon)$. When $\epsilon \approx 1/2$ is close to the critical value, the late time $\ln[n_x]_{\rm typ}$ has not yet converged, and appears parabolic in x, indicative of diffusive dynamics. (**b**) Fitting the localization length from the decay of $\ln[n_x]_{\rm typ} \sim -2x/\zeta$ shows the expected $1/\ln[\epsilon(1-\epsilon)]$ scaling. **Inset**: For small $\epsilon(1-\epsilon)$, ζ^{-1} converges to a nonzero value as T is increased. *Parameters:* $L = 160$ with periodic boundaries, $B_0/\Omega_1 = 1$, $\Omega_1/\Omega_2 = (1+\sqrt{5})/2$, $\Omega_1 T/(2\pi) = 2584$, $\delta/\Omega_1 = 0.09$, $\Delta/\Omega_1 = 0.7$, and $J/\Omega_1 = 0.305$. 300 disorder configurations and initial phases are used for averages in $\ln[n_x]_{\rm typ}$, with plotted error bars giving one standard error of the mean (often too small to be visible). Values of ϵ and T used are marked in yellow in the color bars.

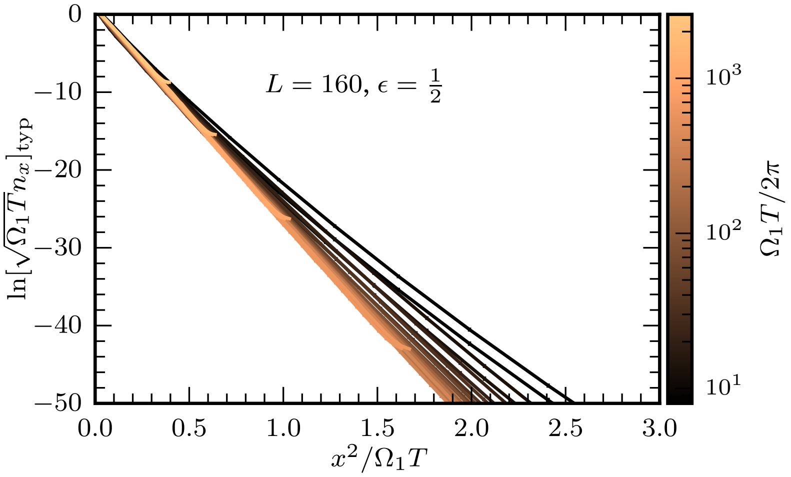

Figure 4·6: *Data collapse in site occupations.*—Rescaling x^2 by time (T, the integration time (4.20)) produces data collapse in $\ln[n_x]_{\rm typ}$ at $\epsilon = 1/2$, consistent with diffusive dynamics (4.22). The collapse is improved by including the subleading correction predicted by diffusion, $\frac{1}{2}\ln \Omega_1 T$. *Parameters:* $\epsilon = 1/2$, and as in Fig. 4·5.

$J^2\epsilon(1-\epsilon)/\Delta$. Thus

$$\zeta^{-1} = O\left(\ln\left[\frac{J^2}{\Delta\delta}\epsilon(1-\epsilon)\right]\right) \quad \text{for} \quad \frac{J^2}{\Delta}\epsilon(1-\epsilon) \ll \delta. \tag{4.21}$$

We see this scaling in Fig. 4·5(b).

Close to the self-dual point $\epsilon = 1/2$, $\ln[n_x(t)]_{\rm typ}$ appears parabolic at numerical time scales:

$$\ln[n_x(t)]_{\rm typ} \sim -\frac{x^2}{Dt}, \tag{4.22}$$

with some $D > 0$. Indeed, rescaling x^2 by t produces data collapse in $\ln[n_x(t)]_{\rm typ}$ for small x^2/t (Fig. 4·6).

Equation (4.22) is characteristic of a diffusive regime in dynamics. The finite-size scaling analysis of Sec. 4.3.3 suggests that for $\epsilon \neq 1/2$, this diffusive behavior is a finite-size effect associated to an isolated critical point, rather than a diffusive phase.

While localization is vital for the stability of the QP pump, it does not reveal its topological properties. The energy transferred between the drives is the interest-

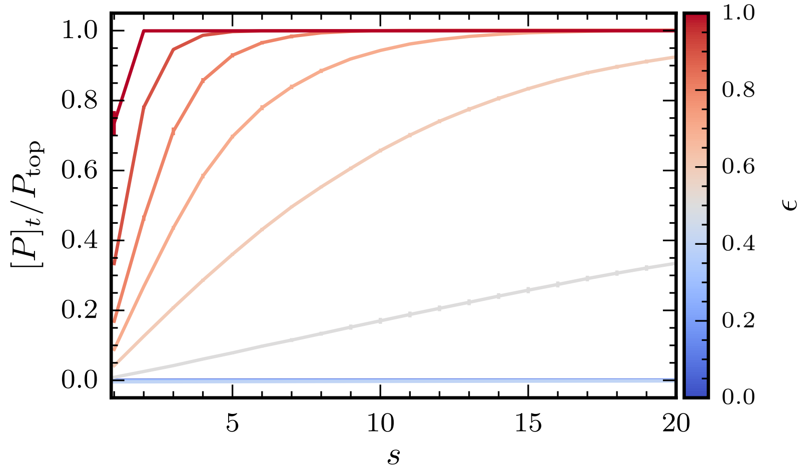

Figure 4·7: *Edge modes in the coupled layer model.*—The topological edge modes responsible for pumping are exponentially localized. This is revealed by computing the dependence of the average pumping rate $[P]_t$ on the filling s (Fig. 4·2). $[P]_t$ converges exponentially to its topological value $P_{\mathrm{top}}W$ outside a critical region around $\epsilon = 1/2$. *Parameters:* As in Fig. 4·5, but with open boundary conditions. $[P]_t$ is averaged over 200 disorder and initial phase samples. $\epsilon \in [0, 1]$ is taken in steps of 0.1. (Note that all curves with $\epsilon \leq 0.4$ overlap.)

ing observable in this context, and it is this we use to numerically demonstrate the presence of the topological phase. Specifically, the order parameter in Fig. 4·2 is the average rate of energy transfer between the drives, $[P]_t$ (4.4).

To numerically measure $[P]_t$, we integrate the expectation value of $P(t) = -\Omega_2 \partial_{\theta_2} H$ (Eq. (4.3)), which gives the power transferred into the drive of frequency Ω_2. The total work done on this drive is

$$\Delta E_2(t) = \int_0^t \mathrm{d}t' \ \mathrm{Tr}\, P(t')\rho(t'), \tag{4.23}$$

where $\rho(t')$ is a time evolved state.

The initial state $\rho(0)$ would, ideally, be the pumping mode itself. This is difficult to prepare, and even numerically we do not know its precise form. However, as the pumping mode is localized near the edge, taking $\rho(0) = \rho_s$, the Slater-determinant state with the first s sites near the edge filled (Fig. 4·2(a)), ensures the pumping mode is completely occupied, up to an exponentially small weight outside the range s (Fig. 4·7). No other modes pump, except the edge mode at the opposite edge, so all pumping is due to the occupied edge mode. Thus, one expects to find

$$\Delta E_2(t) = P_{\text{top}} W t + O(e^{-s/\zeta}, t^0) \tag{4.24}$$

when $\rho = \rho_s$. (In fact, one may also populate any additional sites in the bulk much further than ζ from the edges. This does not affect the average pumping rate, but our numerics do not use such states.)

The late time average $\Delta E_2/t$ converges to $[P]_t$, but several numerical techniques can make the estimation of $[P]_t$ more reliable. While Eq. (4.24) holds in each disorder realization and for any initial phase $\vec{\theta}_0$, averaging $\Delta E_2(t)$ over disorder and initial phase reduces the subleading corrections for finite s and t. Then, fitting the late time data (we use the last half of the observed time series) to a straight line provides an estimate for the average pumping rate $[P]_t$ which biases the longest time scales.

In Fig. 4·2(b), we find that $[P]_t$ is quantized to the expected topological values of 0 (small ϵ) or 1 (large ϵ) outside of a critical region near the self-dual point ($\epsilon = 1/2$). Further, this critical region sharpens with increasing L and s, suggesting the smooth crossover could be a finite size effect. The exponential convergence of $[P]_t$ to the quantized value with increasing s is shown in Fig. 4·7.

4.3.2 Frequency Lattice Localization

Anomalous localized topological phases (ALTPs) are localized in real space, but also in the synthetic dimensions. The numerics of this chapter use carefully chosen values of the model parameters for which states are well localized in both the spatial and synthetic dimensions.

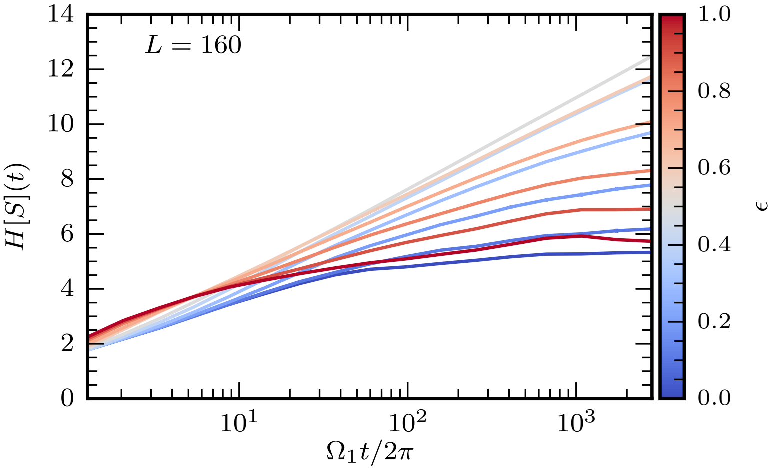

Figure 4·8: *Spectral entropy in the coupled layer model.*—The average spectral entropy $H[S](t)$ grows logarithmically with the observation time t in a delocalized phase. Deep in the localized phase, away from $\epsilon = 1/2$, $H[S](t)$ saturates at a finite value. The finite size scaling analysis of Sec. 4.3.3 suggests that all $H[S](t)$ curves except that for $\epsilon = 1/2$ will saturate. *Parameters:* As in Fig. 4·5, except $\delta/\Omega_1 = 0.15$. The spacing $\mathrm{d}t$ between time points used in $C_{ab}(x,t)$ when computing the Fourier transform is $\Omega_1 \mathrm{d}t = 0.1$. Error bars are typically smaller than the line width.

To numerically quantify the extent of eigenstates in both the spatial and synthetic dimensions we used an *average spectral entropy*, $H[S](t)$ [38]. This does not require us to solve for the quasienergy states—the definition only depends on the values of correlation functions.

First, define the single-particle states

$$|z_0\rangle = c^\dagger_{0\uparrow}|0\rangle\,,\ |x_0\rangle = \tfrac{1}{\sqrt{2}}(c^\dagger_{0\uparrow} + c^\dagger_{0\downarrow})\,|0\rangle\,, \text{and}\ |y_0\rangle = \tfrac{1}{\sqrt{2}}(c^\dagger_{0\uparrow} + ic^\dagger_{0\downarrow})\,|0\rangle\,, \tag{4.25}$$

(with time evolved states $|\alpha_0(t)\rangle$) and the quadratic local observables

$$\Sigma^\alpha_x = \sigma^\alpha_{\mu\nu} c^\dagger_{x\mu} c_{x\nu}. \tag{4.26}$$

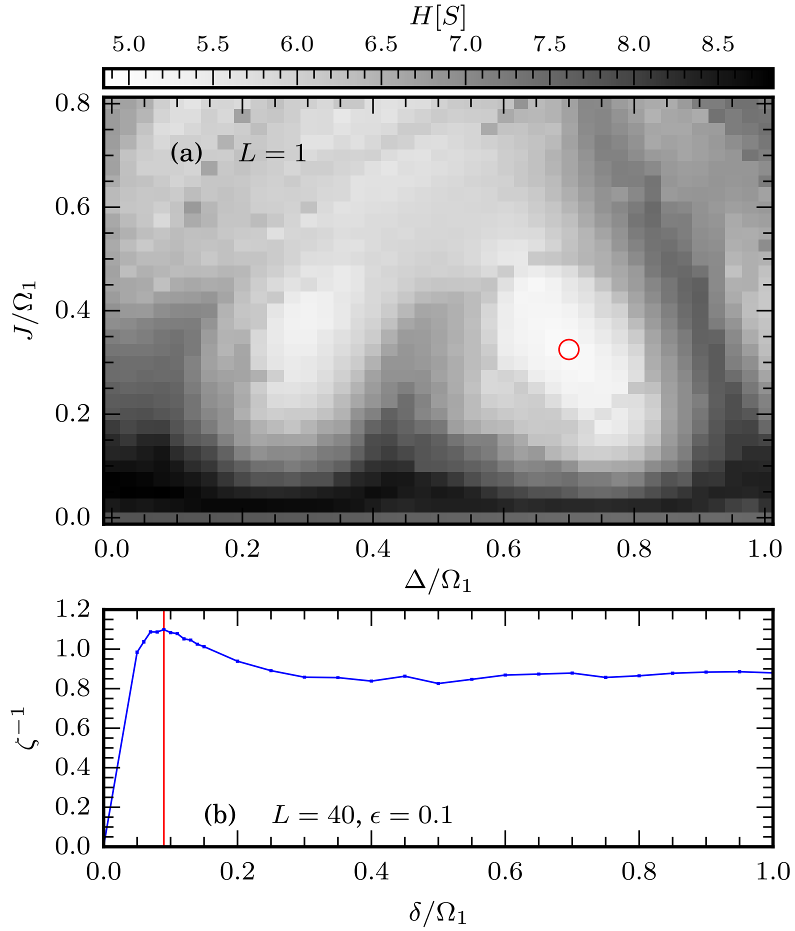

Figure 4·9: *Parameters in the coupled layer model.*—(**a**) Working parameters for J and Δ are found by minimizing the average spectral entropy $H[S]$ in the single-site problem. The optima are found to be $J/\Omega_1 \approx 0.305$ and $\Delta/\Omega_1 \approx 0.7$ (red circle). (**b**) The disorder strength δ is subsequently optimized by minimizing the localization length (as measured in Fig. 4·5) in an extended chain. The optimum is found to be $\delta/\Omega_1 \approx 0.09$ (red line). Note that in no case is the localization behavior monotonic in these parameters. *Parameters:* $\epsilon = 0.1$. (**a**) The maximum observation time for $C_{\alpha\beta}$ is $\Omega_1 t/2\pi \approx 2800$, $L = 1$, $B_0/\Omega_1 = 1$. (**b**) $L = 40$, periodic boundary conditions.

Then the correlation functions

$$C_{\alpha\beta}(x,t) = \langle\alpha_0(t)|\, \Sigma_x^\beta \,|\alpha_0(t)\rangle \tag{4.27}$$

probe both the spatial extent of a particle initialized at position $x = 0$ and its time dependent evolution within a single site. A large frequency lattice localization length is indicated in $C_{\alpha\beta}(x,t)$ by quasiperiodic oscillations with significant weight in many harmonics.

More precisely, the power spectrum

$$S_{\alpha\beta}(x,\omega) = |\mathcal{F}\{C_{\alpha\beta}\}(x,\omega)|^2 \tag{4.28}$$

will have support on many x and ω if the frequency lattice extent is large (where $\mathcal{F}\{\cdot\}$ is the Fourier transform with respect to time). On the other hand, if the quasienergy states are localized then *all* power spectra $S_{\alpha\beta}$ should only have significant weight on a few x and ω.

To be sensitive to delocalization in any observable, we use the averaged power spectrum

$$S(x,\omega) = \frac{1}{9} \sum_{\alpha,\beta\in\{x,y,z\}} S_{\alpha\beta}(x,\omega). \tag{4.29}$$

The extent of the support of S is quantified by its (Shannon) entropy,

$$H[S] = -\sum_{x,\omega} p(x,\omega) \ln p(x,\omega), \tag{4.30}$$

where,

$$p(x,\omega) = S(x,\omega)/\sum_{x',\omega'} S(x',\omega'). \tag{4.31}$$

Numerically, we can only compute S at finitely many points in x and ω. Delocalization is revealed by an unbounded growth of $H[S]$ when the system size and integration time are increased. We will denote the average spectral entropy with an explicit time dependence, $H[S](t)$, to emphasize this (Fig. 4·8).

Even a single site can have infinite extent in the frequency lattice when driven quasiperiodically. To determine working values for the hopping strength J (4.16) (H_{hop} has an on-site component which flips $(\pm)$ pumping states to $(\mp)$ states) and the on-site detuning Δ (4.17), we computed $H[S](t)$ for a fine grid of values and a fixed large t (Fig. 4·9).

Note that $H[S]$ is not monotonic with either Δ or J. Indeed, taking $J \to 0$ produces quasienergy states which have a Chern number, which must be delocalized. On the other hand, taking any energy scale much larger than $|\vec{\Omega}|$ produces a model in the frequency lattice where the hopping terms are much larger than the inhomogeneity, which tends to delocalize. The optimal values of Δ and J are both $O(1)$:

$$J/\Omega_1 \approx 0.305, \quad \Delta/\Omega_1 \approx 0.7. \tag{4.32}$$

Of course, the spatial disorder strength δ (Eq. (4.17)) also controls the localization properties of the extended model with $L > 1$. With J and Δ fixed as in Eq. (4.32), we can subsequently find a working value for δ by minimizing the localization length ζ, as computed in Fig. 4·5 for fixed $\epsilon = 0.1$. Again, the localization length is not a monotonic function of the disorder. The optimal value is found to be

$$\delta/\Omega_1 \approx 0.09. \tag{4.33}$$

For these parameters, the spatial localization length is roughly one lattice site. This can be made smaller still by tuning $\epsilon(1-\epsilon)$ closer to zero.

4.3.3 Critical point

In several numerical studies of the QP pump, it has not been clear whether the topological and trivial phases are separated by an isolated critical point, or an intervening critical phase [1, 65]. The coupled layer model enjoys a self-duality which fixes a value that must be delocalized, $\epsilon = 1/2$, and simplifies finite-size scaling analysis. Our findings are consistent with $\epsilon = 1/2$ being an isolated critical point.

The dynamical exponent, z, describes the scaling relationship between length and time at the critical point. Prompted by the parabolic shape of late time $\ln[n_x(t)]_{\text{typ}}$, it is natural to suspect that the critical point is diffusive, with $z = 2$ [138].

If, indeed, $z = 2$, rescaling time as t/x^2 (with x some length scale) should produce data collapse in observable quantities. The length scale we rescale by is s, the finite extent of the initial Slater-determinant state. The observable we inspect is $\Delta E_2(t, s, \epsilon)$ (noting the dependence on s and ϵ explicitly). (Rescaling x^2 by t in $\ln[n_x(t)]$ also produces data collapse as in Eq. (4.22); see Fig. 4·6)

Fig. 4·10(a) shows that the measured $\Delta E_2(t, s, \epsilon = 1/2)$ is consistent with the scaling form

$$\Delta E_2(t, s, \epsilon = 1/2) \sim s^z \mathcal{E}_2(t/s^z) \tag{4.34}$$

with $z = 2$. With this scaling relation, the lines $\Delta E_2 \propto t$ are fixed. Additionally, well before the time scale for diffusion by length s, $\Omega_1 t/s^2 \ll 1$,[1] the rate of pumping is precisely half the quantized value:

$$\Delta E_2(t, s, \epsilon = 1/2) \sim P_{\text{top}} t/2, \quad \Omega_1 t/s^2 \ll 1. \tag{4.35}$$

By making s larger, this half-integer pumping can be made to persist for an arbitrarily long time.

If the $\epsilon = 1/2$ critical point is isolated, then a nonzero value of $\epsilon - 1/2$ introduces a finite localization length ζ. The divergence of ζ defines another important critical

---

[1] In identifying s^2/Ω_1 as the timescale for diffusion by length s, we assume that the diffusion constant is set by dimensional analysis: $D = O(a^2\Omega_1)$, where a is the lattice constant. Fig. 4·10(a) indicates $\Omega_1 t/s^2 \ll 1$ is sufficient to see half-quantized pumping, from which we infer that diffusion away from the edge is limited on this timescale.

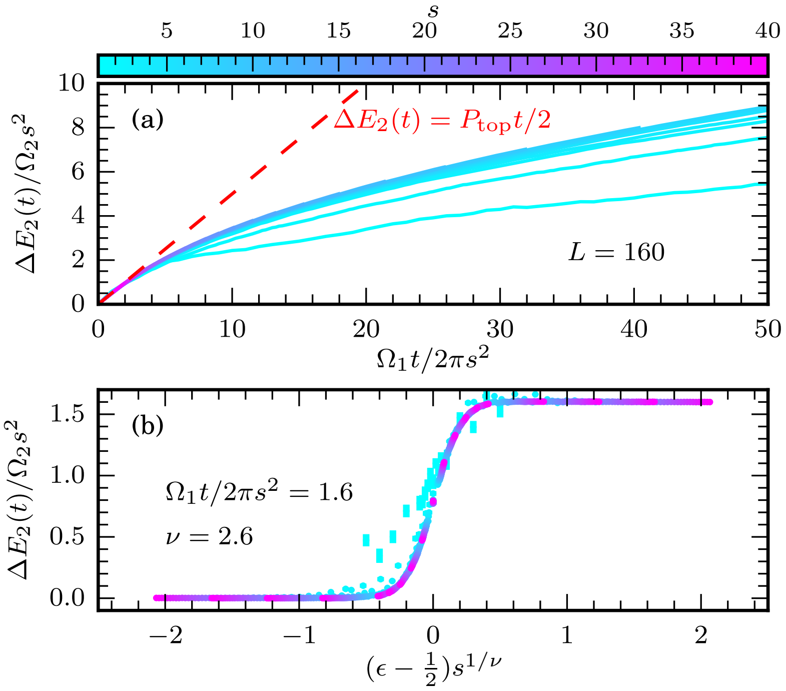

Figure 4·10: *Finite-size scaling collapse around the critical point.*— (**a**) Rescaling t by s^2 at the critical point $\epsilon = \epsilon_c = 1/2$ collapses the energy curves $\Delta E_2(t)$, showing that the critical point is diffusive (dynamical exponent $z = 2$). At short times, $\Omega_1 t/2\pi s^2 \ll 1$, the average power is half the topological value. (**b**) Rescaling $\epsilon - 1/2$ by $s^{1/2.6}$ produces a good data collapse for E_2 at fixed $\Omega_1 t/2\pi s^2$ and large s, consistent with the critical exponent ν for the two-dimensional quantum Hall effect transition. *Parameters:* As in Fig. 4·5 with open boundary conditions. $\Delta E_2(t)$ is averaged over 200 disorder and initial phase samples.

exponent, ν:

$$\zeta \sim A(\epsilon - \tfrac{1}{2})^{-\nu}. \tag{4.36}$$

We assess a corresponding scaling form for $\Delta E_2(t, s, \epsilon)$,

$$\Delta E_2(t, s, \epsilon) \sim s^z \mathcal{E}_2(t/s^z, (\epsilon - \tfrac{1}{2})s^{1/\nu}). \tag{4.37}$$

There is a relatively broad range of $\nu \in [2.2, 2.8]$ which produce acceptable collapse in our data. The particular value $\nu = 2.6$ is shown in Fig. 4·10(b). Beyond some small s transient behavior, all rescaled data lie on the same curve.

The scaling form (4.37) with any positive ν suggests that keeping s/L fixed and taking $s \to \infty$ faster than $\sqrt{t}$ sharpens the curve for $[P]_t$ in Fig. 4·2 to a step function. (In Fig. 4·2, $t = T$ is taken to be a large fixed value.) Further, there is a unique critical point with diffusive dynamics and a half-integer energy current, $[P]_t = P_{\text{top}}/2$.

We note that half-integer quantization of the topological response has long been recognized in the context of the integer quantum Hall effect [139–143], and more recently in the analogous setting of quasiperiodically driven spins [28, 64]. In the quantum Hall context, the analogous quantity to the pumping rate is the Hall conductivity σ_{xy}, the scaling theory for which predicts an unstable half-integer fixed point at the transition [139–143]. For noninteracting particles, the critical point is also diffusive ($z = 2$), with a critical exponent for the divergence of the correlation length $\nu = 2.593 \pm 0.005$ [144–146].

The quantum Hall phenomenology is consistent with our observations in Fig. 4·10. It is tantalizing to make strong comparisons between the integer quantum Hall transition and the QP pump transition, especially given the cartoons for the QP pump in Figs. 4·3 and 4·4.

Nonetheless, a precise argument indicating that the QP pump transition is in the universality class of the two-dimensional integer quantum Hall transition remains elusive. Quantum Hall systems and the QP pump share a similar coupled layer construction (Fig. 4·3), but the disorder along $\hat{\Omega}_\perp$ in the QP pump is correlated [2]. This may alter critical exponents compared to those with uncorrelated disorder.

Further, comparing $[P]_t$ and σ_{xy} in the picture of Fig. 4·3 is problematic—σ_{xy} is defined in terms of linear response, while $[P]_t$ arises from edge physics in the coupled layer picture. Especially at the transition, it becomes unclear why a half-integer σ_{xy} should relate to a half-integer $[P]_t$. Recent work has explored the presence and nature of edge states at the transitions between topological phases, including in quantum Hall systems [147–149]. However, a complete understanding of the edge state properties has not yet been achieved.

4.4 Effect of Interactions

The QP pump is proposed to be an infinitely long lived phase of matter even with weak interactions [1, 2] (chapter 5). Localization is essential here, as it protects the system from absorbing energy from the drives and heating to a featureless infinite temperature state [69, 70, 150]. While the asymptotic stability of localization in interacting strongly disordered systems has recently been brought into debate [72–77, 151–153], it remains universally accepted that such systems remain localized for a sufficiently long time to give rise to prominent *prethermal* regimes [154]. The existence of such a prethermal regime also extends to quasiperiodically driven systems [33].

Topological pumping persists when adding weak interactions to the coupled layer model (Fig. 4·11). In the parameter regimes accessible by our numerics, this behavior is prethermal. It persists for a long, but finite, time in any finite size system.

We consider the time-dependent interaction (recall that the pumping mode number operators $n_{x\pm}(\vec{\theta})$ depend quasiperiodically on time, Eq. (4.11))

$$H_{\text{int}}(\vec{\theta}) = U \sum_{x=0}^{L-1} \left[n_{x+}n_{x-} + n_{x-}n_{(x+1)+} \right], \tag{4.38}$$

which preserves the self-duality of model (4.15). This ensures that any localized trivial phase with $\epsilon < 1/2$ must be mirrored by a localized topological phase with $\epsilon > 1/2$.

Fig. 4·11(a) shows that the transferred energy $\Delta E_2(t)$ in the interacting model $H + H_{\text{int}}$ is extremely close to the noninteracting prediction. Even after 1000 cycles of the first drive, only around 5 of the expected 1000 energy quanta have not been pumped into drive 2.

However, the model is delocalized for the parameters in Fig. 4·11. Localization in the interacting model can be assessed by measuring the half-cut entanglement entropy, S_{ent}, for an initial product state. In a localized phase, S_{ent} should increase logarithmically until it eventually saturates due to finite-size effects [155–157]. Fig. 4·11(b) shows that S_{ent} appears to increase faster than logarithmically prior to finite-size saturation, indicating that the system is not localized in accessible parameter regimes.

This lack of localization can be understood through the analysis of Ref. [2] (chapter 5). Reference [2] finds that the QP pump is stable, even with interactions, provided that the many-body localization length ξ is below a critical value[2]

$$\xi \leq \xi_c = (2 \ln 4)^{-1}. \tag{4.39}$$

The noninteracting coupled layer model is arbitrarily well-localized for $\epsilon(1-\epsilon) \ll 1$, but Eq. (4.21) and Fig. 4·5 show that the single-particle localization length only approaches zero logarithmically. Comparison of Fig. 4·5 to Eq. (4.39) shows that $\epsilon \lesssim 0.05$ (or $1 - \epsilon \lesssim 0.05$) is necessary to have $\zeta < \xi_c$. Further, even $\epsilon \lesssim 0.05$ is

---

[2] Here, we are taking the local Hilbert space dimension to be 4, as is appropriate for spinful fermions, unlike Ref. [2], which considered qubit chains.

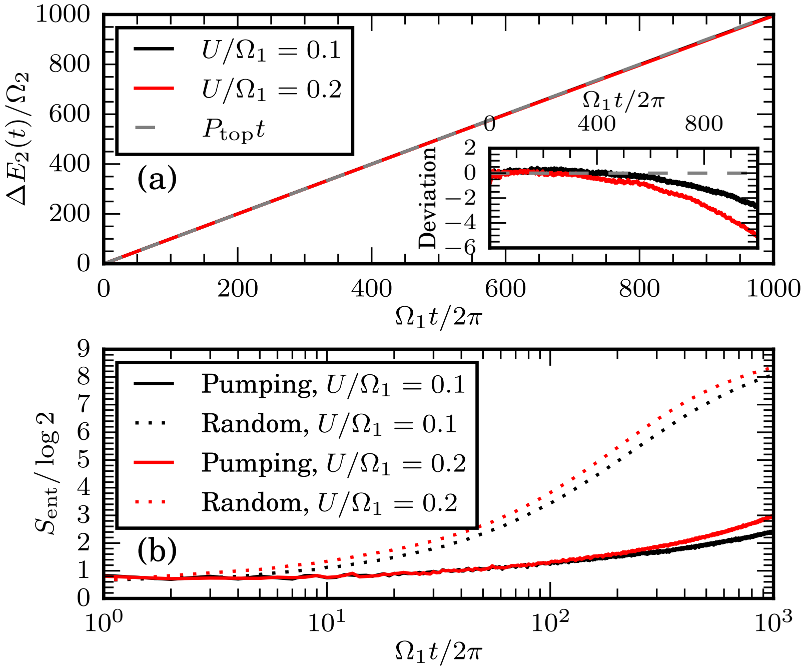

Figure 4·11: *Interactions in the coupled layer model.*—(**a**) The energy pumped into drive 2 is very close to the topological value $\Delta E_2(t) = P_{\rm top}t$, even with nonzero interaction strength U. This indicates the existence of a long-lived prethermal regime where topological pumping persists. (**b**) Nonetheless, these parameter values are delocalized. The half-cut entanglement entropy, $S_{\rm ent}$, increases faster than logarithmically to its saturation value in a random initial product state, indicative of thermalization. The pumping state with s sites filled from the $x = 0$ edge, which is far from random, thermalizes much slower. *Parameters:* $L = 10$, $s = 5$, $\Omega_1 T/2\pi = 1000$, $\epsilon = 0.9$. $\Delta E_2(t)$ and $S_{\rm ent}$ are averaged over 200 samples of initial product states, disorder realizations and initial phases. All other parameters as in Fig. 4·5.

likely an overestimate for the stability of localization. Interactions should be expected to renormalize ζ significantly when calculating the many-body localization length ξ. Thus, very small values of ϵ would be required to observe asymptotic many-body localization (MBL) in the coupled layer model. This is problematic in finite time numerics, as an integration time of many times $2\pi/\epsilon$ is required to observe the effects of the hopping term, and thus even have the possibility of observing thermalization.

Part of the reason for the extremely long lifetime of pumping is the highly non-thermal initial state, ρ_s, in which the system is prepared. It takes much longer for the fermions to diffuse from the left-hand side (say) of the system to uniformity than it does for a random initial distribution to thermalize. This can be seen by comparing the half-cut entanglement entropy of the pumping initial state to a random product state (Fig. 4·11(b)). The entropy in the random state increases faster than logarithmically to its saturation value, while the pumping state entropy increases very little on the observed timescale.

4.5 General Construction

Any $(1 + D)$-dimensional ALTP can be constructed through coupled layers, as in Sec. 4.2. With a careful coupling of critically tuned sites driven by D incommensurate frequencies, these models retain the self-duality properties from the $D = 2$ case.

The uncoupled starting point of the construction is formally similar to Sec. 4.2:

$$H_0(\vec{\theta}) = \sum_{x=0}^{L-1} c^{\dagger}_{x\mu} \left[-(\vec{B} + \vec{B}_{\mathrm{CD}}) \cdot \vec{\Gamma} \right]_{\mu\nu} c_{x\nu}. \tag{4.40}$$

In the new context, $\vec{\theta}$ is a vector of D drive phases, with the corresponding vector of frequencies $\vec{\Omega}$; the Γ_j give some convenient operator basis for the single-site Hamiltonian; and B_j and $B_{\mathrm{CD},j}$ are their coefficients. The eigenvalues of $-\vec{B}(\vec{\theta}) \cdot \vec{\Gamma}$ form continuous *bands* as a function of $\vec{\theta}$. This structure is analogous to the band theory of solids, where $\vec{k}$ (the crystal momentum) plays the same role as $\vec{\theta}$.

The uncoupled model (4.40) can be fine tuned to possess chiral topological states. When the number of tones $D = 2n$ is even, $\vec{B}(\vec{\theta})$ can be chosen so that the projector p_- onto the eigenstates of $-\vec{B}(\vec{\theta}) \cdot \vec{\Gamma}$ with negative energy—the *lower bands*—has a nonzero nth Chern number, C_n [158]. (We will give a particular example for the second Chern number below.) Then, $\vec{B}_{\mathrm{CD}}(\vec{\theta})$ should be chosen to eliminate excitations between the lower and upper bands induced by the drive. Writing p_- for the projector onto the lower bands, the necessary and sufficient condition for the suppression of excitations out of the lower bands is [136]

$$[-i\partial_t B_j \Gamma_j + [B_k \Gamma_k, B_{\mathrm{CD},l} \Gamma_l], p_-] = 0, \tag{4.41}$$

(where summation is implied). This gives a linear equation for $B_{\mathrm{CD},l}$ in terms of $B_j(\vec{\theta})$ and the coefficients f_{jkl} in an expansion of the commutator $[\Gamma_k, \Gamma_l] = f_{jkl}\Gamma_j$.

$$(i\vec{\Omega} \cdot \nabla_\theta B_j + B_k B_{\mathrm{CD},l} f_{jkl})[\Gamma_j, p_-] = 0 \tag{4.42}$$

Solutions to this equation are not unique.

Now the sites must be coupled. A generic hopping between sites will typically allow for a localized phase, but to unambiguously identify the edge state in some limit the coupling must be carefully chosen. We denote the $\vec{\theta}$-dependent fermion annihilation operators in each band as $c^{\pm}_{x\mu}(\vec{\theta})$ with a superscript ± depending on whether the band has positive or negative energy in $-\vec{B} \cdot \vec{\Gamma}$. The definition of these operators require a choice of gauge, which cannot be smooth if any Chern number is nonzero. The hopping term between sites is, with open boundary conditions,

$$H_{\text{hop}} = J_{\mu\nu}(\vec{\theta}) \sum_{x=0}^{L-2} (1-\epsilon) c^{+\dagger}_{x\mu} c^{-}_{x\nu} + \epsilon c^{+\dagger}_{(x+1)\mu} c^{-}_{x\nu} + J_{\mu\nu}(\vec{\theta})(1-\epsilon) c^{+\dagger}_{(L-1)\mu} c^{-}_{(L-1)\nu} + \text{H.c.} \tag{4.43}$$

As the $c^{+\dagger}_{x\mu} c^{-}_{x'\nu}$ hopping terms are not smooth, the hopping coefficients $J_{\mu\nu}(\vec{\theta})$ must be chosen so as to vanish sufficiently quickly around any singularities, leaving H_{hop} smooth and well-defined. Otherwise, there is significant freedom in the choice of $J_{\mu\nu}(\vec{\theta})$. Any choice leaves the upper bands (those with positive energy) uncoupled at $x = 0$ when $\epsilon = 1$ (Fig. 4·3).

An on-site disorder term is responsible for localization:

$$H_{\text{dis}} = \sum_{x=0}^{L-1} \delta_{x+} p_{x+} + \delta_{x-} p_{x-}, \tag{4.44}$$

where $p_{x\pm}$ is the projector onto the upper (lower) bands on site x, and $\delta_{x\pm}$ are independent and identically distributed random numbers.

The total Hamiltonian is

$$H = H_0 + H_{\text{hop}} + H_{\text{dis}}. \tag{4.45}$$

This model has the same $\epsilon \leftrightarrow 1-\epsilon$ self-duality as the two-tone model. It has uncoupled, perfectly localized edge modes with nth Chern number $\pm C_n$ when $\epsilon = 1$.

The winding number invariant, W, of the bulk model is given by C_n in the nontrivial phase.

4.5.1 Four-dimensional quantum Hall edge states

The simplest ALTP beyond the QP pump has $d + D = 5$. The general coupled layer construction shows that this phase has edges states with a nontrivial second

Chern number C_2, as appearing in the four-dimensional integer quantum Hall effect [135, 158]. In this section, we explore this case in more detail. In a related $(2+3)$-dimensional model constructed from the coupled layer approach (Fig. 4·12), we describe the physical observable associated to the edge states—a nonlinear (in synthetic field strength) energy pumping response.

Just as a nonzero first Chern number implies a quantized linear response to a weak electric field, a nonzero second Chern number implies a quantized quadratic response to an electric *and* magnetic field. In the frequency lattice, the electric field is the vector $\vec{\Omega}$. It is not possible to implement a magnetic field in the $(0+D)$-dimensional geometry of the edge in the coupled layer construction. Instead, one should seek a $(2+3)$-dimensional model (with a $(1+3)$-dimensional edge), where a magnetic field in the synthetic dimensions may be emulated through a spatially dependent initial phase $\vec{\theta}_0(y)$ in the drive [47].

Our starting point remains the coupled layer model. To give an example of a particular $\vec{B}$ which gives $C_2 = 1$ for the $x = 0$ edge state, we may take

$$B_0 = 3 - \sum_{j=1}^{4} \cos\theta_j(t), \quad B_{1\leq j\leq 4} = \sin\theta_j(t) \tag{4.46}$$

where the 4×4 Γ_j matrices may be expressed as tensor products of Pauli matrices σ^α and τ^β:

$$\Gamma_0 = \tau^x,\ \Gamma_1 = \sigma^z\tau^z,\ \Gamma_2 = \sigma^x\tau^z,\ \Gamma_3 = \sigma^y\tau^z,\ \text{and}\ \Gamma_4 = \tau^y. \tag{4.47}$$

The coupled layer model is then defined through the general construction above.

To find a $(2+3)$-dimensional model, we exchange one synthetic dimension for a spatial dimension [1]. The mapping to accomplish this is provided by the frequency lattice description: Fourier modes of drive 1 are hopping terms in synthetic space, which, at a formal level, may be declared to be an actual spatial dimension. At

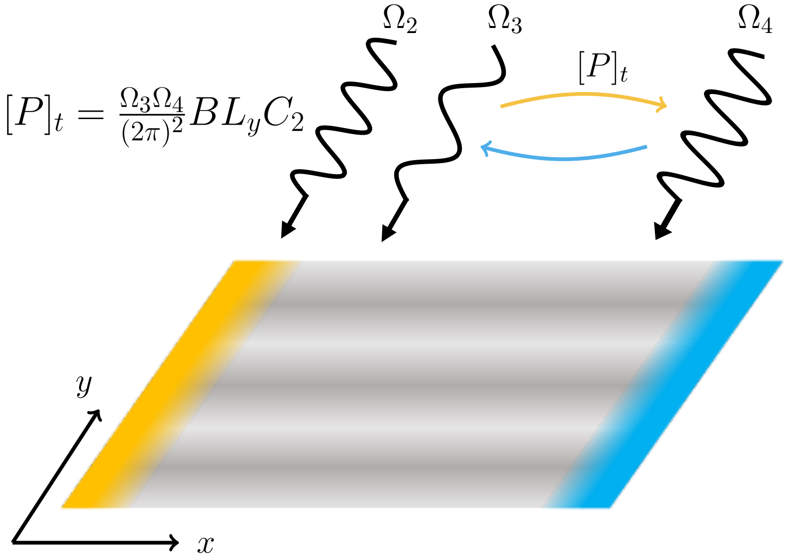

Figure 4·12: *Synthetic four-dimensional quantum Hall effect.*—The coupled layer construction may be used to model a $(2+3)$-dimensional ALTP. The edge states (yellow, blue) possess a nontrivial second Chern number $\pm C_2$ which is equal (up to a sign depending on which edge is being considered) to the bulk winding number W. Their response is analogous to the nonlinear response in the four-dimensional quantum Hall effect. A magnetic flux B per plaquette is introduced in the $(\hat{y}, \hat{e}_2)$ plane by a linear winding of the initial phase $\theta_{02} = By$ in space (grey stripes). The average energy pumping rate between drives 3 and 4 depends on both the magnetic field B and the electric field $\vec{\Omega}$: $[P]_t/L_y = \Omega_3\Omega_4 B C_2/(2\pi)^2$. L_y is the length of the pumping edge.

the most direct level, the synthetic electric field $\Omega_1\hat{e}_1$ should be replaced by a linear potential in real space. Alternatively, a different form of spatial inhomogeneity may be introduced, provided that it causes localization and does not change the topological phase of the model.

In more detail, the Hamiltonian for a $(1+D)$-dimensional ALTP may be written as a sum of quadratic terms,

$$H(\vec{\theta}) = \sum_{x,x'} h^{\mu\nu}_{xx'}(\vec{\theta}) c^\dagger_{x\mu} c_{x'\nu}. \tag{4.48}$$

The θ_1 Fourier components of $h^{\mu\nu}_{xx'}(\vec{\theta})$,

$$h^{\mu\nu}_{\vec{x}\vec{x}'}(\vec{\theta}_{\hat{1}}) = \frac{1}{2\pi}\int \mathrm{d}\theta_1\, h^{\mu\nu}_{xx'}(\vec{\theta})e^{i(y-y')\theta_1}, \tag{4.49}$$

may be interpreted as hopping matrices. Here, $\vec{x} = x\hat{x} + y\hat{y}$, $y - y'$ indexes the Fourier component, and $\vec{\theta}_{\hat{1}} = \sum_{j=2}^{D}\theta_j\hat{e}_j$ is $\vec{\theta}$ with the θ_1 component removed. A Hamiltonian for a $(2 + (D-1))$-dimensional ALTP is then

$$H'(\vec{\theta}_{\hat{1}}) = H'_{\mathrm{dis}} + \sum_{\vec{x},\vec{x}'} h^{\mu\nu}_{\vec{x}\vec{x}'}(\vec{\theta}_{\hat{1}})c^{\dagger}_{\vec{x}\mu}c_{\vec{x}'\nu}, \tag{4.50}$$

where H'_{dis} includes a disorder potential in the y dimension (a linear potential, or otherwise). In this construction, the quasiperiodic hopping coefficients $h^{\mu\nu}_{\vec{x}\vec{x}'}$ decay exponentially in $|y - y'|$, but are only strictly local in the x dimension.

In a strip geometry for H', with $0 \leq 1 - \epsilon \ll 1/2$, C_2 edge states exist at the one-dimensional boundaries parallel to y (Fig. 4·12). In the frequency lattice, there is a linear potential (electric field) along $\vec{\Omega}_{\hat{1}} = \sum_{j=2}^{D}\Omega_j\hat{e}_j$. To observe the quadratic response of a four-dimensional quantum Hall state, we must have a way of introducing a magnetic field through a plane which includes two of $(\hat{y}, \hat{e}_2, \hat{e}_3, \hat{e}_4)$.

In fact, Ref. [47] has already demonstrated how this may be done in a $(1+3)$-dimensional wire model (where $C_2 \neq 0$ requires adiabaticity or fine tuning). The initial phase $\vec{\theta}_0$ appears in the frequency lattice as a vector potential. Including a spatially varying initial phase introduces a nonzero flux in short loops in the frequency lattice. Taking

$$\vec{\theta}_0 = By\hat{e}_2 \tag{4.51}$$

introduces a flux B through each square plaquette in the $(\hat{y}, \hat{e}_2)$-plane. (Physical response only depends on $B \mod 2\pi$.)

By analogy to the (continuum) response of a four-dimensional Hall insulator, the average energy current between the θ_3 and θ_4 drives is found to be [47]

$$[P]_t = \frac{\Omega_3 \Omega_4}{(2\pi)^2} B L_y C_2 + O(B^2), \tag{4.52}$$

where L_y is the length of the pumping boundary. This agrees with Eq. (4.2), as $C_2 = W$. Observing pumping requires, as usual, filling a distance $s \gg \zeta$ from the boundary with fermions.[3]

4.6 Topological Classification

The coupled layer construction provides a useful toy model for $(1+D)$-dimensional ALTPs. It is useful to keep these examples in mind as we proceed to the general topological classification.

The topological classification is most naturally expressed through the micromotion operator (2.8) [90]

$$V(\vec{\Phi}, \vec{\theta}) = \sum_{\alpha} |\phi_\alpha(\vec{\theta})\rangle\langle\alpha|, \tag{4.53}$$

where $|\alpha\rangle$ is a basis for the system's Hilbert space and $\vec{\Phi}$ is a vector of fluxes twisting the periodic boundary conditions of the spatial dimensions (we have suppressed the dependence of the quasienergy states $\vec{\Phi}$). In a localized phase the micromotion $V(\vec{\Phi}, \vec{\theta})$ is a smooth map from the $(d+D)$-dimensional torus defined by $\vec{\Phi}$ and the drive phases $\vec{\theta}$ to the unitary group. It is well known that such maps are classified by an integer winding number $W[V]$ when $d + D$ is odd, defined by [8, 158–160]

$$W[V] = C_{d+D} \int \mathrm{d}^d\Phi \, \mathrm{d}^D\theta \, \epsilon^{j \cdots k} \, \mathrm{Tr}\, (V^\dagger \partial_j V) \cdots (V^\dagger \partial_k V) \tag{4.54}$$

where the integral is over the torus, $\epsilon^{j \cdots k}$ is the Levi-Civita symbol, ∂_j is differentiation with respect to one of Φ_j or θ_j, and

---

[3] There may be subextensive corrections from the corners of the sample, which can be canceled by driving the corners [47].

$$C_{d+D} = \frac{(\frac{d+D-1}{2})!}{(d+D)!(2\pi i)^{(d+D+1)/2}} \tag{4.55}$$

is a constant.

The classification of ALTPs is accomplished by the following theorem, to be proved in Sec. 4.6.2.

Theorem. The winding number $W[V]$ is an integer valued topological invariant characterizing localized phases with $d + D > 1$. That is, if the two Hamiltonian-frequency pairs $(H_0(\vec{\theta}), \vec{\Omega}_0)$ and $(H_1(\vec{\theta}), \vec{\Omega}_1)$ are joined by a connected path $(H_s(\vec{\theta}), \vec{\Omega}_s)$ (where $s \in [0, 1]$) such that all the $(H_s(\vec{\theta}), \vec{\Omega}_s)$ have localized quasienergy states, then $W[V_0] = W[V_1]$.

As promised, the classification depends only on the frequency lattice dimension $d + D$. Note that the Floquet classification of anomalous phases without symmetry is reproduced with $D = 1$ [90].

In the spirit of having a cohesive language for spatial and synthetic dimensions, we overload the notation $\vec{\theta}$ with the fluxes from the spatial dimensions,

$$\vec{\theta} = \sum_{j=1}^{d} \Phi_j \hat{e}_j + \sum_{j=d+1}^{d+D} \theta_j \hat{e}_j. \tag{4.56}$$

The micromotion operator $V(\vec{\theta})$ may be regarded as a map from the torus $\mathbb{T}^{d+D}$ of fluxes and phase angles to the unitary group,

$$V : \mathbb{T}^{d+D} \to U(N). \tag{4.57}$$

It is well known that the (stable) homotopy class of such maps is characterized by the integer defined in Eq. (4.54) [8, 158–160].[4] With this fact in hand, the missing element of the proof is that, under the conditions of the theorem, the path V_s is continuous, and that $W[V]$ is gauge independent. Then the theorem follows from the homotopy invariance of W (that is, invariance under continuous deformations of V).

---

[4] Strictly speaking, this characterizes maps from the $(d + D)$-sphere to the unitary group. We are ignoring lower homotopy groups of the unitary group and focusing on this so called *strong* invariant [90, 158, 161].

4.6.1 Gauge invariance of $W[V]$

The micromotion operator $V(\vec{\theta})$ is not unique. It changes under the gauge transformation of the quasienergy states. If $W[V]$ is to have any physical meaning, it cannot change under the gauge transformation (2.22). We prove this is so for $d + D > 1$.

In the $d + D = 1$ case, $W[V]$ gives the familiar winding number $\frac{1}{2\pi i}\oint \frac{\mathrm{d}z}{z}$ for the complex number $z = \det(V)$. This can be altered by an arbitrary integer through the gauge transformation (2.22), and so $W[V]$ has no physical meaning for a $(0+1)$-dimensional localized phase—a periodically driven qudit. Even so, an integer classification of zero-dimensional Floquet systems has been reported in, for instance, Ref. [90].

$W[V]$ is always zero for $d + D$ even, so we will focus on the non-trivial case of $d + D$ being odd.

The gauge invariant unitary operator characterizing the system is the evolution operator:

$$U(t_1, t_0; \vec{\theta}_0) = \sum_\alpha |\psi_\alpha(t_1; \vec{\theta}_0)\rangle\langle\psi_\alpha(t_0; \vec{\theta}_0)| \tag{4.58}$$

$$= V(\vec{\theta}_{t_1}) e^{-i(t_1 - t_0)H_F} V^\dagger(\vec{\theta}_{t_0}), \tag{4.59}$$

where $H_F = \sum_\alpha \epsilon_\alpha |\alpha\rangle\langle\alpha|$ is the Floquet Hamiltonian. Any transformation of V and H_F which preserves the form of this decomposition does not affect the physical operator U.

Transformations preserving (4.59) include the gauge transformations (2.22) and rotations of the reference basis $|\alpha\rangle \mapsto |\beta_\alpha\rangle$. We can handle both of these operations at once by writing

$$V(\vec{\theta}) \mapsto V(\vec{\theta})\tilde{U}(\vec{\theta}) \tag{4.60}$$

where $\tilde{U}(\vec{\theta}) = \sum_\alpha e^{i\vec{n}_\alpha\cdot\vec{\theta}}|\alpha\rangle\langle\beta_\alpha|$ is unitary and $\vec{n}_\alpha$ are arbitrary vectors of integers.

It is convenient to express $W[V]$ in a coordinate independent form. In the language of differential forms, we define $\tilde{n}_V = -iV^\dagger \mathrm{d}V$, where d is the exterior derivative. Then $W[V]$ is expressed

$$W[V] = i^{d+D} C_{d+D} \int\limits_{\mathbb{T}^{d+D}} \mathrm{Tr}\, \tilde{n}_V^{\wedge(d+D)} \tag{4.61}$$

$$= \tilde{C}_{d+D} \int\limits_{\mathbb{T}^{d+D}} \mathrm{Tr}\, \tilde{n}_V \wedge (i\mathrm{d}\tilde{n}_V)^{\wedge(d+D-1)/2}, \tag{4.62}$$

where $\tilde{C}_\delta = i^\delta C_\delta$ and we used the fact that

$$\mathrm{d}\tilde{n}_V = -i\mathbb{1}\mathrm{d}(V^\dagger \mathrm{d}V) = -iV^\dagger V \mathrm{d}V^\dagger \wedge \mathrm{d}V = iV^\dagger \mathrm{d}V \wedge V^\dagger \mathrm{d}V = -i\tilde{n}_V \wedge \tilde{n}_V. \tag{4.63}$$

The second equality follows from $V^\dagger V = \mathbb{1}$ and $\mathrm{d}(V^\dagger \mathrm{d}V) = \mathrm{d}V^\dagger \wedge \mathrm{d}V + V^\dagger \mathrm{d}^2 V$ with $\mathrm{d}^2 = 0$. The third equality uses $V\mathrm{d}V^\dagger = -(\mathrm{d}V)V^\dagger$, obtained by differentiating $VV^\dagger = \mathbb{1}$.

We further compute that

$$\tilde{n}_{V\tilde{U}} = -i(\tilde{U}^\dagger(V^\dagger \mathrm{d}V)\tilde{U} + \tilde{U}^\dagger \mathrm{d}\tilde{U}) = \tilde{U}^\dagger \tilde{n}_V \tilde{U} + \tilde{n}_{\tilde{U}} \tag{4.64}$$

where

$$\tilde{n}_{\tilde{U}} = \sum_\alpha \vec{n}_\alpha |\beta_\alpha\rangle\langle\beta_\alpha| \tag{4.65}$$

is a constant independent of $\vec{\theta}$. Thus, substituting (4.64) into the formula for the winding number (4.62), all the derivatives of $\tilde{n}_{\tilde{U}}$ vanish, and we obtain

$$W[V\tilde{U}] = W[V] + B \tag{4.66}$$

where

$$B = \tilde{C}_{d+D} \int \mathrm{Tr}\, \tilde{U} \tilde{n}_{\tilde{U}} \tilde{U}^\dagger \wedge (i\mathrm{d}\tilde{n}_V)^{\wedge(d+D-1)/2} \tag{4.67}$$

$$= \tilde{C}_{d+D} \sum_\alpha \vec{n}_\alpha \cdot \langle \alpha | \left(\int (i\mathrm{d}\tilde{n}_V)^{\wedge(d+D-1)/2} \right) |\alpha\rangle \,. \tag{4.68}$$

The integrand is a total derivative of

$$i\tilde{n}_V \wedge (i\mathrm{d}\tilde{n}_V)^{\wedge(d+D-3)/2}, \tag{4.69}$$

and so $B = 0$.

Thus, $W[V\tilde{U}] = W[V]$ and the winding number is gauge invariant.

4.6.2 Proof of classification

We now prove the theorem classifying localized phases.

That $W[V]$ is an integer and invariant under smooth deformations of V is well known, and we will assume this fact [8, 158–160]. More precisely, $W[V]$ is a homotopy invariant. We show that, under the conditions of the theorem, the path between the micromotion operators V_s is continuous. Thus, the winding number of all micromotion operators on the path, in particular the end-points, must be equal.

The proof is most straightforward in the frequency lattice. The continuous family $(H_s, \vec{\Omega}_s)$ defines a continuous family of quasienergy operators K_s. The assumptions of the theorem require each K_s to have a complete set of normalizable eigenstates $|\tilde{\phi}_\gamma(s)\rangle$ with associated eigenvalues $\epsilon_\gamma(s)$, where γ indexes the frequency lattice Hilbert space. We show that eigenstate indices can be organized so that each $|\tilde{\phi}_\gamma(s)\rangle$ is a continuous functions of $s \in [0, 1]$.

Assuming for now that each $|\tilde{\phi}_\gamma(s)\rangle$ is continuous in s, the result follows straightforwardly as we have outlined. Any set of independent representatives for the quasienergy state equivalence classes (formed by (2.22) and which we will indexed by α) defines a continuous family of micromotion operators $V_s = \sum_\alpha |\phi_\alpha(s)\rangle\langle\alpha|$. The homotopy invariance of W then implies that $W[V_s] = W[V_{s'}]$ for all s and s'. In particular $W[V_0] = W[V_1]$.

Organizing the eigenstates $|\tilde{\phi}_\gamma(s)\rangle$ into continuous families is difficult (if it is possible) for general infinite dimensional gapless operators like K_s. Localization allows us to construct these families with the same ease as in finite dimensional systems.

We fix an eigenstate $|\tilde{\phi}_\gamma(s)\rangle$ of K_s, and consider eigenstates $|\tilde{\phi}_{\gamma'}(s')\rangle$ of $K_{s'}$ when s' is close to s.

First, observe that there are only finitely many $|\tilde{\phi}_{\gamma'}(s')\rangle$ which can plausibly be matched to $|\tilde{\phi}_\gamma(s)\rangle$. This is intuitive from localization: there are only finitely many quasienergy states localized near where $|\tilde{\phi}_\gamma(s)\rangle$ has significant weight in the frequency lattice. Formally, we define a finite set of frequency lattice sites A such that

$$\langle\tilde{\phi}_\gamma(s)|\, P_A\, |\tilde{\phi}_\gamma(s)\rangle > 1-\delta \tag{4.70}$$

where $P_A = \sum_{\vec{n}\in A} |\vec{n}\rangle\langle\vec{n}|$ is the projector onto A and $\delta > 0$. This is possible because $|\tilde{\phi}_\gamma(s)\rangle$ is square-summable (being localized). This subset of the frequency lattice will be where we focus our attention.

We consider a projection of $K_{s'}$ onto A, $P_A K_{s'} P_A$. As $K_{s'}$ is local, if $|\tilde{\phi}_{\gamma'}(s')\rangle$ is almost entirely supported in the region A, in the sense that $\langle\tilde{\phi}_{\gamma'}(s')|\, P_A\, |\tilde{\phi}_{\gamma'}(s')\rangle > 1-\delta$, then $|\tilde{\phi}_{\gamma'}(s')\rangle$ is close to an eigenstate $|\chi_{\gamma'}(s')\rangle$ of $P_A K_{s'} P_A$. That is, if we write $d(\psi,\phi)$ for the distance between states $|\psi\rangle$ and $|\phi\rangle$ (not being specific about the metric on state space), then for each $|\tilde{\phi}_{\gamma'}(s')\rangle$ and any $\epsilon > 0$ there is a $\delta > 0$ (a large enough A) such that an eigenstate $|\chi_{\gamma'}(s')\rangle$ of $P_A K_{s'} P_A$ satisfies

$$d(\tilde{\phi}_{\gamma'}(s'), \chi_{\gamma'}(s')) < \epsilon. \tag{4.71}$$

Continuous families of eigenstates $|\chi_{\gamma'}(s')\rangle$ can be unambiguously identified for the corresponding family of *finite dimensional* hermitian operators $P_A K_{s'} P_A$ (discarding the null space of P_A) for smooth enough paths [162, Chapter 2]. This lets us make a choice for γ so that $|\chi_\gamma(s')\rangle$ is continuous in s'.

The proximity of an eigenstate of $K_{s'}$ to $|\chi_\gamma(s')\rangle$, as in (4.71), then induces a choice for $|\tilde{\phi}_\gamma(s')\rangle$. The family $|\tilde{\phi}_\gamma(s')\rangle$ defined in this way is continuous: there is a $\delta' > 0$ so that $d(\chi_\gamma(s), \chi_\gamma(s')) < \epsilon$ whenever $|s - s'| < \delta'$ and so

$$d(\tilde{\phi}_\gamma(s), \tilde{\phi}_\gamma(s')) \leq d(\tilde{\phi}_\gamma(s), \chi_\gamma(s)) + d(\chi_\gamma(s), \chi_\gamma(s')) + d(\chi_\gamma(s'), \tilde{\phi}_\gamma(s')) < 3\epsilon, \quad (4.72)$$

where we used the triangle inequality repeatedly and (4.71).

This shows that the smooth path $(H_s, \vec{\Omega}_s)$ induces continuous paths for the frequency lattice eigenstates, and completes the proof of the theorem.

4.7 Observable Consequences

The formal classification of ALTPs is physically interesting only because it predicts quantized observables. The physical observables depend on d. We identify these for $d \in \{0, 1\}$ when $d + D = 3$. The Floquet case $d = 2$ is well studied [11, 126], and $d = 1$ is the QP pump. See Ref. [66] for $d = 3$.

The chiral energy circulation captures the topological response of (0+3)-dimensional ALTPs—qudits driven by three incommensurate tones (Fig. 4·13). In more detail, the Heisenberg operator for the instantaneous rate of work done on the qudit is $U^\dagger \partial_t H(\vec{\theta}_t) U = \sum_j \Omega_j U^\dagger \partial_j H(\vec{\theta}_t) U$, where $U = U(t, 0)$ is the evolution operator from time 0 to t. As energy input into the qudit must come from the drives, it is natural to identify $U^\dagger \partial_j H U := -\dot{n}_j$ as the rate of photon transfer out of the jth drive. An operator measuring the rate at which photons circulate between the drives (Fig. 4·1(a)) is then

$$M(t) = \frac{1}{4}(\vec{n} \times \dot{\vec{n}}) \cdot \hat{\Omega} + \text{H.c.}, \quad (4.73)$$

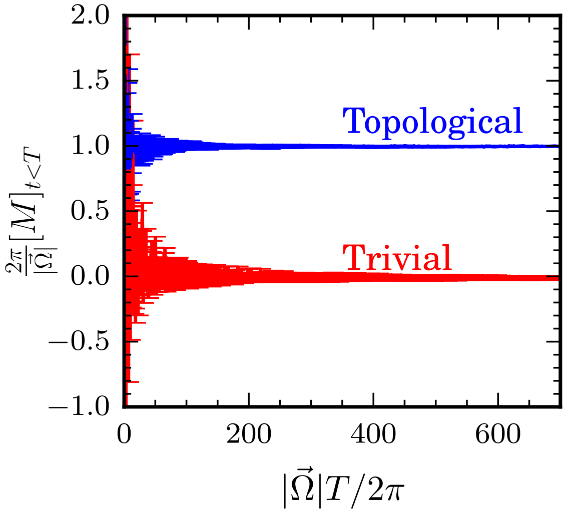

Figure 4·13: *Quantized energy circulation.*—The energy circulation $[M]_{t<T}$ in a three-tone-driven qubit converges to a quantized value as the averaging time T is increased. Details of the model and parameter values are reported in Ref. [1].

where $\vec{n}$ is the integral of $\dot{\vec{n}}$, and we can drop the constant of integration (Sec. 4.7.1). Introducing the notation $[A]_{t<T} := \frac{1}{T}\int_0^T \mathrm{d}t\ \mathrm{Tr}\, A(t)$, we prove in Sec. 4.7.1 that

$$[M]_{t<T} = \frac{|\vec{\Omega}|}{2\pi} W[V] + O(T^{-1}). \tag{4.74}$$

That is, the long-time average of the circulation in an initial mixed state $\rho \propto \mathbb{1}$ is quantized and proportional to the winding number (Fig. 4·13).

A quantized circulation is also present in $(1+2)$-dimensional ALTPs—the QP pump. However, in contrast to the $(0+3)$-dimensional ALTP, there are also *edge* signatures of topology, as displayed by the coupled layer model.

The topological *energy current* between the drives at the edge of the QP pump (Fig. 4·1(b)) is a robust feature of any two-tone-driven wire with nontrivial topology, not just the coupled layer model. The frequency lattice for the driven wire has a slab geometry (Fig. 4·4). A nonzero winding number in the bulk is accompanied by current-carrying edge states, which must run perpendicular to $\vec{\Omega}$, due to Stark localization by the electric field $\vec{\Omega}$ (Fig. 4·1(d)). If $\vec{\Omega} = \Omega_2\hat{e}_2 + \Omega_3\hat{e}_3$ (reserving $\hat{e}_1$ for the spatial lattice direction), the edge current is parallel to $\Omega_3\hat{e}_2 - \Omega_2\hat{e}_3$. That is, photons are transferred from drive 3 to drive 2 (or drive 2 to drive 3, depending on the sign of $W[V]$) in an energy current.

Quantitatively, the long-time average of the energy current into drive j, $P_j(t) = \Omega_j\dot{n}_j(t)$, in an initial state localized near an edge is (now noting explicitly the dependence on the filling s)

$$[P_j]_{s,T} := [P_j\rho_s]_T = \pm P_{\mathrm{top}}W[V] + O(T^{-1}, e^{-s/\zeta}). \tag{4.75}$$

Here, ρ_s is a projector onto lattice sites localized within s sites of the edge (Fig. 4·2), ζ is the single-particle localization length, and the sign depends on which drive j is being considered. Experimentally, this is the response of a noninteracting wire filled with fermions up to a distance s from the edge. Eq. (4.75) is proved in Sec. 4.7.2.

4.7.1 Quantized Energy Circulation

We prove that the energy-charge circulation, generalizing the magnetization of the anomalous Floquet-Anderson insulator (AFAI) [11, 126], is quantized and proportional to the winding number.

For brevity of notation we will assemble the fluxes Φ_j twisting the periodic boundary conditions of any spatial dimensions of the system and the drive phases θ_j into a single three-dimensional vector $\vec{\theta}$, as in (4.56). In this notation $\vec{\Omega}$ is zero in any entry corresponding to a spatial dimension. Thus, we understand $\vec{\theta}_t = \vec{\Omega}t + \vec{\theta}_0$ to only vary in time in the components corresponding to the drives.

The component of the Heisenberg operator

$$\dot{\vec{n}}(t;\vec{\theta}_0) = U^\dagger(t,0;\vec{\theta}_0)(-\nabla_\theta H)(\vec{\theta}_t)U(t,0;\vec{\theta}_0) \tag{4.76}$$

corresponding to drive j measures the photon current into drive j. The component corresponding to the jth spatial axis measures a physical current. Thus, we identify its integral with a displacement in the frequency lattice,

$$\Delta\vec{n}(t;\vec{\theta}_0) = \int\limits_0^t \mathrm{d}t\,\dot{\vec{n}}(t) = -iU^\dagger(t,0;\vec{\theta}_0)\nabla_{\theta_0}U(t,0;\vec{\theta}_0). \tag{4.77}$$

This formula is most straightforwardly checked by differentiating the right hand side and applying the Schrödinger equation $i\partial_t U = HU$ to obtain (4.76). Also observe that $\Delta\vec{n}(0;\vec{\theta}_0) = 0$ as $U(0,0;\vec{\theta}_0) = \mathbb{1}$ is independent of initial phase.

The component of $\Delta\vec{n}$ corresponding to drive j is interpreted as the change in photon number of drive j. The component corresponding to the jth spatial axis is interpreted as the displacement along this dimension, divided by the length of the system in that dimension, $\Delta r_j/L_j$. An arbitrary choice of initial conditions for $\vec{n}(t;\vec{\theta}_0) = \vec{n}(0;\vec{\theta}_0) + \Delta\vec{n}(t;\vec{\theta}_0)$ defines a position in the frequency lattice.

The energy-charge circulation is defined by

$$M(t) = \frac{1}{4}(\vec{n}\times\dot{\vec{n}})\cdot\hat{\Omega} + \text{h.c.} \tag{4.78}$$

and we prove it takes the quantized average value

$$[M]_{t<T} = \frac{1}{T}\int\limits_0^T \mathrm{d}t\ \mathrm{Tr}\,M(t) = \frac{|\vec{\Omega}|}{2\pi}W[V] + O(T^{-1}, e^{-L/\xi}) \tag{4.79}$$

in the anomalous localized phase for any initial phase $\vec{\theta}_0$. Furthermore, we show that a local version of this quantity—the circulation density—is also quantized when one of the dimensions is spatial.

As a preliminary issue, note that the long time average does not depend on the initial condition $\vec{n}(0)$ in the localized phase. Adding an arbitrary constant to $\vec{n}$ in (4.78) adds a term proportional to $\frac{1}{T}\int_0^T \mathrm{d}t\,\dot{\vec{n}} = O(T^{-1})$, where we used that $\Delta\vec{n}(t)$

is bounded in the localized phase.

4.7.1.1 Manipulation of winding number density

Before we begin, it is convenient to first prove a lemma about the expression of the winding number density in terms of coordinates. The winding number density can be expressed in a coordinate-free form as

$$w[V] = \frac{i}{3!(2\pi)^2} \operatorname{Tr} \tilde{n} \wedge \tilde{n} \wedge \tilde{n} \tag{4.80}$$

where $\tilde{n}(\vec{\theta}) = -iV^\dagger \mathrm{d}V$ and $V(\vec{\theta})$ is the micromotion operator. To relate this to an expression with coordinates (such as $M(t)$) we prove

$$\operatorname{Tr} \tilde{n}_1 \partial_2 \tilde{n}_3 \, \mathrm{d}^3\theta = -\frac{i}{6} \operatorname{Tr} \tilde{n} \wedge \tilde{n} \wedge \tilde{n} + \mathrm{d}\omega \tag{4.81}$$

where subscript numerals index any local set of coordinates (which need not necessarily extend to a *global* set of coordinates), we have defined a coordinate expression of $\tilde{n}$ as $\tilde{n} = \sum_{i=1}^{3} \tilde{n}_i \mathrm{d}\theta_i$, $\mathrm{d}\omega$ is a total derivative and $\mathrm{d}^3\theta = \mathrm{d}\theta_1 \wedge \mathrm{d}\theta_2 \wedge \mathrm{d}\theta_3$ is the volume element of the torus. That is, we relate the coordinate-free expression on the right hand side of (4.81) to a particular form involving the components of $\tilde{n}$ on the left hand side.

Indeed, we have

$$\tilde{n}_1 \partial_2 \tilde{n}_3 = -i\tilde{n}_1 \partial_2 (V^\dagger \partial_3 V) \tag{4.82}$$

$$= -i\tilde{n}_1 (\partial_2 V^\dagger \partial_3 V + V^\dagger \partial_2 \partial_3 V). \tag{4.83}$$

Inserting $V^\dagger V = \mathbb{1}$ in the first term and using $V \partial V^\dagger = -\partial V V^\dagger$ (obtained by differentiating $VV^\dagger = \mathbb{1}$) we see

$$\tilde{n}_1 \partial_2 \tilde{n}_3 = -i\tilde{n}_1 \tilde{n}_2 \tilde{n}_3 - i\tilde{n}_1 (V^\dagger \partial_2 \partial_3 V). \tag{4.84}$$

The second term may be be further manipulated as

$$\begin{aligned} -i\tilde{n}_1(V^\dagger\partial_2\partial_3 V) &= \partial_3(\tilde{n}_1\tilde{n}_2) - (\partial_3\tilde{n}_1)\tilde{n}_2 + i\tilde{n}_1(\partial_3 V^\dagger\partial_2 V) \\ &= \partial_3(\tilde{n}_1\tilde{n}_2) - (\partial_3\tilde{n}_1)\tilde{n}_2 + i\tilde{n}_1\tilde{n}_3\tilde{n}_2. \end{aligned} \quad (4.85)$$

This gives the full expression

$$\tilde{n}_1\partial_2\tilde{n}_3 = \partial_3(\tilde{n}_1\tilde{n}_2) - (\partial_3\tilde{n}_1)\tilde{n}_2 - i\tilde{n}_1[\tilde{n}_2,\tilde{n}_3], \quad (4.86)$$

which upon taking the trace and using the cyclic property thereof, becomes

$$\operatorname{Tr}\tilde{n}_1\partial_2\tilde{n}_3 = \partial_3\operatorname{Tr}\tilde{n}_1\tilde{n}_2 - \operatorname{Tr}\tilde{n}_2\partial_3\tilde{n}_1 - i\operatorname{Tr}\tilde{n}_1[\tilde{n}_2,\tilde{n}_3]. \quad (4.87)$$

The first of these terms is a total derivative, and the final one appears in a coordinate expression of the winding number density. The second is of the same form as the left hand side (with the indices cyclically permuted), and so we may apply the same formula recursively. Doing this three times gives

$$\operatorname{Tr}\tilde{n}_1\partial_2\tilde{n}_3 = \partial_3\operatorname{Tr}\tilde{n}_1\tilde{n}_2 - \partial_1\operatorname{Tr}\tilde{n}_2\tilde{n}_3 + \partial_2\operatorname{Tr}\tilde{n}_3\tilde{n}_1 - \operatorname{Tr}\tilde{n}_1\partial_2\tilde{n}_3 - i\operatorname{Tr}\tilde{n}_1[\tilde{n}_2,\tilde{n}_3], \quad (4.88)$$

where some terms have been canceled. The cyclicity of the trace may be further exploited to derive

$$\operatorname{Tr}\tilde{n}_1[\tilde{n}_2,\tilde{n}_3] = \frac{1}{3}\epsilon^{ijk}\operatorname{Tr}\tilde{n}_i\tilde{n}_j\tilde{n}_k, \quad (4.89)$$

where summation over repeated indices is implied on the right hand side. The right hand side of (4.89) is proportional to the coefficient of $\mathrm{d}^3\theta$ in $\operatorname{Tr}\tilde{n}\wedge\tilde{n}\wedge\tilde{n}$. Moving the duplicate term $-\operatorname{Tr}\tilde{n}_1\partial_2\tilde{n}_3$ to the left hand side of (4.88) and multiplying by the volume element $\mathrm{d}^3\theta$ gives the required expression

$$\operatorname{Tr}\tilde{n}_1\partial_2\tilde{n}_3\,\mathrm{d}^3\theta = -\frac{i}{6}\operatorname{Tr}\tilde{n}\wedge\tilde{n}\wedge\tilde{n} + \mathrm{d}\omega \quad (4.90)$$

where

$$\omega = \frac{1}{2}\mathrm{Tr}\left[\tilde{n}_1\tilde{n}_2\,\mathrm{d}\theta_1\wedge\mathrm{d}\theta_2\;\; -\tilde{n}_2\tilde{n}_3\,\mathrm{d}\theta_2\wedge\mathrm{d}\theta_3+\tilde{n}_3\tilde{n}_1\,\mathrm{d}\theta_3\wedge\mathrm{d}\theta_1\right]. \tag{4.91}$$

4.7.1.2 Proof of quantized energy-charge circulation

We now use (4.81) to prove (4.79). Portions of the following calculation are essentially a reproduction of the proof of quantized magnetization of the AFAI in Ref. [126].

We define local coordinate vectors $\hat{\ell}_1$ and $\hat{\ell}_2$ which form an orthonormal triple with $\hat{\Omega} = \hat{\ell}_1 \times \hat{\ell}_2$. (Note that as $\hat{\Omega}$ is incommensurate in general, these local coordinate vectors cannot be used to define a *global* system of smooth coordinates on the torus.)

First, we manipulate the formula for the winding number using (4.81). The winding number density can be expressed in terms of our chosen coordinates as

$$w[V] = \frac{-1}{(2\pi)^2}\,\mathrm{Tr}\,\tilde{n}_2\partial_\Omega\tilde{n}_1\mathrm{d}^3\theta+\mathrm{d}\omega \tag{4.92}$$

where we have denoted $\partial_\Omega = \hat{\Omega}\cdot\nabla_\theta$. Integrating by parts and using the cyclicity of the trace, (4.92) becomes

$$w[V] = \frac{1}{8\pi^2}\,\mathrm{Tr}\,(\tilde{n}\times\partial_\Omega\tilde{n})\cdot\hat{\Omega}\mathrm{d}^3\theta+\mathrm{d}\omega'. \tag{4.93}$$

The winding number is the integral over the torus of this density, $W[V] = \int_{\mathbb{T}^3} w[V]$, which removes the total derivative $\mathrm{d}\omega'$.

We replace the Ω derivative by using the chain rule $|\vec{\Omega}|\partial_\Omega A(\vec{\theta}_t) = \partial_t A(\vec{\theta}_t)$, valid for any A defined on the torus. We thus have for the winding number

$$|\vec{\Omega}|W[V] = \frac{1}{8\pi^2}\int \mathrm{d}^3\theta\;\mathrm{Tr}\,(\tilde{n}\times\dot{\tilde{n}})\cdot\hat{\Omega}. \tag{4.94}$$

The orbit $\{\vec{\Omega}t+\vec{\theta}_0\;:\;t\in\mathbb{R}\}$ is ergodic in the torus when $\vec{\Omega}$ is incommensurate. In the spatial dimensions where $\vec{\Omega}$ has zero components, localization implies that the above quantity, which may be expressed as the trace of a Hermitian operator, depends only exponentially weakly on the threaded flux Φ_j. Thus, we may replace an average over all the variables $\vec{\theta}$ with an average over just the orbit—schematically $\frac{1}{(2\pi)^3}\int \mathrm{d}^3\theta = \frac{1}{T}\int_0^T \mathrm{d}t + O(T^{-1}, e^{-L/\xi})$, where L is the linear system size and ξ is the localization length. For the winding number, we find

$$|\vec{\Omega}|W[V] = \frac{1}{8\pi^2}\frac{(2\pi)^3}{T}\int\limits_0^T \mathrm{d}t\ \mathrm{Tr}\,(\tilde{n}\times\dot{\tilde{n}})\cdot\hat{\Omega} + O(T^{-1}, e^{-L/\xi}). \tag{4.95}$$

We must now express (4.95) in terms of $\vec{n}$, rather than $\tilde{n}$. Using that $V(\vec{\theta}_t) = U(t,0;\vec{\theta}_0)V(\vec{\theta}_0)e^{iH_F t}$ (as may be obtained from (4.59)) and that $\mathrm{d}V(\vec{\theta}_t)$ has the components of $\nabla_{\theta_0}V(\vec{\theta}_t)$, we have that

$$\tilde{n}(\vec{\theta}_t) = e^{-iH_F t}V_0^\dagger \vec{n}(t;\vec{\theta}_0)V_0 e^{iH_F t}. \tag{4.96}$$

Here we have denoted $V(\vec{\theta}_0) = V_0$ and took for convenience that $\vec{n}(0;\vec{\theta}_0) = V_0\tilde{n}(\vec{\theta}_0)V_0^\dagger$. Taking the time derivative we find

$$\dot{\tilde{n}} = e^{-iH_F t}V_0^\dagger\left(\dot{\vec{n}}(t) + \left[\vec{n}(t), V_0 H_F V_0^\dagger\right]\right)V_0 e^{iH_F t}. \tag{4.97}$$

Substituting (4.96) and (4.97) into (4.95) and focusing on the $T\to\infty$ limit, we have

$$\frac{|\vec{\Omega}|}{2\pi}W[V] = \lim_{T\to\infty}\frac{1}{T}\int\limits_0^T \mathrm{d}t\ \Big(\mathrm{Tr}\,\tfrac{1}{2}(\vec{n}\times\dot{\vec{n}})\cdot\hat{\Omega} \tag{4.98}$$

$$+\,\mathrm{Tr}\,\tfrac{1}{2}(\vec{n}\times i[\vec{n}, V_0 H_F V_0^\dagger])\cdot\hat{\Omega}\Big). \tag{4.99}$$

The first term (4.98) is the expression we are looking for.

We must now argue that the last term (4.99) is zero. We observe that the remaining terms in (4.98) are invariant under the gauge transformation (2.22), so (4.99) must also be gauge invariant. We will show this is enough to conclude that it is, in fact, zero.

We write $V_0 H_F V_0^\dagger = \sum_\alpha \epsilon_\alpha \rho_\alpha$ where $\rho_\alpha = |\phi_\alpha(\vec{\theta}_0)\rangle\langle\phi_\alpha(\vec{\theta}_0)|$. Then (4.99) becomes

$$\sum_\alpha \epsilon_\alpha \lim_{T\to\infty} \frac{1}{T} \int_0^T \mathrm{d}t \ \mathrm{Tr}\, \tfrac{1}{2}(\vec{n} \times i\,[\vec{n}, \rho_\alpha]) \cdot \hat{\Omega}. \tag{4.100}$$

Under a gauge transformation of $|\phi_\beta(\vec{\theta})\rangle \mapsto e^{i\vec{k}\cdot\vec{\theta}}\,|\phi_\beta(\vec{\theta})\rangle$, the quasienergies transform as $\epsilon_\alpha \mapsto \epsilon_\alpha + \vec{k}\cdot\vec{\Omega}\delta_{\alpha\beta}$, and the term (4.100) is shifted by

$$\vec{k}\cdot\vec{\Omega} \lim_{T\to\infty} \frac{1}{T} \int_0^T \mathrm{d}t \ \mathrm{Tr}\, \tfrac{1}{2}(\vec{n} \times i\,[\vec{n}, \rho_\beta]) \cdot \hat{\Omega} = 0 \tag{4.101}$$

for any $\vec{k} \in \mathbb{Z}^3$ and β. Gauge invariance demands (4.101) is zero. As $\vec{k}\cdot\vec{\Omega} \neq 0$ for at least some $\vec{k}$, it is the second factor that must be zero for all β. However, these are precisely the terms occurring in (4.100), so in fact (4.100) is also zero.

We are left with our desired term

$$\frac{|\vec{\Omega}|}{2\pi} W[V] = \lim_{T\to\infty} \frac{1}{T} \int_0^T \mathrm{d}t \ \mathrm{Tr}\, \tfrac{1}{2}(\vec{n} \times \dot{\vec{n}}) \cdot \hat{\Omega}. \tag{4.102}$$

The integrand is the trace of the product of two Hermitian operators, and so is real. Thus, we can take the hermitian part of the operator $\frac{1}{2}(\vec{n} \times \dot{\vec{n}}) \cdot \hat{\Omega}$ in this formula. This is the energy-charge circulation (4.78). Finally, we have

$$\frac{|\vec{\Omega}|}{2\pi} W[V] = \lim_{T\to\infty} \frac{1}{T} \int_0^T \mathrm{d}t \ \mathrm{Tr}\, M(t). \tag{4.103}$$

4.7.1.3 Quantized circulation density

In addition to the total circulation (4.78) being quantized, the *circulation density* is also quantized.

The total circulation is defined using a trace over all states in a system with

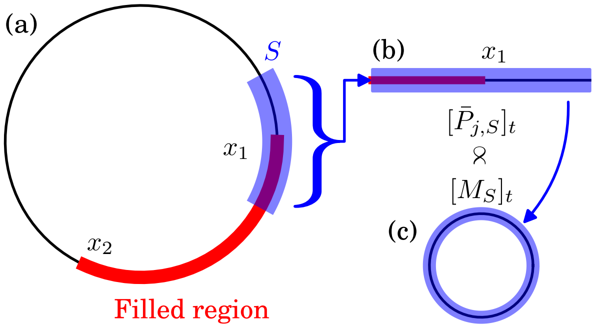

Figure 4·14: *Geometry of Sec. 4.7.1.3.*—**(a)** A large $(1+2)$-dimensional ALTP, with all states in the red region filled with fermions. The energy current between the drives near one edge of the filled region (in blue), $[P_{j,S}]_t$, is equal (with exponentially small corrections) to the total energy current in a system with open boundary conditions obtained by cutting out the region S around x_1, $[\bar{P}_j]_t$, shown in **(b)**. It is shown in Sec. 4.7.2 that the current in **(b)** is proportional to the circulation $[M_S]_t$ in the system with periodic boundary conditions **(c)** obtained by joining the ends of **(b)** together. The total circulation of **(c)** must be equal to the circulation density in region S of **(a)**, as a localized system is insensitive to its boundary conditions. Thus the circulation of **(c)** is equal to the appropriately scaled average circulation density over S, $\frac{L}{|S|}[M\rho_S]_t$. Then $[P_{j,S}]_t = -[P_{j,S'}]_t$ (with S' near x_2) gives that $\frac{L}{|S|}[M\rho_S]_t = \frac{L}{|S'|}[M\rho_{S'}]_t$.

periodic boundary conditions. It should be regarded as the average of a locally defined circulation density for systems with at least one spatial dimension. In Ref. [126] it was shown that not only is the magnetization quantized in a $(2+1)$-dimensional system, but the magnetization *density* is also quantized in a mesoscopic region filled with fermions. The equivalent claim in a $(1+2)$-dimensional ALTP (the QP pump) is also true; the circulation density is quantized, as we will now argue. The corresponding claim for a $(0+3)$-dimensional ALTP is meaningless; with no spatial extent there is no sensible notion of density.

We can calculate the average circulation density in a mesoscopic region by projecting the total circulation M onto some set of consecutive sites S with $\xi \ll |S| \ll L$, where ξ is the localization length, $|S|$ is the number of sites and L is the system size. That is, writing $m(r_1) = L\rho_{r_1} M \rho_{r_1}$ for the circulation density, where ρ_{r_1} is the projector into site $|r_1\rangle$, and $[A]_t = \lim_{T\to\infty} \int_0^T \mathrm{d}t \; \mathrm{Tr}\, A(t)$ as usual, we have

$$\sum_{r_1 \in S} [m(r_1)] = L[M\rho_S], \tag{4.104}$$

where $\rho_S = \sum_{r_1 \in S} \rho_{r_1}$ is the projector onto the sites S.

We aim to show that

$$\tfrac{L}{|S|}[M\rho_S]_t = \tfrac{L}{|S'|}[M\rho_{S'}]_t + O(e^{-|S|/\xi}, e^{-|S'|/\xi}) \tag{4.105}$$

for any S and S' centered at x_1 and x_2 respectively. In words—that the magnetization density is uniform on mesoscopic scales. The result follows from a relation between the energy current between the drives and the circulation which we prove in Sec. 4.7.2, but will assume for now.

Consider the average energy current into drive j in an initial state with fermions completely filling the region between x_1 and x_2:

$$[P_j]_{[x_1,x_2],t} = \lim_{T\to\infty} \frac{1}{T} \int\limits_0^T \mathrm{d}t \; \mathrm{Tr}\, P_j(t) \rho_{[x_1,x_2]}. \tag{4.106}$$

Here $P_j(t) = \Omega_j \dot{n}_j(t)$ and $\rho_{[x_1,x_2]}$ is the projector onto the sites between x_1 and x_2. Due to the localization of the quasienergy states, the only non-zero contributions to this integral can come from the ends of the filled region near x_1 or x_2. In the interior the localization of the quasienergy states ensures that $\dot{\vec{n}}$ averages to zero, while the integrand is explicitly zero outside the filled region. In fact, the total integral must also be zero as the boundedness of $n_j(t)$ in time in a localized phase implies that the average of $\dot{n}_j(t)$ vanishes in any initial state.

We can extract the energy current contribution to (4.106) from the sites S near x_1 by considering a system consisting only of the sites S with open boundary conditions (Fig. 4·14(a) and (b)). Due to the localization of the quasienergy states, the observable energy current in this segment only depends exponentially weakly on the different boundary conditions. Denoting operators on the system with open boundary conditions with a bar and writing $[P_{j,S}]_t$ for the energy current near x_1 in the original system, we have

$$[P_{j,S}]_t = [\bar{P}_j]_t + O(e^{-|S|/\xi}). \tag{4.107}$$

In Sec. 4.7.2 we relate $[\bar{P}_j]_t$ to the average circulation of the system with periodic boundary conditions obtained by joining the ends of the open system (Fig. 4·14(b) and (c)). Calling this quantity $[M_S]_t$, we have

$$[\bar{P}_j]_t \propto [M_S]_t. \tag{4.108}$$

The circulation $[M_S]$ can now be related to our original quantity of interest $[M\rho_S]_t$. Indeed, localization implies the operators $|S|M_S$ and $L\rho_S M\rho_S$ coincide for states away from the boundaries of S. The factors of system size $|S|$ and L are present as the conjugate variable to the flux threading the small system (Fig. 4·14(c)) is $r/|S|$, while in the large system (Fig. 4·14(a)) it is r/L. Thus M carries an implicit factor $1/L$, while M_S has a factor $1/|S|$. Accounting for exponential corrections due to states localized near the boundary of S, we have

$$\tfrac{L}{|S|}[M\rho_S]_t = [M_S]_t + O(e^{-|S|/\xi}). \tag{4.109}$$

Following through the same logic at x_2 with S', and paying careful attention to a minus sign due to the orientation at that boundary being opposite, we conclude that

$$[P_j]_{[x_1,x_2],t} \propto \tfrac{L}{|S|}[M\rho_S]_t - \tfrac{L}{|S'|}[M\rho_{S'}]_t + O(e^{-|x_1-x_2|/\xi}). \tag{4.110}$$

However, recall the left hand side must be zero as the average of $\dot{n}_j(t)$ vanishes in any initial state. We then deduce that $\frac{L}{|S|}[M\rho_S] = \frac{L}{|S'|}[M\rho_{S'}]$ up to exponentially small corrections. That is, the mesoscopic average of the circulation densities at x_1 and x_2 are equal.

4.7.2 Quantized Edge Pumping

In addition to the quantized circulation of Sec. 4.7.1, the QP pump also has topological edge effects. Namely, there is a quantized pumping of energy between the drives (an energy current) when the wire is prepared in an initial state with fermions filling all lattice sites near an edge (c.f. Refs. [44, 47]).

The presence and nature of the edge states can be deduced intuitively by considering a commensurate approximation to the incommensurately driven problem of interest. As noted in Sec. 2.2.2, this commensurate approximation compactifies the frequency lattice model into a cylinder, which may be threaded by a flux Φ (Fig. 4·15(a)). The $(2+1)$-dimensional ALTP (the AFAI) of equivalent geometry consists of a driven annulus and possesses edge states which carry a charge current along the two rings of the annulus (Fig. 4·15(b)). The movement of charge around this cylinder in the AFAI corresponds in the frequency lattice to the transport of a state through different photon occupation states $|\vec{n}\rangle$. That is, a current of energy between the drives.

The same conclusion may be drawn by inspecting the quasienergy band structure of the $(2+1)$-dimensional model. The quasienergies of the edge states wind $W[V]$ times around their domain of periodicity as a quantum of flux twists the periodic boundary conditions. In the quasiperiodic limit (the infinite system size limit of the periodic dimension) the dependence of the gradient of the quasienergy on the threaded flux disappears Ref. [38]. This results in quasienergy bands of constant gradient proportional to $W[V]$ (Fig. 4·15(c)). The gradient of the quasienergy itself is directly proportional to the long-time average of the pumped power Ref. [38].

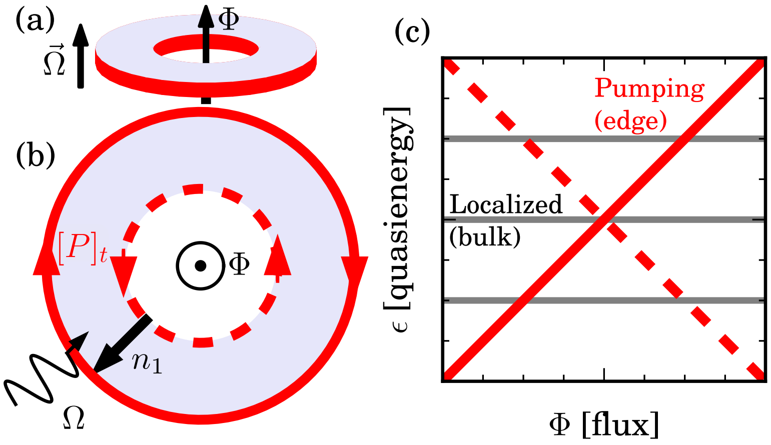
(a)
$\vec{\Omega}$
Φ
(b)
$[P]_t$
Φ
n_1
Ω
(c)
Pumping
(edge)
Localized
(bulk)
ϵ [quasienergy]
Φ [flux]

Figure 4·15: *Edge states in a commensurate approximation.*—**(a)** The (3 + 0)-dimensional frequency lattice corresponding to a one-dimensional system driven by two *commensurate* tones is a cylinder. **(b)** The corresponding $(2 + 1)$-dimensional system is a driven annulus. A charge current in the $(2 + 1)$-dimensional system corresponds to an energy current between the drives $[P]_t$ in the $(1 + 2)$-dimensional system. **(c)** The spectral flow of the quasienergy states as a quantum of flux twists the periodic boundary conditions. The edge states responsible for the energy current wind around the domain of periodicity of the quasienergy, while the localized bulk states are unaffected.

With this intuition we now proceed to the formal proof, which does not make use of any commensurate approximation. The proof, not surprisingly, mirrors the corresponding proof for the AFAI [126].

We consider a one-dimensional lattice of sites $|n_1\rangle$ driven by two incommensurate tones $\vec{\Omega} = \Omega_2\hat{e}_2 + \Omega_3\hat{e}_3$. The winding number invariant, $W[V]$, of this system is associated with periodic boundary conditions in the n_1 direction, being given explicitly by (4.54). We will show the winding number $W[V]$ is related to energy current at the edge of a chain with *open* boundary conditions, but which is identical to the periodic system in the bulk.

Unlike Sec. 4.7.1, we will use the standard coordinate axes, so $\partial_1 = \partial_{\Phi_1}$ (with Φ_1 being a flux) while $\partial_{2,3} = \partial_{\theta_{02,03}}$. As in Sec. 4.7.1, we write $n_j(t;\vec{\theta}_0) = n_j(0;\vec{\theta}_0) - iU^\dagger\partial_j U(t,0;\vec{\theta}_0)$ for the frequency lattice position along the j axis, and $\dot{n}_j(t;\vec{\theta}_0) = -\bar{U}^\dagger\partial_j\bar{H}(\vec{\theta}_t)\bar{U}$ for its derivative. We will denote operators in the system with open boundary conditions by a bar, so that the open system has Hamiltonian $\bar{H}$, micromotion $\bar{V}$ and so on.

We will prove that the average energy current into drive two (three) is quantized when the lattice is initialized in a state with fermions completely filling all sites localized near one of the edges. That is,

$$[\bar{P}_{2,3}]_{s,t<T} := \frac{1}{T}\int_0^T \mathrm{d}t\ \mathrm{Tr}\,\bar{P}_{2,3}(t)\rho_s = \pm\frac{\Omega_2\Omega_3}{2\pi}W[V] + O(T^{-1}, e^{-s/\xi}, e^{-L/\xi}) \tag{4.111}$$

where $\bar{P}_j(t) = \Omega_j\dot{\bar{n}}_j(t)$ $(j \in \{2,3\})$ is the Heisenberg operator for the current into drive j, ρ_s is a projector onto the sites $|n_1\rangle$ within a distance s of the edge, L is the length of the chain and ξ is the single-particle localization length.

First we relate $\bar{P}_j(t)$ to a Berry curvature. This calculation is standard in the literature [9, 11, 37, 38]. Using the product rule, we have

$$-\bar{U}^\dagger \partial_j \bar{H} \bar{U} = -\partial_j(\bar{U}^\dagger \bar{H} \bar{U}) + (\partial_j \bar{U}^\dagger)\bar{H}\bar{U} + \bar{U}^\dagger \bar{H}(\partial_j \bar{U}). \tag{4.112}$$

Using the Schrödinger equation $i\partial_t \bar{U} = \bar{H}\bar{U}$, this becomes

$$-\bar{U}^\dagger \partial_j \bar{H} \bar{U} = -i\partial_j(\bar{U}^\dagger \partial_t \bar{U}) + i(\partial_j \bar{U}^\dagger \partial_t \bar{U} - \partial_t \bar{U}^\dagger \partial_j \bar{U}). \tag{4.113}$$

The first term, when substituted back into the integral gives a contribution proportional to $\partial_j \left(\frac{1}{T}\int \mathrm{d}t \ \mathrm{Tr}\, \bar{U}^\dagger \bar{H} \bar{U} \rho_s\right)$, which is the θ_{0j} derivative of the average energy. In the $T \to \infty$ limit the average energy becomes insensitive to the initial phase, and so this term is zero. This can be seen by first noting that in the bulk of the filled region the integral becomes $\frac{1}{T}\int \mathrm{d}t \, \partial_j \, \mathrm{Tr}\, \bar{H} = \frac{1}{(2\pi)^3}\int \mathrm{d}^3\theta \, \partial_j \, \mathrm{Tr}\, \bar{H} + O(T^{-1})$ which is the integral of a total derivative over the torus, and so is zero. Away from the boundary of the lattice all the quasienergy states are localized in the frequency lattice, and so their instantaneous energy also has the periodicity of the torus, and their derivatives integrate to zero.

The remaining term in (4.113) is indeed a Berry curvature. By inserting $\bar{U}\bar{U}^\dagger = \mathbb{1}$ and using $(\partial \bar{U}^\dagger)\bar{U} = -\bar{U}^\dagger \partial \bar{U}$ we put the full expression (4.111) in the form

$$[\bar{P}_j]_{s,t<T} = -\frac{i\Omega_j}{T}\int_0^T \mathrm{d}t \ \mathrm{Tr}\, [\bar{n}_t, \bar{n}_j]\, \rho_s \tag{4.114}$$

where we denoted $\bar{n}_k = -i\bar{U}^\dagger \partial_k \bar{U}$. Using the fact that $\mathrm{Tr}\,[A,B]\,C = -\mathrm{Tr}\, B\,[A,C]$ this is

$$[\bar{P}_j]_{s,t<T} = \frac{i\Omega_j}{T}\int_0^T \mathrm{d}t \ \mathrm{Tr}\, \bar{n}_j[\bar{n}_t, \rho_s]. \tag{4.115}$$

Eq. 4.115 may be related to the model with periodic boundary conditions through the use of an auxiliary gauge transformation of the form

$$|n_1\rangle \mapsto |n_1\rangle\,, \quad n_1 \leq s \tag{4.116}$$

$$|n_1\rangle \mapsto e^{i\Phi_1}\,|n_1\rangle\,, \quad n_1 > s \tag{4.117}$$

which is implemented by the unitary $G_{\Phi_1} = e^{i\Phi_1(\mathbb{1}-\rho_s)}$. As this is a pure gauge transformation on the system with open boundary conditions in the n_1 direction, it does not affect expectation values of physical observables. Then, defining $\bar{A}(\Phi_1) = G^\dagger_{\Phi_1}\bar{A}G_{\Phi_1}$ and using that G_{Φ_1} and ρ_s commute we have

$$[\bar{P}_j]_{s,t<T} = \frac{i\Omega_j}{T}\int\limits_0^T \mathrm{d}t\ \mathrm{Tr}\,\bar{n}_j(\Phi_1)[\bar{n}_t(\Phi_1), \rho_s]. \tag{4.118}$$

The commutator in this expression can be expressed as a derivative,

$$[\bar{n}_t(\Phi_1), \rho_s] = i\partial_1\bar{n}_t(\Phi_1), \tag{4.119}$$

giving the expression

$$[\bar{P}_j]_{s,t<T} = -\frac{\Omega_j}{T}\int\limits_0^T \mathrm{d}t\ \mathrm{Tr}\,\bar{n}_j(\Phi_1)\partial_1\bar{n}_t(\Phi_1). \tag{4.120}$$

We now relate this expression involving operators on the chain with open boundary conditions (with bars) to a similar expression on the system with periodic boundary conditions (with no decorations). That is, we consider a one-dimensional system with periodic boundary conditions, a circle, driven by two periodic tones with a flux Φ_1 twisting the boundary conditions. The Hamiltonian $H(t;\Phi_1,\theta_{02},\theta_{03})$ on the circle is identical to $G^\dagger_{\Phi_1}\bar{H}(t;\theta_{02},\theta_{03})G_{\Phi_1}$ in the interior of the chain.

Due to the assumed localization of the bulk of the chain, the operators $\bar{n}_k$ are all themselves local. This means that on the circle $n_t(\Phi_1)$ depends only exponentially weakly on Φ_1. This weak dependence on the twisted boundary condition Φ_1 and the posited matching of H and $\bar{H}$ in the interior implies $i\partial_1 \bar{n}_t(\Phi_1) = i\partial_1 n_t(\Phi_1) + O(e^{-L/\xi})$. We also see from (4.115) that the only states making significant contribution to the integrand are those near $n_1 = s$—this is the only region where ρ_s is not locally proportional to the identity, and so is the only place the commutator can be non-zero. For large enough s this is well within the bulk of the chain, where the $\bar{n}_k$ operators match the operators on the circle. We conclude that we may replace the chain operators in (4.120) with their periodic boundary condition equivalents, with only exponentially small corrections in L/ξ and s/ξ, which we suppress. This gives

$$[\bar{P}_j]_{s,t<T} = -\frac{\Omega_j}{T} \int_0^T \mathrm{d}t \; \operatorname{Tr} n_j(\Phi_1) \partial_1 n_t(\Phi_1). \tag{4.121}$$

The integrand here is an expression to which the result of Sec. 4.7.1.1 (4.81) applies. This result may be applied repeatedly to show (suppressing Φ_1 dependence)

$$\operatorname{Tr} n_j \partial_1 n_t = -\operatorname{Tr} n_1 \partial_t n_j + \partial_j \operatorname{Tr} n_1 n_t. \tag{4.122}$$

The product rule then gives

$$\operatorname{Tr} n_1 \partial_t n_j = \tfrac{1}{2} \operatorname{Tr} n_1 \partial_t n_j - n_j \partial_t n_1 + \tfrac{1}{2} \partial_t \operatorname{Tr} n_j n_1, \tag{4.123}$$

so that the integrand is

$$-\operatorname{Tr} n_j \partial_1 n_t = \tfrac{1}{2} \operatorname{Tr} n_1 \partial_t n_j - n_j \partial_t n_1 - \partial_j \operatorname{Tr} n_1 n_t + \tfrac{1}{2} \partial_t \operatorname{Tr} n_j n_1. \tag{4.124}$$

The first of these terms is $\pm \operatorname{Tr} \frac{1}{2}(\vec{n} \times \dot{\vec{n}}) \cdot \hat{e}_k$, where $k \neq j$ and the sign is positive for $j = 2$ and negative for $j = 3$.

Substituting (4.124) into (4.121), we see

$$[\bar{P}_j]_{s,t<T} = \pm\frac{\Omega_j}{T}\int\limits_0^T \mathrm{d}t\ \mathrm{Tr}\,\tfrac{1}{2}(\vec{n}\times\dot{\vec{n}})\cdot\hat{e}_k - \partial_j\,\mathrm{Tr}\,n_1 n_t + \partial_t\,\mathrm{Tr}\,\tfrac{1}{2}n_j n_1. \tag{4.125}$$

Both of the total derivative terms average to zero in the $T\to\infty$ limit. This can be seen explicitly for the time derivative:

$$\frac{1}{T}\int\limits_0^T \mathrm{d}t\,\partial_t\,\mathrm{Tr}\,\tfrac{1}{2}n_j n_1 = \frac{1}{T}\,\mathrm{Tr}\,\tfrac{1}{2}n_j n_1\Big|_0^T = O(T^{-1}) \tag{4.126}$$

as $\vec{n}$ is bounded in time by the assumed localization in both space and the frequency lattice.

The other derivative term is an initial phase derivative of the long-time average of an observable, and so is also zero. Explicitly, expanding the trace in a basis of quasienergy states:

$$\begin{aligned}\mathrm{Tr}\,n_1 n_t = &\sum_{\alpha,\beta}\langle\psi_\alpha(t)|\,\partial_1\,|\psi_\beta(t)\rangle\,\langle\psi_\beta(t)|\,\partial_t\,|\psi_\alpha(t)\rangle\\ &= \sum_{\alpha,\beta}\Big(\langle\phi_\alpha(\vec{\theta}_t)|\,\partial_1\,|\phi_\beta(\vec{\theta}_t)\rangle\,\langle\phi_\beta(\vec{\theta}_t)|\,\partial_t\,|\phi_\alpha(\vec{\theta}_t)\rangle\\ &\qquad - i\epsilon_\alpha\,\langle\phi_\alpha(\vec{\theta}_t)|\,\partial_1\,|\phi_\alpha(\vec{\theta}_t)\rangle\,\delta_{\alpha\beta}\Big),\end{aligned} \tag{4.127}$$

which is periodic on the torus $\vec{\theta}_t$, and so its initial phase derivatives vanish upon averaging.

We are left with

$$[\bar{P}_j]_{s,t<T} = \pm\Omega_j[\tfrac{1}{2}(\vec{n}\times\dot{\vec{n}})\cdot\hat{e}_k]_{t<T}. \tag{4.128}$$

We want to relate this to $[\frac{1}{2}(\vec{n}\times\dot{\vec{n}})\cdot\hat{\Omega}]_{t<T} = [M]_{t<T}$, so that we can use the main result of Sec. 4.7.1 (4.79) to relate this to the winding number. The spatial system is localized, and so cannot absorb energy indefinitely. Thus, the long-time average of

the energy current into the system is zero. That is,

$$[\tfrac{1}{2}(\vec{n}\times\dot{\vec{n}})\cdot(-\Omega_2\hat{e}_3+\Omega_3\hat{e}_2)]_{t<T} = -[\bar{P}_2]_{s,t<T} - [\bar{P}_3]_{s,t<T} \\ = [\partial_t \bar{H}]_{s,t<T} = O(T^{-1}). \quad (4.129)$$

Writing $\hat{\ell} = (-\Omega_2\hat{e}_3+\Omega_3\hat{e}_2)/|\vec{\Omega}|$, we see that $[\frac{1}{2}(\vec{n}\times\dot{\vec{n}})]_{t<T}$ has no component along $\hat{\ell}$ in the long time limit. Then we can decompose $\hat{e}_k = (\hat{\ell}\cdot\hat{e}_k)\hat{\ell} + (\hat{\Omega}\cdot\hat{e}_k)\hat{\Omega}$ in (4.128), and discard the part with $\hat{\ell}$. This leaves just

$$[\bar{P}_j]_{s,t<T} = \pm\frac{\Omega_j\Omega_k}{|\vec{\Omega}|}[\tfrac{1}{2}(\vec{n}\times\dot{\vec{n}})\cdot\hat{\Omega}]_{t<T} + O(T^{-1}). \quad (4.130)$$

Using the main result of Sec. 4.7.1, this is

$$[\bar{P}_j]_{s,t<T} = \pm\frac{\Omega_2\Omega_3}{2\pi}W[V] + O(T^{-1}, e^{-s/\xi}, e^{-L/\xi}), \quad (4.131)$$

where we restored the suppressed exponential corrections.

4.8 Summary and Discussion

This chapter provided an explicit coupled layer model for the QP pump, which we analyzed in detail. Further, we made a general classification of ALTPs in any spatial dimension d and number of driving tones D. The general analysis shows that the quantized pumping of energy by the coupled layer edge mode is a generic feature of all QP pump models.

Toy models capturing the physics of a system are essential in the study of complicated effects [9, 137, 163]. The coupled layer construction for the QP pump allows for the straightforward identification of localized pumping modes at the edge, and an improved understanding of the topological-trivial transition. Similar models of ALTPs with more drives enable a comparably straightforward analysis of the edge modes, including the synthetic four-dimensional quantum Hall response of the (2+3)-dimensional ALTP.

With these models in hand, a systematic study of the observable responses of higher D ALTPs can be made. This is crucial when seeking technological applications of ALTPs, and a necessary ingredient for a more complete theoretical understanding of these phases. Some applications of ALTP phenomenology are known—energy pumping can be used to prepare highly excited nonclassical cavity states [3]—but finding ways to exploit other behaviors of ALTPs remains an interesting opening for future research.

In a similar direction, finding experimentally feasible models for ALTPs would be very useful. The coupled layer models serve as a theoretical toy—they are not obviously suitable for realization in the laboratory. However, they could serve as a guide towards what features are necessary in an experimental Hamiltonian. The effect of dissipation and decoherence (as occurs in any experimental realization) on the energy pumping response should also be considered.

Our discussion of the coupled layer model focused on edge modes, but ALTPs also possess a quantized bulk response (Sec. 4.7.1.3) [1, 65]. In the QP pump, the bulk energy circulation can be understood qualitatively through the coupled layer model (Fig. 4·3). Extending this qualitative understanding to a quantitative one could provide access to bulk observables in higher D ALTPs, and potentially illuminate the nature of the bulk-edge correspondence in these phases.

Our analysis of the QP pump transition was consistent with the two-dimensional quantum Hall transition universality class [139–146]. However, our finite size scaling does not fix the critical exponents with high precision, nor is the theoretical connection concrete. A more extensive study of this transition may provide confirmation of this conjectured universality class. Due to the similarity of the coupled layer model to an

SSH model in a rotating frame, it may be amenable to a real-space renormalization group analysis [164–166]. Alternatively, a network model for the transition, similar to the Chalker-Coddington model, would make the connection to quantum Hall systems transparent [144].

The topological pumping response of the QP pump persists for an extremely long time when weak interactions are introduced. However, we have not observed a regime where the coupled layer model is asymptotically localized. Given that current numerical studies of MBL can no longer confirm such a phase in static systems [72–77, 151–153], it seems unlikely that a larger numerical study will be able to observe such a regime in quasiperiodically driven systems. Instead, it would be interesting to better understand the mechanism of thermalization in the accessible parameter regime. In static systems, this is likely due to many-body resonances between macroscopically distinct states [76, 167–173]. Extending the improved understanding of such resonances in static systems to the quasiperiodically driven setting would be interesting.

Beyond the QP pump, all $(0+D)$-dimensional ALTPs—driven qudits—are within immediate experimental reach in a number of solid-state and optical architectures [174–176]. Signatures of topology in the adiabatic limit have already been observed with two-tone driven nitrogen vacancy centers [28]. Investigation of ALTPs with still higher $d + D$ provides access to the topological physics of driven systems in four dimensions and higher. To date, such responses have been observed only in the adiabatic limit [135, 177].

Chapter 5

Many-Body Localization With Quasiperiodic Driving

Strong periodic driving generates new phases of matter with no analogueue in static systems [12, 116, 178]. Examples include anomalous topological insulators with chiral edge modes [11, 90, 126, 179], and discrete time crystals with sub-harmonic response to the drive [119, 120, 180]. Several optical and solid-state experiments have observed signatures of these dynamical phases [131, 181–184].

As we saw in chapter 4, quasiperiodic driving by multiple incommensurate tones [13–24, 185] generates orders not accessible in either static *or* periodically-driven systems [1, 27, 33, 34, 37, 44, 46, 64, 65, 186–191], some of which have been experimentally observed [28, 29, 135, 177, 192, 193]. For instance, anomalous localized phases support energy currents between the drives at their edges [1, 44, 65], and spin chains without any assumed symmetry exhibit coherent edge states [34]. In both cases, the orders rely on localization in the bulk to forbid heating to a featureless infinite-temperature state [67, 69–71, 150, 156, 157, 194–200].

However, with interactions and quasiperiodic driving, it is unclear if the bulk can remain localized indefinitely, and thus if these orders characterize genuine dynamical phases of matter. Localization in quasiperiodically-driven systems is likely to be delicate, as even qubits can have ergodic dynamics and act as a local heat bath for nearby degrees of freedom [1, 16, 17, 65]. Indeed, this is why there is no localization in classical spin chains [201, 202].

This chapter provides analytical and numerical evidence that quasiperiodically-driven many-body localization (MBL) is a stable dynamical phase for smooth two-

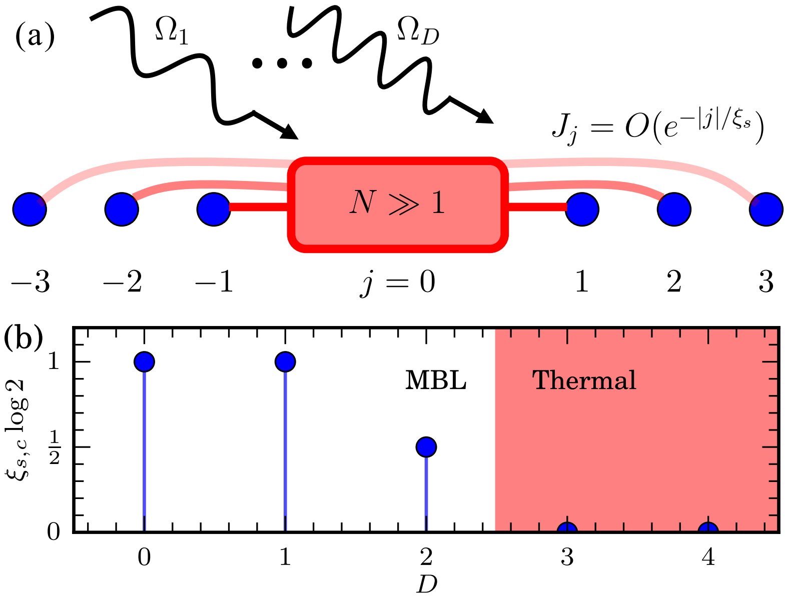

Figure 5·1: (**a**) *Thermal inclusions.*—The dominant mechanism of thermalization for a randomly disordered driven chain is the occurrence of a thermal region, say at site $j = 0$. The system is driven by D tones with frequencies $\Omega_1, \ldots, \Omega_D$, and the N-level thermal region has exponentially decaying couplings $J_j = O(e^{-|j|/\xi_s})$ to l-bits a distance j from the thermal region. (**b**) *Critical localization length.*— MBL is stable to the inclusion of a thermal region for $D = 0$ (static systems), $D = 1$ (periodically driven), $D = 2$, and not for any $D \geq 3$. The critical localization length below which MBL is stable is reduced to $\xi_{s,c} = (2 \log 2)^{-1}$ for two-tone driving.

tone driving. Here, few-level systems generically have pure point spectra (Sec. 5.5). Analogous arguments to those in static MBL then show that perturbations do not lead to the proliferation of long-range many-body resonances [167, 169, 170] (Sec. 5.7).

However, other potential instabilities remain—in particular, for MBL by random disorder, a large thermal region with N levels may absorb nearby spins and initiate a thermal avalanche [78, 200] (Fig. 5·1). Here, the spectrum being pure point does not guarantee stability. Intuitively, the number of harmonics must grow slowly enough with N (Sec. 5.4). We show that the scaling with N allows for stable MBL when the localization length is less than a critical value,

$$\xi_{s,c} = (2\log 2)^{-1}. \tag{5.1}$$

Notably, the critical localization length is reduced as compared to the static and periodically-driven cases (Fig. 5·1).

With three or more tones in the drive, sufficiently large thermal inclusions show continuous spectra [1, 44]. Just as in classical systems, a putatively-MBL chain is not stable to such an inclusion. Thus, quasiperiodically-driven MBL with random disorder does not exist with three or more tones (Sec. 5.6).

It should be noted that the validity of the arguments which lead to Eq. (5.1) have been questioned recently in the context of static systems [72–77], though there is not yet consensus in the community on this issue. The objections to the stability of MBL are primarily supported by numerical evidence, and show that, at the very least, asymptotic stability of MBL occurs at far larger disorder strengths than previously believed. If, in fact, there is no static MBL phase, then there is also no quasiperiodically driven MBL phase. Our conclusion that MBL cannot be stable for three or more tone driving is less affected by this debate.

Two of our intermediate results are of independent interest. We characterize l-bits with quasiperiodic driving in terms of the frequency lattice (Sec. 5.2), which requires careful attention to the structure of the frequency lattice in many-body systems (Sec. 5.1). We also adapt the eigenstate thermalization hypothesis (ETH) [203–207] to quasiperiodically driven systems, and test its predictions numerically (Sec. 5.3).

In what follows, we focus on thermal inclusions in randomly disordered chains, before addressing the perturbative stability of MBL. The former is more constraining in its implications for MBL, and provides mathematical machinery with which to analyze the latter.

5.1 Frequency lattice for interacting systems

The frequency lattice organizes the Fourier content of the long-time steady states of quasiperiodically-driven systems [13, 16, 17, 30, 36, 208] (chapter 2). It is well suited to discussions of formally infinite-time properties, such as localization. However, there are several subtleties that arise in the treatment of many-body Hamiltonians in this context, which we explain in this section.

We begin by recalling the frequency lattice construction. We consider one-dimensional quantum systems with smooth quasiperiodic time dependence consisting of D incommensurate tones. Such a Hamiltonian may be parameterized in terms of D phase variables $\theta_j(t) = \Omega_j t$, where Ω_j is the angular frequency of the jth drive. For convenience, we assemble the phases into a vector

$$\vec{\theta}_t = \sum_{j=1}^{D} \theta_j(t)\hat{e}_j. \tag{5.2}$$

The time-dependent Hamiltonian may then be written as

$$H(t) = H(\vec{\theta}_t), \quad \text{where} \quad H(\vec{\theta} + 2\pi\hat{e}_j) = H(\vec{\theta}) \tag{5.3}$$

is periodic in each phase variable, with period 2π. Incommensurability of the frequencies is stated mathematically as

$$\vec{n} \cdot \vec{\Omega} = 0 \quad \Longleftrightarrow \quad \vec{n} = 0, \tag{5.4}$$

where $\vec{n} \in \mathbb{Z}^D$ is a vector of integers. (For $D = 2$, this is equivalent to Ω_1/Ω_2 being irrational.) The drive is not periodic, but is instead, in a sense that can be made precise, almost periodic.

In analoguey to the stationary state solutions of the Schrödinger equation with a static Hamiltonian, the steady states of a quasiperiodically driven system are the *quasienergy states* [13, 17, 87]

$$|\psi_\alpha(t)\rangle = e^{-i\epsilon_\alpha t}\,|\phi_\alpha(\vec{\theta}_t)\rangle\,, \tag{5.5}$$

where $|\psi_\alpha(t)\rangle$ is a solution to the Schrödinger equation $i\partial_t\,|\psi_\alpha(t)\rangle = H(t)\,|\psi_\alpha(t)\rangle$, α indexes a basis of the Hilbert space, ϵ_α is the *quasienergy* and the quasienergy state $|\phi_\alpha(\vec{\theta}_t)\rangle$ is smooth on the torus. The states

$$|\phi_\alpha(\vec{\theta})\rangle = \sum_{\vec{n}\in\mathbb{Z}^D} |\phi_{\alpha\vec{n}}\rangle\, e^{-i\vec{n}\cdot\vec{\theta}} \tag{5.6}$$

may be calculated after a Fourier transform from the eigenvalue equation

$$\sum_{\vec{m}\in\mathbb{Z}^D} K_{\vec{n}\vec{m}}\,|\phi_{\alpha\vec{m}}\rangle = \epsilon_\alpha\,|\phi_{\alpha\vec{n}}\rangle\,, \tag{5.7}$$

where

$$K_{\vec{n}\vec{m}} = H_{\vec{n}-\vec{m}} - \vec{\Omega}\cdot\vec{n}\delta_{\vec{n}\vec{m}}, \tag{5.8}$$

and $H_{\vec{n}}$ are the Fourier components of $H(\vec{\theta}) = \sum_{\vec{n}} H_{\vec{n}} e^{-i\vec{n}\cdot\vec{\theta}}$. The quasienergy states being smooth on the torus is equivalent to the Fourier components $|\phi_{\alpha\vec{n}}\rangle$ being localized in $\vec{n}$. If the eigenstates of $K_{\vec{n}\vec{m}}$ are delocalized, the quasienergy states are not well-defined.

The operator $K_{\vec{n}\vec{m}}$ is a static lattice Hamiltonian in an extended *frequency lattice.* It has translationally-invariant hopping matrices given by $H_{\vec{n}-\vec{m}}$, and an on-site linear potential $-\vec{\Omega}\cdot\vec{n}$ which breaks translational symmetry. This linear potential would arise in real-space from a uniform electric field given by $\vec{\Omega}$, so we sometimes refer to $\vec{\Omega}$ in this context as an electric field.

The frequency lattice has additional *synthetic dimensions* corresponding to each of the periodic drives (Fig. 5·2). We make this explicit by appending states $|\vec{n}\rangle$ to the

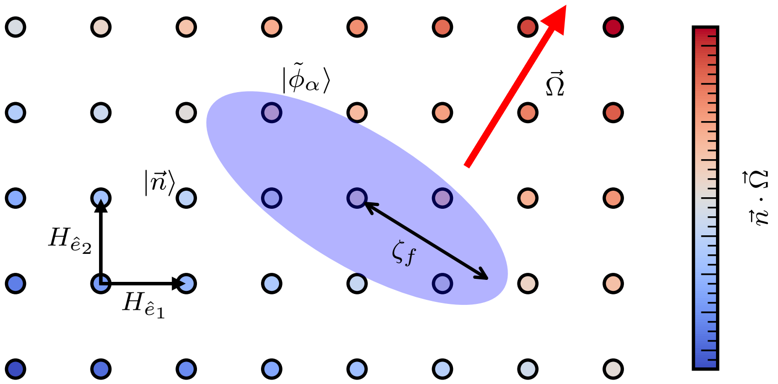

Figure 5·2: *The frequency lattice.*—The steady states of a system driven by D incommensurate tones are the eigenstates of a static lattice problem in an extended frequency lattice. This lattice has additional synthetic dimensions, with sites labeled by $\vec{n} \in \mathbb{Z}^D$ (each site shown has all of the degrees of freedom of the spatial Hilbert space). The hopping matrices $H_{\vec{n}-\vec{m}}$ in the frequency lattice are given by Fourier components of the driven Hamiltonian. The on-site linear potential is $-\vec{n}\cdot\vec{\Omega}$, as might arise from a uniform electric field $\vec{\Omega}$. The quasienergy states $|\tilde{\phi}_\alpha\rangle$ are localized with localization length ζ_f. The degree of localization parallel to $\vec{\Omega}$ is greater than that perpendicular to $\vec{\Omega}$.

Hilbert space and defining [13, 16, 17, 36]

$$\tilde{K} = \sum_{\vec{n},\vec{m}\in\mathbb{Z}^D} K_{\vec{n}\vec{m}} |\vec{n}\rangle\langle\vec{m}|, \tag{5.9}$$

and similarly $|\tilde{\phi}_\alpha\rangle = \sum_{\vec{n}} |\phi_{\alpha\vec{n}}\rangle\,|\vec{n}\rangle$. Explicitly, the extended Hilbert space is

$$\mathcal{K} = \mathcal{H} \otimes \ell^2(\mathbb{Z}^D), \tag{5.10}$$

where $\mathcal{H}$ is the Hilbert space in the temporal domain, and $\ell^2(\mathbb{Z}^D)$ denotes the space of square-summable complex valued functions on the square lattice $\mathbb{Z}^D$.

In this chapter, we will decorate states in, and operators on, $\mathcal{K}$ with a tilde, to make a clear distinction between those objects that have the extra factor $\ell^2(\mathbb{Z}^D)$, and those that do not.

Extending the Hilbert space introduces a new gauge freedom related to the position of the origin in the synthetic dimensions. Translations in the synthetic dimensions do not produce observable effects on real-time dynamics, as may be seen explicitly from the quasienergy states. A translation of a quasienergy state $|\tilde{\phi}_\alpha\rangle$ by a lattice vector $\vec{m}$,

$$|\tilde{\phi}_\alpha^{\vec{m}}\rangle = \sum_{\vec{n}} |\phi_{\alpha\vec{n}}\rangle\,|\vec{n}+\vec{m}\rangle\,, \tag{5.11}$$

is another quasienergy state of $\tilde{K}$, with quasienergy $\epsilon_\alpha - \vec{m}\cdot\vec{\Omega}$. The actual solution to the Schrödinger equation, however, does not change:

$$|\psi_\alpha^{\vec{m}}(t)\rangle = e^{-i(\epsilon_\alpha - \vec{m}\cdot\vec{\Omega})t} e^{-i\vec{m}\cdot\vec{\Omega}t}\,|\phi_\alpha(\vec{\theta})\rangle = |\psi_\alpha(t)\rangle\,. \tag{5.12}$$

An operator $O(\vec{\theta})$ on $\mathcal{H}$ corresponds to an operator on $\mathcal{K}$ defined by

$$\tilde{O} = \sum_{\vec{n},\vec{m}} O_{\vec{n}-\vec{m}} |\vec{n}\rangle\langle\vec{m}|, \tag{5.13}$$

which is constructed so that $O(\vec{\theta})\,|\phi(\vec{\theta})\rangle \leftrightarrow \tilde{O}\,|\tilde{\phi}\rangle$. We see that physical operators are naturally translationally invariant (gauge invariant) in the frequency lattice.

When $\mathcal{H}$ is a many-body Hilbert space for a spatially extended system, the character of the spatial dimensions is different from the synthetic frequency lattice dimensions. If we consider a finite subsystem of the frequency lattice for a spin-$\frac{1}{2}$ chain with L spins and M synthetic sites, the Hilbert space dimension supported on this subsystem is $2^L M$. The synthetic part of the problem is thus analogueous to a single-particle system, even in the many-body setting.

Furthermore, the structure of tensor products in the frequency lattice is more complicated than in the temporal domain. The origin of this complication is that there is only one factor of $\ell^2(\mathbb{Z}^D)$ in the frequency lattice Hilbert space, even in a tensor product system. Explicitly, if $\mathcal{H} = \mathcal{H}_1 \otimes \mathcal{H}_2$, then

$$\mathcal{K} = \mathcal{H}_1 \otimes \mathcal{H}_2 \otimes \ell^2(\mathbb{Z}^D) \neq \mathcal{K}_1 \otimes \mathcal{K}_2, \tag{5.14}$$

where $\mathcal{K}_j = \mathcal{H}_j \otimes \ell^2(\mathbb{Z}^D)$. As a consequence, given states $|\phi_j(\vec{\theta})\rangle \in \mathcal{H}_j$ and corresponding frequency lattice states $|\tilde{\phi}_j\rangle \in \mathcal{K}_j$, the frequency lattice state corresponding to $|\phi_1(\vec{\theta})\rangle \otimes |\phi_2(\vec{\theta})\rangle$ is obtained as a convolution, for which we use the symbol $*$,

$$|\tilde{\phi}_1\tilde{\phi}_2\rangle = |\tilde{\phi}_1\rangle * |\tilde{\phi}_2\rangle = \sum_{\vec{n}} \left(\sum_{\vec{m}} |\phi_{1,\vec{n}-\vec{m}}\rangle\, |\phi_{2,\vec{m}}\rangle \right) |\vec{n}\rangle\,, \tag{5.15}$$

and not as a tensor product of the states $|\tilde{\phi}_j\rangle$.

Such tensor convolutions are somewhat more elegantly stated for operators. An operator $O_j(\vec{\theta})$ on $\mathcal{H}_j$ corresponds to an operator $\tilde{O}_j$ on $\mathcal{K}_j$ defined as in Eq. (5.13). The frequency lattice operator for the tensor product $O_1(\vec{\theta}) \otimes O_2(\vec{\theta})$ is

$$\widetilde{O_1 O_2} = (\tilde{O}_1 \otimes \mathbb{1}_2)(\mathbb{1}_1 \otimes \tilde{O}_2) = \tilde{O}_1\tilde{O}_2 = \tilde{O}_2\tilde{O}_1, \tag{5.16}$$

where in the last two expressions we use the convention that $\tilde{O}_1$ acting in $\mathcal{K}$ is regarded as acting as the identity on the space $\mathcal{H}_2$, and similarly for $\tilde{O}_2$ acting on $\mathcal{H}_1$.

5.2 Quasiperiodically-driven Many-Body Localization

We present a definition of MBL in a quasiperiodically driven setting that recovers much of the phenomenology present in static systems. In static systems, MBL may be characterized by a complete set of quasilocal integrals of motion, *l-bits* τ_j^z, for which

$$\langle\psi(t)|\,\tau_j^z\,|\psi(t)\rangle = \text{const.} \tag{5.17}$$

for any initial state $|\psi(0)\rangle$. This property results in the many striking features of MBL: memory of the initial state, pure point spectra of local observables, and so on [71, 156, 157].

Similarly, we define a complete set of l-bits $\tau_j^z(\vec{\theta})$ with explicit $\vec{\theta}$ dependence. The l-bits commute with the time evolution operator, so that

$$\langle\psi(t)|\,\tau_j^z(\vec{\theta}_t)\,|\psi(t)\rangle = \text{const.} \tag{5.18}$$

for any initial state $|\psi(0)\rangle$.

A quasiperiodically driven system is many-body localized if there is a complete set of l-bits that are (quasi)local in both the frequency and spatial lattices. That is, a set of frequency lattice operators

$$\tilde{\tau}_j^z = \sum_{\vec{n},\vec{m}\in\mathbb{Z}^D} \tau_{j,\vec{n}-\vec{m}}^z|\vec{n}\rangle\langle\vec{m}| \tag{5.19}$$

such that $[\tilde{\tau}_j^z, \tilde{K}] = 0$, $[\tilde{\tau}_j^z, \tilde{\tau}_k^z] = 0$, and with $\tilde{\tau}_j^z$ having localization center j. More precisely, decomposing $\tau^z_{j,\vec{n}}$ into terms $\tau^z_{j,\vec{n},r}$ supported within a spatial range r of j:

$$\tau^z_{j,\vec{n}} = \sum_r \tau^z_{j,\vec{n},r} \quad \text{where} \quad \|\tau^z_{j,\vec{n},r}\| = O(e^{-|\vec{n}|/\zeta_f - r/\zeta_s}). \tag{5.20}$$

Here, we have introduced a frequency localization length ζ_f, and a spatial localization length ζ_s.

The complete set of l-bits split the Hilbert space into 2^L sectors (for a spin-$\frac{1}{2}$ chain of length L). Each sector contains only one physically inequivalent quasienergy state, and may be labeled by its eigenvalues under each $\tilde{\tau}^z_j$. Furthermore, we require these quasienergy states to be localized in the synthetic dimensions—that is, that they have smooth quasiperiodic time dependence in the temporal domain.[1]

Explicitly, if we label the quasienergy state $|\tilde{\phi}_\alpha\rangle$ translated by the frequency lattice vector $\vec{n}$ as $|\tilde{\phi}^{\vec{n}}_\alpha\rangle$, then the frequency lattice l-bits may be written as

$$\tilde{\tau}^z_j = \sum_{\vec{n},\alpha} \tau^z_{j\alpha} |\tilde{\phi}^{\vec{n}}_\alpha\rangle\langle\tilde{\phi}^{\vec{n}}_\alpha|, \tag{5.21}$$

where $\tau^z_{j\alpha}$ is an $\vec{n}$ independent eigenvalue (recall that any physical operator must be translationally invariant in the synthetic dimensions). Eq. (5.21) also makes clear that the frequency lattice localization length of the l-bits, ζ_f, is also that of the quasienergy states (Fig. 5·2).

In later sections, we only use the frequency lattice operators $\tilde{\tau}^z_j$. The corresponding temporal operators are conserved quantities with explicit time dependence, as we show below.

In the temporal domain, $\tilde{\tau}^z_j$ corresponds to a smooth, quasilocal, quasiperiodic operator

---

[1] Our definition requires the quasienergy states $|\phi_\alpha(\vec{\theta})\rangle$ to be smooth on the torus. From Eq. (5.23) we can see that the requirement that $\tau^z_j(\vec{\theta})$ be smooth (that is, that $\tilde{\tau}^z_j$ be a quasilocal operator) implies that the projector $|\phi_\alpha(\vec{\theta})\rangle\langle\phi_\alpha(\vec{\theta})|$ must be smooth. Even so, the requirement that $|\phi_\alpha(\vec{\theta})\rangle$ be smooth is an independent assumption which excludes the case of $|\phi_\alpha(\vec{\theta})\rangle$ not admitting a globally smooth gauge—for instance, because it has a non-trivial Chern number.

$$\tau_j^z(t) = \tau_j^z(\vec{\theta}_t) = \sum_{\vec{n}} \tau_{j,\vec{n}}^z e^{-i\vec{n}\cdot\vec{\theta}_t} \tag{5.22}$$

such that $\tau_j^z(\vec{\theta})\,|\phi_\alpha(\vec{\theta})\rangle = \tau_{j\alpha}^z\,|\phi_\alpha(\vec{\theta})\rangle$. That is

$$\tau_j^z(\vec{\theta}) = \sum_\alpha \tau_{j\alpha}^z |\phi_\alpha(\vec{\theta})\rangle\langle\phi_\alpha(\vec{\theta})| \tag{5.23}$$

is diagonal in the quasienergy state basis, even in the temporal domain.

The temporal domain operators do not necessarily commute with the instantaneous Hamiltonian, $[\tau_j^z(\vec{\theta}), H(\vec{\theta})] \neq 0$. Rather, the Heisenberg operators

$$\tau_j^{z,H}(t) = U(t)^\dagger \tau_j^z(\vec{\theta}_t) U(t) \tag{5.24}$$

(where $U(t) = U(t,0)$ is the unitary evolution operator) are constant in time

$$\mathrm{d}_t \tau_j^{z,H}(t) = 0 \tag{5.25}$$

so that the l-bits are conserved quantities with explicit time dependence. Taking an expectation value in $|\psi(0)\rangle$ yields Eq. (5.18).

Unlike in static MBL, the Hamiltonian $H(\vec{\theta})$ cannot be expressed as a sum of products of the l-bits [156, 157]. Instead, the quasienergy operator in the frequency lattice has the analogueous property that there exists a quasilocal unitary $\tilde{W}$ in the frequency lattice so that

$$\tilde{W}\tilde{K}\tilde{W}^\dagger = -\sum_{\vec{n}} \vec{\Omega}\cdot\vec{n}|\vec{n}\rangle\langle\vec{n}| + \sum_j h_j \tilde{\sigma}_j^z + \sum_{j,j'} h_{jj'} \tilde{\sigma}_j^z \tilde{\sigma}_{j'}^z + \cdots . \tag{5.26}$$

That is, a quasilocal rotation allows $\tilde{K}$ to be expressed as a sum of products of Pauli $\tilde{\sigma}^z$ operators, up to a term that breaks the translational invariance.

The definition of MBL implies that all local observables O have pure point power spectra [16, 17], as is the case in static MBL.

5.2.1 Equivalence of Definitions of Quasiperiodically-Driven MBL

There has already been a definition of quasiperiodically-driven MBL presented in the literature [33, Section II D]. The definition proposed in Sec. 5.2 is equivalent to that in Ref. [33].

Ref. [33] defines quasiperiodically-driven MBL by first supposing a Floquet-Bloch decomposition of the evolution operator of the form

$$U(t,0) = P(\vec{\theta}_t) e^{-itH_F} P(\vec{\theta}_0)^\dagger, \tag{5.27}$$

where $P(\vec{\theta})$ is a quasilocal unitary. This is equivalent to our requirement of the existence of a complete set of smooth quasienergy states, as may be seen by taking

$$P(\vec{\theta}) = \sum_\alpha |\phi_\alpha(\vec{\theta})\rangle\langle\alpha|, \quad H_F = \sum_\alpha \epsilon_\alpha |\alpha\rangle\langle\alpha|, \tag{5.28}$$

where some locality structure must be imposed on the basis $|\alpha\rangle$ to make sense of P being quasilocal. For instance, the basis could be taken to be the product basis of uncoupled spins.

Given this decomposition exists, Ref. [33] defines a quasiperiodically-driven system to be MBL if there is a complete set of quasilocal integrals of motion for H_F, which we can express in terms of the basis $|\alpha\rangle$ as

$$\tau_j^{z\prime} = \sum_\alpha \tau_{j\alpha}^z |\alpha\rangle\langle\alpha|. \tag{5.29}$$

The relation between this $\tau_j^{z\prime}$ and our $\tau_j^z(\vec{\theta})$ is given by what Ref. [33] calls "reverse [Heisenberg] evolution".

$$\tau_j^z(\vec{\theta}_t) = P(\vec{\theta}_t) \tau_j^{z\prime} P(\vec{\theta}_t)^\dagger \tag{5.30}$$

Thus, the quasilocality of one of these objects implies the quasilocality of the other, and the two definitions of quasiperiodically-driven MBL are equivalent.

5.3 Thermal Region Ansatz

In this section, we present an ansatz which characterizes matrix elements of *thermalizing quasiperiodically-driven systems*, in the style of the eigenstate-thermalization hypothesis (ETH) [203–207]. This ansatz characterizes low-disorder regions in a quasiperiodically-driven putatively-MBL chain.

Our ansatz is a statistical description of finite quasiperiodically-driven quantum systems with pure point spectra. In the thermodynamic limit, the spectrum becomes continuous. However, it is also possible to have a continuous spectrum in a finite quasiperiodically-driven system for $D \geq 3$ (Sec. 5.6). To develop an ETH ansatz here, the spectrum should be made discrete with commensurate approximations (Sec. 5.8).

Consider an N-dimensional Hilbert space with a quasiperiodic Hamiltonian $H_B(\vec{\theta}_t)$ (the "bath Hamiltonian"). Assume that there exists a complete set of smooth quasienergy states $|\psi_\alpha(t)\rangle = e^{-i\epsilon_\alpha t} |\phi_\alpha(\vec{\theta}_t)\rangle$—that is, that the eigenstates of the corresponding quasienergy operator are localized in the synthetic dimensions, with localization length ζ_f.

The ansatz concerns matrix elements of generic local operators $V(\vec{\theta}_t)$ (V in this chapter is not to be mistaken for the micromotion operator) between quasienergy states,

$$\begin{aligned} V_{\alpha\beta}(t) &= \langle\psi_\alpha(t)| \, V(\vec{\theta}_t) \, |\psi_\beta(t)\rangle \\ &= e^{-i\omega_{\beta\alpha} t} \, \langle\phi_\alpha(\vec{\theta}_t)| \, V(\vec{\theta}_t) \, |\phi_\beta(\vec{\theta}_t)\rangle \, , \end{aligned} \tag{5.31}$$

where $\omega_{\beta\alpha} = \epsilon_\beta - \epsilon_\alpha$, and we choose particular representative quasienergy states $|\phi_\alpha(\vec{\theta}_t)\rangle$ to fix ϵ_α.

The frequency lattice operator corresponding to V is $\tilde{V} = \sum_{\vec{n},\vec{m}} V_{\vec{n}-\vec{m}} \otimes |\vec{n}\rangle\langle\vec{m}|$, and the quasienergy states are denoted $|\tilde{\phi}_\alpha^{\vec{n}}\rangle$ (5.11). Then an arbitrary matrix element of $\tilde{V}$ in the quasienergy state basis has the form

$$\begin{aligned}\tilde{V}^{\vec{n}\vec{m}}_{\alpha\beta} &= \langle\tilde{\phi}^{\vec{n}}_{\alpha}|\,\tilde{V}\,|\tilde{\phi}^{\vec{m}}_{\beta}\rangle \\ &= \sum_{\vec{j},\vec{k}} \langle\phi_{\alpha\vec{j}}|\,V_{\vec{j}-\vec{k}+\vec{n}-\vec{m}}\,|\phi_{\beta\vec{k}}\rangle\,,\end{aligned} \tag{5.32}$$

which is the coefficient of $\delta(\omega - \Delta^{\vec{n}\vec{m}}_{\alpha\beta})$ in the Fourier transform of $V_{\alpha\beta}(t)$, and $\Delta^{\vec{n}\vec{m}}_{\alpha\beta} = \omega_{\beta\alpha} + (\vec{n} - \vec{m}) \cdot \vec{\Omega}$ is the quasienergy difference between $|\tilde{\phi}^{\vec{m}}_{\beta}\rangle$ and $|\tilde{\phi}^{\vec{n}}_{\alpha}\rangle$. As $\tilde{V}$ is translationally invariant, the matrix element $\tilde{V}^{\vec{n}\vec{m}}_{\alpha\beta} = \tilde{V}^{\vec{n}-\vec{m}}_{\alpha\beta}$ only depends on the separation between $\vec{n}$ and $\vec{m}$, which we call $\vec{l} = \vec{n} - \vec{m}$. Subsequently, we only keep the $\vec{l}$ dependence in our notation.

We first state the ansatz, and then define and motivate each of the terms appearing in the equation. The ansatz is

$$\tilde{V}^{\vec{l}}_{\alpha\beta} = \bar{V}_{\vec{l}}\delta_{\alpha\beta} + \frac{f_{\vec{l}}(\Delta^{\vec{l}}_{\alpha\beta})}{\sqrt{N\xi_f^{D-1}}} R_{\alpha\beta,\vec{l}}. \tag{5.33}$$

Consider the first term. Equation (5.33) must recover the infinite-temperature expectation value of $V(\vec{\theta})$ in a quasienergy state, as it models a thermal system. (As energy is not conserved in a quasiperiodically driven system, thermal expectation values should be taken at infinite temperature.) We define $\bar{V}(\vec{\theta})$ to be this expectation value,

$$\bar{V}(\vec{\theta}) = \frac{1}{N}\operatorname{Tr} V(\vec{\theta}) = \sum_{\vec{l}} \bar{V}_{\vec{l}} e^{-i\vec{l}\cdot\vec{\theta}}. \tag{5.34}$$

The Fourier components $\bar{V}_{\vec{l}}$ appear in the first term of Eq. (5.33). Fluctuations to the expectation value are given by the second term in Eq. (5.33), but these vanish as the number of levels $N \to \infty$.

The second term is motivated by the intuition that the components $|\phi_{\alpha\vec{n}}\rangle$ appear as independent random vectors [207], with an assumed exponentially decaying norm with $|\vec{n}|$ (Fig. 5·2).

The factors $R_{\alpha\beta,\vec{l}}$ are independent (usually complex) random variables with mean zero and unit variance, and model the apparently random nature of the quasienergy states. We will not need to assume any particular distribution for these variables, or even that they are identically distributed for different $\vec{l}$. However, if $V(\vec{\theta})$ is Hermitian, then there is a constraint $R_{\alpha\beta,\vec{l}} = R^*_{\beta\alpha,-\vec{l}}$, where z^* is the complex conjugate of z.

The spectral functions $f_{\vec{l}}(\omega)$ appearing in the second term encode the dependence of the off-diagonal matrix elements on the quasienergy difference ω. The spectral functions also carry an explicit dependence on the frequency lattice separation $\vec{l}$. The former is usual for an ETH ansatz—matrix elements typically depend on energy differences of eigenstates. The latter dependence on $\vec{l}$ has no analogue in the usual ETH for static or periodically-driven systems—it encodes the localization of the quasienergy states (and hence the matrix elements) perpendicular to $\vec{\Omega}$ in the frequency lattice. Displacements $\vec{l}$ parallel to $\vec{\Omega}$ affect the quasienergy difference $\omega = \Delta^{\vec{l}}_{\alpha\beta}$, but those perpendicular to $\vec{\Omega}$ do not. As ω is insensitive to this displacement, the additional dependence of $f_{\vec{l}}(\omega)$ on $\vec{l}$ is required to correctly describe the localization perpendicular to $\vec{\Omega}$. Namely, for large $|\vec{l}|$, we demand that

$$|f_{\vec{l}}(\omega)| = O(e^{-|\vec{l}|/\xi_f}), \tag{5.35}$$

where ξ_f is a frequency lattice localization length. If $V_{\vec{n}} = O(e^{-|\vec{n}|/\zeta_V})$, then $\xi_f = O(\max\{\zeta_f, \zeta_V\})$. When the localization length of the quasienergy states is large, $\xi_f = O(\zeta_f)$.

The localization of $f_{\vec{l}}$ in the direction parallel to the electric field $\vec{\Omega}$ in the frequency lattice is much stronger than in the $D-1$ perpendicular directions. This is due to Stark localization by the linear potential $\vec{n} \cdot \vec{\Omega}$, which causes a super-exponential localization like

$$\log|f_{\vec{l}}(\omega)| \sim -\omega_{\vec{l}} \log \omega_{\vec{l}}, \tag{5.36}$$

where $\omega_{\vec{l}} = \vec{l} \cdot \hat{\Omega}$ is much larger than a localization length parallel to the electric field, $\omega_{\vec{l}} \gg \xi_{\parallel}$ [91].

The localization length $\xi_{\parallel}$ controls the preasymptotic exponential decay of $|f_{\vec{l}}(\omega)|$, and depends only weakly on N. In a driven many-body system, $\xi_{\parallel}$ is a function of $W/|\vec{\Omega}|$, where W is the bandwidth of the static part of the Hamiltonian. For a generic spin system this varies as $W = O(\sqrt{L}) = O(\sqrt{\log_2 N})$, which results in a very weak growth with N. States at a distance $\omega_{\vec{l}} \gg \xi_{\parallel}$ are far detuned, resulting in super-exponential localization.

The localization length ξ_f also appears in the denominator of the second term in Eq. (5.33), which may be interpreted as the square root of an effective Hilbert space dimension

$$N_{\text{eff}} = N \xi_f^{D-1}. \tag{5.37}$$

For a given $|\tilde{\phi}_\alpha^{\vec{n}}\rangle$, N_{eff} is roughly the number of other states with which $|\tilde{\phi}_\alpha^{\vec{n}}\rangle$ has a significant matrix element. More precisely, the volume factor of ξ_f^{D-1} in N_{eff} ensures that

$$\sum_\alpha \langle \tilde{\phi}_\alpha | \tilde{V}^\dagger \tilde{V} | \tilde{\phi}_\alpha \rangle = \int \frac{\mathrm{d}^D \theta}{(2\pi)^D} \operatorname{Tr} V^\dagger V(\vec{\theta}) = O(N). \tag{5.38}$$

The exponent is $D-1$, and not D, because the strong localization in the $\vec{\Omega}$ direction means that the relevant volume is (asymptotically for large N) just that perpendicular to $\vec{\Omega}$.

As a final comment, there may be $D-1$ distinct localization lengths in the plane perpendicular to $\vec{\Omega}$ in the frequency lattice. Eq. (5.33) is modified accordingly; specifically, ξ_f^{D-1} is replaced with the product of principal localization lengths, $\prod_{j=1}^{D-1} \xi_{f,j}$. More generally, this denominator is determined by the requirement of normalization. In later sections, we neglect such refinements and use Eq. (5.33) as stated, as our primary focus is $D = 2$, where there is a unique localization length ξ_f perpendicular to $\vec{\Omega}$.

The predictions of our ansatz (5.33) can be checked in numerical simulations of thermalizing quasiperiodically-driven systems. In the remainder of this section we check several statistics of the off-diagonal matrix elements $\tilde{V}^{\vec{l}}_{\alpha\beta}$ for $D = 2$, and find that they are consistent with (5.33).

5.3.1 Model

We first define a model that we work with numerically. In principle, this should be a non-integrable many-body quantum system driven quasiperiodically. However, it has already been established numerically that the expectation values of operators in eigenstates of *static* thermalizing Hamiltonians are well-described by random matrix theory, through ETH [203–207]. The content of our ansatz that requires new analysis is the frequency lattice structure.

To separate the frequency lattice structure from a test of ETH, we choose a model that already consists of random matrices, and add quasiperiodic driving. The result is a Gaussian unitary ensemble (GUE) random Hamiltonian with nearest-neighbor hops on the frequency lattice. That is,

$$H(\vec{\theta}) = H_0 + J(H_1 e^{-i\theta_1} + H_2 e^{-i\theta_2} + \text{H.c.}), \tag{5.39}$$

where H_0 is a GUE random matrix with root-mean-square (rms) energy

$$\sqrt{\frac{1}{N}\operatorname{Tr} H_0^\dagger H_0} = W + o(1), \tag{5.40}$$

J sets the driving amplitude (and is a hopping amplitude in the frequency lattice), and H_1 and H_2 are complex Gaussian random matrices with unit rms energy. We take $\theta_j = \Omega_j t$, with $\Omega_1/\Omega_2 = (1+\sqrt{5})/2$ given by the golden ratio.

We restrict our attention to the case of $D = 2$ tones, which is the most numerically tractable. As the ansatz (5.33) assumes no structure beyond that imposed by the assumption of localization and normalization, we expect that if the RMT phenomenology holds for $D = 2$ it will also hold for more tones, provided the larger D models are localized in the frequency lattice.

We take V in Eq. (5.33) to be a static GUE random operator with unit rms energy.

5.3.2 Statistics of Matrix Elements in Commensurate Approximations

Numerically extracting the quasienergy states $|\phi_\alpha(\vec{\theta})\rangle$ from the quasiperiodically driven model (5.39) can be challenging. It usually requires solving the model on the frequency lattice, which increases the size of the problem substantially. It is much easier instead to make a commensurate approximation to the incommensurate frequency vector $\vec{\Omega}$ and solve the corresponding Floquet problem in the time domain. If the incommensurate model is localized in the frequency lattice, which is a requirement of our ansatz, then the incommensurate limit may be safely described by a limit of commensurate approximations.[2]

We consider commensurate approximations

$$\vec{\Omega}_n = \Omega_1 \hat{e}_1 + \Omega_1 \frac{p_n}{q_n} \hat{e}_2 \tag{5.41}$$

where $p_n = F_{n-1}$ and $q_n = F_n$ are consecutive Fibonacci numbers. As $n \to \infty$, we have that $\vec{\Omega}_n \to \vec{\Omega}$.

Each commensurate approximation is periodic with period $T_n = q_n \frac{2\pi}{\Omega_1}$. Thus, we can find the quasienergy states at $\vec{\theta} = 0$ and their corresponding quasienergies by

---

[2] Indeed, a commensurate approximation to $\vec{\Omega}$ may be regarded as introducing periodic boundary conditions in the frequency lattice [1, 37, 38].

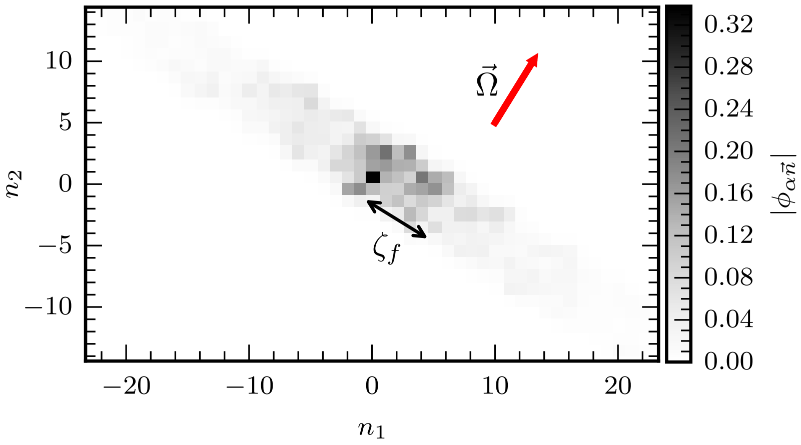

Figure 5·3: *Frequency lattice quasienergy state.*—Quasienergy states are well described by a sum $|\tilde{\phi}_\alpha\rangle = \sum_{\vec{n}} |\phi_{\alpha\vec{n}}\rangle\,|\vec{n}\rangle$, where $|\phi_{\alpha\vec{n}}\rangle$ are random vectors. The norm $|\phi_{\alpha\vec{n}}|$ of the components decreases exponentially in the direction perpendicular to $\vec{\Omega}$, with localization length ζ_f. They decrease faster than exponentially parallel to $\vec{\Omega}$. *Parameters:* $N = 20$, $J/W = 0.1$, $\Omega_1/W = 0.6$, $q = 233$

diagonalizing the Floquet operator

$$\begin{aligned} U(T_n, 0) &= \mathcal{T} \exp\left(-i \int_0^{T_n} \mathrm{d}t\, H(\vec{\theta}_t) \right) \\ &= \sum_\alpha e^{-i\epsilon_\alpha T_n} |\phi_\alpha(0)\rangle\langle\phi_\alpha(0)|, \end{aligned} \tag{5.42}$$

where $\mathcal{T}$ denotes time ordering. The quasienergy states at any other $\vec{\theta}_t$ can then be calculated as

$$|\phi_\alpha(\vec{\theta}_t)\rangle = e^{i\epsilon_\alpha t} U(t, 0)\, |\phi_\alpha(0)\rangle\,. \tag{5.43}$$

We use a second-order Suzuki-Trotter approximation [209] to compute $U(T_n, 0)$, and subsequently calculate $|\phi_\alpha(\vec{\theta})\rangle$ on an $F_{n-1} \times F_n$ grid in the $\vec{\theta}$ torus. We fix a gauge for this state by requiring that the highest weight component in the corresponding frequency lattice state $|\tilde{\phi}_\alpha\rangle = \sum_{\vec{n}} |\phi_{\alpha\vec{n}}\rangle\,|\vec{n}\rangle$ be $|\phi_{\alpha 0}\rangle$. In this gauge, if the quasienergy states are well-localized, we may regard our chosen representative states as being centered at the origin in the frequency lattice (Fig. 5·3).

With $|\phi_\alpha(\vec{\theta})\rangle$ found, we can compute the matrix elements $\tilde{V}^{\vec{l}}_{\alpha\beta}$ as the two-dimensional Fourier coefficients of

$$V_{\alpha\beta}(\vec{\theta}) = \langle\phi_\alpha(\vec{\theta})|\, V(\vec{\theta})\, |\phi_\beta(\vec{\theta})\rangle\, . \tag{5.44}$$

Using this method, we can directly compute the matrix elements $\tilde{V}^{\vec{l}}_{\alpha\beta}$ in small commensurate approximations. We address the behavior of the matrix elements for $\vec{l}$ perpendicular to and parallel to the electric field $\vec{\Omega}$ separately. We begin with $\vec{l} \perp \vec{\Omega}$ (Fig. 5·4).

We have assumed that the standard deviation $\Delta\tilde{V}_{\vec{l}}$ of the matrix elements with fixed $\vec{l}$ should decrease exponentially for large $|\vec{l}|$ in this direction (the mean vanishes). Specifically, we predict for the off-diagonal matrix elements that

$$\Delta\tilde{V}_{\vec{l}} \sim \frac{\|f_{\vec{l}}\|}{\sqrt{N_{\text{eff}}}}, \tag{5.45}$$

where

$$\|f_{\vec{l}}\|^2 = \int \mathrm{d}\omega\, |f_{\vec{l}}(\omega)|^2 \tag{5.46}$$

decays exponentially. This exponential decay is visible for small N in Fig. 5·4(a), but we are unable to reach commensurate approximations that allow us to see the decay clearly for larger N.

We can also observe that $\Delta\tilde{V}_0$ decays faster than $N^{-1/2}$ for fixed $\vec{l} = 0$. This is also predicted by our ansatz, as the localization length ξ_f may grow with N, so that N_{eff} grows faster than N. Indeed, Sec. 5.5 gives that $\xi_f = O(N)$ for $D = 2$, so that $\Delta\tilde{V}_0 = O(N^{-1})$.

We did not require that the matrix elements be normally distributed, as is often done in ETH. Indeed, in the tails of a localized wavefunction the wavefunction amplitudes, and hence matrix elements, should be log-normally distributed [210]. We can check if the matrix elements we compute numerically are normally distributed by

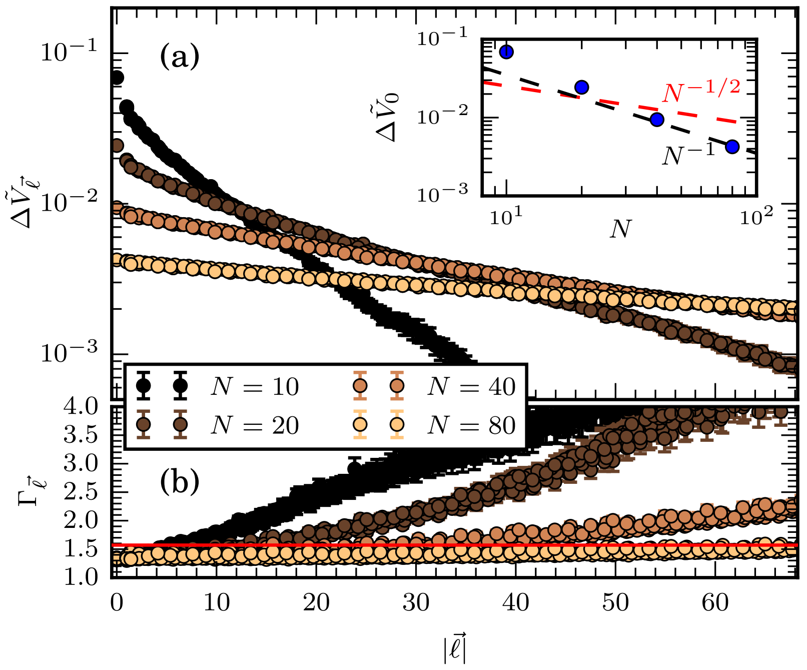

Figure 5·4: *Matrix elements perpendicular to* $\vec{\Omega}$.—We examine the statistics of matrix elements $\tilde{V}^{\vec{l}}_{\alpha\beta}$ for $|\vec{l}\cdot\vec{\Omega}_n| < W$ (almost perpendicular to the electric field). (**a**) Eq. (5.33) conjectures that the matrix elements should have a standard deviation which decreases exponentially in $|\vec{l}|$. This feature is visible for small N. (**Inset**) The standard deviation of the $\vec{l} = 0$ matrix elements decreases faster than $N^{-1/2}$ (red dashed), as we predict. Sec. 5.5 predicts a scaling of N^{-1} (black dashed), which is a better fit for large N, though Sec. 5.5.3 provides much better evidence for this scaling. (**b**) The ratio $\Gamma_{\vec{l}}$ should be $\pi/2$ (red line) for a Gaussian distribution of matrix elements. We see this is not the case for large $|\vec{l}|$. *Parameters:* $J/W = 0.1$, $\Omega_1/W = 0.6$, $q = 233$, with $N_{\text{samp}} \approx 1200/N$ random matrix samples.

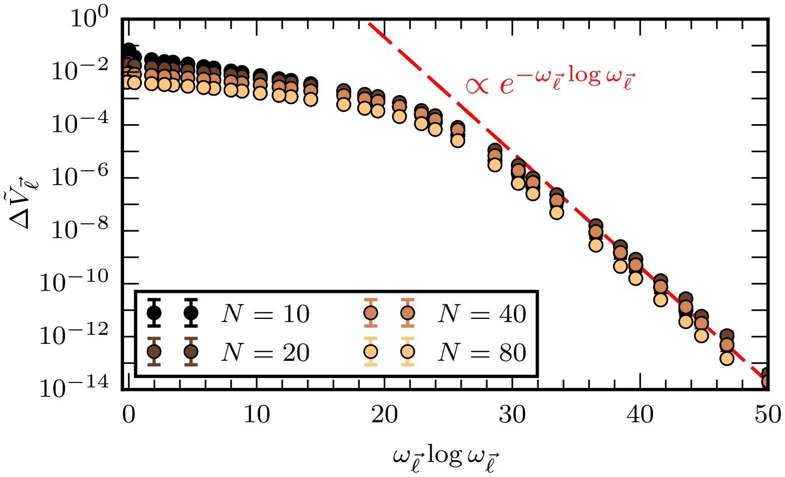

Figure 5·5: *Matrix elements parallel to* $\vec{\Omega}$.—We examine the statistics of matrix elements $\tilde{V}^{\vec{l}}_{\alpha\beta}$ for $|\vec{l} \times \vec{\Omega}_n| < |\vec{\Omega}_n|$ (almost parallel to the electric field). Eq. (5.36) predicts that the standard deviation of the matrix elements should decay much faster as compared to the perpendicular direction. This is reflected in our numerics, where the decay is faster than exponential: consistent with $\log \Delta\tilde{V}_{\vec{l}} \sim -\omega_{\vec{l}} \log \omega_{\vec{l}}$ (where $\omega_{\vec{l}} = \vec{l} \cdot \hat{\Omega}$) for large $\omega_{\vec{l}}$. Furthermore, the localization length of the matrix elements does not grow with N—increasing N only decreases the matrix elements. *Parameters:* $J/W = 0.1$, $\Omega_1/W = 0.6$, $q = 233$, with $N_{\text{samp}} \approx 1200/N$ random matrix samples.

computing the ratio [211]

$$\Gamma_{\vec{l}} = \frac{[|V^{\vec{l}}_{\alpha\beta}|^2]_{\alpha\beta}}{[|V^{\vec{l}}_{\alpha\beta}|]^2_{\alpha\beta}}, \tag{5.47}$$

where $[\cdot]_{\alpha\beta}$ indicates an average over off-diagonal elements $V^{\vec{l}}_{\alpha\beta}$ for fixed $\vec{l}$, and within a window of the quasienergy difference $\Delta^{\vec{l}}_{\alpha\beta}$. $\Gamma_{\vec{l}}$ is $\pi/2$ if the matrix elements are Gaussian-distributed for fixed $\vec{l}$, within a small quasienergy window.

We see in Fig. 5·4(b) that most matrix elements are not Gaussian-distributed. For small deviations from $\pi/2$, this may be because the windows we have used for $\Delta^{\vec{l}}_{\alpha\beta}$ are too large. Taking smaller windows while still maintaining good statistics requires larger N. The large deviations visible at small N and large $|\vec{l}|$ cannot be explained in this way; they represent departures from Gaussianity.

Our ansatz predicts qualitatively different behavior of the matrix elements with $|\vec{l}|$ when $\vec{l}$ is parallel to the electric field $\vec{\Omega}$. These predictions are verified in Fig. 5·5. Namely, the standard deviation $\Delta\tilde{V}_{\vec{l}} = O(e^{-\omega_{\vec{l}} \log \omega_{\vec{l}}})$ decreases faster than exponentially for $\omega_{\vec{l}} \gg \xi_{\|}$, and $\xi_{\|}$ does not depend on N. (For a typical spin system with high-frequency quasiperiodic driving $\xi_{\|}$ should depend weakly on N, because the bandwidth of the static part of the Hamiltonian grows. Our model (5.39) has a fixed bandwidth, so $\xi_{\|}$ should not depend on N.)

Indeed, faster-than-exponential decay of $\Delta\tilde{V}_{\vec{l}}$ is visible in Fig. 5·5. Furthermore, increasing N only decreases $\Delta\tilde{V}_{\vec{l}}$ (due to the factor $N_{\text{eff}}^{-1/2}$), without extending the localization length $\xi_{\|}$.

The features of the ansatz listed in this section are those most relevant for this chapter. We have verified that they are effective descriptions of the frequency lattice structure of matrix elements in the localized (in the synthetic dimensions) regime.

5.4 Spatial Localization Assuming Synthetic Localization

In this section, we show that quasiperiodically-driven MBL is self-consistently stable to the inclusion of a thermal region, provided the frequency lattice localization length grows at most as a power law with the Hilbert space dimension of the thermal region, $\xi_f = O(N^\nu)$.

Intuitively, in the ETH ansatz (5.33) the effective density of states grows as

$$\rho_{\text{eff}} = O(N_{\text{eff}}) = O(N^{1+\nu(D-1)}). \tag{5.48}$$

For MBL to be self-consistently stable, the product of this density of states and a typical matrix element of a perturbation must be much less than unity. Testing when this is true, as in Ref. [78], leads to the conclusion that MBL may be stable for spatial localization lengths obeying

$$\xi_s < \xi_{s,c} = ([1 + \nu(D-1)] \log 2)^{-1}. \tag{5.49}$$

Eq. (5.49) is our main result of this section.

A technical proof of Eq. (5.49) is more involved, as the density of states in the frequency lattice is formally infinite at all energies, and the matrix elements $\tilde{V}^{\vec{l}}_{\alpha\beta}$ do not have a single scale. To characterize precisely how the infinite density of states is defeated by exponential localization in the matrix elements, we use the *fidelity susceptibility* in the frequency lattice. The typical value of this quantity is

$$\chi_\star = \left(\lim_{\Delta \to 0} \left[\frac{1}{2\Delta} \sum_{|\Delta^{\vec{l}}_{\beta\alpha}| < \Delta} |\tilde{V}^{\vec{l}}_{\beta\alpha}| \right]_{\text{dis}} \right)^2, \tag{5.50}$$

where the sum is over states in a narrow quasienergy window Δ, and the square brackets $[\cdot]_{\text{dis}}$ indicate an ensemble average, which we discuss further below. This quantity is well-defined in the frequency lattice.

In a static system $\sqrt{\chi_\star} = \rho[|V|]_{\text{dis}}$ reduces to the familiar product of the density of states ρ and the average (absolute value of the) off-diagonal matrix element [212].

We note that Eq. (5.49) is consistent with investigations of MBL in classical spin systems [201, 202]. As a thermal classical spin presents a continuous spectrum to the adjacent non-chaotic spins, it completely thermalizes a putatively-MBL chain, so that MBL is not stable in classical systems. In our case also, if ξ_f grows faster than a power law, $\nu \to \infty$ (which includes the case of the spectrum being continuous at finite N), the critical localization length is zero.

In Sec. 5.4.1 we state our model of a thermal inclusion in a quasiperiodically-driven putatively MBL chain. Then in Sec. 5.4.2 we derive Eq. (5.49).

5.4.1 Model

The Hilbert space (in the temporal domain) for the putatively MBL chain is $\mathcal{H} = \mathcal{H}_B \otimes \mathcal{H}_{\mathrm{MBL}}$, where $\mathcal{H}_B$ is the N-dimensional Hilbert space of the thermal inclusion (the "bath"), and $\mathcal{H}_{\mathrm{MBL}}$ is the Hilbert space of the MBL chain, which we regard as a tensor product of two-level systems—the l-bits.

The Hamiltonian on this system is $H(t) = H_0(\vec{\theta}_t) + H_{\mathrm{int}}(\vec{\theta}_t)$, where $H_0(\vec{\theta})$ consists of the uncoupled Hamiltonians of the thermal region and the MBL chain, and $H_{\mathrm{int}}(\vec{\theta})$ is the interaction between them.

In the frequency lattice, we have a quasienergy operator $\tilde{K} = \tilde{K}_0 + \tilde{K}_{\mathrm{int}}$, with

$$\tilde{K}_0 = -\sum_{\vec{n}} \vec{\Omega} \cdot \vec{n} |\vec{n}\rangle\langle\vec{n}| + \tilde{K}_B \otimes \mathbb{1}_{\mathrm{MBL}} + \mathbb{1}_B \otimes \tilde{K}_{\mathrm{MBL}}, \tag{5.51}$$

where $\tilde{K}_a$ for $a \in \{B, \mathrm{MBL}, \mathrm{int}\}$ is a translationally invariant term, and

$$\tilde{K}_{\mathrm{int}} = \sum_j J_j (\tilde{V} \tilde{\tau}_j^+ + \tilde{V}^\dagger \tilde{\tau}_j^-). \tag{5.52}$$

Here, $\tilde{V}$ is a not-necessarily-Hermitian operator acting on the bath with $O(1)$ operator norm, and $\tilde{\tau}_j^\pm$ are the raising and lowering operators for the l-bit $\tilde{\tau}_j^z$. Localization of the l-bits implies that the coefficients $J_j = O(e^{-|j|/\xi_s})$ decay exponentially in space. We have suppressed a dependence on j from the terms $\tilde{V}$.

The assumed form of the interaction (5.52) is incomplete. We have neglected products of l-bit operators, and have not included a term like $J_j' \tilde{V}' \tilde{\tau}_j^z$ which does not flip l-bits. These additional terms do not change the results of our analysis [212].

5.4.2 Thermal Avalanches

5.4.2.1 The Fidelity Susceptibility in the Frequency Lattice

We consider l-bits two at a time—one on each side of the thermal region, which we position at $j = 0$ (Fig. 5·1).

To quantify when the l-bits at $\pm j$ are thermalized by the thermal inclusion, we will use the *fidelity susceptibility* in the frequency lattice. The fidelity susceptibility χ_j quantifies the strength of hybridization between uncoupled eigenstates that differ in the $\pm j$th l-bit when said l-bits are coupled to the bath.

Uncoupled frequency lattice quasienergy states of the thermal region and the two l-bits take the form of a convolution (Sec. 5.1),

$$|\tilde{\phi}_\alpha \tilde{\tau}_j \tilde{\tau}_{-j}\rangle = |\tilde{\phi}_\alpha\rangle * |\tilde{\tau}_j\rangle * |\tilde{\tau}_{-j}\rangle \,, \tag{5.53}$$

with quasienergy

$$\epsilon_\alpha + h_j \tau_j + h_{-j} \tau_{-j} \tag{5.54}$$

where $\tau_j, \tau_{-j} = \pm 1$ and α indexes the Hilbert space of the thermal region. (We have neglected products of l-bit operators in $\tilde{K}_{\mathrm{MBL}}$ by assuming this form of the quasienergy.)

The fidelity susceptibility can be regarded as the norm of the correction to this state in the first order of perturbation theory, regarding the coupling $\tilde{K}_{\mathrm{int}}$ as a perturbation,

$$\chi_\alpha = \sum_{\beta,\vec{l},h} \left| \frac{\tilde{V}^{\vec{l}}_{\beta\alpha}}{\omega_{\alpha\beta} + \vec{l}\cdot\vec{\Omega} - 2h} \right|^2 . \tag{5.55}$$

Here, the sum excludes $(\beta, \vec{l}) = (\alpha, 0)$, but it includes $\beta = \alpha$ when $\vec{l} \neq 0$. The matrix elements $\tilde{V}^{\vec{l}}_{\beta\alpha} = \langle \tilde{\phi}^{\vec{l}}_\beta | \tilde{V} | \tilde{\phi}_\alpha \rangle$ will be taken to be of the form proposed in (5.33). The denominator

$$\Delta^{\vec{l}}_{\beta\alpha} = \omega_{\alpha\beta} + \vec{l}\cdot\vec{\Omega} - 2h \tag{5.56}$$

is the quasienergy difference between the states $|\tilde{\phi}_\alpha\{\tilde{\tau}\}\rangle$ and $|\tilde{\phi}^{\vec{l}}_\beta\{\tilde{\tau}'\})\rangle$, so that

$$h \in \{2h_j\tau_j, 2h_{-j}\tau_{-j}\} \tag{5.57}$$

depending on whether l-bit j or l-bit $-j$ is flipped by $\tilde{K}_{\text{int}}$. (At the first order of perturbation theory, only one can be flipped.)

In the static case, the distribution of χ_α within a particular random matrix ensemble for V can be calculated in many cases [212]. In all cases, it has a broad distribution with a power-law tail. As we show in Sec. 5.4.2.3, this is also true in the frequency lattice.

That is, χ_α has a distribution function with asymptotic behavior,

$$f_{\text{FS}}(\chi) \overset{\chi\to\infty}{\sim} \sqrt{\frac{\chi_{\star,j}}{\chi^3}}, \tag{5.58}$$

where the typical scale of the distribution is given by

$$\sqrt{\chi_{\star,j}} = \lim_{\Delta\to 0}\left[\frac{1}{2\Delta}\sum_{|\Delta^{\vec{l}}_{\beta\alpha}|<\Delta}|\tilde{V}^{\vec{l}}_{\beta\alpha}|\right]_{\text{dis}}. \tag{5.59}$$

Here, the sum is over all uncoupled quasienergy states $|\tilde{\phi}^{\vec{l}}_\beta\{\tilde{\tau}'\})\rangle$ such that $|\Delta^{\vec{l}}_{\beta\alpha}| < \Delta$, and the square brackets indicate an average over the distribution of matrix elements $|\tilde{V}^{\vec{l}}_{\beta\alpha}|$ (determined by the distribution of the random numbers $R_{\beta\alpha,\vec{l}}$ of (5.33)) and of the level spacings $|\Delta^{\vec{l}}_{\beta\alpha}|$. We have not been specific about the distributions for the matrix element or level spacing for two reasons: first, $\sqrt{\chi_{\star,j}}$ is well-defined given only very weak conditions on the distributions (the probability density that $\Delta^{\vec{l}}_{\beta\alpha} = 0$ is finite, and the averages of $|\tilde{V}^{\vec{l}}_{\beta\alpha}|$ are summable over $\vec{l}$); and secondly, we will only be concerned with the scaling properties of $\sqrt{\chi_{\star,j}}$. To calculate the actual value of $\sqrt{\chi_{\star,j}}$ we would need these distributions, but they are unnecessary to deduce the fidelity susceptibility's asymptotic behavior with j.

The dimensionless quantity $J_j\sqrt{\chi_{\star,j}}$ formalizes the notion of the product of a matrix element and a density of states in the frequency lattice.

5.4.2.2 Growth of the Thermal Region

If the spin chain is thermal, the dimensionless combination $J_j\sqrt{\chi_j}$ remains large as $j \to \infty$—all uncoupled quasienergy states hybridize strongly to form highly entangled thermal eigenstates. In an MBL system, $J_j\sqrt{\chi_j}$ decreases to zero, indicating that l-bits distant from the thermal inclusion are only slightly dressed by their coupling to said inclusion. Our aim is to show that the latter scenario of $J_j\sqrt{\chi_j} \to 0$ is possible. In this stage, we mimic the arguments of Ref. [78].

We make the pessimistic assumption that all l-bits up to and including $\pm|j-1|$ are perfectly absorbed by the thermal region. Then the system consisting of the thermal region and the first $2(j-1)$ l-bits is still described by the random matrix ansatz (5.33), but with a larger Hilbert space dimension $N_{j-1} = N2^{2(j-1)}$. This in turn generically affects the frequency lattice localization length $\xi_f = \xi_f(N_{j-1})$, and subsequently affects the spectral functions $|f_{\vec{l}}| = O(e^{-|\vec{l}|/\xi_f(N_{j-1})})$.

Considering some fixed quasienergy window Δ, there are on the order of

$$N_{\mathrm{eff},j-1} = N_{j-1}\xi_f(N_{j-1})^{D-1} \tag{5.60}$$

terms in the sum that contribute to $\sqrt{\chi_{\star,j}}$ before the exponential suppression from $|f_{\vec{l}}|$ makes further terms negligible. (Recall from Sec. 5.3 that the relevant frequency lattice volume is ξ_f^{D-1}, and not ξ_f^D, because the extent of the quasienergy state in the direction parallel to $\vec{\Omega}$ scales weakly, i.e. slower than a power law, with N.)

Meanwhile, each of the terms within the localization length scales as $N_{\mathrm{eff},j-1}^{-1/2}$, in order to fix the normalization of V. Thus, we see that

$$\sqrt{\chi_{\star,j}} = O\left(\sqrt{N_{\mathrm{eff},j-1}}\right). \tag{5.61}$$

By assumption of MBL, we have that $J_j = O(e^{-|j|/\xi_s})$, so for the dimensionless quantity $J_j\sqrt{\chi_{\star,j}}$, we have,

$$\log(J_j\sqrt{\chi_{\star,j}}) = O\left(-\frac{j}{\xi_s} + j\log 2 + \frac{D-1}{2}\log\frac{\xi_f(N2^{2j})}{\xi_f(N)}\right). \tag{5.62}$$

The thermal avalanche will eventually stop if

$$\lim_{j\to\infty}\left[-\frac{j}{\xi_s} + j\log 2 + \frac{D-1}{2}\log\frac{\xi_f(N2^{2j})}{\xi_f(N)}\right] = -\infty. \tag{5.63}$$

This requires that the frequency lattice localization length grows at most as a power law in the Hilbert space dimension of the bath,

$$\xi_f(N) = O(N^\nu), \tag{5.64}$$

that is, at most exponentially in the number of thermal spins.

Assuming (5.64), there is a critical spatial localization length $\xi_{s,c}$ below which MBL is stable, just as in the case of static MBL. In the quasiperiodically driven case, this is given by

$$\xi_{s,c}^{-1} = [1+\nu(D-1)]\log 2. \tag{5.65}$$

For spatial localization lengths below this value, $\xi_s < \xi_{s,c}$, the susceptibility $J_j\sqrt{\chi_{\star,j}}$ decreases exponentially with j. Otherwise, the thermal region grows to encompass the entire system.

We note that the result (5.65) has Floquet MBL as a special case with $D = 1$. In that case, the critical localization length is the same as the static case, $(\log 2)^{-1}$, as is already well known from other arguments based on the Floquet Hamiltonian [170, 195, 213].

We also observe that the quasiperiodically driven MBL phase is less stable than the static phase, in the sense that the critical localization length is strictly smaller than that in the static case. This is because the presence of the frequency lattice allows the effective Hilbert space dimension N_{eff} to grow faster than 2^{2j}.

5.4.2.3 Typical Frequency Lattice Fidelity Susceptibility

This section completes the technical details of our argument with a proof of Eq. (5.59). Restated here, we show that the fidelity susceptibilities of frequency lattice eigenstates are distributed according to a power law

$$f_{\text{FS}}(\chi) \sim \sqrt{\frac{\chi_{\star,j}}{\chi^3}} \tag{5.66}$$

where the typical scale is

$$\sqrt{\chi_{\star,j}} = \lim_{\Delta\to 0} \left[\frac{1}{2\Delta} \sum_{|\Delta^{\vec{l}}_{\beta\alpha}|<\Delta} |\tilde{V}^{\vec{l}}_{\beta\alpha}| \right]_{\text{dis}} . \tag{5.67}$$

We split the sum in (5.55) into a sum for each frequency lattice site, $\chi_\alpha = \sum_{\vec{l}} \chi_{\alpha,\vec{l}}$, where

$$\chi_{\alpha,\vec{l}} = \sum_{\beta,h} \left| \frac{\tilde{V}^{\vec{l}}_{\beta\alpha}}{\omega_{\beta\alpha} + \vec{l}\cdot\vec{\Omega} - 2h} \right|^2 . \tag{5.68}$$

Due to the presence of small denominators $\Delta^{\vec{l}}_{\beta\alpha} = |\omega_{\beta\alpha} + \vec{l}\cdot\vec{\Omega} - 2h|$, this sum tends to be dominated by its largest element. Then we can write

$$\chi_{\alpha,\vec{l}} \approx \frac{|\tilde{V}^{\vec{l}}_{\beta\alpha}|^2}{|\Delta^{\vec{l}}_{\beta\alpha}|^2}, \tag{5.69}$$

where β and h are chosen to minimize $|\Delta^{\vec{l}}_{\beta\alpha}|^2$. The distribution of fidelity susceptibilities $f_{\text{FS}}(\chi|\omega_{\beta\alpha}, \vec{l})$ can then be calculated as [212]

$$f_{\text{FS}} = \int \mathrm{d}V \int \mathrm{d}\Delta\, \delta\left(\chi - \tfrac{|V|^2}{|\Delta|^2}\right) f_{\text{ME}}(V) f_{\text{LS}}(\Delta) \tag{5.70}$$

$$= \frac{1}{2\chi^{3/2}} \int \mathrm{d}V\, |V| f_{\text{ME}}(V) f_{\text{LS}}(\tfrac{V}{\sqrt{\chi}}) \tag{5.71}$$

where f_{ME} and f_{LS} are distributions for the matrix element and minimum level spacing $\Delta^{\vec{l}}_{\beta\alpha}$ respectively. Both depend on $\vec{l}$. This calculation shows that $f_{\mathrm{FS}} \sim \sqrt{\chi_{\star,\vec{l}}/\chi^3}$ has a power-law dependence on χ. The scale $\chi_{\star,\vec{l}}$ may be extracted as

$$\chi_{\star,\vec{l}} = \lim_{\chi\to\infty} \chi^3 f_{\mathrm{FS}}^2 \tag{5.72}$$

$$= \left(\lim_{\Delta\to 0} \frac{1}{2} \int \mathrm{d}V \, |V| f_{\mathrm{ME}}(V) f_{\mathrm{LS}}(\Delta) \right)^2 . \tag{5.73}$$

Schematically, this may be written $\chi_{\star,\vec{l}} = [|V^{\vec{l}}|]^2_{\mathrm{dis}} \rho^2_{\vec{l}}$, where $[|V^{\vec{l}}|]_{\mathrm{dis}}$ is an average of the absolute value of the matrix elements $\tilde{V}^{\vec{l}}_{\beta\alpha}$ as the random variables $R_{\beta\alpha,\vec{l}}$ from Eq. (5.33) are varied. The quantity $\rho_{\vec{l}}$ is a density of states at the relevant quasienergy, restricted to the site $\vec{l}$. However, it will be more useful later to instead express $\sqrt{\chi_{\star,\vec{l}}}$ explicitly as

$$\sqrt{\chi_{\star,\vec{l}}} = \lim_{\Delta\to 0} \left[\frac{1}{2\Delta} \sum_{|\Delta^{\vec{l}}_{\beta\alpha}|<\Delta} |\tilde{V}^{\vec{l}}_{\beta\alpha}| \right]_{\mathrm{dis}} , \tag{5.74}$$

where $\vec{l}$ is fixed in the sum, and square brackets indicate an average over the variables $R_{\beta\alpha,\vec{l}}$ and over the quasienergies $\epsilon_\beta - 2h$. We have not specified the distributions f_{ME} and f_{LS} over which this average is to be performed because, for our purposes, all we require is that the average $[|V^{\vec{l}}|]_{\mathrm{dis}}$ exists, and that the probability density $f_{\mathrm{LS}}(0)$ is finite. The specific distribution of the matrix elements and quasienergies will affect the value of $\sqrt{\chi_{\star,\vec{l}}}$, but not its asymptotic scaling as the avalanche progresses, which is our only concern.

If we then make the approximation that the random variables $\chi_{\alpha,\vec{l}}$ on different sites are independent, we can calculate the typical scale $\chi_{\star,j}$ of χ_α in terms of the distributions on the sites $\vec{l}$. We define the cumulant generating functions

$$K_{\vec{l}}(t) = \log[e^{i\chi_{\alpha,\vec{l}}t}]_{\mathrm{dis}}, \tag{5.75}$$

where the square brackets indicate an average over $\chi_{\alpha,\vec{l}}$, appropriately weighted by the distribution $f_{\rm FS}$.

As the asymptotic form of the fidelity distribution is $f_{\rm FS} \sim \chi_{\star,\vec{l}}^{1/2}/\chi^{3/2}$ for $\chi \to \infty$, the cumulant generating function must behave asymptotically for $t \to 0$ as

$$K_{\vec{l}}(t) \sim C\sqrt{t\chi_{\star,\vec{l}}}, \tag{5.76}$$

where $C = (-1+i)\sqrt{2\pi}$ is a constant [212]. The cumulant generating function for a sum of independent random variables is the sum of their cumulant generating functions, thus

$$K(t) \sim C\sqrt{t}\sum_{\vec{l}} \sqrt{\chi_{\star,\vec{l}}}. \tag{5.77}$$

That is, we have a full distribution of χ_α with the same power-law tail, and a scale $\chi_{\star,j}$ given by

$$\sqrt{\chi_{\star,j}} = \sum_{\vec{l}} \sqrt{\chi_{\star,\vec{l}}} = \lim_{\Delta\to 0}\left[\frac{1}{2\Delta}\sum_{|\Delta^{\vec{l}}_{\beta\alpha}|<\Delta} |\tilde{V}^{\vec{l}}_{\beta\alpha}|\right]_{\rm dis}. \tag{5.78}$$

The sum is over $|\tilde{\phi}^{\vec{l}}_\beta\{\tilde{\tau}'\}\rangle$ satisfying the condition $|\Delta^{\vec{l}}_{\beta\alpha}| < \Delta$. With fixed $\vec{l}$ this sum is finite, with at most $2N$ terms for any $\vec{l}$. The infinite sum over $\vec{l}$ converges if $|\tilde{V}^{\vec{l}}_{\beta\alpha}|$ decays exponentially in $|\vec{l}|$, as we have assumed. The $\Delta \to 0$ limit converges if $f_{\rm LS}(0)$ is finite for all $\vec{l}$. Thus, $\sqrt{\chi_{\star,j}}$ is a finite quantity for any $N, \xi_f < \infty$.

Let us return to the assumption that the random variables $\chi_{\alpha,\vec{l}}$ are independent for different $\vec{l}$. The matrix elements $\tilde{V}^{\vec{l}}_{\beta\alpha}$ appearing at distinct $\vec{l}$ are independent random variables within our ansatz, but the energy denominators $\Delta^{\vec{l}}_{\beta\alpha}$ do have correlations between them. These correlations arise because the change in a given energy denominator is given deterministically by the change in the $\vec{l}\cdot\vec{\Omega}$ term. This results in special separations $\vec{l}_*$ where $\vec{l}_*\cdot\vec{\Omega} \approx 0$, and so the energy denominators are almost the same. On this point, we observe that these special $\vec{l}_*$ occur no more frequently than would be expected for random shifts in quasienergy, so even if they do introduce some correlation, it is unlikely to affect the asymptotic behavior we have identified.

In more detail, for a badly approximable $\vec{\Omega} \in \mathbb{R}^2$, there is a $C > 0$ such that [33, 100, 214]

$$|\vec{l} \cdot \vec{\Omega}| \geq \frac{C|\vec{\Omega}|}{|\vec{l}|}. \tag{5.79}$$

(A similar statement may be made for almost all $\vec{\Omega} \in \mathbb{R}^2$ by replacing $|\vec{l}|$ with $|\vec{l}|^{1+\epsilon}$ for any $\epsilon > 0$.) Thus, if $|\vec{l}_* \cdot \vec{\Omega}| < \delta$ is especially small, then

$$|\vec{l}_*| \geq C|\vec{\Omega}|/\delta = O(\delta/|\vec{\Omega}|)^{-1}. \tag{5.80}$$

In words, to find a potential $\vec{l}_* \cdot \vec{\Omega}$ that is smaller than δ, one must search within a distance $O(\delta/|\vec{\Omega}|)^{-1}$ in the frequency lattice. Similarly, if the potentials $\vec{l} \cdot \vec{\Omega}$ were actually random, one would expect to have to sample $O(\delta/|\vec{\Omega}|)^{-1}$ of them to find one that is smaller than δ.

5.5 Synthetic Localization for Two-Tone Driving

In this section we argue that (5.64) generically holds for $D = 2$ with $\nu = 1$, and thus that quasiperiodically-driven MBL is stable to thermal inclusions in the case of two-tone driving, with a critical localization length

$$\xi_{s,c} = (2\log 2)^{-1}. \tag{5.81}$$

The localization of quasienergy states for smooth two-tone driving can be understood as Anderson localization in the $D - 1 = 1$ dimensional surface perpendicular to $\vec{\Omega}$ in the frequency lattice. That is, it is essentially a *single-particle* effect, even in this many-body setting.

Note that the localization is "generic"—there are finely-tuned examples in the literature of smooth two-tone driving resulting in delocalized quasienergy states [17, 38].

For $D = 2$, Stark localization produces a quasi-one-dimensional model of width roughly $\xi_{\parallel} \approx W/|\vec{\Omega}|$ along which quasienergy states could delocalize, where W is the bandwidth of the static part of the Hamiltonian. We lump together sites along the width of this strip to form new sites with increased Hilbert space dimension $N' \approx NW/|\vec{\Omega}|$ and bandwidth $W' \approx 2W$. In this coarse-grained model, localization is nearly complete in the direction parallel to $\vec{\Omega}$. We drop the primes on N' and W', and consider the one-dimensional model thus formed below.

The sequence of sites included in the one-dimensional model are those closest to the line with tangent $\vec{p} = \Omega_2 \hat{e}_1 - \Omega_1 \hat{e}_2$ (Fig. 5·6). Label these sites by the index k such that $\vec{n}_k = \vec{n}_{k-1} \pm \hat{e}_{i_k}$, where the sign of $\pm\hat{e}_{i_k}$ is determined by the sign of Ω_1 and Ω_2, and $i_k \in \{1, 2\}$ is a sequence determined by the number theoretic properties of Ω_1/Ω_2. For instance, when $\Omega_1/\Omega_2 = (1+\sqrt{5})/2$ is the golden ratio, i_k is the Fibonacci word of the elements $\{1, 2\}$ [215, 216, Chapter 2].

The quasienergy states are then approximated by the mid-spectrum eigenstates of the one-dimensional single-particle tight-binding model[3]

$$K_{\text{1-dim}} = \sum_{k,k' \in \mathbb{Z}} (H_{kk'} - \omega_k \delta_{kk'}) |k\rangle\langle k'|, \tag{5.82}$$

with N orbitals per site and where $H_{kk'} = H_{\vec{n}_k - \vec{n}_{k'}}$ still decays exponentially in $|k - k'|$, but is not necessarily translationally invariant in k. The on-site potential $\omega_k = \vec{n}_k \cdot \vec{\Omega}$ is defined up to a constant by the recursion

$$\omega_k = \omega_{k-1} + (-1)^{i_k} \Omega_{i_k}, \tag{5.83}$$

where we have chosen k to increase in the direction of $\vec{p} = \Omega_2 \hat{e}_1 - \Omega_1 \hat{e}_2$.

---

[3] The states in the middle of the spectrum have localization centers in the middle of the coarse-grained strip, and are thus least affected by the truncation to a one-dimensional model.

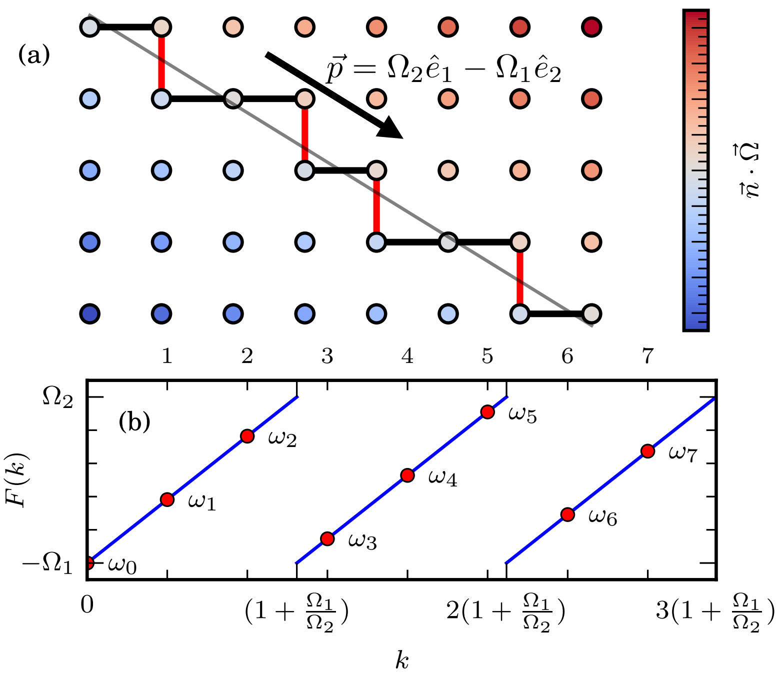
(a)
$\vec{p} = \Omega_2\hat{e}_1 - \Omega_1\hat{e}_2$
$\vec{n}\cdot\vec{\Omega}$
1
2
3
4
5
6
7
(b)
Ω_2
$F(k)$
$-\Omega_1$
ω_0
ω_1
ω_2
ω_3
ω_4
ω_5
ω_6
ω_7
0
$(1+\frac{\Omega_1}{\Omega_2})$
$2(1+\frac{\Omega_1}{\Omega_2})$
$3(1+\frac{\Omega_1}{\Omega_2})$
k

Figure 5·6: *Quasi-one-dimensional model.*—(**a**) Restricting the full two-dimensional (coarse-grained) frequency lattice to those sites closest to a given equipotential (grey line) with tangent $\vec{p}$ produces a one-dimensional model (5.82). The model has a quasiperiodic potential and distinct hopping matrices on the horizontal and vertical bonds. (**b**) The on-site potentials $\omega_k = \vec{n}_k \cdot \vec{\Omega}$ for sites $\vec{n}_k$ in the one-dimensional model are quasiperiodic. They are obtained by sampling a sawtooth function $F(k)$ incommensurately to its period of $1 + \Omega_1/\Omega_2$. The discontinuity in F favors localization in the one-dimensional model.

The potentials ω_k are quasiperiodic in the sense that they may be obtained by sampling a periodic function $F(k)$ at a rate incommensurate to the period of F. Indeed, one can check that taking

$$F(k+\beta) = F(k) = \Omega_2 k + C \quad \text{for } k \in [0, \beta) \tag{5.84}$$

as piecewise linear with period $\beta = 1 + \Omega_1/\Omega_2$ (so that F is a sawtooth, Fig. 5·6(b)) recovers $F(k) - F(k-1) = (-1)^{i_k}\Omega_{i_k}$.

The Hamiltonian (5.82) is an inhomogeneous one-dimensional hopping problem. Such a model has exponentially localized eigenstates if the on-site potential is random and the hopping is quasilocal [67]. Although the potentials ω_k in (5.83) are not random, we argue that the intuition from Anderson localization is correct in this case, and that the localization of the model (5.82) is captured by the associated Anderson model

$$K_{\text{random}} = \sum_{k,k' \in \mathbb{Z}} (H_{kk'} - \omega'_k \delta_{kk'})|k\rangle\langle k'|, \tag{5.85}$$

where ω'_k are independent random variables sampled from the uniform distribution on $[C, C + \Omega_1 + \Omega_2)$.

5.5.1 Localization in the Anderson Model

The localization of the Anderson chain K_{random} is controlled by the ratio r of typical hopping amplitudes to the scale of the disorder. By estimating r, we obtain a prediction for the dependence of the localization length of the quasienergy states ζ_f (and hence that for the matrix elements, $\xi_f = O(\zeta_f)$), on the number of orbitals N.

We begin by estimating the effective scale of the disorder in the N-band model Eq. (5.85). A quasienergy state with quasienergy ϵ_0 in the uncoupled model, with $H_{kk'}$ set to zero for $k \neq k'$, will hybridize with states with a similar quasienergy. This justifies considering the delocalization of this state as only involving the energy levels on each site closest to ϵ_0. The uncoupled energy levels of $H_0 = H_{kk}$ have a typical density of states in the middle of the spectrum given by $\rho = N/W$. If H_0 is modeling a many-body Hamiltonian on $L \gg 1$ spins, then $W = O(\sqrt{L})$, and $|\vec{\Omega}| \ll W$ at large L—the on-site potential is small compared to the bandwidth. Then we can approximate the density of states at quasienergy ϵ_0 on every other site in the chain as also being $\rho = N/W$. The effective disorder strength in the Anderson model (5.85) is thus set by the typical level spacing between these states: W/N.

If the hopping matrices $H_{kk'}$ have typical scale $\|H_{kk'}\| = J$, where J depends on the driving protocol, then the typical scale of the matrix element between the resonant levels is $J/\sqrt{N}$. The factor of $\sqrt{N}$ comes from an assumption that the eigenstates of H_0 present themselves in matrix elements of $H_{kk'}$ as random vectors [207].

The hopping $J/\sqrt{N}$ is asymptotically larger than the "disorder" W/N, so as $N \to \infty$ the model (5.85) must enter the low-disorder regime. Indeed,

$$r = \frac{J/\sqrt{N}}{W/N} = (J/W)\sqrt{N}. \tag{5.86}$$

grows without bound with N.

In the large r regime, the localization length scales with r^2 [217], giving

$$\xi_f = O(r^2) = O\left(\left(\tfrac{J}{W}\right)^2 N\right). \tag{5.87}$$

This provides $\nu = 1$. Not only is ξ_f finite for all finite N, it grows only linearly with N (that is, as 2^L in a spin chain).

5.5.2 Localization in the Quasiperiodic Model

While the inhomogeneous on-site potentials ω_k in the model (5.82) are not random, we find the associated Anderson model (5.85) to be an effective description of the localization properties of the system. This can be verified numerically, and partially justified analytically.

The prediction of exponential localization with $\nu = 1$ can be checked numerically in a driven random matrix model. Detailed descriptions of these numerics are presented below in Sec. 5.5.3, but we summarize some findings here. By taking a commensurate approximation to $\vec{\Omega}$ it is possible to calculate quasienergy states (Sec. 5.5.3.2). Fig. 5·7 shows the *inverse participation ratio* (IPR) (5.97) of the quasienergy states in a series of commensurate approximations indexed by Fibonacci numbers $q = F_n$. The IPR is roughly IPR $\propto \xi_f^{-1}$, so seeing the IPR saturate as $q \to \infty$ indicates the localization length is finite in the incommensurate limit. Rescaling the IPR by N and q by $1/N$ produces a good data collapse, consistent with $\nu = 1$.

The one-dimensional model (5.82) can also be simulated directly (Sec. 5.5.3.3). This produces a more quantitative prediction that

$$\nu = 1.001 \pm 0.009, \tag{5.88}$$

which is also consistent with $\nu = 1$.

The model (5.82) evades the mechanism of delocalization in many well-known quasiperiodic models, such as the Aubry-André model [218, 219]. Determining the localization properties of quasiperiodic tight-binding models, such as Eq. (5.82), is assisted by the existence of a duality transformation of these models [218–224]. For simplicity, suppose the hopping matrices $H_{kk'} = H_{k-k'}$ are translationally invariant (which amounts to an isotropy condition in the two-dimensional frequency lattice: $H_{\hat{e}_1} = H_{\hat{e}_2}$, etc.). Then the dual model is related to Eq. (5.82) by Fourier transform. Indeed, if $|\tilde{\phi}\rangle = \sum_k |\phi_k\rangle |k\rangle$ is an eigenstate of $K_{\text{1-dim}}$, then substituting the Fourier transform

$$|\phi_k\rangle = C \sum_x |\phi_x\rangle e^{-2\pi i x k/\beta} \tag{5.89}$$

(where C is a normalization constant) into the eigenvalue equation $K_{\text{1-dim}} |\tilde{\phi}\rangle = \epsilon |\tilde{\phi}\rangle$

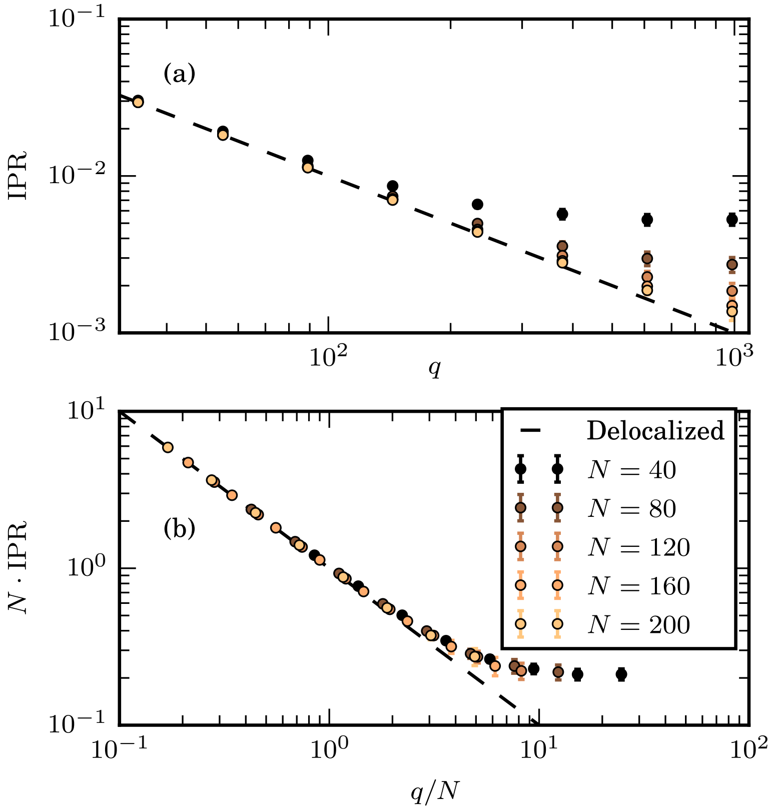

Figure 5·7: *IPR in commensurate approximations.*—(**a**) Inverse participation ratio averaged over both eigenstate index α and $N_{\text{samp}} \approx 1200/N$ samples in the random matrix model of Sec. 5.5.3.1. Successive commensurate approximations are indexed by Fibonacci numbers $q = F_n$. For small q, the IPR decreases as $1/q$ (dashed line), but for large q the IPR saturates, indicating a finite localization length in the incommensurate limit. (**b**) Scaling by N leads to a good data collapse, consistent with $\nu = 1$. *Parameters for model* (5.93)*:* $J/W = 0.2$, $\Omega_1/W = 0.6$, $q \in \{34, \ldots, 987\}$, with $N_{\text{samp}} \approx 1200/N$ random matrix samples.

reveals that $\sum_x |\phi_x\rangle\, |x\rangle$ is an eigenstate of

$$K^{\text{dual}}_{\text{1-dim}} = \sum_{x,x' \in \mathbb{Z}} (H(x)\delta_{xx'} - F_{x-x'})|x\rangle\langle x'|, \tag{5.90}$$

where

$$H_k = C \sum_x H(x) e^{2\pi i x k/\beta}, \tag{5.91}$$

$$F(k) = C \sum_x F_x e^{-2\pi i x k/\beta}. \tag{5.92}$$

If an eigenstate $|\tilde{\phi}\rangle$ of $K^{\text{dual}}_{\text{1-dim}}$ is localized, then the dual eigenstate of $K_{\text{1-dim}}$ must be delocalized [224]. In the self-dual Aubry-André model [218, 219], this guarantees the existence of a delocalized phase. Similarly, whenever the on-site potential $F(k)$ is smooth and the hopping amplitudes $H_{k-k'}$ decay exponentially, the dual model also has a smooth potential and exponentially decaying hopping amplitudes. At least one of the two models related by duality must be delocalized, and as both models have a similar structure, it is not possible for quasiperiodic models with smooth potentials to generically be localized.

In contrast, we observe that the on-site potential $F(k)$ in Eq. (5.84) is not smooth as a function of k—it has a finite jump—and so the hops F_x in the dual model are power-law decaying. In the absence of other special structure, we expect that the long-range model $K^{\text{dual}}_{\text{1-dim}}$ will be delocalized, which allows the quasilocal hopping model $K_{\text{1-dim}}$ to generically be localized.

While it is possible for both $K_{\text{1-dim}}$ and $K^{\text{dual}}_{\text{1-dim}}$ to be delocalized, once the inhomogenous model $K_{\text{1-dim}}$ evades any condition preventing it from localizing, the intuition from Anderson localization is that it will do so. Our numerical results provide a strong case for generic localization with $\nu = 1$.

5.5.3 Numerical Evidence of Synthetic Localization for Two-Tone Driving

Our calculations in Sec. 5.5 on the behavior of ξ_f with N for $D = 2$ can be verified through a number of numerical experiments. In this section, we report on two such experiments, one based on real-time evolution in a sequence of commensurate approximations to the quasiperiodic drive (Sec. 5.5.3.2), and one based on the one-dimensional model (5.82) in the frequency lattice (Sec. 5.5.3.3). In both cases, our results are consistent with $\xi_f = O(\zeta_f) = O(N)$.

5.5.3.1 Model

We use the model (5.39) from Sec. 5.3.1 for our numerics. This is a model of driven random matrices with nearest-neighbor hops on the frequency lattice. Restating it here:

$$H(\vec{\theta}) = H_0 + J(H_1 e^{-i\theta_1} + H_2 e^{-i\theta_2} + \text{H.c.}), \tag{5.93}$$

where H_0 is a GUE random matrix with rms energy W (as defined in Eq. (5.40)), J is a hopping amplitude, and H_1 and H_2 are complex Gaussian random matrices with unit rms energy. We take $\theta_j = \Omega_j t$, with $\Omega_1/\Omega_2 = (1+\sqrt{5})/2$ given by the golden ratio.

5.5.3.2 Commensurate Approximations

Ideally, we could directly compute the quasienergy states $|\phi_\alpha(\vec{\theta})\rangle$ from the quasiperiodically driven model (5.39), but as we noted in Sec. 5.3.2, this is numerically challenging, and so instead we make a commensurate approximation to the incommensurate frequency vector $\vec{\Omega}$, and we solve the corresponding Floquet problem.

Recall that the commensurate approximations we use are

$$\vec{\Omega}_n = \Omega_1 \hat{e}_1 + \Omega_1 \frac{p_n}{q_n} \hat{e}_2 \tag{5.94}$$

where $p_n = F_{n-1}$ and $q_n = F_n$ are consecutive Fibonacci numbers. We use a second-order Suzuki-Trotter approximation [209] to compute $U(T_n, 0)$, and subsequently calculate $|\phi_\alpha(\theta_2 \hat{e}_2)\rangle$ at q points along the line $\theta_1 = 0$.

Localization in the frequency lattice can be probed by calculating the Fourier coefficients of the density matrix

$$\rho_\alpha(\theta_2 \hat{e}_2) = |\phi_\alpha(\theta_2 \hat{e}_2)\rangle\langle\phi_\alpha(\theta_2 \hat{e}_2)| = \sum_n \rho'_{\alpha n} e^{-in\theta_2}, \tag{5.95}$$

which are related to the two-dimensional Fourier coefficients of the density matrix $\rho_{\alpha\vec{n}}$ by

$$\rho'_{\alpha n} = \sum_{n_1} \rho_{\alpha, n_1 \hat{e}_1 + n \hat{e}_2}. \tag{5.96}$$

Computing $\rho'_{\alpha n}$, rather than $\rho_{\alpha\vec{n}}$, is less expensive numerically (in both time and memory), and allows us to probe larger commensurate approximations. We calculate the density matrix, rather than the kets $|\phi_\alpha(\vec{\theta})\rangle$, to avoid having to find a smooth gauge for the states.

To quantify the localization of these states, we use the inverse participation ratio, defined as

$$\mathrm{IPR}_\alpha = \sum_n \|\rho'_{\alpha n}\|_F^4, \tag{5.97}$$

where $\|\cdot\|_F$ is the Frobenius norm. This quantity is 1 for a perfectly localized state, and $1/q$ for a completely delocalized state on q sites. (We do not have an infinite system as we calculate $\rho_\alpha(\theta_2 \hat{e}_2)$ at only q points.) Roughly, $1/\mathrm{IPR}_\alpha$ is the number of frequency lattice sites that a state has significant weight on, and is proportional to ζ_f, the localization length of the quasienergy states. As we observed in Sec. 5.3, the localization length of the matrix elements has the same scaling: $\xi_f = O(\zeta_f)$. Thus, it is sufficient to compute ζ_f.

The numerically calculated inverse participation ratios for the model (5.39) are shown in Fig. 5·7. For every N in Fig. 5·7, the IPR saturates as q becomes very large, indicating that all N have a finite localization length, as we have predicted.

Furthermore, rescaling q by $1/N$ and the IPR by N produces a collapse of the data. This amounts to rescaling lengths in the frequency lattice by $1/N$, so the data collapse indicates the existence of a single length scale, $\xi_f = O(\zeta_f)$, which grows proportionally to N. Thus, these numerics agree with our prediction of $\nu = 1$.

5.5.3.3 One-dimensional Approximation

We can probe even larger distances in the frequency lattice, and larger Hilbert space dimensions N, by instead studying the one-dimensional approximation (5.82) directly.

There are many numerical methods effective in solving one-dimensional tight binding models. For the purpose of extracting the localization length ζ_f (which has the same scaling as ξ_f), we use a transfer matrix method [225, 226].

The eigenvalue equation for $|\tilde{\phi}_\alpha\rangle = \sum_k |\phi_{\alpha,k}\rangle |k\rangle$ may be written

$$(H_0 + \omega_k) |\phi_{\alpha,k}\rangle + J(H_{i_k} |\phi_{\alpha,k-1}\rangle + H^\dagger_{i_{k+1}} |\phi_{\alpha,k+1}\rangle) = \epsilon_\alpha |\phi_{\alpha,k}\rangle \,, \tag{5.98}$$

where $i_k \in \{1, 2\}$ is the same quasiperiodic sequence from Sec. 5.5, and H_0, H_1 and H_2 are given as in the model (5.39).

The eigenvalue equation (5.98) may be expressed as a transfer matrix equation for $|\phi_{\alpha,k+1}\rangle$ given $|\phi_{\alpha,k}\rangle$ and $|\phi_{\alpha,k-1}\rangle$:

$$|\Phi_{\alpha,k+1}\rangle = \begin{pmatrix} |\phi_{\alpha,k+1}\rangle \\ |\phi_{\alpha,k}\rangle \end{pmatrix} = T_{k+1}(\epsilon_\alpha) \begin{pmatrix} |\phi_{\alpha,k}\rangle \\ |\phi_{\alpha,k-1}\rangle \end{pmatrix} , \tag{5.99}$$

where

$$T_{k+1}(\epsilon) = \begin{pmatrix} -\frac{1}{J} H^{-\dagger}_{i_{k+1}} (H_0 + \omega_k - \epsilon) & -H^{-\dagger}_{i_{k+1}} H_{i_k} \\ \mathbb{1} & 0 \end{pmatrix} , \tag{5.100}$$

and we have written $A^{-\dagger} = (A^{-1})^\dagger = (A^\dagger)^{-1}$.

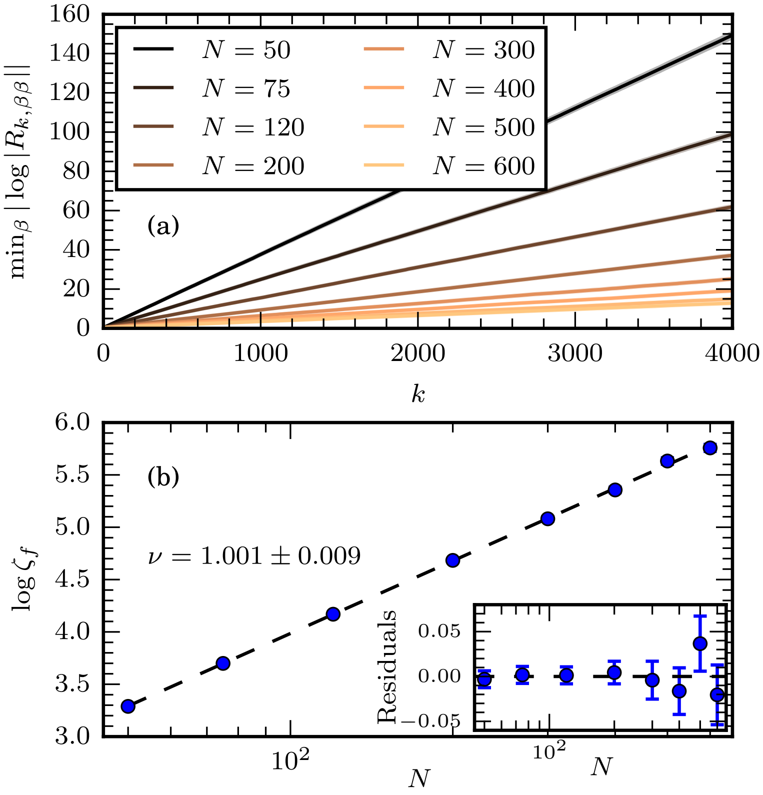

Figure 5·8: *Scaling of ζ_f in a one-dimensional approximation.*— (**a**) The inverse localization length ζ_f^{-1} may be extracted from the limiting behavior of the QR-decomposition of a transfer matrix, as described in (5.105). (**b**) Values of ζ_f extracted from the data in (**a**) show the expected linear scaling with N. Fitting a power law $\zeta_f = AN^\nu$ (dashed line) gives $\nu = 1.001 \pm 0.009$, consistent with $\nu = 1$. *Parameters:* $\Omega_1/W = 0.6$, $J/W = 0.2$, $\Omega_1/\Omega_2 = (1+\sqrt{5})/2$, $\epsilon = 0$, chain length $L = 4000$ with between 800 and 200 samples of random matrices, depending on N.

To identify the localization length ζ_f, we need to identify the asymptotic behavior

$$\zeta_f^{-1} = \lim_{k\to\infty} -\frac{1}{k} \log \|\Phi_{\alpha,k}\|. \tag{5.101}$$

The scaling of $\log \|\Phi_{\alpha,k}\|$ can be estimated by computing the eigenvalues of

$$\Pi_k(\epsilon) = T_k T_{k-1} \cdots T_1(\epsilon) \tag{5.102}$$

at a fixed target quasienergy ϵ. The product Π_k has $2N$ eigenvalues $\lambda_{k\beta}$, which may have $|\lambda_{k\beta}| < 1$ corresponding to decay of the wavefunction, or $|\lambda_{k\beta}| > 1$ corresponding to growth of the wavefunction (moving towards the localization center). The longest localization length is extracted as

$$\zeta_f^{-1}(\epsilon) = \lim_{k\to\infty} \min_{\beta} \frac{1}{k} \left|\log |\lambda_{k\beta}|\right|. \tag{5.103}$$

Equation (5.103) is hard to evaluate numerically, as the eigenvalues of $\Pi_k(\epsilon)$ vary over many orders of magnitude for large k, and numerical calculations tend to be dominated by the largest eigenvalue. Fortunately, numerically stable methods to calculate $\zeta_f^{-1}(\epsilon)$ have been developed in the context of calculating Lyapunov exponents in discrete maps [227]. They are based on the QR-decomposition of Π_k,

$$\Pi_k = Q_k R_k \tag{5.104}$$

where Q_k is unitary and R_k is upper triangular. The localization length may be computed as

$$\zeta_f^{-1}(\epsilon) = \lim_{k\to\infty} \min_{\beta} \frac{1}{k} \left|\log |R_{k,\beta\beta}|\right|, \tag{5.105}$$

where $R_{k,\beta\beta}$ is a diagonal element of R_k. By using the techniques of [227], the logarithms $\log |R_{k,\beta\beta}|$ may be computed directly. These are not dominated by the largest value, as the exponential growth with k in the elements $R_{k,\beta\beta}$ appears only as linear growth in the logarithm.

Localization lengths extracted using the transfer matrix method for different values of N and a value of ϵ in the middle of the spectrum are shown in Fig. 5·8. (There is no "middle of the spectrum" in the full frequency lattice model, where the spectrum is unbounded. However, when restricted to a line as is in this section, the spectrum is bounded, and so it has a "middle" where the density of states is maximal, and the one-dimensional model is most representative of the frequency lattice.) We first see that the average of $\min_\beta |\log |R_{k,\beta\beta}||$ over random matrix samples (and even the individual samples, not shown) shows linear behavior with k with a strictly positive slope, so there is indeed exponential localization. Extracting the localization length from these data and fitting a power law $\zeta_f = AN^\nu$ gives

$$\nu = 1.001 \pm 0.009, \tag{5.106}$$

consistent with the predicted $\nu = 1$ from the associated Anderson model.

5.6 Absence of Synthetic Localization with Three or More Tones

Following Sec. 5.5, Stark localization produces a coarse-grained single-particle hopping problem in $D-1$ dimensions. Just as in the $D = 2$ case, said hopping model has a large number of orbitals N, an inhomogeneous on-site potential $\omega_{\vec{k}} = \vec{\Omega} \cdot \vec{n}_{\vec{k}}$ and exponentially decaying (but no longer necessarily translationally invariant) hopping matrices $H_{\vec{k}\vec{k}'}$.

A disordered $(D-1)$-dimensional Anderson model with spin-orbit coupling is not always localized for $D \geq 3$ [228–230]. There is typically a non-zero hopping amplitude to disorder strength ratio r_c above which eigenstates become delocalized. As argued in Sec. 5.5, the relevant ratio in our case is $r = (J/W)\sqrt{N}$ (5.86).

The ratio r grows with N, so for sufficiently large $N > N_c$, the ratio r exceeds the critical value r_c, and the localization length ξ_f becomes infinite. That is, a large enough, but finite, thermal inclusion acquires a genuinely continuous spectrum in the presence of three-tone (or more) driving. This feature destabilizes randomly disordered MBL—it is known from, for instance, Ref. [201] that a finite thermal region that presents a continuous spectrum to the rest of the chain can completely thermalize the system given sufficient time.

That ξ_f can diverge for a finite thermal inclusion is supported by numerical evidence in the existing literature. Refs. [1, 65] identify a phase believed to be delocalized in the frequency lattice for a three-tone-driven qubit ($N = 2$). Larger N only increases the likelihood to delocalize.

We conclude that quasiperiodically-driven MBL with random disorder can only be stable for two-tone-driving. For $D \geq 3$ tones, sufficiently large thermal regions will destabilize a putatively MBL chain.

5.7 Many-Body Resonances

Another mechanism for destroying MBL is the proliferation of *many-body resonances*—if, for all L sufficiently large, a fixed nonzero perturbation to a putatively MBL chain causes a given quasienergy state to hybridize with exponentially many in L other quasienergy states, then MBL is not a stable dynamical phase.

In static systems, demanding perturbative stability of MBL implies that the localization length must be below a critical value $\xi'_{s,c}$. This critical value is bounded from below by $(\log 2)^{-1}$, the critical localization length predicted by the avalanche argument. The bound is saturated when the matrix elements of the perturbation between l-bit states that differ in $\tilde{\tau}^z_{\pm r}$ are sufficiently narrowly distributed. In physical chains, however, the matrix elements at each range r are broadly distributed (approximately log-normally) [231], so that there is a window of disorder strengths accessible at small sizes in which localization in the chain is stable to the formation of many-body resonances, but not to thermal avalanches [76, 170].

For $D \geq 2$ tones, we show that the critical localization length for perturbative stability is still bounded by $(\log 2)^{-1}$, which is now strictly larger than the localization length provided by the avalanche argument. Thus, we expect that the regime wherein avalanches, and not many-body resonances, control the (in)stability of randomly disordered MBL ($\xi_{s,c} < \xi_s < \xi'_{s,c}$) is broader in quasiperiodically-driven systems than in static and periodically-driven systems.

The reason the bound on $\xi'_{s,c}$ is unaltered from the static case is because the frequency lattice only provides a polynomial enhancement to the effective density of states introduced in Sec. 5.4. Unlike in the case of a thermal avalanche, there is no growing thermal bubble that can expand exponentially in the frequency lattice as it absorbs more spins. Without the required exponential scaling, the effective density of states cannot compete with the decaying matrix elements. The remainder of this section is essentially a formal verification of this intuition.

The frequency lattice fidelity susceptibility (Sec. 5.4.2.1) detects if a perturbation $JV(\vec{\theta})$ to a putatively MBL Hamiltonian $H(\vec{\theta})$ causes large changes to the unperturbed quasienergy states. Strong localization of l-bits places constraints on the fidelity susceptibility, and ensures perturbative stability. This calculation generalizes methods used in Ref. [170] in the static and Floquet contexts.

We assume that the Hermitian operator $V(\vec{\theta})$ is quasilocal in space centered at $j = 0$ (say), and smooth in $\vec{\theta}$. To extract the spatial structure of $\tilde{V}$ it is convenient to decompose it as

$$\tilde{V} = \sum_r \tilde{V}_r \tag{5.107}$$

where $[\tilde{V}_r, \tilde{\tau}^z_j] = 0$ for $|j| > r$, and $[\tilde{V}_r, \tilde{\tau}^z_{\pm r}] \neq 0$. In words, $\tilde{V}_r$ acts trivially on l-bits that are further than a range r from $j = 0$, and non-trivially on those exactly at range r. We define a scaled Frobenius norm for the temporal operator for $\tilde{V}_r$,

$$\|V_r\| = \sqrt{\frac{1}{2^L}\int \frac{\mathrm{d}^D\theta}{(2\pi)^D}\operatorname{Tr} V_r(\vec{\theta})^2} \tag{5.108}$$

where L is the system size. Quasilocality of $\tilde{V}$ in real space is expressed as

$$\log\|V_r\| \sim -\frac{r}{\xi_s}. \tag{5.109}$$

Quasilocality in the synthetic dimensions implies exponential decay of the matrix elements $\tilde{V}^{\vec{l}}_{\beta\alpha}$ with $|\vec{l}|$, with localization length ξ_f, as usual.

We use the assumed exponential decay of $\|V_r\|$ with r to deduce the scaling of the matrix elements appearing in the calculation of the fidelity susceptibility $\chi_\star$. In terms of the matrix elements between quasienergy states $|\tilde{\phi}^{\vec{n}}_\alpha\rangle = |\{\tilde{\tau}\}^{\vec{n}}\rangle$, specified by their l-bit configurations and a translation $\vec{n}$, the norm is

$$\|V_r\|^2 = \frac{1}{2^L}\sum_{\alpha,\beta,\vec{l}} |(\tilde{V}_r)^{\vec{l}}_{\beta\alpha}|^2. \tag{5.110}$$

To estimate $\chi_\star$, we find the average squared matrix element, summed over $\vec{l}$:

$$v(r)^2 = \left[\sum_{\vec{l}} |(\tilde{V}_r)^{\vec{l}}_{\beta\alpha}|^2\right]_{\alpha\beta}, \tag{5.111}$$

where square brackets indicate an average over those α and β such that the matrix element is non-zero. Comparing this to Eqs. (5.108) and (5.110), and noting that there are $N_r = O(2^{2r})$ states $|\tilde{\phi}_\beta\rangle$ for which the matrix element is non-zero with a given α, we have

$$v(r) = \frac{O(e^{-r/\xi_s})}{\sqrt{N_r}}. \tag{5.112}$$

By summing over the frequency lattice before analyzing the scaling of $\chi_\star$, the problem of calculating $\xi'_{s,c}$ is essentially reduced to the static case. The sum was possible due to the exponential decay of $|(\tilde{V}_r)^{\vec{l}}_{\beta\alpha}|^2$ with $|\vec{l}|$, and the fact that there are only polynomially many frequency lattice sites with a given $|\vec{l}|$.

Summarizing the remaining steps in the calculation [170]: one organizes the sum for $\chi_\star$ in terms of operators of increasing range $\tilde{V}_r$, which gives

$$\sqrt{\chi_\star} \leq \sum_{r=1}^{L} \left(\lim_{\Delta \to 0} \left[\frac{1}{2\Delta} \sum_{|\Delta^{\vec{l}}_{\beta\alpha}| < \Delta} |(\tilde{V}_r)^{\vec{l}}_{\beta\alpha}| \right]_{\alpha\beta} \right), \tag{5.113}$$

where we used the triangle inequality. Eq. (5.110) places a restriction on the sum of squares of the matrix elements. Given this restriction, the sum of the absolute values appearing in $\sqrt{\chi_\star}$ is maximal when all the matrix elements are equal. Thus, we obtain an upper bound for $\sqrt{\chi_\star}$ by replacing the sum of matrix elements for each r by the root-mean-square value $v(r) = O(e^{-r/\xi_s} 2^{-r})$ times the number of terms $N_r = O(2^{2r})$. The $\Delta \to 0$ limit introduces an unimportant $O(1)$ factor. Thus, we have

$$\sqrt{\chi_\star} \leq O\left(\sum_{r=1}^{L} 2^r e^{-r/\xi_s} \right). \tag{5.114}$$

Demanding that $\sqrt{\chi_\star}$ converges as $L \to \infty$ for $\xi_s < \xi'_{s,c}$ implies

$$\xi'_{s,c} \geq (\log 2)^{-1}. \tag{5.115}$$

If this condition is met, then by choosing $J \ll 1/\sqrt{\chi_\star}$ we have that the dimensionless quantity $J\sqrt{\chi_\star} \ll 1$, and distant quasienergy states typically do not strongly hybridize when the perturbation $JV(\vec{\theta})$ is added to the Hamiltonian. On the other hand, if the sum for $\sqrt{\chi_\star}$ diverges, then no such J exists in the thermodynamic limit, and the MBL phenomenology is unstable to an arbitrarily small perturbation.

We conclude that MBL phenomenology is stable to many-body resonances for any number of tones D whenever the spatial localization length is below a critical value $\xi'_{s,c} \geq (\log 2)^{-1}$, the bound for which is independent of D.

We reiterate that Eq. (5.115) is *not* the critical localization length for the stability of randomly disordered MBL in the thermodynamic limit. Avalanches are the dominant instability for MBL, and this is particularly stark in quasiperiodically driven MBL for $D \geq 3$.

5.8 Summary and Discussion

We have argued that two-tone-driven randomly-disordered MBL is stable to the occurrence of a large thermal region, and to the addition of a small perturbation to the Hamiltonian. Stability requires that the spatial localization length is below a critical value $\xi_{s,c} = (2\log 2)^{-1}$. With three or more tones, however, putative MBL is always unstable to thermal avalanches.

An immediate consequence of our result is that the two-tone-driven topological orders identified in Refs. [1, 33, 34, 65] (including the QP pump of chapter 4) have infinite lifetime with sufficient disorder. That is, they characterize genuine dynamical phases of matter.

We have not *proven* the existence of quasiperiodically-driven MBL. Rather, we have checked for the stability of putative MBL to two particular mechanisms of thermalization that are believed to be the dominant ones in the thermodynamic limit. There has been a recent debate about the existence of MBL even in static systems [72–74, 77]. Quasiperiodically-driven MBL is not immune to that debate—all objections to static MBL apply just as much to quasiperiodically-driven MBL.

Our results also clarify how quasiperiodic driving enhances the effective Hilbert space dimension of a finite system. This feature could be used to increase the thermalizing ability of small quantum systems, and thus aid in experimental tests of thermalization in nearly-isolated quantum systems [200, 232].

While we have kept our discussion to smooth driving, our results may hold for continuous and piecewise smooth, but non-analytic drives. Non-analyticities result in power-law hops in the frequency lattice, $\tilde{V}^{\vec{l}}_{\alpha\beta} = O(|\vec{l}|^{-p})$. Our conditions on the drive ensure $p > 1$, so that the analogueous Anderson model in the frequency lattice is localized for $D = 2$ [67], and $\chi_{\star,j=0}$ is finite. Stability to avalanches additionally requires that $\chi_{\star,j}$ grows at most exponentially in j. We expect this is so, but we leave this calculation to future work.

Resonance counting in the frequency lattice suggests that discontinuous two-tone drives with $p < 1$ lead to delocalization [67]. Indeed, this has been shown for specific drives in a two-level system [14]. As local regions have continuous spectra, MBL is not stable here, explaining the results in Ref. [31]. The marginal $p = 1$ case is an interesting topic for future research [233].

With $D \geq 2$, we expect that the finite size regime in which a localized chain is stable to many-body resonances but not to thermal avalanches is broader than in static and periodically driven systems [76]. Quasiperiodic driving may thus provide a good experimental setting for the controlled exploration of different instabilities of randomly disordered MBL [197–200].

However, our analysis of many-body resonances was restricted to first order perturbation theory. More sophisticated methods of treating many-body resonances have recently been developed in the context of *prethermal MBL* [173]. Adapting these techniques to the frequency lattice could produce a tighter bound on $\xi'_{s,c}$, conceivably reaching $\xi_{s,c}$. The same techniques also predict the behavior of observables. Whether this behavior is significantly altered in quasiperiodically driven systems is an interesting direction for future work.

If putative MBL is due to quasiperiodic spatial modulation (QPMBL), rather than random disorder, then regions of low disorder do not occur [234, 235]. Avalanches can only occur for $\xi_s > \xi_{s,c}$ if there is some other mechanism to generate large thermal subsystems. This leaves open the possibility that quasiperiodically-driven QPMBL, and the associated topological dynamical phases [1, 33], are stable with any number of tones D. (Though if there is a non-perturbative instability to many-body resonances, such resonances will also destabilize QPMBL.)

Our discussion of the critical localization length $\xi_{s,c}$ largely follows Reference [78]. Ref. [78] identifies a bare localization length that is subject to a renormalization group (RG) scaling [236–239]. The value $\xi_{s,c} = (2\log 2)^{-1}$ should also be interpreted in this way. We leave a more systematic formulation of RG in quasiperiodically-driven MBL to future work.

Local integrals of motion could be explicitly constructed on the frequency lattice (Sec. 5.2) by adapting existing analytical and numerical techniques for static systems [71, 240–244]. We suspect the frequency lattice also provides a formalism to generalize Imbrie's proof of static MBL [71].

Our quasiperiodically-driven ETH-style ansatz (5.33) is appropriate for systems with pure-point spectra: finite systems with quasienergy states localized in the synthetic dimensions of the frequency lattice. With three or more tones, the quasienergy states may be delocalized. The ansatz (5.33) can be adapted to this case by taking commensurate approximations to $\vec{\Omega}$. This collapses the frequency lattice into a cylinder with a finite circumference [1, 37, 38]. Quasienergy states are localized parallel to the length of the cylinder by the electric field $\vec{\Omega}$, but are delocalized around the circumference. The appropriate ETH-style ansatz then becomes

$$\tilde{V}^{\vec{l}}_{\alpha\beta} = \bar{V}_{\vec{l}}\delta_{\alpha\beta} + \frac{f(\Delta^{\vec{l}}_{\alpha\beta})}{\sqrt{N\mu}} R_{\alpha\beta,\vec{l}}, \tag{5.116}$$

where symbols are defined as in Eq. (5.33), and μ is the $(D-1)$-dimensional volume of the cylinder section perpendicular to $\vec{\Omega}$. Note that the spectral function f does not depend on $\vec{l}$, as the states are delocalized perpendicular to the electric field. We conjecture Eq. (5.116) to be the statistical description of three-or-more-tone thermalizing quantum systems with continuous spectra in the incommensurate limit.

Chapter 6

Conclusion

As the experimental control of quantum systems improves, quasiperiodic driving becomes increasing viable as a means of quantum control [28]. Control protocols which rely on topology are particularly attractive, as they are robust to many imperfections which inevitably arise in real experiments.

This dissertation has demonstrated by explicit example that topological effects in quasiperiodically driven systems can be exploited to perform useful tasks. In particular, the phenomenon of topological energy pumping [37, 38] can be used to engineer highly excited non-classical cavity states by *boosting* less excited states [3, 51]. Such states serve as a resource for, for instance, highly sensitive interferometry or the storage of quantum information [52–63]. Further, topological energy pumping, and thus boosting, can occur as a robust edge effect in *anomalous localized topological phases* (ALTPs) [1, 4], which we argue are stable to weak interactions [2].

Quasiperiodic driving also offers a rich ground theoretically. The existence of stable non-equilibrium phases of matter in driven systems was originally noticed in periodically-driven (Floquet) systems, but nontrivial topological phases may also occur with quasiperiodic driving. Indeed, quasiperiodic driving provides topological phases with no periodically-driven analogue, just as periodic driving provided phases with no static analogue [1, 27, 33, 34, 37, 44, 46, 64, 65, 186–191].

Detailed questions regarding the stability of these phases to interactions are also of theoretical interest. Previous work demonstrates that the lifetime of any topological response in quasiperiodically driven systems can extend to a parametrically long *prethermal* regime [33], and our own arguments indicate that this regime may be infinitely long [2]. The abstract algebraic structure which characterizes interacting quasiperiodic phases is not yet complete—the classification in Ref. [33] fails to capture ALTPs, as their topological structure depends on many states, not just one [1, 66]. Extending the classification of quasiperiodically-driven phases to capture ALTPs may well reveal unanticipated interacting topological phases of quasiperiodically driven systems, potentially with useful applications.

Regardless, the most interesting current directions for research on quasiperiodically driven systems are likely experimental. Topological energy pumping has been indirectly demonstrated in nitrogen vacancy centers in diamond [28] and in superconducting qubit architectures [245]. However, direct measurement of an energy current between the drives has not yet been achieved, nor has the coherent effect of boosting been observed. Making this observation is the immediate direction of greatest interest in this class of systems. This should be possible directly in cavity and circuit QED systems. There have also been recent efforts theoretically to identify alternative settings where pumping rates may be high enough to measure without confining any electromagnetic modes [49].

In terms of applications, boosting is likely to be the most advantageous in optical cavity QED systems. While methods exist to prepare Fock states in circuit QED using coherent control [111–113], methods in cavity QED tend to be stochastic—they only prepare a Fock state with some probability, and preparing highly-excited Fock states is exponentially less likely. The experimental exploration of boosting in optical systems is thus of great interest, as it allows the *on-demand* preparation of Fock states.

Quasiperiodically driven systems likely contain many undiscovered phenomena. Their continued study, both in theory and experiment, may uncover a host of new surprises. Discovering unanticipated applications of these phenomena is, with some creativity, also very plausible. While this dissertation demonstrates that surprising physics with genuine applications can arise from quasiperiodically driven systems, it is very far from being an exhaustive study of the subject. More novel physical processes likely only await our investigation to be uncovered.

Bibliography

[1] David M. Long, Philip J. D. Crowley, and Anushya Chandran. Nonadiabatic topological energy pumps with quasiperiodic driving. *Physical Review Letters*, 126:106805, Mar 2021. doi: 10.1103/PhysRevLett.126.106805. URL https://link.aps.org/doi/10.1103/PhysRevLett.126.106805.

[2] David M. Long, Philip J. D. Crowley, and Anushya Chandran. Many-body localization with quasiperiodic driving. *Physical Review B*, 105:144204, Apr 2022. doi: 10.1103/PhysRevB.105.144204. URL https://link.aps.org/doi/10.1103/PhysRevB.105.144204.

[3] David M. Long, Philip J. D. Crowley, Alicia J. Kollár, and Anushya Chandran. Boosting the quantum state of a cavity with floquet driving. *Physical Review Letters*, 128:183602, May 2022. doi: 10.1103/PhysRevLett.128.183602. URL https://link.aps.org/doi/10.1103/PhysRevLett.128.183602.

[4] David M. Long, Philip J. D. Crowley, and Anushya Chandran. Coupled layer construction for synthetic hall effects in driven systems. *Physical Review B*, 106:144203, Oct 2022. doi: 10.1103/PhysRevB.106.144203. URL https://link.aps.org/doi/10.1103/PhysRevB.106.144203.

[5] Phillip Weinberg and Marin Bukov. QuSpin: a Python Package for Dynamics and Exact Diagonalisation of Quantum Many Body Systems part I: spin chains. *SciPost Physics*, 2:003, 2017. doi: 10.21468/SciPostPhys.2.1.003. URL https://scipost.org/10.21468/SciPostPhys.2.1.003.

[6] Phillip Weinberg and Marin Bukov. QuSpin: a Python Package for Dynamics and Exact Diagonalisation of Quantum Many Body Systems. Part II: bosons, fermions and higher spins. *SciPost Physics*, 7:020, 2019. doi: 10.21468/SciPostPhys.7.2.020. URL https://scipost.org/10.21468/SciPostPhys.7.2.020.

[7] R. Merlin. Rabi oscillations, floquet states, fermi's golden rule, and all that: Insights from an exactly solvable two-level model. *American Journal of Physics*, 89(1):26–34, 2021. doi: 10.1119/10.0001897. URL https://doi.org/10.1119/10.0001897.

[8] Takuya Kitagawa, Erez Berg, Mark Rudner, and Eugene Demler. Topological characterization of periodically driven quantum systems. *Physical Review B*, 82:235114, Dec 2010. doi: 10.1103/PhysRevB.82.235114. URL https://link.aps.org/doi/10.1103/PhysRevB.82.235114.

[9] Mark S. Rudner, Netanel H. Lindner, Erez Berg, and Michael Levin. Anomalous edge states and the bulk-edge correspondence for periodically driven

two-dimensional systems. *Physical Review X*, 3:031005, Jul 2013. doi: 10.1103/PhysRevX.3.031005. URL https://link.aps.org/doi/10.1103/PhysRevX.3.031005.

[10] Marin Bukov, Luca D'Alessio, and Anatoli Polkovnikov. Universal high-frequency behavior of periodically driven systems: From dynamical stabilization to Floquet engineering. *Advances in Physics*, 64(2):139–226, 2015. ISSN 14606976. doi: 10.1080/00018732.2015.1055918.

[11] Paraj Titum, Erez Berg, Mark S. Rudner, Gil Refael, and Netanel H. Lindner. Anomalous floquet-anderson insulator as a nonadiabatic quantized charge pump. *Physical Review X*, 6:021013, May 2016. doi: 10.1103/PhysRevX.6.021013. URL https://link.aps.org/doi/10.1103/PhysRevX.6.021013.

[12] Takashi Oka and Sota Kitamura. Floquet engineering of quantum materials. *Annual Review of Condensed Matter Physics*, 10(1):387–408, 2019. ISSN 19475462. doi: 10.1146/annurev-conmatphys-031218-013423.

[13] Tak-San Ho, Shih-I Chu, and James V Tietz. Semiclassical many-mode floquet theory. *Chemical Physics Letters*, 96(4):464–471, 1983. URL https://doi.org/10.1016/0009-2614(83)80732-5.

[14] JM Luck, H Orland, and U Smilansky. On the response of a two-level quantum system to a class of time-dependent quasiperiodic perturbations. *Journal of Statistical Physics*, 53(3-4):551–564, 1988. URL https://doi.org/10.1007/BF01014213.

[15] Giulio Casati, Italo Guarneri, and D. L. Shepelyansky. Anderson Transition in a One-Dimensional System with Three Incommensurate Frequencies. *Physical Review Letters*, 62(4):345–348, 1989. ISSN 00319007. doi: 10.1103/PhysRevLett.62.345.

[16] H. R. Jauslin and J. L. Lebowitz. Spectral and stability aspects of quantum chaos. *Chaos*, 1(1):114–121, 1991. ISSN 10541500. doi: 10.1063/1.165809.

[17] P. M. Blekher, H. R. Jauslin, and J. L. Lebowitz. Floquet spectrum for two-level systems in quasiperiodic time-dependent fields. *Journal of Statistical Physics*, 68(1-2):271–310, 1992. ISSN 00224715. doi: 10.1007/BF01048846.

[18] Àngel Jorba and Carles Simó. On the reducibility of linear differential equations with quasiperiodic coefficients. *Journal of Differential Equations*, 98(1):111–124, 1992. ISSN 10902732. doi: 10.1016/0022-0396(92)90107-X.

[19] Ulrike Feudel, Arkady S. Pikovsky, and Michael A. Zaks. Correlation properties of a quasiperiodically forced two-level system. *Physical Review E*, 51:1762–1769,

Mar 1995. doi: 10.1103/PhysRevE.51.1762. URL https://link.aps.org/doi/10.1103/PhysRevE.51.1762.

[20] Dario Bambusi and Sandro Graffi. Time quasi-periodic unbounded perturbations of Schrödinger operators and KAM methods. *Communications in Mathematical Physics*, 219(2):465–480, 2001. ISSN 00103616. doi: 10.1007/s002200100426.

[21] Guido Gentile. Quasi-Periodic Solutions for Two-Level Systems. *Communications in Mathematical Physics*, 242(1):221–250, 2003. ISSN 1432-0916. doi: 10.1007/s00220-003-0943-0. URL https://doi.org/10.1007/s00220-003-0943-0.

[22] Shih I. Chu and Dmitry A. Telnov. Beyond the Floquet theorem: Generalized Floquet formalisms and quasienergy methods for atomic and molecular multiphoton processes in intense laser fields. *Physics Reports*, 390(1-2):1–131, 2004. ISSN 03701573. doi: 10.1016/j.physrep.2003.10.001.

[23] R. Gommers, S. Denisov, and F. Renzoni. Quasiperiodically driven ratchets for cold atoms. *Phys. Rev. Lett.*, 96:240604, Jun 2006. doi: 10.1103/PhysRevLett.96.240604. URL https://link.aps.org/doi/10.1103/PhysRevLett.96.240604.

[24] Julien Chabé, Gabriel Lemarié, Benoit Grémaud, Dominique Delande, Pascal Szriftgiser, and Jean Claude Garreau. Experimental observation of the anderson metal-insulator transition with atomic matter waves. *Physical Review Letters*, 101:255702, Dec 2008. doi: 10.1103/PhysRevLett.101.255702. URL https://link.aps.org/doi/10.1103/PhysRevLett.101.255702.

[25] David Cubero and Ferruccio Renzoni. Asymptotic theory of quasiperiodically driven quantum systems. *Physical Review E*, 97:062139, Jun 2018. doi: 10.1103/PhysRevE.97.062139. URL https://link.aps.org/doi/10.1103/PhysRevE.97.062139.

[26] Sourav Nandy, Arnab Sen, and Diptiman Sen. Steady states of a quasiperiodically driven integrable system. *Physical Review B*, 98:245144, Dec 2018. doi: 10.1103/PhysRevB.98.245144. URL https://link.aps.org/doi/10.1103/PhysRevB.98.245144.

[27] Sayak Ray, Subhasis Sinha, and Diptiman Sen. Dynamics of quasiperiodically driven spin systems. *Physical Review E*, 100:052129, Nov 2019. doi: 10.1103/PhysRevE.100.052129. URL https://link.aps.org/doi/10.1103/PhysRevE.100.052129.

[28] Eric Boyers, Philip J. D. Crowley, Anushya Chandran, and Alexander O. Sushkov. Exploring 2d synthetic quantum hall physics with a quasiperiodically driven qubit. *Physical Review Letters*, 125:160505, Oct 2020. doi: 10.1103/

PhysRevLett.125.160505. URL https://link.aps.org/doi/10.1103/PhysRevLett.125.160505.

[29] Philipp T Dumitrescu, Justin G Bohnet, John P Gaebler, Aaron Hankin, David Hayes, Ajesh Kumar, Brian Neyenhuis, Romain Vasseur, and Andrew C Potter. Dynamical topological phase realized in a trapped-ion quantum simulator. *Nature*, 607(7919):463–467, 2022. ISSN 1476-4687. doi: 10.1038/s41586-022-04853-4. URL https://doi.org/10.1038/s41586-022-04853-4.

[30] Hideo Sambe. Steady states and quasienergies of a quantum-mechanical system in an oscillating field. *Physical Review A*, 7:2203–2213, Jun 1973. doi: 10.1103/PhysRevA.7.2203. URL https://link.aps.org/doi/10.1103/PhysRevA.7.2203.

[31] Philipp T. Dumitrescu, Romain Vasseur, and Andrew C. Potter. Logarithmically slow relaxation in quasiperiodically driven random spin chains. *Physical Review Letters*, 120:070602, Feb 2018. doi: 10.1103/PhysRevLett.120.070602. URL https://link.aps.org/doi/10.1103/PhysRevLett.120.070602.

[32] Kartiek Agarwal and Ivar Martin. Dynamical enhancement of symmetries in many-body systems. *Physical Review Letters*, 125:080602, Aug 2020. doi: 10.1103/PhysRevLett.125.080602. URL https://link.aps.org/doi/10.1103/PhysRevLett.125.080602.

[33] Dominic V. Else, Wen Wei Ho, and Philipp T. Dumitrescu. Long-lived interacting phases of matter protected by multiple time-translation symmetries in quasiperiodically driven systems. *Physical Review X*, 10:021032, May 2020. doi: 10.1103/PhysRevX.10.021032. URL https://link.aps.org/doi/10.1103/PhysRevX.10.021032.

[34] Aaron J. Friedman, Brayden Ware, Romain Vasseur, and Andrew C. Potter. Topological edge modes without symmetry in quasiperiodically driven spin chains. *Physical Review B*, 105:115117, Mar 2022. doi: 10.1103/PhysRevB.105.115117. URL https://link.aps.org/doi/10.1103/PhysRevB.105.115117.

[35] Tristan Martin, Ivar Martin, and Kartiek Agarwal. Effect of quasiperiodic and random noise on many-body dynamical decoupling protocols. *Physical Review B*, 106:134306, Oct 2022. doi: 10.1103/PhysRevB.106.134306. URL https://link.aps.org/doi/10.1103/PhysRevB.106.134306.

[36] Albert Verdeny, Joaquim Puig, and Florian Mintert. Quasi-periodically driven quantum systems. *Zeitschrift fur Naturforschung A: a Journal of Physical Sciences*, 71(10):897–907, 2016. ISSN 09320784. doi: 10.1515/zna-2016-0079.

[37] Ivar Martin, Gil Refael, and Bertrand Halperin. Topological frequency conversion in strongly driven quantum systems. *Physical Review X*, 7:041008,

Oct 2017. doi: 10.1103/PhysRevX.7.041008. URL https://link.aps.org/doi/10.1103/PhysRevX.7.041008.

[38] P. J. D. Crowley, I. Martin, and A. Chandran. Topological classification of quasiperiodically driven quantum systems. *Physical Review B*, 99:064306, Feb 2019. doi: 10.1103/PhysRevB.99.064306. URL https://link.aps.org/doi/10.1103/PhysRevB.99.064306.

[39] K. v. Klitzing, G. Dorda, and M. Pepper. New method for high-accuracy determination of the fine-structure constant based on quantized hall resistance. *Physical Review Letters*, 45:494–497, Aug 1980. doi: 10.1103/PhysRevLett.45.494. URL https://link.aps.org/doi/10.1103/PhysRevLett.45.494.

[40] D. J. Thouless, M. Kohmoto, M. P. Nightingale, and M. den Nijs. Quantized hall conductance in a two-dimensional periodic potential. *Physical Review Letters*, 49:405–408, Aug 1982. doi: 10.1103/PhysRevLett.49.405. URL https://link.aps.org/doi/10.1103/PhysRevLett.49.405.

[41] D. J. Thouless. Quantization of particle transport. *Physical Review B*, 27:6083–6087, May 1983. doi: 10.1103/PhysRevB.27.6083. URL https://link.aps.org/doi/10.1103/PhysRevB.27.6083.

[42] Alexei Kitaev. Anyons in an exactly solved model and beyond. *Annals of Physics*, 321(1):2–111, 2006. ISSN 00034916. doi: 10.1016/j.aop.2005.10.005.

[43] Xiao-Gang Wen. Colloquium: Zoo of quantum-topological phases of matter. *Reviews of Modern Physics*, 89:041004, Dec 2017. doi: 10.1103/RevModPhys.89.041004. URL https://link.aps.org/doi/10.1103/RevModPhys.89.041004.

[44] Michael H. Kolodrubetz, Frederik Nathan, Snir Gazit, Takahiro Morimoto, and Joel E. Moore. Topological floquet-thouless energy pump. *Physical Review Letters*, 120:150601, Apr 2018. doi: 10.1103/PhysRevLett.120.150601. URL https://link.aps.org/doi/10.1103/PhysRevLett.120.150601.

[45] Yang Peng and Gil Refael. Floquet second-order topological insulators from nonsymmorphic space-time symmetries. *Phys. Rev. Lett.*, 123:016806, Jul 2019. doi: 10.1103/PhysRevLett.123.016806. URL https://link.aps.org/doi/10.1103/PhysRevLett.123.016806.

[46] Yang Peng and Gil Refael. Time-quasiperiodic topological superconductors with majorana multiplexing. *Physical Review B*, 98:220509(R), Dec 2018. doi: 10.1103/PhysRevB.98.220509. URL https://link.aps.org/doi/10.1103/PhysRevB.98.220509.

[47] Yang Peng and Gil Refael. Topological energy conversion through the bulk or the boundary of driven systems. *Physical Review B*, 97:134303, Apr 2018. doi: 10.1103/PhysRevB.97.134303. URL https://link.aps.org/doi/10.1103/PhysRevB.97.134303.

[48] Frederik Nathan, Gil Refael, Mark S. Rudner, and Ivar Martin. Quantum frequency locking and downconversion in a driven qubit-cavity system. *Physical Review Research*, 2:043411, Dec 2020. doi: 10.1103/PhysRevResearch.2.043411. URL https://link.aps.org/doi/10.1103/PhysRevResearch.2.043411.

[49] Frederik Nathan, Ivar Martin, and Gil Refael. Topological frequency conversion in weyl semimetals. *Physical Review Research*, 4:043060, Oct 2022. doi: 10.1103/PhysRevResearch.4.043060. URL https://link.aps.org/doi/10.1103/PhysRevResearch.4.043060.

[50] Christina Psaroudaki and Gil Refael. Photon pumping in a weakly-driven quantum cavity–spin system. *Annals of Physics*, 435:168553, 2021. ISSN 0003-4916. doi: https://doi.org/10.1016/j.aop.2021.168553. URL https://www.sciencedirect.com/science/article/pii/S0003491621001597. Special issue on Philip W. Anderson.

[51] Frederik Nathan, Ivar Martin, and Gil Refael. Topological frequency conversion in a driven dissipative quantum cavity. *Physical Review B*, 99:094311, Mar 2019. doi: 10.1103/PhysRevB.99.094311. URL https://link.aps.org/doi/10.1103/PhysRevB.99.094311.

[52] Carlton M. Caves. Quantum-mechanical noise in an interferometer. *Physical Review D*, 23:1693–1708, Apr 1981. doi: 10.1103/PhysRevD.23.1693. URL https://link.aps.org/doi/10.1103/PhysRevD.23.1693.

[53] Vittorio Giovannetti, Seth Lloyd, and Lorenzo Maccone. Quantum-enhanced measurements: Beating the standard quantum limit. *Science*, 306(5700):1330–1336, 2004. doi: 10.1126/science.1104149.

[54] Hugo Cable and Jonathan P. Dowling. Efficient generation of large number-path entanglement using only linear optics and feed-forward. *Physical Review Letters*, 99:163604, Oct 2007. doi: 10.1103/PhysRevLett.99.163604. URL https://link.aps.org/doi/10.1103/PhysRevLett.99.163604.

[55] Rafal Demkowicz-Dobrzański, Marcin Jarzyna, and Jan Kołodyński. Chapter four - quantum limits in optical interferometry. volume 60 of *Progress in Optics*, pages 345–435. Elsevier, 2015. doi: https://doi.org/10.1016/bs.po.2015.02.003. URL https://www.sciencedirect.com/science/article/pii/S0079663815000049.

[56] M. Brune, E. Hagley, J. Dreyer, X. Maitre, A. Maali, C. Wunderlich, J. M. Raimond, and S. Haroche. Observing the progressive decoherence of the "meter" in a quantum measurement. *Physical Review Letters*, 77:4887–4890, Dec 1996. doi: 10.1103/PhysRevLett.77.4887. URL https://link.aps.org/doi/10.1103/PhysRevLett.77.4887.

[57] Isaac L. Chuang, Debbie W. Leung, and Yoshihisa Yamamoto. Bosonic quantum codes for amplitude damping. *Physical Review A*, 56:1114–1125, Aug 1997. doi: 10.1103/PhysRevA.56.1114. URL https://link.aps.org/doi/10.1103/PhysRevA.56.1114.

[58] Brian Vlastakis, Gerhard Kirchmair, Zaki Leghtas, Simon E. Nigg, Luigi Frunzio, S. M. Girvin, Mazyar Mirrahimi, M. H. Devoret, and R. J. Schoelkopf. Deterministically encoding quantum information using 100-photon Schrödinger cat states. *Science*, 342(6158):607–610, 2013. ISSN 10959203. doi: 10.1126/science.1243289.

[59] Mazyar Mirrahimi, Zaki Leghtas, Victor V Albert, Steven Touzard, Robert J Schoelkopf, Liang Jiang, and Michel H Devoret. Dynamically protected cat-qubits: a new paradigm for universal quantum computation. *New Journal of Physics*, 16(4):045014, apr 2014. doi: 10.1088/1367-2630/16/4/045014. URL https://doi.org/10.1088/1367-2630/16/4/045014.

[60] Matthew Reagor, Wolfgang Pfaff, Christopher Axline, Reinier W. Heeres, Nissim Ofek, Katrina Sliwa, Eric Holland, Chen Wang, Jacob Blumoff, Kevin Chou, Michael J. Hatridge, Luigi Frunzio, Michel H. Devoret, Liang Jiang, and Robert J. Schoelkopf. Quantum memory with millisecond coherence in circuit qed. *Physical Review B*, 94:014506, Jul 2016. doi: 10.1103/PhysRevB.94.014506. URL https://link.aps.org/doi/10.1103/PhysRevB.94.014506.

[61] Z. Xiao, T. Fuse, S. Ashhab, F. Yoshihara, K. Semba, M. Sasaki, M. Takeoka, and J. P. Dowling. Fast amplification and rephasing of entangled cat states in a qubit-oscillator system. *Physical Review A*, 99:013827, Jan 2019. doi: 10.1103/PhysRevA.99.013827. URL https://link.aps.org/doi/10.1103/PhysRevA.99.013827.

[62] B M Terhal, J Conrad, and C Vuillot. Towards scalable bosonic quantum error correction. *Quantum Science and Technology*, 5(4):043001, jul 2020. doi: 10.1088/2058-9565/ab98a5. URL https://doi.org/10.1088/2058-9565/ab98a5.

[63] Wen-Long Ma, Shruti Puri, Robert J. Schoelkopf, Michel H. Devoret, S.M. Girvin, and Liang Jiang. Quantum control of bosonic modes with superconducting circuits. *Science Bulletin*, 66(17):1789–1805, 2021. ISSN 2095-9273. doi: https://doi.org/10.1016/j.scib.2021.05.024. URL https://www.sciencedirect.com/science/article/pii/S2095927321004011.

[64] P. J. D. Crowley, I. Martin, and A. Chandran. Half-integer quantized topological response in quasiperiodically driven quantum systems. *Physical Review Letters*, 125:100601, Aug 2020. doi: 10.1103/PhysRevLett.125.100601. URL https://link.aps.org/doi/10.1103/PhysRevLett.125.100601.

[65] Frederik Nathan, Rongchun Ge, Snir Gazit, Mark Rudner, and Michael Kolodrubetz. Quasiperiodic floquet-thouless energy pump. *Physical Review Letters*, 127:166804, Oct 2021. doi: 10.1103/PhysRevLett.127.166804. URL https://link.aps.org/doi/10.1103/PhysRevLett.127.166804.

[66] Bastien Lapierre, Titus Neupert, and Luka Trifunovic. Topologically localized insulators. *Physical Review Letters*, 129:256401, Dec 2022. doi: 10.1103/PhysRevLett.129.256401. URL https://link.aps.org/doi/10.1103/PhysRevLett.129.256401.

[67] P. W. Anderson. Absence of diffusion in certain random lattices. *Physical Review*, 109:1492–1505, Mar 1958. doi: 10.1103/PhysRev.109.1492. URL https://link.aps.org/doi/10.1103/PhysRev.109.1492.

[68] Elihu Abrahams. *50 Years of Anderson Localization*. World Scientific, 2010. ISBN 9789814360883. doi: 10.1142/7663. URL https://doi.org/10.1142/7663.

[69] D. M. Basko, I. L. Aleiner, and B. L. Altshuler. Metal-insulator transition in a weakly interacting many-electron system with localized single-particle states. *Annals of Physics (Amsterdam)*, 321(5):1126–1205, 2006. ISSN 00034916. doi: 10.1016/j.aop.2005.11.014.

[70] Vadim Oganesyan and David A. Huse. Localization of interacting fermions at high temperature. *Physical Review B*, 75:155111, Apr 2007. doi: 10.1103/PhysRevB.75.155111. URL https://link.aps.org/doi/10.1103/PhysRevB.75.155111.

[71] John Z Imbrie. On Many-Body Localization for Quantum Spin Chains. *Journal of Statistical Physics*, 163(5):998–1048, 2016. ISSN 1572-9613. doi: 10.1007/s10955-016-1508-x. URL https://doi.org/10.1007/s10955-016-1508-x.

[72] Jan Šuntajs, Janez Bonča, Toma ž Prosen, and Lev Vidmar. Quantum chaos challenges many-body localization. *Physical Review E*, 102:062144, Dec 2020. doi: 10.1103/PhysRevE.102.062144. URL https://link.aps.org/doi/10.1103/PhysRevE.102.062144.

[73] Dries Sels and Anatoli Polkovnikov. Dynamical obstruction to localization in a disordered spin chain. *Physical Review E*, 104:054105, Nov 2021. doi: 10.1103/PhysRevE.104.054105. URL https://link.aps.org/doi/10.1103/PhysRevE.104.054105.

[74] Dries Sels and Anatoli Polkovnikov. Thermalization of dilute impurities in one-dimensional spin chains. *Physical Review X*, 13:011041, Mar 2023. doi: 10.1103/PhysRevX.13.011041. URL https://link.aps.org/doi/10.1103/PhysRevX.13.011041.

[75] D. A. Abanin, J. H. Bardarson, G. De Tomasi, S. Gopalakrishnan, V. Khemani, S. A. Parameswaran, F. Pollmann, A. C. Potter, M. Serbyn, and R. Vasseur. Distinguishing localization from chaos: Challenges in finite-size systems. *Annals of Physics*, 427:168415, 2021. ISSN 1096035X. doi: 10.1016/j.aop.2021.168415. URL https://doi.org/10.1016/j.aop.2021.168415.

[76] Alan Morningstar, Luis Colmenarez, Vedika Khemani, David J. Luitz, and David A. Huse. Avalanches and many-body resonances in many-body localized systems. *Physical Review B*, 105:174205, May 2022. doi: 10.1103/PhysRevB.105.174205. URL https://link.aps.org/doi/10.1103/PhysRevB.105.174205.

[77] Dries Sels. Bath-induced delocalization in interacting disordered spin chains. *Physical Review B*, 106:L020202, Jul 2022. doi: 10.1103/PhysRevB.106.L020202. URL https://link.aps.org/doi/10.1103/PhysRevB.106.L020202.

[78] Wojciech De Roeck and François Huveneers. Stability and instability towards delocalization in many-body localization systems. *Physical Review B*, 95:155129, Apr 2017. doi: 10.1103/PhysRevB.95.155129. URL https://link.aps.org/doi/10.1103/PhysRevB.95.155129.

[79] Aditi Mitra. Quantum quench dynamics. *Annual Review of Condensed Matter Physics*, 9(1):245–259, 2018. doi: 10.1146/annurev-conmatphys-031016-025451. URL https://doi.org/10.1146/annurev-conmatphys-031016-025451.

[80] A. J. Sabbah and D. M. Riffe. Femtosecond pump-probe reflectivity study of silicon carrier dynamics. *Physical Review B*, 66:165217, Oct 2002. doi: 10.1103/PhysRevB.66.165217. URL https://link.aps.org/doi/10.1103/PhysRevB.66.165217.

[81] Gonzalo Usaj, P. M. Perez-Piskunow, L. E. F. Foa Torres, and C. A. Balseiro. Irradiated graphene as a tunable floquet topological insulator. *Physical Review B*, 90:115423, Sep 2014. doi: 10.1103/PhysRevB.90.115423. URL https://link.aps.org/doi/10.1103/PhysRevB.90.115423.

[82] H. L. Calvo, L. E. F. Foa Torres, P. M. Perez-Piskunow, C. A. Balseiro, and Gonzalo Usaj. Floquet interface states in illuminated three-dimensional topological insulators. *Phys. Rev. B*, 91:241404, Jun 2015. doi: 10.1103/PhysRevB.91.241404. URL https://link.aps.org/doi/10.1103/PhysRevB.91.241404.

[83] Martin C. Fischer, Jesse W. Wilson, Francisco E. Robles, and Warren S. Warren. Invited review article: Pump-probe microscopy. *Review of Scientific Instruments*, 87(3):031101, 2016. doi: 10.1063/1.4943211. URL https://aip.scitation.org/doi/abs/10.1063/1.4943211.

[84] Qingqing Cheng, Yiming Pan, Huaiqiang Wang, Chaoshi Zhang, Dong Yu, Avi Gover, Haijun Zhang, Tao Li, Lei Zhou, and Shining Zhu. Observation of anomalous π modes in photonic floquet engineering. *Physical Review Letters*, 122:173901, May 2019. doi: 10.1103/PhysRevLett.122.173901. URL https://link.aps.org/doi/10.1103/PhysRevLett.122.173901.

[85] J W McIver, B Schulte, F.-U. Stein, T Matsuyama, G Jotzu, G Meier, and A Cavalleri. Light-induced anomalous Hall effect in graphene. *Nature Physics*, 16(1):38–41, 2020. ISSN 1745-2481. doi: 10.1038/s41567-019-0698-y. URL https://doi.org/10.1038/s41567-019-0698-y.

[86] M Budden, T Gebert, M Buzzi, G Jotzu, E Wang, T Matsuyama, G Meier, Y Laplace, D Pontiroli, M Riccò, F Schlawin, D Jaksch, and A Cavalleri. Evidence for metastable photo-induced superconductivity in K3C60. *Nature Physics*, 17(5):611–618, 2021. ISSN 1745-2481. doi: 10.1038/s41567-020-01148-1. URL https://doi.org/10.1038/s41567-020-01148-1.

[87] Gaston Floquet. Sur les équations différentielles linéaires à coefficients périodiques. *Annales Scientifiques de l'École Normale Supérieure*, 12:47–88, 1883. URL http://eudml.org/doc/80895.

[88] André Eckardt and Egidijus Anisimovas. High-frequency approximation for periodically driven quantum systems from a Floquet-space perspective. *New Journal of Physics*, 17(9):093039, 2015. ISSN 13672630. doi: 10.1088/1367-2630/17/9/093039.

[89] Frederik Nathan and Mark S. Rudner. Topological singularities and the general classification of Floquet-Bloch systems. *New Journal of Physics*, 17(12):125014, 2015. ISSN 13672630. doi: 10.1088/1367-2630/17/12/125014. URL http://dx.doi.org/10.1088/1367-2630/17/12/125014.

[90] Rahul Roy and Fenner Harper. Periodic table for floquet topological insulators. *Physical Review B*, 96:155118, Oct 2017. doi: 10.1103/PhysRevB.96.155118. URL https://link.aps.org/doi/10.1103/PhysRevB.96.155118.

[91] David Emin and C. F. Hart. Existence of wannier-stark localization. *Physical Review B*, 36:7353–7359, Nov 1987. doi: 10.1103/PhysRevB.36.7353. URL https://link.aps.org/doi/10.1103/PhysRevB.36.7353.

[92] R Miller, T E Northup, K M Birnbaum, A Boca, A D Boozer, and H J Kimble. Trapped atoms in cavity QED: coupling quantized light and matter. *Journal of Physics B: Atomic, Molecular and Optical Physics*, 38(9):S551–S565, apr 2005. doi: 10.1088/0953-4075/38/9/007. URL https://doi.org/10.1088/0953-4075/38/9/007.

[93] Herbert Walther, Benjamin T H Varcoe, Berthold-Georg Englert, and Thomas Becker. Cavity quantum electrodynamics. *Reports on Progress in Physics*, 69 (5):1325–1382, apr 2006. doi: 10.1088/0034-4885/69/5/r02. URL https://doi.org/10.1088/0034-4885/69/5/r02.

[94] Alexandre Blais, Steven M Girvin, and William D Oliver. Quantum information processing and quantum optics with circuit quantum electrodynamics. *Nature Physics*, 16(3):247–256, 2020. ISSN 1745-2481. doi: 10.1038/s41567-020-0806-z. URL https://doi.org/10.1038/s41567-020-0806-z.

[95] Alexandre Blais, Arne L. Grimsmo, S. M. Girvin, and Andreas Wallraff. Circuit quantum electrodynamics. *Reviews of Modern Physics*, 93:025005, May 2021. doi: 10.1103/RevModPhys.93.025005. URL https://link.aps.org/doi/10.1103/RevModPhys.93.025005.

[96] Xiao-Liang Qi, Yong-Shi Wu, and Shou-Cheng Zhang. Topological quantization of the spin hall effect in two-dimensional paramagnetic semiconductors. *Physical Review B*, 74:085308, Aug 2006. doi: 10.1103/PhysRevB.74.085308. URL https://link.aps.org/doi/10.1103/PhysRevB.74.085308.

[97] B. Andrei Bernevig, Taylor L. Hughes, and Shou-Cheng Zhang. Quantum spin hall effect and topological phase transition in hgte quantum wells. *Science*, 314(5806):1757–1761, 2006. doi: 10.1126/science.1133734. URL https://www.science.org/doi/abs/10.1126/science.1133734.

[98] A. M. Bouchard and Marshall Luban. Bloch oscillations and other dynamical phenomena of electrons in semiconductor superlattices. *Physical Review B*, 52: 5105–5123, Aug 1995. doi: 10.1103/PhysRevB.52.5105. URL https://link.aps.org/doi/10.1103/PhysRevB.52.5105.

[99] M. Z. Hasan and C. L. Kane. Colloquium: Topological insulators. *Reviews of Modern Physics*, 82(4):3045–3067, 2010. ISSN 00346861. doi: 10.1103/RevModPhys.82.3045.

[100] Wolfgang M Schmidt. *Diophantine approximation.* Springer Science & Business Media, Berlin, 1996.

[101] Anton Frisk Kockum, Adam Miranowicz, Simone De Liberato, Salvatore Savasta, and Franco Nori. Ultrastrong coupling between light and matter.

Nature Reviews Physics, 1(1):19–40, 2019. ISSN 2522-5820. doi: 10.1038/s42254-018-0006-2. URL https://doi.org/10.1038/s42254-018-0006-2.

[102] Andreas Bayer, Marcel Pozimski, Simon Schambeck, Dieter Schuh, Rupert Huber, Dominique Bougeard, and Christoph Lange. Terahertz Light–Matter Interaction beyond Unity Coupling Strength. *Nano Letters*, 17(10):6340–6344, oct 2017. ISSN 1530-6984. doi: 10.1021/acs.nanoLetters7b03103. URL https://doi.org/10.1021/acs.nanoLetters7b03103.

[103] Fumiki Yoshihara, Tomoko Fuse, Sahel Ashhab, Kosuke Kakuyanagi, Shiro Saito, and Kouichi Semba. Superconducting qubit–oscillator circuit beyond the ultrastrong-coupling regime. *Nature Physics*, 13(1):44–47, 2017. ISSN 1745-2481. doi: 10.1038/nphys3906. URL https://doi.org/10.1038/nphys3906.

[104] N. K. Langford, R. Sagastizabal, M. Kounalakis, C. Dickel, A. Bruno, F. Luthi, D. J. Thoen, A. Endo, and L. Dicarlo. Experimentally simulating the dynamics of quantum light and matter at deep-strong coupling. *Nature Communications*, 8(1715):1715, 2017. ISSN 20411723. doi: 10.1038/s41467-017-01061-x. URL http://dx.doi.org/10.1038/s41467-017-01061-x.

[105] Wil Kao, Kuan-Yu Li, Kuan-Yu Lin, Sarang Gopalakrishnan, and Benjamin L. Lev. Topological pumping of a 1d dipolar gas into strongly correlated prethermal states. *Science*, 371(6526):296–300, 2021. doi: 10.1126/science.abb4928. URL https://www.science.org/doi/abs/10.1126/science.abb4928.

[106] Michael Victor Berry. Quantal phase factors accompanying adiabatic changes. *Proceedings of the Royal Society of London. A. Mathematical and Physical Sciences*, 392(1802):45–57, 1984. doi: 10.1098/rspa.1984.0023. URL https://royalsocietypublishing.org/doi/abs/10.1098/rspa.1984.0023.

[107] Frank Wilczek and A. Zee. Appearance of gauge structure in simple dynamical systems. *Physical Review Letters*, 52:2111–2114, Jun 1984. doi: 10.1103/PhysRevLett.52.2111. URL https://link.aps.org/doi/10.1103/PhysRevLett.52.2111.

[108] Hanhee Paik, D. I. Schuster, Lev S. Bishop, G. Kirchmair, G. Catelani, A. P. Sears, B. R. Johnson, M. J. Reagor, L. Frunzio, L. I. Glazman, S. M. Girvin, M. H. Devoret, and R. J. Schoelkopf. Observation of high coherence in josephson junction qubits measured in a three-dimensional circuit qed architecture. *Physical Review Letters*, 107:240501, Dec 2011. doi: 10.1103/PhysRevLett.107.240501. URL https://link.aps.org/doi/10.1103/PhysRevLett.107.240501.

[109] D. Zoepfl, P. R. Muppalla, C. M. F. Schneider, S. Kasemann, S. Partel, and G. Kirchmair. Characterization of low loss microstrip resonators as a building

block for circuit qed in a 3d waveguide. *AIP Advances*, 7(8):085118, 2017. doi: 10.1063/1.4992070. URL https://doi.org/10.1063/1.4992070.

[110] Srivatsan Chakram, Andrew E. Oriani, Ravi K. Naik, Akash V. Dixit, Kevin He, Ankur Agrawal, Hyeokshin Kwon, and David I. Schuster. Seamless high-q microwave cavities for multimode circuit quantum electrodynamics. *Physical Review Letters*, 127:107701, Aug 2021. doi: 10.1103/PhysRevLett.127.107701. URL https://link.aps.org/doi/10.1103/PhysRevLett.127.107701.

[111] Max Hofheinz, EM Weig, M Ansmann, Radoslaw C Bialczak, Erik Lucero, M Neeley, AD O'connell, H Wang, John M Martinis, and AN Cleland. Generation of fock states in a superconducting quantum circuit. *Nature*, 454(7202): 310–314, 2008. doi: 10.1038/nature07136.

[112] H. Wang, M. Hofheinz, M. Ansmann, R. C. Bialczak, E. Lucero, M. Neeley, A. D. O'Connell, D. Sank, J. Wenner, A. N. Cleland, and John M. Martinis. Measurement of the decay of fock states in a superconducting quantum circuit. *Physical Review Letters*, 101:240401, Dec 2008. doi: 10.1103/PhysRevLett.101.240401. URL https://link.aps.org/doi/10.1103/PhysRevLett.101.240401.

[113] Reinier W. Heeres, Brian Vlastakis, Eric Holland, Stefan Krastanov, Victor V. Albert, Luigi Frunzio, Liang Jiang, and Robert J. Schoelkopf. Cavity state manipulation using photon-number selective phase gates. *Physical Review Letters*, 115:137002, Sep 2015. doi: 10.1103/PhysRevLett.115.137002. URL https://link.aps.org/doi/10.1103/PhysRevLett.115.137002.

[114] André Eckardt. Colloquium: Atomic quantum gases in periodically driven optical lattices. *Reviews of Modern Physics*, 89:011004, Mar 2017. doi: 10.1103/RevModPhys.89.011004. URL https://link.aps.org/doi/10.1103/RevModPhys.89.011004.

[115] Christian Gross and Immanuel Bloch. Quantum simulations with ultracold atoms in optical lattices. *Science*, 357(6355):995–1001, 2017. doi: 10.1126/science.aal3837. URL https://www.science.org/doi/abs/10.1126/science.aal3837.

[116] Mark S Rudner and Netanel H Lindner. Band structure engineering and non-equilibrium dynamics in Floquet topological insulators. *Nature Reviews Physics*, 2(5):229–244, 2020. ISSN 2522-5820. doi: 10.1038/s42254-020-0170-z. URL https://doi.org/10.1038/s42254-020-0170-z.

[117] Takashi Oka and Hideo Aoki. Photovoltaic hall effect in graphene. *Physical Review B*, 79:081406(R), Feb 2009. doi: 10.1103/PhysRevB.79.081406. URL https://link.aps.org/doi/10.1103/PhysRevB.79.081406.

[118] Ankit S Disa, Tobia F Nova, and Andrea Cavalleri. Engineering crystal structures with light. *Nature Physics*, 17(10):1087–1092, 2021. ISSN 1745-2481. doi: 10.1038/s41567-021-01366-1. URL https://doi.org/10.1038/s41567-021-01366-1.

[119] Vedika Khemani, Achilleas Lazarides, Roderich Moessner, and S. L. Sondhi. Phase structure of driven quantum systems. *Physical Review Letters*, 116: 250401, Jun 2016. doi: 10.1103/PhysRevLett.116.250401. URL https://link.aps.org/doi/10.1103/PhysRevLett.116.250401.

[120] Dominic V. Else, Bela Bauer, and Chetan Nayak. Floquet time crystals. *Physical Review Letters*, 117:090402, Aug 2016. doi: 10.1103/PhysRevLett.117.090402. URL https://link.aps.org/doi/10.1103/PhysRevLett.117.090402.

[121] Vedika Khemani, Roderich Moessner, and S. L. Sondhi. A brief history of time crystals, 2019. URL https://arxiv.org/abs/1910.10745.

[122] Dominic V. Else, Christopher Monroe, Chetan Nayak, and Norman Y. Yao. Discrete time crystals. *Annual Review of Condensed Matter Physics*, 11(1): 467–499, 2020. doi: 10.1146/annurev-conmatphys-031119-050658. URL https://doi.org/10.1146/annurev-conmatphys-031119-050658.

[123] H. M. Blackburn, F. Marques, and J. M. Lopez. Symmetry breaking of two-dimensional time-periodic wakes. *Journal of Fluid Mechanics*, 522:395–411, 2005. doi: 10.1017/S0022112004002095.

[124] Netanel H Lindner, Gil Refael, and Victor Galitski. Floquet topological insulator in semiconductor quantum wells. *Nature Physics*, 7(6):490–495, 2011. ISSN 1745-2481. doi: 10.1038/nphys1926. URL https://doi.org/10.1038/nphys1926.

[125] Mikael C Rechtsman, Julia M Zeuner, Yonatan Plotnik, Yaakov Lumer, Daniel Podolsky, Felix Dreisow, Stefan Nolte, Mordechai Segev, and Alexander Szameit. Photonic floquet topological insulators. *Nature*, 496(7444):196–200, 2013.

[126] Frederik Nathan, Mark S. Rudner, Netanel H. Lindner, Erez Berg, and Gil Refael. Quantized magnetization density in periodically driven systems. *Physical Review Letters*, 119:186801, Oct 2017. doi: 10.1103/PhysRevLett.119.186801. URL https://link.aps.org/doi/10.1103/PhysRevLett.119.186801.

[127] Rahul Roy and Fenner Harper. Floquet topological phases with symmetry in all dimensions. *Physical Review B*, 95(19):33–41, 2017. ISSN 24699969. doi: 10.1103/PhysRevB.95.195128.

[128] Lukas J Maczewsky, Julia M Zeuner, Stefan Nolte, and Alexander Szameit. Observation of photonic anomalous Floquet topological insulators. *Nature Communications*, 8(1):13756, 2017. ISSN 2041-1723. doi: 10.1038/ncomms13756. URL https://doi.org/10.1038/ncomms13756.

[129] Linhu Li, Ching Hua Lee, and Jiangbin Gong. Realistic floquet semimetal with exotic topological linkages between arbitrarily many nodal loops. *Physical Review Letters*, 121:036401, Jul 2018. doi: 10.1103/PhysRevLett.121.036401. URL https://link.aps.org/doi/10.1103/PhysRevLett.121.036401.

[130] Thomas Schuster, Snir Gazit, Joel E. Moore, and Norman Y. Yao. Floquet hopf insulators. *Physical Review Letters*, 123:266803, Dec 2019. doi: 10.1103/PhysRevLett.123.266803. URL https://link.aps.org/doi/10.1103/PhysRevLett.123.266803.

[131] Karen Wintersperger, Christoph Braun, F Nur Ünal, André Eckardt, Marco Di Liberto, Nathan Goldman, Immanuel Bloch, and Monika Aidelsburger. Realization of an anomalous Floquet topological system with ultracold atoms. *Nature Physics*, 16(10):1058–1063, 2020. ISSN 1745-2481. doi: 10.1038/s41567-020-0949-y. URL https://doi.org/10.1038/s41567-020-0949-y.

[132] R. B. Laughlin. Quantized hall conductivity in two dimensions. *Physical Review B*, 23:5632–5633, May 1981. doi: 10.1103/PhysRevB.23.5632. URL https://link.aps.org/doi/10.1103/PhysRevB.23.5632.

[133] S. L. Sondhi and Kun Yang. Sliding phases via magnetic fields. *Physical Review B*, 63:054430, Jan 2001. doi: 10.1103/PhysRevB.63.054430. URL https://link.aps.org/doi/10.1103/PhysRevB.63.054430.

[134] C. L. Kane, Ranjan Mukhopadhyay, and T. C. Lubensky. Fractional quantum hall effect in an array of quantum wires. *Physical Review Letters*, 88:036401, Jan 2002. doi: 10.1103/PhysRevLett.88.036401. URL https://link.aps.org/doi/10.1103/PhysRevLett.88.036401.

[135] Michael Lohse, Christian Schweizer, Hannah M. Price, Oded Zilberberg, and Immanuel Bloch. Exploring 4D quantum Hall physics with a 2D topological charge pump. *Nature (London)*, 553(7686):55–58, 2018. ISSN 14764687. doi: 10.1038/nature25000.

[136] Michael Kolodrubetz, Dries Sels, Pankaj Mehta, and Anatoli Polkovnikov. Geometry and non-adiabatic response in quantum and classical systems. *Physics Reports*, 697:1–87, 2017. ISSN 0370-1573. doi: https://doi.org/10.1016/j.physrep.2017.07.001. URL https://www.sciencedirect.com/science/article/pii/S0370157317301989.

[137] W. P. Su, J. R. Schrieffer, and A. J. Heeger. Solitons in polyacetylene. *Physical Review Letters*, 42:1698–1701, Jun 1979. doi: 10.1103/PhysRevLett.42.1698. URL https://link.aps.org/doi/10.1103/PhysRevLett.42.1698.

[138] P. C. Hohenberg and B. I. Halperin. Theory of dynamic critical phenomena. *Reviews of Modern Physics*, 49:435–479, Jul 1977. doi: 10.1103/RevModPhys.49.435. URL https://link.aps.org/doi/10.1103/RevModPhys.49.435.

[139] D. E. Khmel'nitskii. Quantization of hall conductivity. *Pis' ma Zh. Eksp. Teor. Fiz.*, 38:454, Nov 1983. URL http://jetpletters.ru/ps/1485/article_22668.shtml.

[140] Herbert Levine, Stephen B. Libby, and Adrianus M. M. Pruisken. Electron delocalization by a magnetic field in two dimensions. *Physical Review Letters*, 51:1915–1918, Nov 1983. doi: 10.1103/PhysRevLett.51.1915. URL https://link.aps.org/doi/10.1103/PhysRevLett.51.1915.

[141] R. B. Laughlin. Levitation of extended-state bands in a strong magnetic field. *Physical Review Letters*, 52:2304–2304, Jun 1984. doi: 10.1103/PhysRevLett.52.2304. URL https://link.aps.org/doi/10.1103/PhysRevLett.52.2304.

[142] Dung-Hai Lee, Steven Kivelson, and Shou-Cheng Zhang. Quasiparticle charge and the activated conductance of a quantum hall liquid. *Physical Review Letters*, 68:2386–2389, Apr 1992. doi: 10.1103/PhysRevLett.68.2386. URL https://link.aps.org/doi/10.1103/PhysRevLett.68.2386.

[143] Steven Kivelson, Dung-Hai Lee, and Shou-Cheng Zhang. Global phase diagram in the quantum hall effect. *Physical Review B*, 46:2223–2238, Jul 1992. doi: 10.1103/PhysRevB.46.2223. URL https://link.aps.org/doi/10.1103/PhysRevB.46.2223.

[144] J T Chalker and P D Coddington. Percolation, quantum tunnelling and the integer hall effect. *Journal of Physics C: Solid State Physics*, 21(14):2665–2679, May 1988. doi: 10.1088/0022-3719/21/14/008. URL https://doi.org/10.1088/0022-3719/21/14/008.

[145] Keith Slevin and Tomi Ohtsuki. Critical exponent for the quantum hall transition. *Physical Review B*, 80:041304(R), Jul 2009. doi: 10.1103/PhysRevB.80.041304. URL https://link.aps.org/doi/10.1103/PhysRevB.80.041304.

[146] Martin Puschmann, Philipp Cain, Michael Schreiber, and Thomas Vojta. Integer quantum hall transition on a tight-binding lattice. *Physical Review B*, 99:121301(R), Mar 2019. doi: 10.1103/PhysRevB.99.121301. URL https://link.aps.org/doi/10.1103/PhysRevB.99.121301.

[147] Ruben Verresen. Topology and edge states survive quantum criticality between topological insulators, 2020. URL https://arxiv.org/abs/2003.05453.

[148] Oleksandr Balabanov, Carlos Ortega-Taberner, and Maria Hermanns. Quantization of topological indices in critical chains at low temperatures. *Physical Review B*, 106:045116, Jul 2022. doi: 10.1103/PhysRevB.106.045116. URL https://link.aps.org/doi/10.1103/PhysRevB.106.045116.

[149] Bo Fu, Jin-Yu Zou, Zi-Ang Hu, Huan-Wen Wang, and Shun-Qing Shen. Quantum anomalous semimetals, 2022. URL https://arxiv.org/abs/2203.00933.

[150] David A. Huse, Rahul Nandkishore, Vadim Oganesyan, Arijeet Pal, and S. L. Sondhi. Localization-protected quantum order. *Physical Review B*, 88:014206, Jul 2013. doi: 10.1103/PhysRevB.88.014206. URL https://link.aps.org/doi/10.1103/PhysRevB.88.014206.

[151] M. Schulz, S. R. Taylor, A. Scardicchio, and M. Žnidarič. Phenomenology of anomalous transport in disordered one-dimensional systems. *Journal of Statistical Mechanics: Theory and Experiment*, 2020(2), 2020. ISSN 17425468. doi: 10.1088/1742-5468/ab6de0.

[152] Scott R. Taylor and Antonello Scardicchio. Subdiffusion in a one-dimensional anderson insulator with random dephasing: Finite-size scaling, griffiths effects, and possible implications for many-body localization. *Physical Review B*, 103:184202, May 2021. doi: 10.1103/PhysRevB.103.184202. URL https://link.aps.org/doi/10.1103/PhysRevB.103.184202.

[153] Piotr Sierant and Jakub Zakrzewski. Challenges to observation of many-body localization. *Physical Review B*, 105:224203, Jun 2022. doi: 10.1103/PhysRevB.105.224203. URL https://link.aps.org/doi/10.1103/PhysRevB.105.224203.

[154] Takashi Mori, Tatsuhiko N Ikeda, Eriko Kaminishi, and Masahito Ueda. Thermalization and prethermalization in isolated quantum systems: a theoretical overview. *Journal of Physics B: Atomic, Molecular and Optical Physics*, 51(11):112001, may 2018. doi: 10.1088/1361-6455/aabcdf. URL https://doi.org/10.1088/1361-6455/aabcdf.

[155] Jens H. Bardarson, Frank Pollmann, and Joel E. Moore. Unbounded growth of entanglement in models of many-body localization. *Physical Review Letters*, 109:017202, Jul 2012. doi: 10.1103/PhysRevLett.109.017202. URL https://link.aps.org/doi/10.1103/PhysRevLett.109.017202.

[156] Maksym Serbyn, Z. Papić, and Dmitry A. Abanin. Local conservation laws and the structure of the many-body localized states. *Physical Review Letters*, 111:127201, Sep 2013. doi: 10.1103/PhysRevLett.111.127201. URL https://link.aps.org/doi/10.1103/PhysRevLett.111.127201.

[157] David A. Huse, Rahul Nandkishore, and Vadim Oganesyan. Phenomenology of fully many-body-localized systems. *Physical Review B*, 90:174202, Nov 2014. doi: 10.1103/PhysRevB.90.174202. URL https://link.aps.org/doi/10.1103/PhysRevB.90.174202.

[158] Jeffrey C. Y. Teo and C. L. Kane. Topological defects and gapless modes in insulators and superconductors. *Physical Review B*, 82:115120, Sep 2010. doi: 10.1103/PhysRevB.82.115120. URL https://link.aps.org/doi/10.1103/PhysRevB.82.115120.

[159] Mikio Nakahara. *Geometry, Topology and Physics.* IOP Publishing, Philadelphia, 2 edition, 2003.

[160] Shunyu Yao, Zhongbo Yan, and Zhong Wang. Topological invariants of floquet systems: General formulation, special properties, and floquet topological defects. *Physical Review B*, 96:195303, Nov 2017. doi: 10.1103/PhysRevB.96.195303. URL https://link.aps.org/doi/10.1103/PhysRevB.96.195303.

[161] Alexei Kitaev. Periodic table for topological insulators and superconductors. *AIP Conf. Proc.*, 1134(May 2009):22–30, 2009. ISSN 0094243X. doi: 10.1063/1.3149495.

[162] Tosio Kato. *Perturbation Theory for Linear Operators*. Springer-Verlag Berlin Heidelberg, 2 edition, 1980. doi: 10.1007/978-3-642-66282-9.

[163] F. D. M. Haldane. Model for a quantum hall effect without landau levels: Condensed-matter realization of the "parity anomaly". *Physical Review Letters*, 61:2015–2018, Oct 1988. doi: 10.1103/PhysRevLett.61.2015. URL https://link.aps.org/doi/10.1103/PhysRevLett.61.2015.

[164] Daniel S. Fisher. Critical behavior of random transverse-field ising spin chains. *Physical Review B*, 51:6411–6461, Mar 1995. doi: 10.1103/PhysRevB.51.6411. URL https://link.aps.org/doi/10.1103/PhysRevB.51.6411.

[165] Daniel S. Fisher. Phase transitions and singularities in random quantum systems. *Physica A: Statistical Mechanics and its Applications*, 263(1):222–233, 1999. ISSN 0378-4371. doi: https://doi.org/10.1016/S0378-4371(98)00498-1. URL https://www.sciencedirect.com/science/article/pii/S0378437198004981. Proceedings of the 20th IUPAP International Conference on Statistical Physics.

[166] Gil Refael and Ehud Altman. Strong disorder renormalization group primer and the superfluid–insulator transition. *Comptes Rendus Physique*, 14(8):725–739, 2013. ISSN 1631-0705. doi: https://doi.org/10.1016/j.crhy.2013.09.005. URL https://www.sciencedirect.com/science/article/pii/S1631070513001382.

[167] Sarang Gopalakrishnan, Markus Müller, Vedika Khemani, Michael Knap, Eugene Demler, and David A. Huse. Low-frequency conductivity in many-body localized systems. *Physical Review B*, 92:104202, Sep 2015. doi: 10.1103/PhysRevB.92.104202. URL https://link.aps.org/doi/10.1103/PhysRevB.92.104202.

[168] Vedika Khemani, S. P. Lim, D. N. Sheng, and David A. Huse. Critical properties of the many-body localization transition. *Physical Review X*, 7:021013, Apr 2017. doi: 10.1103/PhysRevX.7.021013. URL https://link.aps.org/doi/10.1103/PhysRevX.7.021013.

[169] Benjamin Villalonga and Bryan K. Clark. Eigenstates hybridize on all length scales at the many-body localization transition. *arXiv:2005.13558*, 2020. URL https://arxiv.org/abs/2005.13558.

[170] Philip J D Crowley and Anushya Chandran. A constructive theory of the numerically accessible many-body localized to thermal crossover. *SciPost Phys.*, 12:201, 2022. doi: 10.21468/SciPostPhys.12.6.201. URL https://scipost.org/10.21468/SciPostPhys.12.6.201.

[171] S. J. Garratt, Sthitadhi Roy, and J. T. Chalker. Local resonances and parametric level dynamics in the many-body localized phase. *Physical Review B*, 104:184203, Nov 2021. doi: 10.1103/PhysRevB.104.184203. URL https://link.aps.org/doi/10.1103/PhysRevB.104.184203.

[172] Samuel J. Garratt and Sthitadhi Roy. Resonant energy scales and local observables in the many-body localized phase. *Physical Review B*, 106:054309, Aug 2022. doi: 10.1103/PhysRevB.106.054309. URL https://link.aps.org/doi/10.1103/PhysRevB.106.054309.

[173] David M. Long, Philip J. D. Crowley, Vedika Khemani, and Anushya Chandran. Phenomenology of the prethermal many-body localized regime, 2022. URL https://arxiv.org/abs/2207.05761.

[174] Morten Kjaergaard, Mollie E. Schwartz, Jochen Braum uller, Philip Krantz, Joel I.-J. Wang, Simon Gustavsson, and William D. Oliver. Superconducting qubits: Current state of play. *Annual Review of Condensed Matter Physics*, 11(1):369–395, 2020. doi: 10.1146/annurev-conmatphys-031119-050605. URL https://doi.org/10.1146/annurev-conmatphys-031119-050605.

[175] D. Leibfried, R. Blatt, C. Monroe, and D. Wineland. Quantum dynamics of single trapped ions. *Reviews of Modern Physics*, 75:281–324, Mar 2003. doi: 10.1103/RevModPhys.75.281. URL https://link.aps.org/doi/10.1103/RevModPhys.75.281.

[176] Marcus W Doherty, Neil B Manson, Paul Delaney, Fedor Jelezko, Jörg Wrachtrup, and Lloyd CL Hollenberg. The nitrogen-vacancy colour centre in diamond. *Physics Reports*, 528(1):1–45, 2013. URL https://doi.org/10.1016/j.physrep.2013.02.001.

[177] Oded Zilberberg, Sheng Huang, Jonathan Guglielmon, Mohan Wang, Kevin P. Chen, Yaacov E. Kraus, and Mikael C. Rechtsman. Photonic topological boundary pumping as a probe of 4D quantum Hall physics. *Nature (London)*, 553 (7686):59–62, 2018. ISSN 14764687. doi: 10.1038/nature25011.

[178] Martin Rodriguez-Vega, Michael Vogl, and Gregory A. Fiete. Low-frequency and Moiré–Floquet engineering: A review. *Annals of Physics*, (xxxx):168434, 2021. ISSN 1096035X. doi: 10.1016/j.aop.2021.168434. URL https://doi.org/10.1016/j.aop.2021.168434.

[179] Hoi Chun Po, Lukasz Fidkowski, Takahiro Morimoto, Andrew C. Potter, and Ashvin Vishwanath. Chiral floquet phases of many-body localized bosons. *Physical Review X*, 6:041070, Dec 2016. doi: 10.1103/PhysRevX.6.041070. URL https://link.aps.org/doi/10.1103/PhysRevX.6.041070.

[180] Frank Wilczek. Quantum time crystals. *Physical Review Letters*, 109:160401, Oct 2012. doi: 10.1103/PhysRevLett.109.160401. URL https://link.aps.org/doi/10.1103/PhysRevLett.109.160401.

[181] J Zhang, P W Hess, A Kyprianidis, P Becker, A Lee, J Smith, G Pagano, I.-D. Potirniche, A C Potter, A Vishwanath, N Y Yao, and C Monroe. Observation of a discrete time crystal. *Nature*, 543(7644):217–220, 2017. ISSN 1476-4687. doi: 10.1038/nature21413. URL https://doi.org/10.1038/nature21413.

[182] Soonwon Choi, Joonhee Choi, Renate Landig, Georg Kucsko, Hengyun Zhou, Junichi Isoya, Fedor Jelezko, Shinobu Onoda, Hitoshi Sumiya, Vedika Khemani, Curt von Keyserlingk, Norman Y Yao, Eugene Demler, and Mikhail D Lukin. Observation of discrete time-crystalline order in a disordered dipolar many-body system. *Nature*, 543(7644):221–225, 2017. ISSN 1476-4687. doi: 10.1038/nature21426. URL https://doi.org/10.1038/nature21426.

[183] Xiao Mi et al. Time-crystalline eigenstate order on a quantum processor. *Nature*, 601(7894):531–536, 2022. ISSN 1476-4687. doi: 10.1038/s41586-021-04257-w. URL https://doi.org/10.1038/s41586-021-04257-w.

[184] Yu-Gui Peng, Cheng-Zhi Qin, De-Gang Zhao, Ya-Xi Shen, Xiang-Yuan Xu, Ming Bao, Han Jia, and Xue-Feng Zhu. Experimental demonstration of anomalous Floquet topological insulator for sound. *Nature Communications*, 7(1): 13368, 2016. ISSN 2041-1723. doi: 10.1038/ncomms13368. URL https://doi.org/10.1038/ncomms13368.

[185] Hongzheng Zhao, Florian Mintert, Roderich Moessner, and Johannes Knolle. Random multipolar driving: Tunably slow heating through spectral engineering. *Physical Review Letters*, 126:040601, Jan 2021. doi: 10.1103/PhysRevLett.126.040601. URL https://link.aps.org/doi/10.1103/PhysRevLett.126.040601.

[186] Feng Mei, Zheng-Yuan Xue, Dan-Wei Zhang, Lin Tian, Chaohong Lee, and Shi-Liang Zhu. Witnessing topological weyl semimetal phase in a minimal circuit-QED lattice. *Quantum Science and Technology*, 1(1):015006, nov 2016. doi: 10.1088/2058-9565/1/1/015006. URL https://doi.org/10.1088/2058-9565/1/1/015006.

[187] Sourav Nandy, Arnab Sen, and Diptiman Sen. Aperiodically driven integrable systems and their emergent steady states. *Physical Review X*, 7:031034, Aug 2017. doi: 10.1103/PhysRevX.7.031034. URL https://link.aps.org/doi/10.1103/PhysRevX.7.031034.

[188] Qian Lin, Xiao Qi Sun, Meng Xiao, Shou Cheng Zhang, and Shanhui Fan. A three-dimensional photonic topological insulator using a two-dimensional ring resonator lattice with a synthetic frequency dimension. *Science Advances*, 4 (10):eaat2774, 2018. ISSN 23752548. doi: 10.1126/sciadv.aat2774.

[189] Ioannis Petrides, Hannah M. Price, and Oded Zilberberg. Six-dimensional quantum hall effect and three-dimensional topological pumps. *Physical Review B*, 98:125431, Sep 2018. doi: 10.1103/PhysRevB.98.125431. URL https://link.aps.org/doi/10.1103/PhysRevB.98.125431.

[190] Tomoki Ozawa and Hannah M Price. Topological quantum matter in synthetic dimensions. *Nature Reviews Physics*, 1(5):349–357, 2019. URL https://doi.org/10.1038/s42254-019-0045-3.

[191] Hongzheng Zhao, Florian Mintert, and Johannes Knolle. Floquet time spirals and stable discrete-time quasicrystals in quasiperiodically driven quantum many-body systems. *Physical Review B*, 100:134302, Oct 2019. doi: 10.1103/PhysRevB.100.134302. URL https://link.aps.org/doi/10.1103/PhysRevB.100.134302.

[192] Eran Lustig, Steffen Weimann, Yonatan Plotnik, Yaakov Lumer, Miguel A. Bandres, Alexander Szameit, and Mordechai Segev. Photonic Topological Insulator in Synthetic Dimensions. *Nature*, 2018. ISSN 1476-4687. doi: 10.1038/s41586-019-0943-7. URL http://arxiv.org/abs/1807.01983.

[193] Avik Dutt, Qian Lin, Luqi Yuan, Momchil Minkov, Meng Xiao, and Shanhui Fan. A single photonic cavity with two independent physical synthetic dimensions. *Science*, 367(6473):59–64, 2020. ISSN 10959203. doi: 10.1126/science.aaz3071.

[194] Arijeet Pal and David A. Huse. Many-body localization phase transition. *Physical Review B*, 82:174411, Nov 2010. doi: 10.1103/PhysRevB.82.174411. URL https://link.aps.org/doi/10.1103/PhysRevB.82.174411.

[195] Pedro Ponte, Z. Papić, François Huveneers, and Dmitry A. Abanin. Many-body localization in periodically driven systems. *Physical Review Letters*, 114:140401, Apr 2015. doi: 10.1103/PhysRevLett.114.140401. URL https://link.aps.org/doi/10.1103/PhysRevLett.114.140401.

[196] Achilleas Lazarides, Arnab Das, and Roderich Moessner. Fate of many-body localization under periodic driving. *Physical Review Letters*, 115:030402, Jul 2015. doi: 10.1103/PhysRevLett.115.030402. URL https://link.aps.org/doi/10.1103/PhysRevLett.115.030402.

[197] Michael Schreiber, Sean S. Hodgman, Pranjal Bordia, Henrik P. Lüschen, Mark H. Fischer, Ronen Vosk, Ehud Altman, Ulrich Schneider, and Immanuel Bloch. Observation of many-body localization of interacting fermions in a quasirandom optical lattice. *Science*, 349(6250):842–845, 2015. ISSN 10959203. doi: 10.1126/science.aaa7432.

[198] J Smith, A Lee, P Richerme, B Neyenhuis, P W Hess, P Hauke, M Heyl, D A Huse, and C Monroe. Many-body localization in a quantum simulator with programmable random disorder. *Nature Physics*, 12(10):907–911, 2016. ISSN 1745-2481. doi: 10.1038/nphys3783. URL https://doi.org/10.1038/nphys3783.

[199] Pranjal Bordia, Henrik Lüschen, Ulrich Schneider, Michael Knap, and Immanuel Bloch. Periodically driving a many-body localized quantum system. *Nature Physics*, 13(5):460–464, 2017. ISSN 1745-2481. doi: 10.1038/nphys4020. URL https://doi.org/10.1038/nphys4020.

[200] Julian Léonard, Matthew Rispoli, Alexander Lukin, Robert Schittko, Sooshin Kim, Joyce Kwan, Dries Sels, Eugene Demler, and Markus Greiner. Signatures of bath-induced quantum avalanches in a many-body–localized system. *arXiv:2012.15270*, 2020. URL https://arxiv.org/abs/2012.15270.

[201] Vadim Oganesyan, Arijeet Pal, and David A. Huse. Energy transport in disordered classical spin chains. *Physical Review B*, 80:115104, Sep 2009. doi: 10.1103/PhysRevB.80.115104. URL https://link.aps.org/doi/10.1103/PhysRevB.80.115104.

[202] D.M. Basko. Weak chaos in the disordered nonlinear schrödinger chain: Destruction of anderson localization by arnold diffusion. *Annals of Physics*, 326(7):1577–1655, 2011. ISSN 0003-4916. doi: https://doi.org/10.1016/j.aop.2011.02.004. URL https://www.sciencedirect.com/science/article/pii/S0003491611000339. July 2011 Special Issue.

[203] R. V. Jensen and R. Shankar. Statistical behavior in deterministic quantum systems with few degrees of freedom. *Physical Review Letters*, 54:1879–1882, Apr 1985. doi: 10.1103/PhysRevLett.54.1879. URL https://link.aps.org/doi/10.1103/PhysRevLett.54.1879.

[204] J. M. Deutsch. Quantum statistical mechanics in a closed system. *Physical Review A*, 43:2046–2049, Feb 1991. doi: 10.1103/PhysRevA.43.2046. URL https://link.aps.org/doi/10.1103/PhysRevA.43.2046.

[205] Mark Srednicki. Chaos and quantum thermalization. *Physical Review E*, 50:888–901, Aug 1994. doi: 10.1103/PhysRevE.50.888. URL https://link.aps.org/doi/10.1103/PhysRevE.50.888.

[206] Marcos Rigol, Vanja Dunjko, and Maxim Olshanii. Thermalization and its mechanism for generic isolated quantum systems. *Nature*, 452(7189):854–858, 2008. ISSN 1476-4687. doi: 10.1038/nature06838. URL https://doi.org/10.1038/nature06838.

[207] Luca D'Alessio, Yariv Kafri, Anatoli Polkovnikov, and Marcos Rigol. From quantum chaos and eigenstate thermalization to statistical mechanics and thermodynamics. *Advances in Physics*, 65(3):239–362, 2016. ISSN 14606976. doi: 10.1080/00018732.2016.1198134. URL https://doi.org/10.1080/00018732.2016.1198134.

[208] Jon H. Shirley. Solution of the schrödinger equation with a hamiltonian periodic in time. *Physical Review*, 138:B979–B987, May 1965. doi: 10.1103/PhysRev.138.B979. URL https://link.aps.org/doi/10.1103/PhysRev.138.B979.

[209] Nathan Wiebe, Dominic Berry, Peter Høyer, and Barry C Sanders. Higher order decompositions of ordered operator exponentials. *Journal of Physics A*, 43(6):065203, 2010. URL https://doi.org/10.1088/1751-8113/43/6/065203.

[210] Antonello Scardicchio and Thimothée Thiery. Perturbation theory approaches to anderson and many-body localization: some lecture notes. *arXiv:1710.01234*, 2017. URL https://arxiv.org/abs/1710.01234.

[211] Tyler LeBlond, Krishnanand Mallayya, Lev Vidmar, and Marcos Rigol. Entanglement and matrix elements of observables in interacting integrable systems. *Physical Review E*, 100:062134, Dec 2019. doi: 10.1103/PhysRevE.100.062134. URL https://link.aps.org/doi/10.1103/PhysRevE.100.062134.

[212] Philip J. D. Crowley and Anushya Chandran. Partial thermalisation of a two-state system coupled to a finite quantum bath. *SciPost Physics*, 12:103, 2022. doi: 10.21468/SciPostPhys.12.3.103. URL https://scipost.org/10.21468/SciPostPhys.12.3.103.

[213] Dmitry A. Abanin, Wojciech De Roeck, and François Huveneers. Theory of many-body localization in periodically driven systems. *Annals of Physics*, 372: 1–11, 2016. ISSN 1096035X. doi: 10.1016/j.aop.2016.03.010. URL http://dx.doi.org/10.1016/j.aop.2016.03.010.

[214] Wolfgang M Schmidt. Norm form equations. *Annals of Mathematics*, 96(3): 526–551, 1972.

[215] Tom C. Brown. Descriptions of the characteristic sequence of an irrational. *Canadian Mathematical Bulletin*, 36(1):15–21, 1993. doi: 10.4153/CMB-1993-003-6.

[216] M. Lothaire. *Algebraic Combinatorics on Words*. Encyclopedia of Mathematics and its Applications. Cambridge University Press, 2002. doi: 10.1017/CBO9781107326019.

[217] D J Thouless. Localization distance and mean free path in one-dimensional disordered systems. *Journal of Physics C: Solid State Physics*, 6(3):L49–L51, feb 1973. doi: 10.1088/0022-3719/6/3/002. URL https://doi.org/10.1088/0022-3719/6/3/002.

[218] Serge Aubry and Gilles André. Analyticity breaking and anderson localization in incommensurate lattices. *Annals of the Israel Physical Society*, 3:133, 1980.

[219] P. G. Harper. Single band motion of conduction electrons in a uniform magnetic field. *Proceedings of the Physical Society. Section A*, 68(10):874–878, oct 1955. doi: 10.1088/0370-1298/68/10/304. URL https://doi.org/10.1088/0370-1298/68/10/304.

[220] Hisashi Hiramoto and Mahito Kohmoto. Electronic spectral and wavefunction properties of one-dimensional quasiperiodic systems: a scaling approach. *International Journal of Modern Physics B*, 06(03n04):281–320, 1992. doi: 10.1142/S0217979292000153. URL https://doi.org/10.1142/S0217979292000153.

[221] J. H. Han, D. J. Thouless, H. Hiramoto, and M. Kohmoto. Critical and bicritical properties of harper's equation with next-nearest-neighbor coupling. *Physical Review B*, 50:11365–11380, Oct 1994. doi: 10.1103/PhysRevB.50.11365. URL https://link.aps.org/doi/10.1103/PhysRevB.50.11365.

[222] Sarang Gopalakrishnan. Self-dual quasiperiodic systems with power-law hopping. *Physical Review B*, 96:054202, Aug 2017. doi: 10.1103/PhysRevB.96.054202. URL https://link.aps.org/doi/10.1103/PhysRevB.96.054202.

[223] A. Chandran and C. R. Laumann. Localization and symmetry breaking in the quantum quasiperiodic ising glass. *Physical Review X*, 7:031061, Sep

2017. doi: 10.1103/PhysRevX.7.031061. URL https://link.aps.org/doi/10.1103/PhysRevX.7.031061.

[224] P J D Crowley, C R Laumann, and A Chandran. Critical behaviour of the quasi-periodic quantum ising chain. *Journal of Statistical Mechanics: Theory and Experiment*, 2022(8):083102, aug 2022. doi: 10.1088/1742-5468/ac815d. URL https://dx.doi.org/10.1088/1742-5468/ac815d.

[225] Hirotsugu Matsuda and Kazushige Ishii. Localization of Normal Modes and Energy Transport in the Disordered Harmonic Chain. *Progress of Theoretical Physics Supplement*, 45:56–86, 05 1970. ISSN 0375-9687. doi: 10.1143/PTPS.45.56. URL https://doi.org/10.1143/PTPS.45.56.

[226] D. J. Thouless. Electrons in disordered systems and the theory of localization. *Physics Reports*, 13(3):93–142, 1974. ISSN 03701573. doi: 10.1016/0370-1573(74)90029-5.

[227] Karlheinz Geist, Ulrich Parlitz, and Werner Lauterborn. Comparison of Different Methods for Computing Lyapunov Exponents. *Progress of Theoretical Physics*, 83(5):875–893, 05 1990. ISSN 0033-068X. doi: 10.1143/PTP.83.875. URL https://doi.org/10.1143/PTP.83.875.

[228] E. Abrahams, P. W. Anderson, D. C. Licciardello, and T. V. Ramakrishnan. Scaling theory of localization: Absence of quantum diffusion in two dimensions. *Physical Review Letters*, 42:673–676, Mar 1979. doi: 10.1103/PhysRevLett.42.673. URL https://link.aps.org/doi/10.1103/PhysRevLett.42.673.

[229] Shinobu Hikami, Anatoly I. Larkin, and Yosuke Nagaoka. Spin-Orbit Interaction and Magnetoresistance in the Two Dimensional Random System. *Progress of Theoretical Physics*, 63(2):707–710, 02 1980. ISSN 0033-068X. doi: 10.1143/PTP.63.707. URL https://doi.org/10.1143/PTP.63.707.

[230] B. L. Altshuler, D. Khmel'nitzkii, A. I. Larkin, and P. A. Lee. Magnetoresistance and hall effect in a disordered two-dimensional electron gas. *Physical Review B*, 22:5142–5153, Dec 1980. doi: 10.1103/PhysRevB.22.5142. URL https://link.aps.org/doi/10.1103/PhysRevB.22.5142.

[231] V. K. Varma, A. Raj, S. Gopalakrishnan, V. Oganesyan, and D. Pekker. Length scales in the many-body localized phase and their spectral signatures. *Physical Review B*, 100:115136, Sep 2019. doi: 10.1103/PhysRevB.100.115136. URL https://link.aps.org/doi/10.1103/PhysRevB.100.115136.

[232] G. Kucsko, S. Choi, J. Choi, P. C. Maurer, H. Zhou, R. Landig, H. Sumiya, S. Onoda, J. Isoya, F. Jelezko, E. Demler, N. Y. Yao, and M. D. Lukin. Critical thermalization of a disordered dipolar spin system in diamond. *Physical Review*

Letters, 121:023601, Jul 2018. doi: 10.1103/PhysRevLett.121.023601. URL https://link.aps.org/doi/10.1103/PhysRevLett.121.023601.

[233] L.S. Levitov. Critical hamiltonians with long range hopping. *Annalen der Physik*, 8(7-9):697–706, 1999. doi: https://doi.org/10.1002/(SICI)1521-3889(199911)8:7/9<697::AID-ANDP697>3.0.CO;2-W.

[234] Shankar Iyer, Vadim Oganesyan, Gil Refael, and David A. Huse. Many-body localization in a quasiperiodic system. *Physical Review B*, 87:134202, Apr 2013. doi: 10.1103/PhysRevB.87.134202. URL https://link.aps.org/doi/10.1103/PhysRevB.87.134202.

[235] Henrik P. Lüschen, Pranjal Bordia, Sebastian Scherg, Fabien Alet, Ehud Altman, Ulrich Schneider, and Immanuel Bloch. Observation of slow dynamics near the many-body localization transition in one-dimensional quasiperiodic systems. *Physical Review Letters*, 119:260401, Dec 2017. doi: 10.1103/PhysRevLett.119.260401. URL https://link.aps.org/doi/10.1103/PhysRevLett.119.260401.

[236] Liangsheng Zhang, Bo Zhao, Trithep Devakul, and David A. Huse. Many-body localization phase transition: A simplified strong-randomness approximate renormalization group. *Physical Review B*, 93:224201, Jun 2016. doi: 10.1103/PhysRevB.93.224201. URL https://link.aps.org/doi/10.1103/PhysRevB.93.224201.

[237] Thimothée Thiery, François Huveneers, Markus Müller, and Wojciech De Roeck. Many-body delocalization as a quantum avalanche. *Physical Review Letters*, 121:140601, Oct 2018. doi: 10.1103/PhysRevLett.121.140601. URL https://link.aps.org/doi/10.1103/PhysRevLett.121.140601.

[238] Anna Goremykina, Romain Vasseur, and Maksym Serbyn. Analytically solvable renormalization group for the many-body localization transition. *Physical Review Letters*, 122:040601, Jan 2019. doi: 10.1103/PhysRevLett.122.040601. URL https://link.aps.org/doi/10.1103/PhysRevLett.122.040601.

[239] Alan Morningstar, David A. Huse, and John Z. Imbrie. Many-body localization near the critical point. *Physical Review B*, 102:125134, Sep 2020. doi: 10.1103/PhysRevB.102.125134. URL https://link.aps.org/doi/10.1103/PhysRevB.102.125134.

[240] V. Ros, M. M uller, and A. Scardicchio. Integrals of motion in the many-body localized phase. *Nuclear Physics B*, 891:420–465, 2015. ISSN 0550-3213. doi: https://doi.org/10.1016/j.nuclphysb.2014.12.014. URL https://www.sciencedirect.com/science/article/pii/S0550321314003836.

[241] Anushya Chandran, Isaac H. Kim, Guifre Vidal, and Dmitry A. Abanin. Constructing local integrals of motion in the many-body localized phase. *Physical Review B*, 91:085425, Feb 2015. doi: 10.1103/PhysRevB.91.085425. URL https://link.aps.org/doi/10.1103/PhysRevB.91.085425.

[242] Louk Rademaker and Miguel Ortuño. Explicit local integrals of motion for the many-body localized state. *Physical Review Letters*, 116:010404, Jan 2016. doi: 10.1103/PhysRevLett.116.010404. URL https://link.aps.org/doi/10.1103/PhysRevLett.116.010404.

[243] David Pekker, Bryan K. Clark, Vadim Oganesyan, and Gil Refael. Fixed points of wegner-wilson flows and many-body localization. *Physical Review Letters*, 119:075701, Aug 2017. doi: 10.1103/PhysRevLett.119.075701. URL https://link.aps.org/doi/10.1103/PhysRevLett.119.075701.

[244] Abishek K. Kulshreshtha, Arijeet Pal, Thorsten B. Wahl, and Steven H. Simon. Behavior of l-bits near the many-body localization transition. *Physical Review B*, 98:184201, Nov 2018. doi: 10.1103/PhysRevB.98.184201. URL https://link.aps.org/doi/10.1103/PhysRevB.98.184201.

[245] Daniel Malz and Adam Smith. Topological two-dimensional floquet lattice on a single superconducting qubit. *Physical Review Letters*, 126:163602, Apr 2021. doi: 10.1103/PhysRevLett.126.163602. URL https://link.aps.org/doi/10.1103/PhysRevLett.126.163602.

CURRICULUM VITAE

[redacted]

[redacted]